APPLICATIONS OF SYNTHESIZED COPPER AND IRON BASED NANOMATERIALS IN WATER POLLUTION AND IN BIOLOGICAL FIELDS

Thesis submitted to

Jadavpur University

by

Bidisha Ghosh

In the partial fulfilment of the requirements for the degree of

Doctor of Philosophy (Ph.D.) in Science

Department of Physics, Jadavpur University

Jadavpur, Kolkata- 700032

India

2023

CERTIFICATE

This is to certify that the thesis entitled **"Applications of Synthesized Copper and Iron Based Nanomaterials in Water pollution and in Biological Fields"** submitted by **Smt Bidisha Ghosh (Registration Number SOPHY1101218, Index No :12/18/Phys/25)** who got her name registered on 31.01.2018 for the award of Ph.D (Science) degree of Jadavpur University is absolutely based upon her own work under the supervision of Dr Kaustuv Das (Supervisor) and Dr Sukhen Das (Co-Supervisor) and that neither this thesis nor any part of it has been submitted for either any degree/diploma or any other academic award anywhere before.

23.06.2023

Dr Kaustuv Das

(Supervisor)

Department of Physics

Jadavpur University

Kolkata-700032, India

Dr Sukhen Das   23/06/2023

Dr Sukhen Das

(Co- Supervisor)

Department of Physics

Jadavpur University

Kolkata-700032, India

Prof. Sukhen Das
Department of Physics,
Jadavpur University
Kolkata - 700 032

Declaration

I hereby, declare the matter described in the thesis entitled, "**Applications of Synthesized Copper and Iron Based Nanomaterials in Water Pollution and in Biological Fields**" is the result of the investigation carried out by me at the Department of Physics, Jadavpur University, Kolkata, India under the supervision of **Dr Kaustuv Das** and under the co-supervision of **Dr Sukhen Das**. Neither this thesis nor any part thereof has been submitted elsewhere for the award of any degree or diploma.

Bidisha Ghosh

Research Scholar
Department of Physics
Jadavpur University
Kolkata-700032, India

DEDICATED TO

My Parents, My Supervisors, my brothers
Soumyadev & Shubham , Boby my friend in
Distress, my Alma Mater Jadavpur University
and to all those who strive each day for a
drop of water …..

Abstract

Applications of Synthesized Copper and Iron Based Nanomaterials in Water Pollution and in Biological Fields

Bidisha Ghosh

Index no: 12/18/Phys./25   *Registration No: SOPHY1101218*

Drinking water pollution through heavy metals, organic phenolic components is an alarming issue worldwide and various indiscriminate anthropological activities, expansion of population and fast pace in industrialization are the root causes of this global quandary leading to major threat to the various biotic and abiotic components of the ecosystem. Alongside improper management in remediating these pollutants culminate in the growth of microorganisms and biofouling. There had been various attempts first of all to devise a good detecting system of heavy metals and materials for removing the organic pollutants as well as the microorganisms that are stamped as the crucial foes of the aqueous habitat. Of all the popular conventional detecting techniques available, fluorescent sensors are now been regarded as the first choice for tracing out heavy metals in water for their efficiency in terms of selectivity and high-end sensitivity. Besides, to address the organic pollutant removal and decontaminating the water environment from the yoke of microorganisms there is urgent need for a suitable material which should serve the salient parameters of being biologically compatible with no burdens of toxicity, quick availability where the material can be synthesized easily and lastly being economically feasible. This research work centralize around transition metals like copper and iron nanomaterials that serves functions of detecting   heavy metals, remediating organic materials and microorganisms. Iron oxyhroxide (α-FeOOH) nanomaterials are been selected to aid in detection of heavy metal ion, hexavalent Chromium (VI)- a model heavy metal ion chosen to study the pattern of detection when the α-FeOOH nanomaterial is decorated with nitrogenous carbon dot. The aggregation of carbon dot is being thwarted by the biocompatible iron oxyhydroxide nanomaterial that acts as a matrix. With an excellent sensing ability this nano-sensor was equally capable in their performance as a biosensor. In this work, the biosensing mechanism was evaluated through *in vitro*

sensing of Cr (VI) in HeLa cells. Additionally copper based semiconductor chalcogenide, copper sulphide (CuS) nanoparticles are chosen to eliminate a potent carcinogen in waste water, para-nitrophenol (pNP) by converting the product to para-amino phenol (pAP) through catalytic reduction using sodium borohydride (NaBH$_4$). CuS nanoparticles were capped with a biocompatible block copolymer Pluronic F-127 and this nanomaterial served dual functions of not only eliminating the waste pollutant but showed excellent antimicrobial activity against a faecal coliform *Eschericia coli* (*Escherichia coli* ATCC 25922) and biofilm forming *Staphylococcus aureus (Staphylococcus aureus* ATCC 25923). The synthesized chalcogenide nanoparticles also showed marked antioxidant activity and cytocompatibility when haemolysis assay was performed. The mentioned transition nanoparticles were subjected through various characterization techniques and thus have been proved to be excellent candidates as nanosensors, nanocatalyst and nano-bio-remediators of the aqueous system with additional qualities of performing as a biosensor and a nanodrug.

Outline of the Thesis

The target of this thesis is to harness the potential of transition metal nanoparticles in remediating water pollution besides utilizing its applications in various biological applications. Thus two transition metal nanoparticles were designed, namely α-FeOOH which were decorated with nitrogenous C-dot and another chalcogenide nanomaterial, CuS was synthesized which was capped with a biocompatible block copolymer Pluronic F-127. The nanoparticles served as a nanosensor, nanocatalyst and a nano bioremediator, the detailed discussion of which is elucidated in the following chapters.

Chapter 1 depicts the background of study, the genesis of the work with a thorough survey of literature regarding water pollution through heavy metals, organic pollutants and microorganisms. The thesis highlights the conventional techniques prevalent in sensing and remediating these factors versus the application of transition metal nanoparticles employed in the same purpose. With this stems the idea of employing copper and iron based semiconductor nanomaterials to address the situation with a glimpse of the various instrumentations so far utilized for their characterization.

Chapter 2 represents the synthesis of a fluorescent nanosensor of hexavalent Cr (VI) wherein a nanomaterial α-FeOOH decorated C-dot was synthesized and a thorough characterization was been made. The efficacy of the nanosensor was judged for sensitivity and selectivity in real water samples.

Chapter 3 explores the biosensing ability of the nanosensor discussed previously in Chapter 2. The nanosensor has been seen to sense the presence of Cr (VI) in living cells leading to the establishment of early stage cancer detection. A theoretical model was prepared using molecular docking techniques that showed the interaction of the nanosensor with the metabolic proteins of the cell.

Chapter 4 will navigate through the synthesis of a chalcogenide, CuS nanocatalyst that has been stabilized through a block copolymer Pluronic F-127 and this nanomaterial was employed for remediating a potent organic pollutant, paranitrophenol (*p*NP) by converting the same into paraaminophenol (*p*AP) through catalytic reduction technique using sodium borohydride (NaBH$_4$).

Chapter 5 explores the antimicrobial efficacy as well as the antioxidant activity and cytocompatibility of the CuS nanocatalyst.

Chapter 6 is the concluding part of the thesis that sums up all the episodes of the research work with an overview of the future scope of the nanomaterials explored so far.

Acknowledgement

"Research is to see what everybody else has seen and to think what nobody else has thought"- Albert Szent-Györgyi

I stumbled across this quotation way back in 2011-2012 at Rajabazar Science College Campus at the Department of Biophysics, where I was working as a novice summer trainee as a part of the Summer Internship Programme for Masters in Science Completion, which I was enrolled in Jadavpur University at the Department of Life Science and Biotechnology. The quote became pertinent after I started my work as a research trainee at the Department of Biophysics, Jadavpur University where I was introduced into a very new concept which I started to work with and based on which this particular journey of the work lies. To think new and to learn, relearn and unlearn what was known is what research is all about. Days of futility had shown that research is all about perseverance. This journey wouldn't had begun if Dr Soumyodev Sarkar (Post-Doctoral Researcher in Arizona State University), my brother and childhood friend had instigated. This thesis can be seen as a bacterial growth curve the exception being that half of the time the exponential phase was little and death phase was absolutely imminent. But the latter didn't happen as there had been strong support systems of my co-supervisor Dr Sukhen Das, Professor, Department of Physics and my supervisor Dr Kaustuv Das, Associate Professor, Dept of Physics, Jadavpur University. Right from managing my clumsiness and relentlessly motivating during the dire times specifically during COVID pandemic and ending in this thesis documentation they had been there with me through and through. This thesis owe to Dr Shubham Roy, Dr Souravi Bardhan & Dr Boby Samai who made me bring this dream to reality. This life will remember Shubham & Souravi as a saviour. Without them this thesis wouldn't have been brought to reality. Boby, my friend and more than a philosopher introduced me to the world of catalysis with nano-materials. I shall never forget Dr Subhas Bhattacharya, ex-Professor, Department of Chemistry who allowed me to use the laboratory for the catalytic reactions. I owe to Dr Soumyadipta Rakshit, who constantly helps me learn about newer techniques related to waste water remediation. I remember veteran professors Dr Sujata Ghosh Dastidar (Ex-Professor, Dept of Pharmacy, Jadavpur University) and Dr Papiya Nandy (Ex- Professor, Dept of Physics, Jadavpur University)guiding me the initial years of my research work. I

List of Abbreviations

μg- microgram

μL- microliter

μM- micromolar

AAS- Atomic Absorption Spectroscopy

AOP- Advanced Oxidation Process

ATCC- American Type Culture Collection

CB- Conduction band

C-dots- Carbon Dots

CuS-copper sulphide

cyt- Cytochrome

DLS- Dynamic Light Scattering

DMEM- Dulbecco Modified Eagle's Medium

DNA- Deoxyribose Nucleic Acid

DPPH- 1,1Diphenyl 2picrylhydrazyl

DTA-TGA- Differential Thermal Analysis & Thermogravimetric Analysis

E.coli- Escherichia coli

EET- Electronic Energy Transfer System

EOC- Emerging Organic Compounds

ETAAS- Electro thermal Atomic Absorption Spectroscopy

eV- electron volt

FeOOH-Ferric Oxyhydroxide

FESEM- Field Emission Scanning Electron Microscopy

FRET-Förster Resonance Energy Transfer

GFAAS- Graphite Furnace Atomic Absorption Spectroscopy

GTF- Glucose Tolerance Factor

HOMO- Highest Occupied Molecular Orbital

I.C – Inhibitory Concentration

ICPMS- Inductive Coupled Plasma Mass Spectroscopy

ICPOS- Inductive Coupled Plasma Optical Emission Spectroscopy

IFE- Inner Filter Effect

IR- Infrared

JCPDS- Joint Committee on Powder Diffraction Standards

keV- kiloelectron volt

LUMO- Lowest Unoccupied Molecular Orbital

M- molar units

MIC-Minimum Inhibitory Concentration

MOF-Metal Organic Framework

mRNA- messanger Ribonucleic Acid

nm- nanometers

nM- nanomolars

O.D- Optical Density

PBS- Phosphate Buffer Saline

PEI- Polyethylenimine

PET- Photo induced Electron Transfer

PL- Photoluminescence Spectroscopy

*p*NP-para nitrophenol

*p*AP-para aminophenol

PVA- Polyvinyl alcohol

PVP- Polyvinyl pyrrolidone

ROS- Reactive Oxygen Species

S.aureus- Staphylococcus aureus

SEM - Scanning Electron Microscopy

SERS- Surface Enhanced Raman Scattering

SV Plot-Stern Volmer's Plot

TEM- Transmission Electron Microscopy

USEPA- United States Environmental Protection Agency

UV-VIS- Ultraviolet Visible Spectroscopy

VB-Valence band

VOC- volatile organic compounds

WHO- World Health Organization

XRD- X-ray diffraction

Table of Contents

List of Publications

1. **Ghosh, B.,** Roy, S., Bardhan, S., Mondal, D., Saha, I., Ghosh, S., . & Das, S. (2022). Biocompatible carbon dot decorated α-FeOOH nanohybrid for an effective fluorometric sensing of Cr (VI) in wastewater and living cells. *Journal of Fluorescence*, *32*(4), 1489-1500.

2. **Ghosh, B.,** Sarkar, S., Sepay, N., Das, K., Das, S., & Dastidar, S. G. (2021). Factors for COVID-19 infection that govern the severity of illness. *SciMedicine Journal*, *3*(2), 177-197.

3. Sarkar, S., Mukherjee, A., Das, S., **Ghosh, B**., Chaudhuri, S., Bhattacharya, D., ... & Gachhui, R. (2019). Nitrogen deprivation elicits dimorphism, capsule biosynthesis and autophagy in Papiliotrema laurentii strain RY1. *Micron*, *124*, 102708.

4. Sinharoy, D., Mukhopadhyay, D., Palchoudhuri, S., **Ghosh, B**., Das, S., & Dastidar, S. G. (2016). Distinct antioxidant activity of a common antidepressant drug imipramine. *Free Radicals and Antioxidants*, *6*(2), 151-154.

5. Palchoudhuri, S.., Mukhopadhyay, D.., Roy, D. S., **Ghosh, B**., Das, S., & Dastidar, S. G. (2017). The antidepressant drug doxepin: A promising antioxidant. *Asian J. Pharm. Clin. Res*, *10*, 1-6.

6. Chaki, S., **Ghosh, B.,** Bandyopadyhay, S., Mookerjee, M., Das, S., & Dastidar, S. G. (2015). Detection of various phytochemical compounds from seeds of A. auriculiformis for possibilities of obtaining potent antimicrobial agents. *Int J Biol Pharm Res*, *6*(2), 120-128.

Book Chapters

1. **Bidisha Ghosh**, Pijush Mallick, Kaustuv Das, Sukhen Das, Recycling of Waste Water through Natural Filtration Techniques: Possibilities and Challenges in Multidisciplinary Review Book, *Taurean Publications,* (ISBN:978-93-91074-40-1), 2022, pp. 1-22

List of Attended Conferences/Seminars

1. Poster Presentation on **"Synthesis and Characterization of CuS nanoparticles and Determination of its Antimicrobial Activity"** at 9th Annual Conference IAMM (West Bengal Chapter) at Nil Ratan Sirkar Medical College on 7th December 2014.

2. Poster Presentation on "**The Wonder Drug *Zincum Oxydatum*"** at the National Symposium on Science Behind Homeopathy at the Birla Industrial and Technological Museum, Kolkata held on 20th February 2016.

3. Poster Presentation on **"Unravelling the photocatalytic reduction and antioxidant properties of block copolymer assisted CuS nanoparticles synthesized via reflux condensation method"** at the National Conference on Recent Developments in Nanoscience & Nanotechnology (NCRDNN) organized by School of Materials Science and Nanotechology, Jadavpur University, Kolkata on 29-31st January 2019.

4. Poster Presentation on **"Synthesis of bimetallic Amp@Ag@Cu nanoparticles for potential biological applications"** at the One Day National Seminar on Modern Trends in Chemistry for Sustainable Development organized by Department of Chemistry, Vijaygarh Jyotish Ray College, Kolkata in Collaboration with The Indian Chemical Society on 3rd March 2020

5. Poster Presentation on **"Fluorometric Sensing of hexavalent chromium in waste water and living cells by C dot decorated biocompatible FeOOH nanoparticles"** at the 1st Virtual International Conference on Biotechnology & Bioinformatics (ICBB-2022) organized by Insight Biosolutions, France in technical collaboration with Indian Science and Technology, India held on 26th-27th February 2022.

Workshops Participated

1. Participated in **Two Day Workshop on Material Characterization Techniques"** held at Jadavpur University on 4th -5th October 2016.

2. Participated in **"One day Workshop on Drugs Virtual Screening by Autodock Vina and Toxicity Prediction by QSAR"** by Indian Science & Technology Foundation, Delhi, India on 26th March 2022

List of Awards

1. Best poster presentation award on "**The Wonder Drug *Zincum Oxydatum***" at the National Symposium on Science Behind Homeopathy at the Birla Industrial and Technological Museum, Kolkata held on 20th February 2016.

2. Best poster presentation award on **"Synthesis of bimetallic Amp@Ag@Cu nanoparticles for potential biological applications"** at the One Day National Seminar on Modern Trends in Chemistry for Sustainable Development organized by Department of Chemistry, Vijaygarh Jyotish Ray College, Kolkata in Collaboration with The Indian Chemical Society on 3rd March 2020.

3. Best poster presentation award on **"Fluorometric Sensing of hexavalent chromium in waste water and living cells by C dot decorated biocompatible FeOOH nanoparticles"** at the 1st Virtual International Conference on Biotechnology & Bioinformatics (ICBB-2022) organized by Insight Biosolutions, France in technical collaboration with Indian Science and Technology, India held on 26th-27th February 2022.

List of Figures

CHAPTER 3

CHAPTER 4

List of Tables

INTRODUCTION, LITERATURE SURVEY & INSTRUMENTATION

CHAPTER 1

1.1 Water Pollution: A Global Conundrum

Water pollution seems the perpetual trouble disturbing almost decades after decades the human pollution on Earth. Being the indispensable component for sustenance the unprecedented challenge of this century is the depletion of available ground water which get sparser with indiscriminate anthropological activities. Consequently, the immediate addressee of this predicament impacts ecological and environmental species of both biotic and abiotic components. Since earlier times from the advent of civilization agricultural activities have posed much threats upon the aquatic milieu mainly rivers and streams [1]. With the advent of time for an aim of faster economic growth and development there had been unprecedented urban growth coupled with elevated levels of population burst. From a pragmatic point of view, it has been observed that water pollution mainly sources out from industrial effluents.

Sources of the contaminants that are released to the aquatic environment that sources mainly from anthropogenic sources mainly leather industries [2-3], textile [4-6], pharmaceutical [7-8] plastic industries [9-11] and also there are fertilizers [12-14] from the agriculture sector that causes the water contamination

Organic effluents in the form of synthetic compounds like benzene, phenolic compounds categorized as "xenobiotics" [15] and VOCs in the form of fumigants, refrigeration materials, solvents [16] along with heavy metals and metalloids [17] are the pivotal threats to the aqueous system.

This research has been aimed to sense the heavy metals in water besides degradation of the toxic dye compounds that gets infiltrated into the environment. Thus, two important nanomaterials have been designed and customized to meet the above requirements and accordingly the choice of the nano materials has been made. Two important groups of nanomaterials are been chosen to meet the requirements. One of them is a transitional metal oxyhydroxide (α-FeOOH) and the other being transitional metal sulphide or more commonly a chalcogenide (CuS) which respectively will serve the function of sensing a heavy metal and the other will degrade toxic organic compounds from the environment.

Before delving further into the details less have a preview of these fundamental atrocities -the heavy metals and the organic compounds which contaminate the aqueous milieu and which gave impetus to this research thesis.

1.1.1 Pollution of water through Heavy Metals: A global quandary-

- **Sources and Properties:**

At the very start of the discussion in this section it is of prime importance to underline the fact that any metal or metalloids starting right from lead (Pb) to manganese, molybdenum (Mb) found in trace amounts can be categorised as contaminant if its presence interfere with the wellbeing of living organisms [18]. In context to heavy metals first of all it needs to be pointed out what counts for a heavy metal. Stephen J Hawkes describes in his paper what is a heavy metal? the answer that he received from his teacher was "A metal that behaves in a heavy metal manner" [19]. Though the answer may remain shrouded in darkness it was described later by scientific groups that metals which have their density of $5g/cm^3$ or more are to be categorised as "heavy metals" [20-22]. The percolation of heavy metals and their subsequent accumulation into the food chain affects various living organisms like including human beings [23-28]. Though there are many heavy metals that are required in trace amounts by organisms that include tungsten [29], cadmium [30], but majority of the heavy metals like arsenic, lead, chromium, mercury poses myriads of adversities to living organisms. As mentioned above about the emergence of industries and their consequent toxic chemical effluents hamper the eco system the sources of heavy metals are also due to other injudicious anthropogenic activities like mining [31-32] smelting [33-34] indiscriminate burning of oils and other fossil fuels [35-36] coupled with various natural sources like volcanic eruptions [37-39] sudden accidental forest fires [40-41], weathering [42-43] leads to the release of a number of heavy metals into the environment.
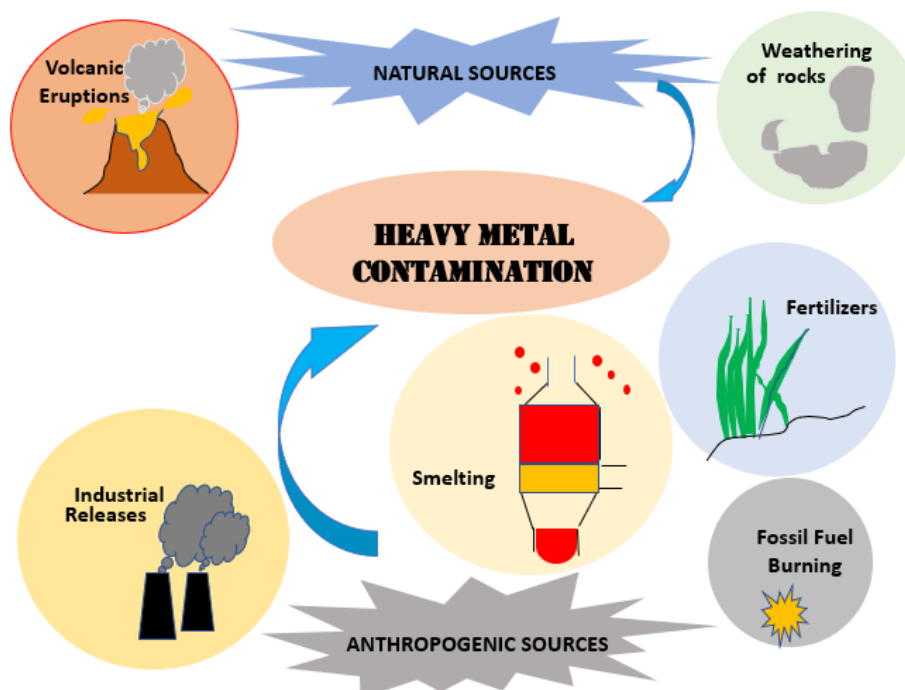
Fig 1.1: A graphical representation of different sources of heavy metal contamination through natural and anthropogenic sources

- **Effects of different heavy metals in the water:**

There are permissible limits for all metals in the environment according to World Health Organization (WHO) [44,45] and since this research work mainly centres around water pollution interaction of the heavy metals with the different biotic components present in the environment are to be addressed in this regard. The heavy metals however in very minute quantities in water poses toxic effects on almost all living organisms. These for example in human beings can cause serious metabolic disorders [46] as well as stems carcinogenic tendency of the cell [47-48].

The different permissible limits and the potential carcinogenic description of different toxic heavy metals are listed in Table 1.1.

Table 1.1: The presence of commonly occurring heavy metals their limits permissible for drinking as advised through WHO and USEPA along with their carcinogenic descriptor [44-45]

Sl. No.	Types of heavy metals	WHO Permissible limit (mg/l) [44]	Carcinogenic factor[45]
1	Arsenic	0.01	A
2	Cadmium	0.003	D
3	Chromium	0.05	D
4	Copper	2.0	D
5	Lead	0.01	B^2
6	Mercury	0.006	D

According to USEPA TT^6 is the action level for copper which is 1.3mg/l,

TT^6 for lead has been set to 0.015mg/l

The Carcinogen descriptors according to USEPA are: A that stands for Human carcinogen; B is "probable human carcinogen"- B1 indicating sufficient human evidence is lacking, B2 indicates though sufficient evidence is obtained in animals very less is known about humans, C indicates it can be a possible carcinogen, D indicates the substance is not classified as a human carcinogen, E indicates that there are evidences of the substance being non-carcinogenic.

- **Chromium: Beneficial Trivalent to Carcinogenic Hazardous Hexavalent form:**

Micronutrient trivalent chromium found its use as dietary supplement [49] and find its role in regulating different metabolic functions of the body mainly in glucose metabolism in which the trivalent form of chromium exists as an inherent element in glucose tolerance factor (GTF) that stimulates insulin production [50]. Dietary chromium is seen to control uptake of glucose by controlling upregulation of the mRNA of various glucose transporters as well as glycogen synthase enzymes [51]. However, in contrast hexavalent chromium significant permeability through sulphur channel as its anionic structure, CrO_4^{2-} ion resembles to that of the sulphate ion (SO_4^{2-}) and arginine in the sulphur channel as well as in phosphate channels through which the Cr (VI) binds stabilizes the Cr (VI) through hydrogen bonding [52-53]. After the entry via mimicking the sulphate and phosphate ion channels the hexavalent Cr (VI) undergoes rapid metabolic reduction to Cr (V), Cr (IV) and ultimately elucidating its DNA binding genotoxic Cr (III) state [54]. The mechanism via which Cr (VI)

undergoes changes in its valence states was well described by Stearns *et* al. The authors pointed out that reduction of hexavalent chromium is dependent on the intracellular level on reducing agents such that at a very low concentration of the available reductants Cr (VI) was seen to get reduced into its Cr lower valence states Cr (VI) ,Cr (V),Cr (IV) andCr (III), wheras when the concentration of reductants is at a definite level the reaction is a rapid reduction process where two electrons are given out from Cr (VI) to form Cr (IV) without the formation of Cr (V) with a one electron loss to yield Cr (III) [55]
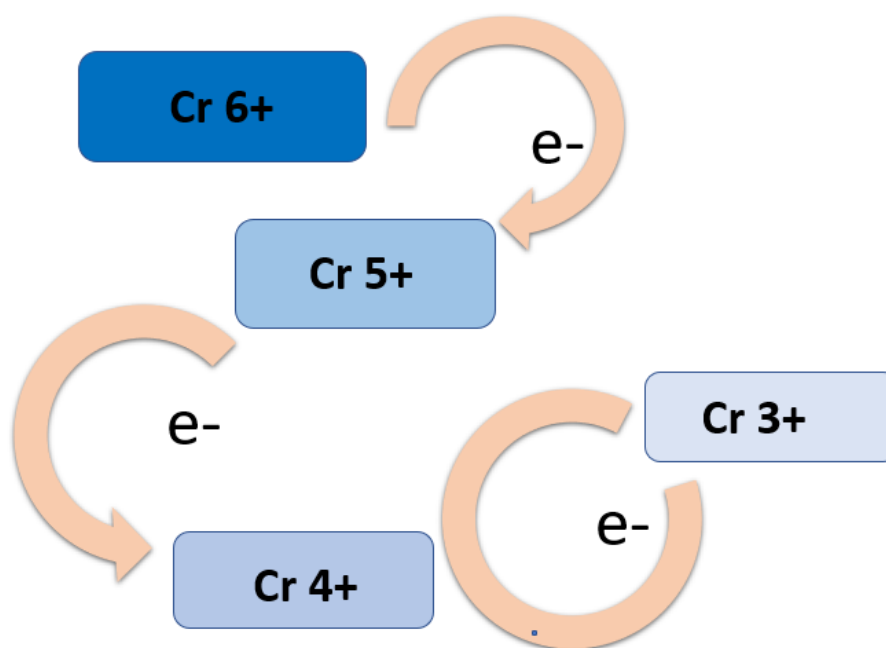
Fig 1.2 The electron transfer process involved in Cr (VI) reduction in the cells at a minimal concentration of the reductants

Formation of trivalent form of Cr (III) species is largely generated out of the reduction of Cr (VI) by various molecules present in the cell like glutathione, the concentration of which largely dictates the reduction of Cr (VI) as shown in Fig 1.2. Chromium (III) formed, though unable to cross the plasma membrane eventually interacts with its six coordination sites with various biological ligands like amino acids, proteins and DNA [56]. The interaction between Cr (III) to that of DNA is a reaction that involves non-oxidative pathways leading to genotoxicity and consequently to intra-strand DNA-Cr (III) crosslinking adduct formation [57] and contributing largely the cell towards cancerous propensity.

Thus, it largely necessitates to check the levels of Cr (VI) in drinking water and thereby its removal from the same. The sensing of Cr (VI) in water thus forms a primary criterion alongside its treatment for removal.

1.1.2 Detection of Cr (VI) in Drinking water:

The necessity for potable drinking water requires thorough assessment primarily to check any traces of heavy metal contamination. In our forementioned section, a discussion has already been made about the most obnoxious presence of Cr (VI). The detection of its can be achieved through various known fabricated sensors available. The sensing techniques should be reliable, cost effective and should be easy to handle.

The various detection methods are now discussed in a nutshell to have a quick idea about the techniques of sensing hexavalent chromium.

- *Spectroscopy based sensor techniques of Cr (VI)*

Of all the spectroscopy-based techniques known one of the widely used spectroscopy based technique is the Raman spectroscopy based sensing techniques that relies on Surface Enhanced Raman Scattering (SERS) typically based on using semiconductor materials labelled with a probe that is further being used for quantitative analysis [58]. Though high degree of sensitivity has been achieved through this technique the method is not always considered helpful because of the lack of sensitivity when assessed in the parameter of time and secondly its reproducibility is not reliable [59].

The next widely used spectroscopic method of identifying heavy metals is Atomic Absorption Spectroscopy (AAS). This analytical process can be used to identify traces of metal that remain as impurities in samples [60]. Atomic absorption spectroscopy can be of varied kinds like Flame Atomic Absorption spectroscopy (FAAS), Electro thermal Atomic Absorption Spectroscopy (ETAAS) and Graphite Furnace Atomic Absorption Spectroscopy (GFAAS). These systems though are accurate and give high precision values, suffers from a number of disadvantages. These various AAS techniques has different matrix related interferences [61]. Other interferences in AAS can be absorption of source radiation of other element rather than the desired one, formation of lower absorption due to ionization [62].

Inductive Coupled Plasma Mass Spectroscopy (ICPMS) and Inductive Coupled Plasma Optical Emission Spectroscopy (ICPOS) are the other spectroscopic techniques that can be seen as a "black box" for ultra trace detection of metals. These spectroscopic measurements rely on plasma that forms when a stream of argon gas flows through quartz tubes. The argon plasma is used to ionize and excite an array of different metals at the same time achieving detection of multiple elements [63]. Though a high- end instrumentation technique the limitation of interference is also associated with this type of spectroscopy as well. Spectral interferences are seen to originate in case of ICPMS from chromium isotopes like ^{52}Cr and ^{53}Cr which cannot be distinguished from two polyatomic elements like C and Cl which generally present in the plasma as $Ar^{12}C^+$ and $Cl^{16}O^+$. The interference of these undesired elements should be warded off for correct quantification of Chromium. [64].

- *Electrochemical based sensor technique of Cr (VI) in waste water*

The bane of the industrial revolution and advent of new agricultural practices in the course of urbanization has paved way for the impregnation of a number of contaminants in the ecological system and the abundance and persistence of heavy metals leached from these sources into the aqueous environment in particular interfere with the sustenance of the fauna and flora of the same [65]. The high cost, robust instrumentation and the interference of undesired elements as mentioned in the earlier section, spectroscopic methods are sort of avoided and in place a number of sensitive detection methods are been used. One of them is the electrochemical sensor based heavy metal detection system which are potable and are of high sensitivity and reproducibility. The system relies on the transducing principle that the information received from the chemical species present in the analyte is converted into electrochemical signal [66]. Most of the electrochemical methods are built on the basic principle of voltammetry. Stripping Voltammetry that can be categorised generally into anodic and cathodic stripping voltametric electrochemical sensing is one of the widely used technique for heavy metal detection in ppb quantities of a concentration of metal just by measuring the pH of the solution [67]. This method has won over the conventional spectroscopic techniques like ICPMS and ICPOES where the metal sample does not need pre acidification [67]. Stripping voltametric are been used for the detection of Cr (VI) in various levels of concentration ranging from milli-

molars to nanomolar levels as seen in ion transfer stripping voltammetry, a more developed electrochemical sensor where instead of using mercury electrodes that renders toxicity the system is built on glass carbon electrode wrapped on double polymers for entrapment of the Cr (VI) ions [68]. Further, newer advancement in electrochemical sensors is widely gaining prominence like "miniaturization" where the device is made up of fewer micro-meters planned on a placing small three electrodes on a platform of insulated material known as screen printed electrodes (SPEs) for allowing very small quantity of analyte to be assessed [69]. Screen printed electrodes mainly are vogue for overcoming the drawbacks of "electrode fouling" [70]. Cr (VI) detection has been possible using graphite screen electrodes [71] with a limit of detection of 19 μgL^{-1}. Newer modifications of electrochemical sensors make use of polycrystalline materials [72-73] for the high selective identification of Cr (VI) in water.

- ***Fluorescent sensors as widespread Cr (VI) detectors***

Fluorescent chemo-sensors rest on the principle of physiochemical transition as the sensing system is built on three basic requirements that composes of a receptor moiety, a fluorescent molecule or a fluorophore and to link these two substances a spacer molecule forming the widely known "fluorophore- receptor- spacer scaffold". The binding of a fluorescent probe with a receptor moiety results in change in the fluorescent intensity or lifetime decay measurements [74]. Fluorescence based detection can either be achieved through Photo induced Electron Transfer (PET) mechanism wherein the sensing mechanism is based on a "off-on" system as when the receptor moiety interacts and detaches with the fluorescent molecule in contrast to fluorescence quenching in   Electronic Energy Transfer System [EET] the sensing mechanism is via interaction between the metal ions and the fluorophore through orbital overlapping [74]. Utilizing this above mechanism, a large number of fluorescent sensors are available for hexavalent chromium like Metal Organic Frameworks (MOFs) which have attractive properties in terms of their structure, porosity and surface area [75]. Besides organic dyes [76] like fluorescent materials are trapped in various minerals and clay materials that serves the function of preventing quenching of the fluorescence.

- *Colorimetric sensors for easy Cr (VI) detectors*

Complexity of techniques as well high-end cost of the instruments like AAS, stripping voltammetry has limited use of the spectroscopic and electrochemical sensing techniques. Thus, novel optical colorimetric sensors are developed nowadays to meet the demand of detecting heavy metal contamination at substantially low concentration with greater reproducibility. A number of polymer based colorimetric sensors [77-78], membrane based [79-80] and multifunctional Schiff's bases as well as various organic molecules are available for detecting heavy metal contamination [81]. Heavy metal hexavalent Cr (VI) sensing can be achieved through fabrication of these mentioned ligands to specific materials of interest.

1.1.3 Pollution in water through organic pollutants:

The vast extent of water pollution globally is not only attributed to the presence of heavy metals in blue resources but also due to the trespassing of a number of organic pollutants, dyes sourcing out of urbanization and rapid industrial advancement. A number of polluting substances known as emerging organic compounds (EOCs) of varied types pollute the environment that are found in a number of industrial products right from pharmaceuticals, agricultural veterinary by products to name a few [82]. The compounds of major concern are phenols and substituted phenolic derivatives that are been categorized as hazardous and noxious substances (HNS) disturb the ecological stability of the aqueous system [83].

Phenol and its derivatives can either be sinker (S) having a solubility ranging between 2.15-8.28g or a sinker- dissolver (SD) having a solubility range between 2.27-2.59g in 100ml water with significant lethal toxicity [83]. Besides, most of the organic compounds that have genotoxic potential have -NO_2 attached to benzene ring that forms nitroaromatic compounds. The position of nitro groups in the various positions of the benzene ring like in *ortho* and *meta* positions render the nitroaromatics prone to repel electrophilic substances and in addition making them more stable in the environment and less prone to degradation [84]. Nitrophenols are considered as "priority pollutants" by U.S Environment Protection Agency (EPA) [85] and amends are to be made to remove them from the environment in spite of their unavoidable usage in different industrial sectors.

- *Para nitrophenol (pNP) : A major nitroaromatic water pollutant*

*p*NP is a one of the major recalcitrant nitroaromatics which has high solubility and stability and is a major water pollutant that disrupts the ecosystem[86] . It has been widely used in various pharmaceutical industries in making leather products and in agricultural sectors as a fungicide [87]. Hydrolytic and photolytic degradation of insecticides and herbicides like parathion, nitrofen may lead to the formation of para nitrophenol (*p*NP) [86,88] .The United States Environmental Protection Agency (USEPA) list has categorized it as one of the most toxic hazardous materials with an allowed concentration in the range of 1-20ppb in water [86] and the Agency for Toxic Substances and Disease Registry of the U.S Public health has categorized *p*NP on the 14th of the other 1177 hazardous materials in the National Priority List (NPL) [89].

Substituted nitro-benzenes has propensities of getting reduced to arylhydroxylamines. These products attack C8 position in the guanine of DNA in the cell by the electrophilic nitrogen present in their structure and has been found to exhibit chromosomal aberrations in mammalian cells [90].
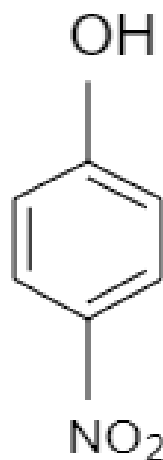
Fig 1.3: Structural representation of para nitrophenol (*p*NP)

(Structural representation was drawn through ChemDraw Software)

Besides, *p*NP has found to exhibit toxic activities against a large number of soil microalgae like *Scenedesmus bijugatus* and *Chlorella vulgaris* where *p*NP has been found to interfere with metabolic activities inhibiting electron transport process in photosynthesis and marked reduction in chlorophyll content [91].

Advanced Oxidation Processes (AOPs) in the treatment of pNP

Being one of the hazardous waste materials there is a great necessity for the efficient removal of *p*NP from the aqueous environment as water is the major elixir of life. A number of mechanisms have been devised to properly manage the waste pollutant.

Advanced oxidation process (AOPs) forms a major platform in eradicating obnoxious organic waste pollutants from water mainly textile dyes, pesticides, antibiotics, and varied range of phenolic hydrocarbons. Advanced Oxidation processes includes two types of catalysis mainly homogenous and heterogenous catalytic reactions [92] and includes processes like photocatalysis, Fenton- Fenton reaction, electrochemical processes, UV and γ irradiation based organic pollutant removal techniques [93]. AOPs are devised on the principle of generation of oxidants and radicals most commonly like hydroxyl radicals that attacks an organic compound and generates a carbon centred radical ($R^{\cdot}$ **-OH)** which further reacts with O_2 to reactive superoxide anion ($O_2^{\cdot}$) through the pathway of organic peroxyl radical formation that culminates ultimately into the degradation of these organic compounds [94]. There are several drawbacks of the Fenton reaction as there is always a requirement of higher concentration of H_2O_2 as well as $FeSO_4$ during the treatment processes [95]. Photocatalysis is one of the most popular AOPs that is employed for waste water treatment. The choice of the materials for photocatalytic waste removals are semiconductor metals immobilized on inorganic solid support like clay, resins and zeolite circumvent the crisis of recalcitrant organic waste pollution in water. [96-98]. The overall mechanism of the photocatalytic reaction can be seen as formation of e^- /h^+ as a result of charge separation [99] when the light is absorbed by the metal complex acting as a catalyst with the simultaneous conduction of the charge carrier from the valence band to the conduction band depending upon the band structure of the semiconductor material which can be made small by the addition of dopants [100] .
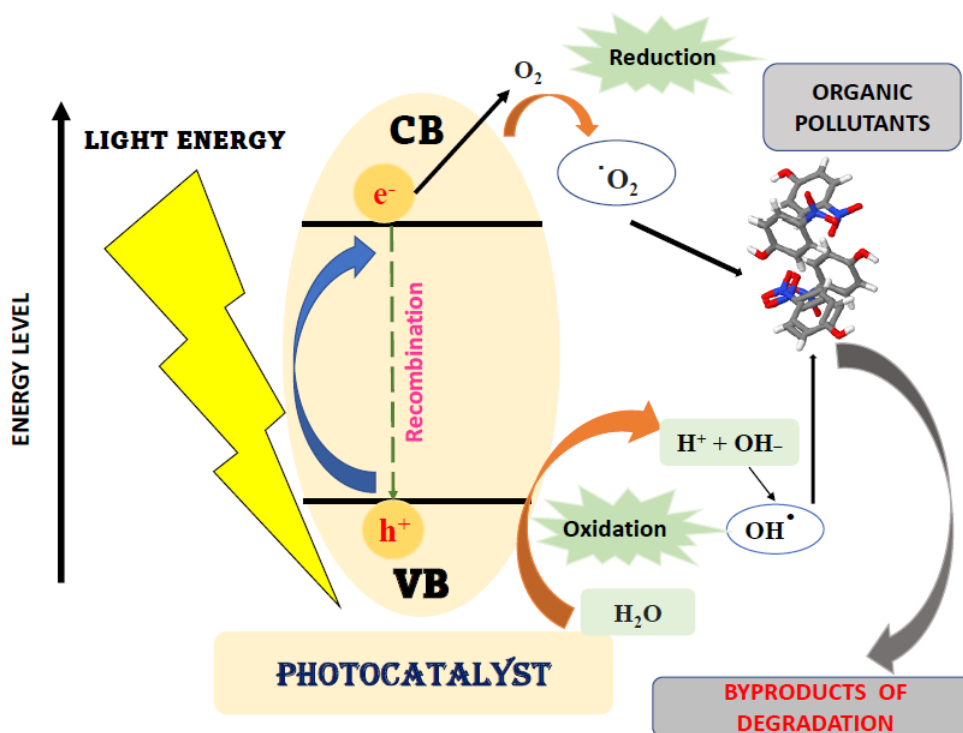
Fig 1.4 A schematic diagram showing photocatalysis of organic pollutants

Ultrasound Irradiation as a Modification of AOPs

Besides photocatalysis another useful method in treating wastewater infested with nitroaromatics is through ultrasound irradiation for its effective eradication. This method has several advantages as it does not generate any secondary products and has high penetrating ability [101]. Ultrasound irradiation generates cavitation where minute bubbles are generated and are collapsed at a given interval of time [102]. The hydrophobic organic compounds are degraded and comparatively lesser hydrophobic compounds are degraded by the OH˙ those that has resulted during the cavitation process [101]. Cavitation processes are generally of two types one acoustic cavitation and the other being hydrodynamic cavitation. In recent years for the removal of pNP are being removed through cavitation technique [103]. Both of the methods of acoustic cavitation and hydrodynamic cavitation either individually or in combination are used for the removal of the major recalcitrant nitroaromatics. Hydrodynamic cavitation is a newer modification of treating waste water. This particular methodology relies on the principle of pressure difference when fluid is allowed to pass through a valve or orifice [104]. Lately, hydrodynamic cavitation in alone and in combination with Fenton's reagent is being used for the removal of *p*NP in waste

water [105-106]. In combined synergistic approach of using hydrodynamic cavitation and Fenton's chemistry the operating pH is seen to be a pivotal parameter in carrying out the degradation reaction [107].

- ***Drawbacks of AOPs- Search for New Methodology:***

Though considered as one of the efficient strategies to remove organic effluents specifically nitroaromatics, there are several disadvantages associated with advanced oxidation processes. Advanced Oxidation processes like Fenton's Reaction requires robust procedures of storage. It has been observed that formation of Fe (III) complexes hinders mineralization which is unable to degradation by OH˙ [108]. Advanced Oxidation Processes have a disadvantage of producing secondary contaminants which can be toxic to the aquatic zooplanktons [109], besides this process is a concentration dependant reaction and requires OH free radical to be produced in abundance to accomplish the degradation system. The source of light used in AOPs like UV entails huge cost and thus most of the time are not appropriate for the degradation of the organic effluents [110]. So, the process of AOPs should be modified with the introduction of new inexpensive catalyst with modified methodology to address the predicament.

1.1.4 Pollution in water through microorganisms

Apart from the obnoxious presence of heavy metals and organic effluents in water another alarming factor that endangers the aqueous realm is the infestation of pathogenic microorganisms which are ubiquitous in the environment. Till date despite the advent of modern medical and technological advancement there is a huge lacuna of proper antimicrobial that could combat the predicament. Drinking water is sparse and the colonization of microorganisms poses threat to the lives of almost a significant section of the global population which is under privileged. It has been reported that the surface water of most of the developed countries are contaminated with pathogens and are mainly of bacteria, protozoa and virus of which the dominated category of bacteria are the coliforms belonging to the family *Enterobacteriaceae* [111]. The frequently occurring coliform is *Escherichia coli.* Apart from this leading opportunistic pathogen that mainly inhabit the water systems there is another adversity that is frequent *Staphylococcus aureus*. This gram- positive bacteria has been seen to cause significant food poisoning when present in water [112]. However,

the most alarming among all these factors is the ability of both these pathogens is to form biofilms. These biofilms are aggregated mass of cells that remains within an exopolysaccharide produced by them and are seen to for a consortium on a surface that can be either a biotic organism or an abiotic solid substratum [113]. Biofilm formation occurs by virtue of several biomolecules like polysaccharide intercellular adhesin (PIA) besides other proteins and DNA [114]. Health hazards are seen to be associated with drinking water contaminated with *S. aureus* [115]. Deterioration of drinking water quality is attributed to the fact that these biofilms inhabit the interior lumen of the water pipelines and can get detached and in its worst may enter into the vicinity of any water source [116]. The formation of biofilms is predominantly seen to occur in water systems as these notorious biofilms and are almost refractory to the action of disinfectants and potent antimicrobials [117]. Recent reports have suggested the use of organo-selenium compounds that could address this biofouling by *E. coli* and *S. aureus* [118]. But these compounds are not preferred for their potential toxic effects as selenium reacts with disulphides present in proteins and form seleno-trisulphides which in due course suffer reduction to form seleno persulphides which are highly reactive and causes cellular oxidative stress [119-120].

So, there should be search for newer materials that could simultaneously combat the microbial contamination by the said microorganisms along with addressing the side effects of toxicity.

1.2 Application of nanoparticles: Its benevolence from sensor to remediator.

For the purpose of developing advanced materials with versatile properties, nanotechnology has been evolved to customise materials having extraordinary potential to meet different applications in varied spectrums of human life. The science of this nanotechnology involves modifying substances at the atomic or molecular level to produce novel, unusual nanoscale materials with tremendous potential. The need for novel materials and devices is growing, which motivates material scientists to create new materials with intriguing features.

Materials that have had their size reduced to the nano regime exhibit different properties from those of bulk materials. The "quantum size effect," which changes the electrical characteristics of solids, is more pronounced as the system's size shrinks.

The mechanical, thermal, and catalytic properties of materials change considerably when the surface area to volume ratio rises. Nanomaterials can be used in many ways thanks to all these distinctive features.

The distinctive electronic, catalytical, sensing, optical, biological and other physico-chemical properties of these nano-materials parts them from the bulk counterparts and the high surface-to-volume ratios of nanomaterials and their surface modifications through a variety of chemical and bioconjugate reactions have shaped nanotechnology through the intersection of chemistry, materials science, and biology towards interdisciplinary science.

Due to their distinctive features based on their intrinsic huge surface-to-volume ratios and quantum size effects, metal NPs with small diameters and a narrow size distribution have drawn a lot of attention in scientific study and industrial applications [121].

In view of the situation described above regarding the contamination of drinking water, nanoparticles for their various noted properties are harnessed as a sensor, a catalyst for pollutant removal as well a remediator for biofilm and also an antimicrobial are chosen Before delving into the details of the choice of the nanoparticles we now discuss in a nutshell how all these important properties are been served by nanoparticles.

1.2.1 Heavy metal sensing potential of nanoparticles

Modern technologies hint at using materials which will be easy to handle, highly economical with high end productivity. The advent of nanotechnology thus meets all the above parameters that could be utilized for the development of smart materials for sensing purpose. Earlier literatures guide in the development of nano-sensors with the help of noble metals like gold, silver and platinum. Gold nanoparticles are largely been employed than the other two metals as silver have the disadvantage of being reactive during the course of reaction and the expensive value of platinum hinders its usage despite having potential for the same [122]. Surface functionalized gold nanoparticles are seen to sense toxic heavy metals lead [123], arsenic [124], mercury [125], hexavalent [126] and trivalent chromium [127]. The mechanism via which primarily gold and other noble metals sense the heavy metals are typically through their localized surface plasmon resonance arising out of the cumulative oscillation of

the conduction band electrons in the nanomaterial with the source of light [128]. In spite of their high sensing ability the gold nanoparticles aren't been preferred due to their high cost. For this there are a number of other alternatives in the form of metal as well as non-metal nanoparticles that are effective as sensors. Most of the nanomaterials that are used these days relies on spectroscopic techniques, colorimetric and fluorescent techniques which were elaborately discussed earlier. Among all these sensing devices the smart method so far has been proved to be productive is the fluorescence quenching method wherein the fluorescent signal change occurring due to the interaction of nanomaterial with the ligand molecule can be monitored by the parameters like fluorescent lifetime, changes in its intensity of the fluorescent nanomaterial. These are found to be more attractive and sensitive than the established mechanism of colorimetry. The sensing methodology commonly followed are Förster Resonance Energy Transfer (FRET) [129], Inner Filter Effect (IFE) [130] Static and Dynamic Quenching mechanisms [131].

1.2.2 Catalytic function of nanoparticles in pollutant removal from water

Apart from the trespassing of heavy metals in waste water, the infiltration of dyes and other phenolic compounds leaching out of different industrial, pharmaceutical and agricultural effluents poses a serious trouble to the aquatic system. The urge to remove these waste pollutants in water calls for the necessity of a material which are excellent in eradicating them so that water is rendered safe for drinking purpose. For this the choice of nanoparticles is the most judicious decision so far proved. The mechanism of degrading the organic pollutants by the nanoparticles is photocatalysis which utilizes the function of a metal nanoparticle which when excited by any source of light will enable movement of electrons from valence band (VB) to conduction band (CB) with the generation of holes in the valence band [132]. Nanoparticles mostly in the form of metal semiconductor like titanium dioxide (TiO_2) are in use for long to address the alarming issue. However, the use of TiO_2 as semiconductor nanoparticles have a disadvantage in terms of catalysis is that they are effective only when the source of UV radiation being a wide gap semiconductor [133]. So apart from these the other types of semiconductors like the oxides and sulphides of various metals are used for the above purpose. The choice of transition metals in the form of their oxides and chalcogenides are commonly used because the positions of CB and VB are thermodynamically favourable [132]. These metallic nanoparticles are been

popularly used in catalytic reactions to ward off the toxic contaminants out of waste water.

1.2.3 Biological application of the nanoparticles

The last most important application about nanoparticles is their biological applications. It provides a broader avenue for a number of applications in therapeutic fields. Being particles of ultra-small dimensions nanoparticles can be used for a plethora of purposes right from detecting pathogens, aiding in delivery of drug of choice and gene to their diversity as effective antimicrobial and potent anti-cancerous agents, an idea schematically represented in Fig 1.5. Via different surface modifications like trans-esterification and amidation processes the surface of the nanoparticles can be modified and linked through various surface ligands for their purpose to interact with different biomolecules like proteins, nucleic acid inside the biological system [134] These surface modifications using various ligands like biocompatible polymers like chitosan, collagen and biomolecules like antibodies are important for probing various cellular actions like detecting various proteins and pathogens [135]. Nanoparticles that are generally used for the vast applications in biology are either metallic nanoparticle [136] or are ceramic or polymeric in nature [137]. Nanoparticles as antimicrobials target the cell wall of bacteria and will thereby will cause cytoplasmic contents to leak out [138]. Nanoparticles after entering into the cell can also trigger formation of reactive oxygen species (ROS) and those will combine with bacterial DNA to form DNA adducts leading to bacterial cell death [139]. One of the promising aspects of nanoparticles is to combat with the biggest bane, cancer. Potent anti-cancerous drugs can be encapsulated within polymer coat of nanoparticle dimension [140] or are conjugated with a nanoparticle tailored against a cancer affected organ [141]. Hydroxyapatite nanoparticles derived from various natural sources like egg shells, fish bones act as "bio-calcium" that are used for tissue bone engineering [142]. Nanoparticles can be labelled with a variety of fluorescent molecules to detect the presence of any pathogens which is a landmark of biosensing. Carbon dot nanoparticles are the examples which alone may serve the function of sensing [143] and are further been utilized as effective candidates in bioimaging purposes [144]. In addition to the different anticancer agents, nanoparticles are also been efficient candidates for photodynamic therapy. Specific drug molecules called photosensitizers being hydrophobic suffers hindrance in the biological system and

thus are encapsulated within either semiconductor, or silica or polymer-based nanoparticles [145] are excited with the help of a specific wavelength of either visible light or near infrared that generates oxygen molecules. This reactive oxygen molecules in turn are reactive and will target the diseased or damaged cells [146].
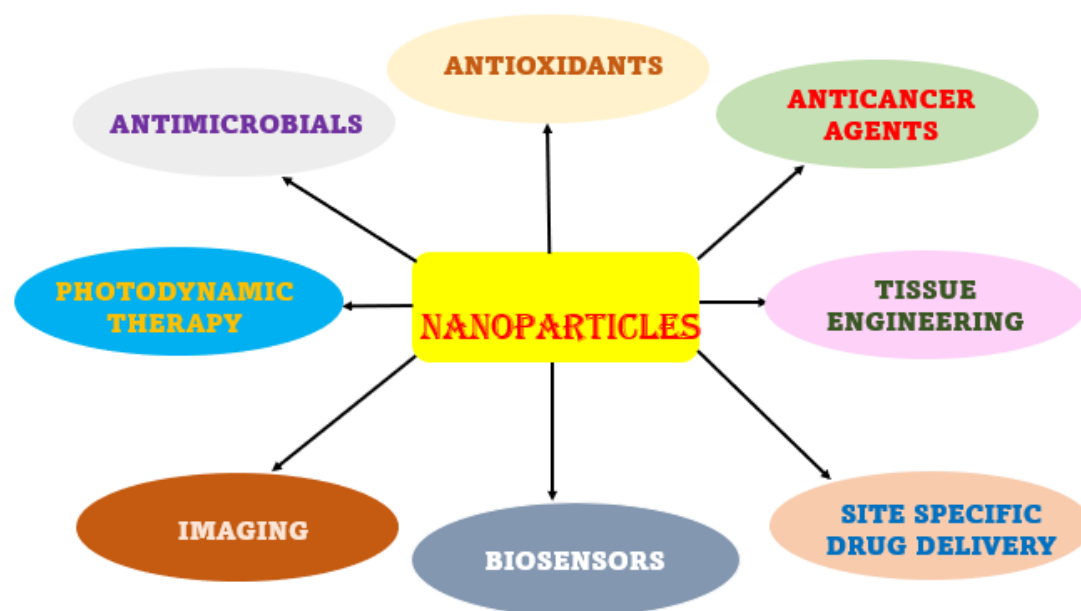
Fig 1.5 Schematic diagram showing the potential biological application of nanoparticles

2.1 Genesis of the Present Work

2.1.1 Choice of Nanomaterials for sensing, catalysis and biological functioning: Iron oxyhydroxides (α- FeOOH) and Copper Sulphide (CuS) nanoparticles

Semiconductor nanoparticles are widely employed for their several unique contributions that arise mainly from their small size effect. At a very low concentration they possess the quality to be effective even working at effectively mild conditions of temperature [147]. Semiconductor nanoparticles includes their myriads of forms ranging from transition metals both in the form of their oxides, sulphides, various rare earth metals of diverse applications and other oxides of importance [148]. Their distinctive properties lie in their application in different electronic and other physical and chemical properties. We here focus among all other semiconductor nanoparticles one of the most prevalent contributions of semiconductor transition metal nanoparticles. The usage of the transition metal nanoparticles has gained

considerable momentum in recent years for their excellent contributions in an array of domains being nano-catalysis, oxidation-reduction reactions, heavy metal sensing and in diverse biological application. As a known factor it has been thoroughly an accepted fact that nanoparticles of semiconductor category have their excellent ability to perform in various redox reactions owing to their size effect. Transition metal semiconductor nanoparticles and their contributions in the broad spectrum can be discussed in the light of transition metal hydroxides and sulphides. Semiconductor transition metals are widely been discussed in this thesis in the light of their role in environmental remediation and in their biological applications.

 The nanomaterials that are selected for carrying out the above three properties of the nanoparticles are iron and copper-based nanomaterials. The reason for such a selection is that these nanomaterials are quite cheap than those of the prevalent noble nanomaterials carrying out these various properties. For the purpose of sensing the nanomaterials of our choice is iron oxyhydroxide nanoparticles. The sensing of the hexavalent chromium in waste water is accomplished by nitrogenous carbon dots (C-dots) synthesized *in situ*. But these carbon dots suffer from aggregation and thus leads to loss of fluorescence [149]. Thus, a suitable matrix is being selected to overcome such a difficulty. Iron oxyhydroxide or goethite (α- FeOOH) are minerals and are wide band gap semiconductor [150]. These nanoparticles were chosen as the first choice for sensing in contrast to other matrices because of its effective biocompatibility and easy handling [151]. Moreover, these nanoparticles when conjugated with C-dots brings about biosensing within the living cells.

The next nanomaterial that was selected for catalysis and an effective antimicrobial agent against coliforms like *E.coli* and biofilm forming *S. aureus* is a another transitional metal semiconductor chalcogenide copper sulphide (CuS) nanoparticles. Though there had been reports of synthesizing these nanoparticles [152] that carries out the function of catalysing organic pollutants pNP this is a novel approach where the nanoparticles were synthesized simply via reflux condensation method with the help of a block copolymer Pluronic F-127. Pluronic capped CuS nanoparticles were used for catalytic reduction of *p*NP using $NaBH_4$ as the reducing agent. This method was in fact contrast to the conventional photocatalysis method where the source and intensity of light is important. *p*NP with the help of $NaBH_4$ gets converted into para-amino phenol (*p*AP) which have wide use in the pharmaceutical industries [153].

Pluronic capped nanoparticles show brilliant capability of being dispersible in aqueous media and thus these nanoparticles were harnessed to assess their antimicrobial potential to be used in remediating the microbial pollutants from water, to act against biofilms and also their use for topical purposes.

2.1.2 Instrumentation, Materials Required & Methods

There are several approaches undertaken to characterise the synthesized transition metal nanoparticles. X-ray diffraction (XRD) has been employed to determine the crystallite nature of the synthesized nanoparticles along with Scanning Electron Microscopy (SEM), Transmission Electron Microscopy (TEM) that are used to determine the size, shape of the particles. Nevertheless, high resolution TEM along with selected area electron diffraction, and have all been used to determine the crystal structure of transition metal nanoparticles. UV-Vis and fluorescence spectrophotometry are frequently utilised in the analysis of the distinctive optical characteristics. Optical absorption and photoluminescence (PL) spectroscopy have been used to explore the interaction pattern of the nanoparticles with different sample molecules. Fourier Transform Infra-red (FTIR) and Raman spectroscopy have been used to clarify the presence of different functional groups in the synthesized samples. The parameters of mass loss, melting point and other phase transitions were achieved by Differential Thermal Analysis & Thermogravimetric Analysis (DTA-TGA).

This chapter discusses all of the materials used along with the characterisation strategies and experimental approaches.

- *X Ray Diffraction (XRD)*

The primary objective of x-ray crystallography lies to extract a three-dimensional molecular structure of a crystal material. A high concentration of a purified crystal material are then subjected to an x-ray beam and the processed diffraction patterns can be used to deduce the crystal packing symmetry and the size of the repeating unit that makes up the crystal. Structure of semi crystalline or polycrystalline materials can be derived from X-ray Crystallography [154]. This is derived from the diffraction spot pattern [155]. When molecules are organised in a regular crystalline array, X-ray crystallography is frequently employed to image molecular structure at extremely high resolution which does not require optics and place no strict demands on the detector's resolution as shown in Fig 1.6. The signal is amplified by the specimen's

many copies, and their regular positioning focuses the far-field diffraction pattern into distinct Bragg peaks [156]. When a beam of light is passed through a sample crystal, there is constructive interference seen in the scattered rays (shown in Fig1.3) which governs the different parameters of a crystal using Bragg's law [157-158]

$$n\lambda = 2d_{(h\,k\,l)} \sin\theta \qquad ..... \text{eq} \quad (1)$$

where n is the order, λ is the X-Ray wavelength, $d_{(h\,k\,l)}$ is the inter planar spacing in the atomic lattice of the crystal planes, and θ is the measured angle between the incident and scattering planes.
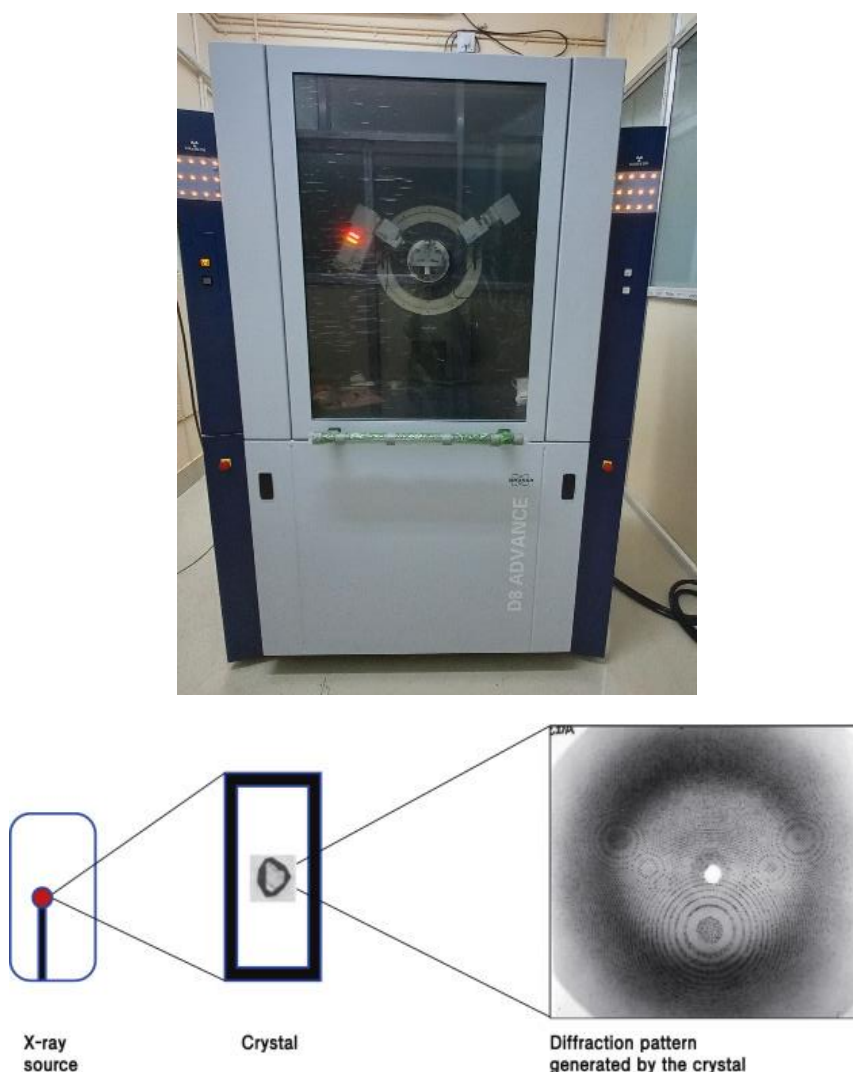
Fig 1.6: X Ray Crystallography Instrument and its brief working principle [157]

The width of a powder X-ray diffraction reflection is related to the size of the coherent diffraction domain and it also infers that the reflection width grows as the size of the coherent diffraction domain decreases. This relationship is been given by Scherrer equation which is as follows:

$$d = K\lambda / \beta \cos \theta \quad \ldots\ldots \text{eq (2)}$$

where d= the coherent domain size, λ is the wavelength of the X-ray, K is the constant, β is the full width at half maximum and θ is the angle of diffraction.

In this work the crystallographic insight was characterized using a X-Ray Diffractometer (Model D8 Advanced, Bruker AXS with a mono- chromatized Cu Kα radiation where λ is 1.5405 Å. The scanning rate was fixed at 0.02 steps/ sec in 2θ range of 10° to 80°. The synthesized nano crystal was placed in a sample holder and an operating current and voltage for collection of the X ray data was fixed at 35mA and 35kV respectively.

Rietveld analysis:

In powder diffraction analysis, there are a few other useful whole-pattern fitting approaches. One option is to freely refine the two values and intensities of peaks to characterise each reflection in the absence of a structural model for auto indexing to find unit cell parameters [158]. Rietveld demonstrates the potential of recreating the results of diffraction pattern measurements using pattern calculation that is made to match the peak profile of the calculation with the peak profile of the observation [159]. Nanomaterials are been employed for determination of their fine structures like lattice parameters, bond angles, bond lengths with additional parameters of phase purity [160]. The Rietveld analysis was carried out using the Rietveld-based programme MAUD v.2.99 (Material Analysis Using Diffraction) and the refined structures were shown using VESTA v.3.0 (Visualisation for Electronic Structural Analysis).

- ### *Fourier Transform Infrared (FTIR) Spectroscopy:*

The technique of the infrared (IR) spectroscopy primarily rests on the different molecular interactions and vibrations between the molecules [161] that roughly translate of the fact that by absorbing IR radiation, a molecule can be excited to a higher vibrational state. The likelihood of an IR frequency being absorbed is determined by the interaction between the frequency and the molecule and the peaks obtained thus can be counted as the "finger print" of the sample that arise mainly

through the vibration of different functional groups associated with the molecule [162]. This method is regarded as a workhorse for quantitative analysis as the amount of infrared energy absorbed by a molecule is proportional to the concentration of the analyte [162-163]. Infrared spectroscopy measures the intensity of an infrared radiation beam before and after it interacts with a sample as a function of light frequency and the obtained infrared spectrum is a plot of relative intensity versus frequency [164].There is considerable change in molecular vibrations upon absorption of the electromagnetic radiation in the IR region which is contributed by transition of the vibrational and rotational energy at the lowermost energy level [162] along with the quantification of impurities present by spectral measurements [163].

An Infrared spectrophotometer consists of three basic components of a radiation source, an interferometer, and a detector. The interferometer generates radiant beams producing an optical path difference between them, and interference signals that the detector measures as a function of the optical path difference. The interferometer commonly used Michaelson Inferometer generates interference signals that contain IR spectral information generated after passing through the sample, illustrated in Fig 1.7.
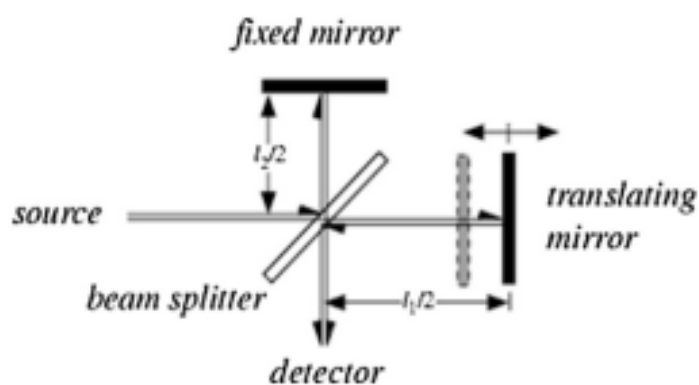
Fig 1.7 : Components of Michaelson Inferometer [163]

The beam splitter divides a collimated light beam from the IR source that is directed to the Michelson interferometer. One half of the beam is reflected by a fixed mirror, while the other half is reflected by a moving mirror roughly shown in Fig 1.8. After returning from the mirrors, the two light beams recombine to form a reconstructed beam, which is optically an interference wave [164].
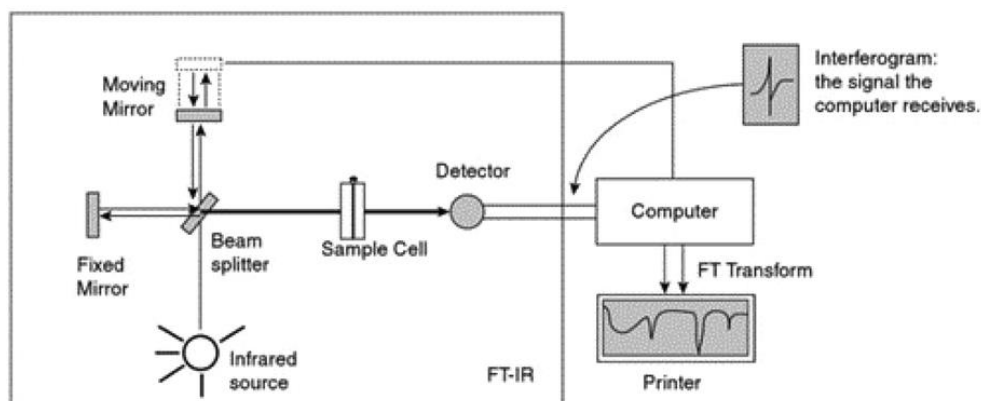
Fig 1.8: A schematic image showing working action of a FTIR machine [165]

It is necessary to have a method of "decoding" the individual frequencies. The intensity-time output of the interferometer is then converted to the familiar infrared spectrum using a well-known mathematical technique known as the Fourier transformation [166]. This is given by the following equation:

$$S(v) = 2 \int_0^\infty I(x) \cos(2\pi\bar{v}\, x)\, dx \;\; ...... \;\; \text{eq (3)}$$

where $S(v)$ is the spectrum, x is retardation, $I(x)$,interferogram and $\bar{v}$ any wavenumber.

While performing our experiments we typically followed the KBr pellet technique in which the functionalized metallic nanoparticles were at first grounded well in a pestle and mortar and then mixed with KBr at a ratio of 1:50. This mixture was then subjected to pelletizing in a hydraulic press at 5tonns for 5mins. The obtained pellets were again dried at 60°-70°C for to remove any remaining moisture that might hinder the process of experimental analysis.

- *Raman Spectroscopy*

Raman spectroscopy is a type of spectroscopy that relies on the inelastic scattering of monochromatic light, typically from a laser source which results in the change of the frequency of photons in monochromatic light due to inelastic scattering when a sample is present Laser photons are absorbed by the sample and then reemitted. The Raman effect occurs when the frequency of reemitted photons is shifted up or down in comparison to the original monochromatic frequency [167].

Raman Spectroscopy differs from the infrared spectroscopy in the fundamental principle where a sample gets irradiated by harnessing a single frequency of radiation which is in contrast to the infrared spectroscopy where a range of frequencies are being used to irradiate the sample of interest. In Infrared Spectroscopy vibrations generated from the molecule coincides to that of the frequency of the incident beam which is unlike Raman Spectroscopy where there is inelastic scattering where there is transfer of energy from incident photon to the scattered photon [168].

A Raman spectrometer schematically shown in Fig 1.9 shows that the machine is made up of four parts: a light source, a monochromator, a sample holder, and a detector. High signal-to-noise ratio, for example, can have an impact on Raman spectral analysis Instrument stability and adequate resolution. The design of an effective FT Raman spectrometers uses NIR or red excitation and avoids the phenomenon of fluorescence. Dispersive Raman spectroscopy and Fourier transform Raman spectroscopy are the two major technologies used to collect Raman spectra, with differences in their laser sources and how Raman scattering is detected and analysed [169].
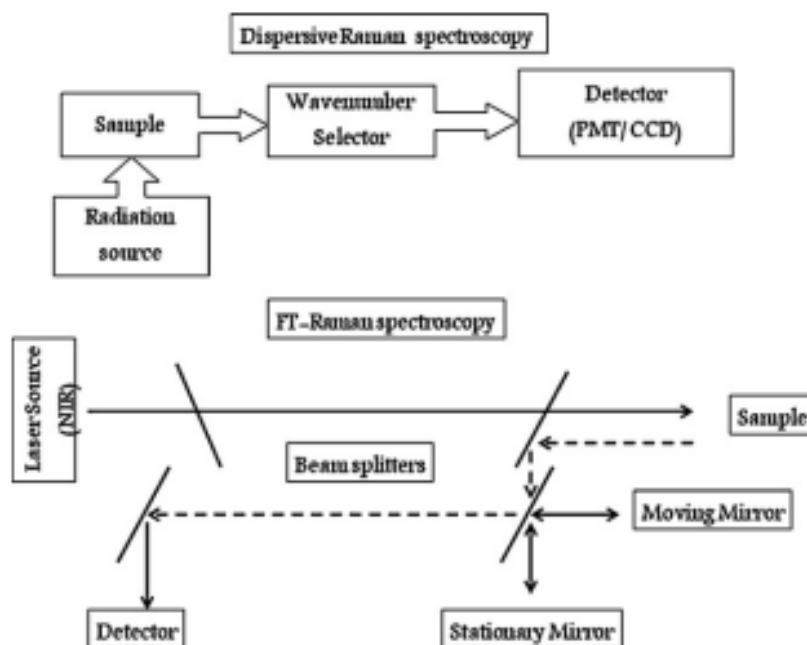
Fig 1.9: Basic Instrumentation of a Raman spectrometer [169]

In our experimental work with transitional metal chalcogenide (CuS) nanoparticles were being assessed through Raman Spectroscopy. Raman Spectra was recorded using Lab

Ram HR Jovin Yvon Raman spectrometer equipped with a laser beam of 488nm excitation of Argon laser light.

- ***Scanning Electron Microscopy (SEM)***

A scanning electron microscope is a device that uses a focused beam of high-energy electrons to image topography and obtain material information from conductive specimens and to capture the surface of the specimens, a beam of electrons is deflected in a magnetic field that performs a scanning movement in a raster pattern [170] which is in contrast to optical microscopy technique where visible light is used as the electron source [171]. Subsequently electrons interact with the sample, producing a variety of signals that can be detected and displayed on the screen of a cathode ray tube [172]. Scanning electron microscopy finds its practical applications in various arenas like characterizing different internal structures of minerals [173], in various fields of nanotechnology [174-176] in the field of biology [177-178].

SEM can provide qualitative detailed insights about a specimen such as its topography, morphological details, crystallographic information. In other words, it describes the surface features and texture, as well as the shape, size, and arrangement of the particles on the sample's surface [179]. Certain requirements are must to be met by the specimen before subjecting it to SEM. It must be able to withstand vacuum and electron bombardment, as well as essentially it needs to be electrically conductive and to be dried and cleaned [179].

SEMs typically operates with a 15KeV voltage originating from a thermo-ionic cathode. Here the incident beam was focused in a 10-100 nm spot on the specimen surface [180]

This scanning electron microscope is been equipped with a sample holder where the stub has been fixed for the sample to be placed on its surface whereby a carbon tap is generally used to adhere the sample to the stub. Then a thin layer or a small amount of material should be applied to the carbon tap because the thin layer properly adheres to the carbon tap, reducing the charging problem and assisting in obtaining a good image. This is followed by sputtering with gold or other non- conductive elements like platinum that minimises the chance of charging.
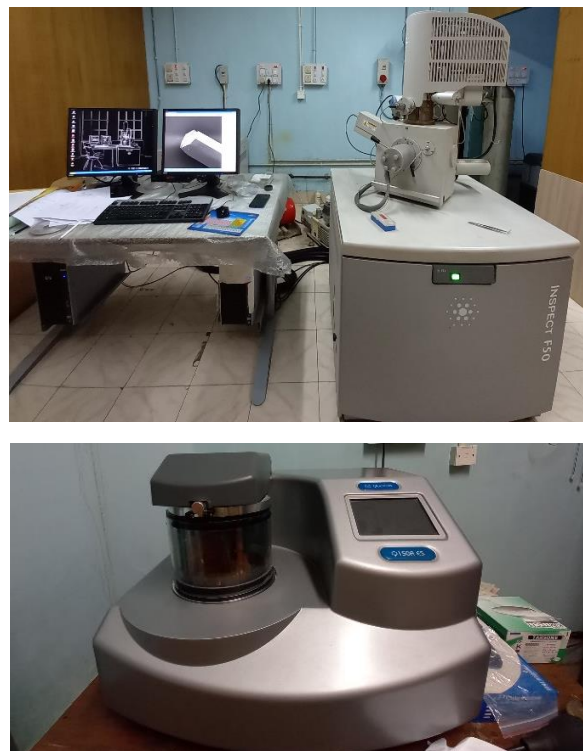
Fig 1.10: Scanning Electron Microscope along with sputter coater

In our experimental work the morphological details of the synthesized C dot@ FeOOH and CuS nanoparticles were prepared by placing the powdered samples in a carbon coated grid and the accelerating voltage was fixed between 10kV and 20kV using a Inpect- F50 Field Emission Microscope.

- *Transmission Electron Microscope (TEM)*

Transmission electron microscopy forms the basis of elucidating the size and structural details of the nanostructures. The application of TEM entails a wider application not only for determining the size regime of materials but it also forms the basis of imaging the structural details of the cytoskeleton [181] by utilizing the theory of passage of electrons through a sample to be to be examined where the wavelength of the electrons is way beyond high than that of the visible light. A thin sample is passed through the TEM by a stream of high energy electrons with energies ranging from 100 to 400 eV. High energy electrons are essential because they reduce scattering. A high vacuum, approximately 10-6 mmHg, is also required because electrons are easily scattered in air.

For TEM analysis for particle size determination JEOL-JM 2010 was used and it operated around 200kV. A diluted solution of few micro-litre of sample of both the transitional metal nanoparticles was placed on a carbon coated copper grid and the thin film was dried in a vacuum desiccator overnight before it is used for analysis.

Fig 1.11: Transmission electron microscope instrument

- *UV-Vis Spectrophotometer:*

UV-Visible spectroscopy is a technique for measuring the amount of light absorbed and scattered by a sample (a quantity known as the extinction, which is defined as the sum of absorbed and scattered light). Because nanoparticles have optical properties that are sensitive to size, shape, concentration, agglomeration state, and refractive index near the nanoparticle surface, UV-Visible spectroscopy is an important tool for identifying, characterising, and studying these materials. UV- Vis spectrophotometer is based upon the Lambert - Beer that states absorption of light by a sample is proportional to the path length and the concentration of the absorbing species.

$$\text{Absorbance, } A = \log I_0/I = \varepsilon lc \ldots \text{eq (4)}$$

where I_0 is the incident radiation intensity and I is the transmitted radiation intensity that emerges from the absorbing medium, c is the concentration expressed in mole litre^{-1}, ε is the the molar absorptivity or molar extinction coefficient (units, litre mole-1 cm^{-1}), and l is the path length (units, cm).

The absorption measurements were carried out using Perkin Elmer Lambda 365 UV-Vis spectrophotometer. The samples for the experiment were first made a dilute solution in Millipore water in a quartz cuvette and was subjected to experimentation.

Fig 1.12: UV- Vis Spectrophotometer used for analysis of the sample

- *Fluorescence Microscopy:*

Photoluminescence (PL) spectroscopy is a very efficient, non-destructive, and widely used technique for analysing a material's optoelectronic properties. Photoluminescence is defined as the spontaneous emission of light from a material under optical excitation, and it can thus be used to provide detailed information on

discrete electronic states involving both intrinsic optical processes and the wide variety of defects that are endemic in practical semiconductor materials, as well as extrinsic optical processes (internal transitions involving defects and their energy levels) by applying an external light with energy hν [182].

Fig 1.13: Fluorescence Spectrophotometer Instrument in the laboratory

The measurement of fluorescence spectra of the samples was carried out using a Cary Eclipse Fluorescence Spectrophotometer, Agilent Technologies following the same sample preparation protocol as that of the UV Vis spectrophotometer having excitation slit 5nm and emission wavelength 2.5nm.

- *Dynamic Light Scattering (DLS)*

When light falls on a solution there is a propensity of random changes in the intensity of the scattered light in the solution and this gives an idea about the particle size of the material in the solution. The method is commonly known as Dynamic Light Scattering (DLS).

There is thermal motion generated due to Brownian motion which is modelled by Stokes-Einstein theory where size of the particle can be calculated using translational diffusion coefficient.

DLS measurement of the samples were carried out using a Nano ZS Zetasizer, Nanoseries Malvern where the source of light used was a He-Ne laser of wavelength 632.8nm operating at 4mW in a thermos stated sample chamber.

- *DTA- TGA*

The change in the physical or chemical property of a sample against time can be monitored through a quantitative method called thermogravimetric analysis [182]. The analysis stresses on the extent through which a material of choice can be stable under the influence of temperature and changes in weight of a particular sample upon increasing the temperature can be analysed [183]. DTA TGA stands as an important parameter in judging the quality of a nanomaterial as transitional nature, stability in oxidation and measurements like melting points can be assessed [184].

In our experiment DTA TGA analysis of FeOOH @Cdot were performed using DTG-60H, Shimadzu under nitrogen rich atmosphere using platinum crucibles.

REFERENCES

1. Bashir, I., Lone, F. A., Bhat, R. A., Mir, S. A., Dar, Z. A., & Dar, S. A. (2020). Concerns and Threats of Contamination on Aquatic Ecosystems. *Bioremediation and Biotechnology: Sustainable Approaches to Pollution Degradation*, 1–26.

2. 2 Lofrano, G., Meriç, S., Zengin, G. E., & Orhon, D. (2013). Chemical and biological treatment technologies for leather tannery chemicals and wastewaters: A review. *Science of the Total Environment*, *461*, 265-281

3. Chowdhury, M., Mostafa, M. G., Biswas, T. K., Mandal, A., & Saha, A. K. (2015). Characterization of the effluents from leather processing industries. *Environmental Processes*, *2*(1), 173-187.

4. Sreedharan, V., & Bhaskara Rao, K. V. (2019). Biodegradation of textile azo dyes. *Nanoscience and biotechnology for environmental applications*, 115-139.

5. Tkaczyk, A., Mitrowska, K., & Posyniak, A. (2020). Synthetic organic dyes as contaminants of the aquatic environment and their implications for ecosystems: A review. *Science of the total environment*, *717*, 137222

6. Berradi, M., Hsissou, R., Khudhair, M., Assouag, M., Cherkaoui, O., El Bachiri, A., & El Harfi, A. (2019). Textile finishing dyes and their impact on aquatic environs. *Heliyon*, *5*(11), e02711.

7. Bielen, A., Šimatović, A., Kosić-Vukšić, J., Senta, I., Ahel, M., Babić, S., ... & Udiković-Kolić, N. (2017). Negative environmental impacts of antibiotic-contaminated effluents from pharmaceutical industries. *Water research*, *126*, 79-87.

8. Wang, K., Zhuang, T., Su, Z., Chi, M., & Wang, H. (2021). Antibiotic residues in wastewaters from sewage treatment plants and pharmaceutical industries: Occurrence, removal and environmental impacts. *Science of the Total Environment*, *788*, 147811.

9. Hirai, H., Takada, H., Ogata, Y., Yamashita, R., Mizukawa, K., Saha, M., ... & Ward, M. W. (2011). Organic micropollutants in marine plastics debris from the open ocean and remote and urban beaches. *Marine pollution bulletin*, *62*(8), 1683-1692.

10. Hu, D., Shen, M., Zhang, Y., & Zeng, G. (2019). Micro (nano) plastics: an un-ignorable carbon source?. *Science of The Total Environment*, *657*, 108-110

11. Lomonaco, T., Manco, E., Corti, A., La Nasa, J., Ghimenti, S., Biagini, D., ... & Castelvetro, V. (2020). Release of harmful volatile organic compounds (VOCs) from photo-degraded plastic debris: a neglected source of environmental pollution. *Journal of hazardous materials*, *394*, 122596.

12. McIsaac, G. (2003). Surface water pollution by nitrogen fertilizers. *Encyclopedia of Water Science*, *950*.

13. Ribbe, L., Delgado, P., Salgado, E., & Flügel, W. A. (2008). Nitrate pollution of surface water induced by agricultural non-point pollution in the Pocochay watershed, Chile. *Desalination*, *226*(1-3), 13-20.

14. Maghanga, J. K., Kituyi, J. L., Kisinyo, P. O., & Ng'Etich, W. K. (2013). Impact of nitrogen fertilizer applications on surface water nitrate levels within a Kenyan tea plantation. *Journal of chemistry*, *2013*.

15. Jaiswal, S., Kumar Gupta, G., Panchal, K., Mandeep, & Shukla, P. (2021). Synthetic Organic Compounds From Paper Industry Wastes: Integrated Biotechnological Interventions. *Frontiers in bioengineering and biotechnology*, *8*, 592939

16. Williams, P., Benton, L., Warmerdam, J., & Sheehan, P. (2002). Comparative risk analysis of six volatile organic compounds in California drinking water. *ACS Publications,*4721-4728.

17. Zamora-Ledezma, C., Negrete-Bolagay, D., Figueroa, F., Zamora-Ledezma, E., Ni, M., Alexis, F., & Guerrero, V. H. (2021). Heavy metal water pollution: A fresh look about hazards, novel and conventional remediation methods. *Environmental Technology & Innovation*, *22*, 101504.

18. Sharma, R. K., & Agrawal, M. (2005). Biological effects of heavy metals: an overview. *Journal of environmental Biology*, *26*(2), 301-313.

19. Hawkes, S. J. (1997). What is a" heavy metal"? *Journal of chemical education*, *74*(11), 1374.

20. Järup, L. (2003). Hazards of heavy metal contamination. *British medical bulletin*, *68*(1), 167-182.

21. Ali, H., & Khan, E. (2018). What are heavy metals? Long-standing controversy over the scientific use of the term 'heavy metals'–proposal of a comprehensive definition. *Toxicological & Environmental Chemistry*, *100*(1), 6-19.

22. Briffa, J., Sinagra, E., & Blundell, R. (2020). Heavy metal pollution in the environment and their toxicological effects on humans. *Heliyon*, *6*(9), e04691.

23. Jezierska, B., Ługowska, K., & Witeska, M. (2009). The effects of heavy metals on embryonic development of fish (a review). *Fish physiology and biochemistry*, *35*(4), 625-640.

24. Wu, G., Kang, H., Zhang, X., Shao, H., Chu, L., & Ruan, C. (2010). A critical review on the bio-removal of hazardous heavy metals from contaminated soils: issues, progress, eco-environmental concerns and opportunities. *Journal of hazardous materials*, *174*(1-3), 1-8.

25. Pandey, G., & Madhuri, S. (2014). Heavy metals causing toxicity in animals and fishes. *Research Journal of Animal, Veterinary and Fishery Sciences*, *2*(2), 17-23.

26. Badr, F. M., & El-Habit, O. (2018). Heavy metal toxicity affecting fertility and reproduction of males. In *Bioenvironmental Issues Affecting Men's Reproductive and Sexual Health* (pp. 293-304). Academic Press.

27. Fu, Z., & Xi, S. (2020). The effects of heavy metals on human metabolism. *Toxicology mechanisms and methods*, *30*(3), 167-176

28. Paschoalini, A. L., & Bazzoli, N. (2021). Heavy metals affecting Neotropical freshwater fish: A review of the last 10 years of research. *Aquatic Toxicology*, *237*, 105906.

29. Andreesen, J. R., & Makdessi, K. (2008). Tungsten, the surprisingly positively acting heavy metal element for prokaryotes. *Annals of the New York Academy of Sciences*, *1125*(1), 215-229

30. Lane, T. W., & Morel, F. M. (2000). A biological function for cadmium in marine diatoms. *Proceedings of the National Academy of Sciences*, *97*(9), 4627-4631

31. Fashola, M. O., Ngole-Jeme, V. M., & Babalola, O. O. (2016). Heavy metal pollution from gold mines: environmental effects and bacterial strategies for resistance. *International journal of environmental research and public health*, *13*(11), 1047

32. Zhang, X., Yang, H., & Cui, Z. (2017). Migration and speciation of heavy metal in salinized mine tailings affected by iron mining. *Water Science and Technology*, *76*(7), 1867-1874

33. Fang, Q., Zhao, Q., Chai, X., Li, Y., & Tian, S. (2020). Interaction of industrial smelting soot particles with pulmonary surfactant: Pulmonary toxicity of heavy metal-rich particles. *Chemosphere*, *246*, 125702.

34. Xu, D. M., Fu, R. B., Liu, H. Q., & Guo, X. P. (2021). Current knowledge from heavy metal pollution in Chinese smelter contaminated soils, health risk implications and associated remediation progress in recent decades: A critical review. *Journal of Cleaner Production*, *286*, 124989

35. 35.Rauckyte, T., Hargreaves, D. J., & Pawlak, Z. (2006). Determination of heavy metals and volatile aromatic compounds in used engine oils and sludges. *Fuel*, *85*(4), 481-485.

36. Nzihou, A., & Stanmore, B. (2013). The fate of heavy metals during combustion and gasification of contaminated biomass—a brief review. *Journal of hazardous materials*, *256*, 56-66

37. Gauthier, P. J., & Le Cloarec, M. F. (1998). Variability of alkali and heavy metal fluxes released by Mt. Etna volcano, Sicily, between 1991 and 1995. *Journal of Volcanology and Geothermal Research*, *81*(3-4), 311-326.

38. Varrica, D., Aiuppa, A., & Dongarrà, G. (2000). Volcanic and anthropogenic contribution to heavy metal content in lichens from Mt. Etna and Vulcano island (Sicily). *Environmental Pollution*, *108*(2), 153-162.

39. 39.Yalcin, M. G., Battaloglu, R., & Ilhan, S. (2007). Heavy metal sources in Sultan Marsh and its neighborhood, Kayseri, Turkey. *Environmental geology*, *53*(2), 399-415.

40. Abraham, J., Dowling, K., & Florentine, S. (2017). The unquantified risk of post-fire metal concentration in soil: A review. *Water, Air, & Soil Pollution*, *228*(5), 1-33

41. Baieta, R., Vieira, A. M., Vaňková, M., & Mihaljevič, M. (2022). Effects of forest fires on soil lead elemental contents and isotopic ratios. *Geoderma*, *414*, 115760

42. Lu, L., Wang, R., Chen, F., Xue, J., Zhang, P., & Lu, J. (2005). Element mobility during pyrite weathering: implications for acid and heavy metal pollution at mining-impacted sites. *Environmental geology*, *49*(1), 82-89

43. Wu, W., Qu, S., Nel, W., & Ji, J. (2020). The impact of natural weathering and mining on heavy metal accumulation in the karst areas of the Pearl River Basin, China. *Science of The Total Environment*, *734*, 139480.

44. Guidelines for Drinking water quality, WHO 2011

45. Guidelines for Carcinogen Risk Assessment, Forum US Environmental Agency,Washington DC, 1986.

46. Slivinska, L. G., Vlizlo, V. V., Shcherbatyy, A. R., Lukashchuk, B. O., Gutyj, B. V., Drach, M. P., ... & Yaremchuk, V. Y. (2021). Influence of heavy metals on metabolic processes in cows. *Ukrainian Journal of Ecology*, *11*(2), 284-291

47. Koedrith, P., Kim, H., Weon, J. I., & Seo, Y. R. (2013). Toxicogenomic approaches for understanding molecular mechanisms of heavy metal mutagenicity and carcinogenicity. *International journal of hygiene and environmental health*, *216*(5), 587-598

48. Kim, H. S., Kim, Y. J., & Seo, Y. R. (2015). An overview of carcinogenic heavy metal: molecular toxicity mechanism and prevention. *Journal of cancer prevention*, *20*(4), 232

49. Prasad, S., Yadav, K. K., Kumar, S., Gupta, N., Cabral-Pinto, M. M., Rezania, S., ... & Alam, J. (2021). Chromium contamination and effect on environmental health and its remediation: A sustainable approaches. *Journal of Environmental Management*, *285*, 112174

50. Zha, L. Y., Zeng, J. W., Chu, X. W., Mao, L. M., & Luo, H. J. (2009). Efficacy of trivalent chromium on growth performance, carcass characteristics and tissue chromium in heat-stressed broiler chicks. *Journal of the Science of Food and Agriculture*, *89*(10), 1782-1786

51. Tian, H., Guo, X., Wang, X., He, Z., Sun, R., Ge, S., & Zhang, Z. (2013). Chromium picolinate supplementation for overweight or obese adults. *Cochrane Database of Systematic Reviews*, (11).

52. Saha, R., Nandi, R., & Saha, B. (2011). Sources and toxicity of hexavalent chromium. *Journal of Coordination Chemistry*, *64*(10), 1782-1806.

53. Wise Jr, J. P., Young, J. L., Cai, J., & Cai, L. (2022). Current understanding of hexavalent chromium [Cr (VI)] neurotoxicity and new perspectives. *Environment international*, *158*, 106877.

54. 54.Nickens, K. P., Patierno, S. R., & Ceryak, S. (2010). Chromium genotoxicity: a double-edged sword. *Chemico-biological interactions*, *188*(2), 276-288.

55. Stearns, D. M., Courtney, K. D., Giangrande, P. H., Phieffer, L. S., & Wetterhahn, K. E. (1994). Chromium (VI) reduction by ascorbate: role of reactive intermediates in DNA damage in vitro. *Environmental health perspectives*, *102*(suppl 3), 21-25

56. O'Brien, T. J., Ceryak, S., & Patierno, S. R. (2003). Complexities of chromium carcinogenesis: role of cellular response, repair and recovery mechanisms. *Mutation Research/Fundamental and Molecular Mechanisms of Mutagenesis*, *533*(1-2), 3-36.

57. Sobol, Z., & Schiestl, R. H. (2012). Intracellular and extracellular factors influencing Cr (VI and Cr (III) genotoxicity. *Environmental and molecular mutagenesis*, *53*(2), 94-100.

58. Ji, W., Wang, Y., Tanabe, I., Han, X., Zhao, B., & Ozaki, Y. (2015). Semiconductor-driven "turn-off" surface-enhanced Raman scattering spectroscopy: application in selective determination of chromium (VI) in water. *Chemical Science*, *6*(1), 342-348

59. Dvoynenko, O., Lo, S. L., Chen, Y. J., Chen, G. W., Tsai, H. M., Wang, Y. L., & Wang, J. K. (2021). Speciation analysis of Cr (VI) and Cr (III) in water with surface-enhanced Raman spectroscopy. *ACS omega*, *6*(3), 2052-2059.

60. Robinson, J. W. (1960). Atomic absorption spectroscopy. *Analytical Chemistry*, *32*(8), 17A-29A

61. Zhang, J., & Li, S. (2021). Sensors for detection of Cr (VI) in water: a review. *International Journal of Environmental Analytical Chemistry*, *101*(8), 1051-1073

62. Farrukh, M. A. (Ed.). (2012). *Atomic absorption spectroscopy*. BoD–Books on Demand.

63. Montaser, A. (Ed.). (1998). *Inductively coupled plasma mass spectrometry*. John Wiley & Sons.

64. Gürleyük, H., & Wallschläger, D. (2001). Determination of chromium (III) and chromium (VI) using suppressed ion chromatography inductively coupled plasma mass spectrometry. *Journal of Analytical Atomic Spectrometry*, *16*(9), 926-930

65. Maceda-Veiga, A., Monroy, M., & de Sostoa, A. (2012). Metal bioaccumulation in the Mediterranean barbel (Barbus meridionalis) in a Mediterranean River receiving effluents from urban and industrial wastewater treatment plants. *Ecotoxicology and Environmental Safety*, *76*, 93-101

66. Pandey, S. K., Singh, P., Singh, J., Sachan, S., Srivastava, S., & Singh, S. K. (2016). Nanocarbon-based electrochemical detection of heavy metals. *Electroanalysis*, *28*(10), 2472-2488.

67. Borrill, A. J., Reily, N. E., & Macpherson, J. V. (2019). Addressing the practicalities of anodic stripping voltammetry for heavy metal detection: a tutorial review. *Analyst*, *144*(23), 6834-6849.

68. Izadyar, A., Al-Amoody, F., & Arachchige, D. R. (2016). Ion transfer stripping voltammetry to detect nanomolar concentrations of Cr (VI) in drinking water. *Journal of Electroanalytical Chemistry*, *782*, 43-49.

69. Liu, X., Yao, Y., Ying, Y., & Ping, J. (2019). Recent advances in nanomaterial-enabled screen-printed electrochemical sensors for heavy metal detection. *TrAC Trends in Analytical Chemistry*, *115*, 187-202

70. Palchetti, I., Mascini, M., Minunni, M., Bilia, A. R., & Vincieri, F. F. (2003). Disposable electrochemical sensor for rapid determination of heavy metals in herbal drugs. *Journal of pharmaceutical and biomedical analysis*, *32*(2), 251-256

71. Hallam, P. M., Kampouris, D. K., Kadara, R. O., & Banks, C. E. (2010). Graphite screen printed electrodes for the electrochemical sensing of chromium (VI). *Analyst*, *135*(8), 1947-1952.

72. Wang, Y., Ma, J. X., Zhang, Y., Xu, N., & Wang, X. L. (2021). A series of cobalt-based coordination polymer crystalline materials as highly sensitive electrochemical sensors for detecting trace Cr (VI), Fe (III) ions, and ascorbic acid. *Crystal Growth & Design*, *21*(8), 4390-4397

73. Wang, X., Mao, W., Wang, D., Hu, X., Liu, B., & Su, Z. (2023). Hourglass shaped polyoxometalate-based materials as electrochemical sensors for the detection of trace Cr (VI) in a wide pH range. *Talanta*, *257*, 124270.

74. Dutta, M., & Das, D. (2012). Recent developments in fluorescent sensors for trace-level determination of toxic-metal ions. *TrAC Trends in Analytical Chemistry*, *32*, 113-132

75. Jain, S., Nehra, M., Dilbaghi, N., Kumar, R., & Kumar, S. (2022). Boric-acid-functionalized luminescent sensor for detection of chromate ions in aqueous solution. *Materials Letters*, *306*, 130933

76. Wei, Y., Mei, L., Li, R., Liu, M., Lv, G., Weng, J., ... & Lu, L. (2018). Fabrication of an AMC/MMT Fluorescence Composite for its Detection of Cr (VI) in Water. *Frontiers in Chemistry*, *6*, 367.

77. Zhang, M., Zhang, L., Tian, H., & Lu, A. (2020). Universal preparation of cellulose-based colorimetric sensor for heavy metal ion detection. *Carbohydrate polymers*, *236*, 116037.

78. Ramdzan, N. S. M., Fen, Y. W., Anas, N. A. A., Omar, N. A. S., & Saleviter, S. (2020). Development of biopolymer and conducting polymer-based optical sensors for heavy metal ion detection. *Molecules*, *25*(11), 2548.

79. Ghobashy, M. M., & Mohamed, T. M. (2018). Radiation preparation of conducting nanocomposite membrane based on (copper/polyacrylic acid/poly vinyl alcohol) for rapid colorimetric sensor of mercury and silver ions. *Journal of Inorganic and Organometallic Polymers and Materials*, *28*, 2297-2305.

80. 80.Azmi, N. A., Ahmad, S. H., & Low, S. C. (2018). Detection of mercury ions in water using a membrane-based colorimetric sensor. *RSC advances*, *8*(1), 251-261

81. Liu, B., Zhuang, J., & Wei, G. (2020). Recent advances in the design of colorimetric sensors for environmental monitoring. *Environmental Science: Nano*, *7*(8), 2195-2213

82. Rojas, S., & Horcajada, P. (2020). Metal–organic frameworks for the removal of emerging organic contaminants in water. *Chemical reviews*, *120*(16), 8378-8415

83. Duan, W., Meng, F., Cui, H., Lin, Y., Wang, G., & Wu, J. (2018). Ecotoxicity of phenol and cresols to aquatic organisms: a review. *Ecotoxicology and environmental safety*, *157*, 441-456

84. Ju, K. S., & Parales, R. E. (2010). Nitroaromatic compounds, from synthesis to biodegradation. *Microbiology and molecular biology reviews*, *74*(2), 250-272

85. Sponza, D. T., & Kuscu, Ö. S. (2011). Relationships between acute toxicities of para nitrophenol (p-NP) and nitrobenzene (NB) to Daphnia magna and Photobacterium phosphoreum: Physicochemical properties and metabolites under anaerobic/aerobic sequentials. *Journal of hazardous materials*, *185*(2-3), 1187-1197

86. Mishra, K. P., & Gogate, P. R. (2011). Intensification of sonophotocatalytic degradation of p-nitrophenol at pilot scale capacity. *Ultrasonics sonochemistry*, *18*(3), 739-744

87. Pradhan, A. A., & Gogate, P. R. (2010). Degradation of p-nitrophenol using acoustic cavitation and Fenton chemistry. *Journal of hazardous materials*, *173*(1-3), 517-522

88. Kothaplamoottil Sivan, S., Padinjareveetil, A. K., Padil, V. V., Pilankatta, R., George, B., Senan, C., ... & Varma, R. S. (2019). Greener assembling of MoO 3 nanoparticles supported on gum arabic: cytotoxic effects and catalytic efficacy towards reduction of p-nitrophenol. *Clean Technologies and Environmental Policy*, *21*, 1549-1561

89. Buser, M., Klein, R., Haire, K., Balachandran, R., Roney, N., Derrick, H., ... & Gao, A. (1992). Toxicological profile for nitrophenols: 2-nitrophenol 4-nitrophenol.

90. Eichenbaum, G., Johnson, M., Kirkland, D., O'neill, P., Stellar, S., Bielawne, J., ... & Tonelli, A. (2009). Assessment of the genotoxic and carcinogenic risks of p-nitrophenol when it is present as an impurity in a drug product. *Regulatory Toxicology and Pharmacology*, *55*(1), 33-42

91. Megharaj, M., Pearson, H. W., & Venkateswarlu, K. (1992). Effects of phenolic compounds on growth and metabolic activities of Chlorella vulgaris and Scenedesmus bijugatus isolated from soil. *Plant and soil*, *140*, 25-34

92. Dewil, R., Mantzavinos, D., Poulios, I., & Rodrigo, M. A. (2017). New perspectives for advanced oxidation processes. *Journal of environmental management*, *195*, 93-99

93. Munter, R. (2001). Advanced oxidation processes–current status and prospects. Proc. Estonian Acad. Sci. Chem, 50(2), 59-80].

94. Deng, Y., & Zhao, R. (2015). Advanced oxidation processes (AOPs) in wastewater treatment. *Current Pollution Reports*, *1*, 167-176

95. Mandal, T., Maity, S., Dasgupta, D., & Datta, S. (2010). Advanced oxidation process and biotreatment: Their roles in combined industrial wastewater treatment. *Desalination*, *250*(1), 87-94

96. Cheng, M., Ma, W., Chen, C., Yao, J., & Zhao, J. (2006). Photocatalytic degradation of organic pollutants catalyzed by layered iron (II) bipyridine complex–clay hybrid under visible irradiation. *Applied Catalysis B: Environmental*, *65*(3-4), 217-226

97. Zhang, X., Wang, J., Xiao, B., Pu, Y., Yang, Y., Geng, J., ... & Zhu, Y. (2022). Resin-based photo-self-Fenton system with intensive mineralization by the synergistic effect of holes and hydroxyl radicals. *Applied Catalysis B: Environmental*, *315*, 121525

98. Fukahori, S., Ichiura, H., Kitaoka, T., & Tanaka, H. (2003). Photocatalytic decomposition of bisphenol A in water using composite TiO2-zeolite sheets prepared by a papermaking technique. *Environmental science & technology*, *37*(5), 1048-1051.

99. Mian, M. M., & Liu, G. (2018). Recent progress in biochar-supported photocatalysts: synthesis, role of biochar, and applications. *RSC advances*, *8*(26), 14237-14248

100. Yang, Y., Zhong, H., & Tian, C. (2011). Photocatalytic mechanisms of modified titania under visible light. *Research on Chemical Intermediates*, *37*, 91-102

101. Pang, Y. L., Abdullah, A. Z., & Bhatia, S. (2011). Review on sonochemical methods in the presence of catalysts and chemical additives for treatment of organic pollutants in wastewater. *Desalination*, *277*(1-3), 1-14

102. Gogate, P. R. (2002). Cavitation: an auxiliary technique in wastewater treatment schemes. *Advances in Environmental Research*, *6*(3), 335-358

103. Kotronarou, A., Mills, G., & Hoffmann, M. R. (1991). Ultrasonic irradiation of p-nitrophenol in aqueous solution. *the journal of physical chemistry*, *95*(9), 3630-3638

104. Tao, Y., Cai, J., Huai, X., Liu, B., & Guo, Z. (2016). Application of hydrodynamic cavitation to wastewater treatment. *Chemical engineering & technology*, *39*(8), 1363-1376

105. Capocelli, M., Prisciandaro, M., Lancia, A., & Musmarra, D. (2014). Hydrodynamic cavitation of p-nitrophenol: a theoretical and experimental insight. *Chemical Engineering Journal*, *254*, 1-8.

106. Roy, K., & Moholkar, V. S. (2021). p–nitrophenol degradation by hybrid advanced oxidation process of heterogeneous Fenton assisted hydrodynamic cavitation: discernment of synergistic interactions and chemical mechanism. *Chemosphere*, *283*, 131114.

107. Pradhan, A. A., & Gogate, P. R. (2010). Removal of p-nitrophenol using hydrodynamic cavitation and Fenton chemistry at pilot scale operation. *Chemical Engineering Journal*, *156*(1), 77-82

108. Oturan, M. A., & Aaron, J. J. (2014). Advanced oxidation processes in water/wastewater treatment: principles and applications. A review. *Critical reviews in environmental science and technology*, *44*(23), 2577-2641]

109. Liu, L., Chen, Z., Zhang, J., Shan, D., Wu, Y., Bai, L., & Wang, B. (2021). Treatment of industrial dye wastewater and pharmaceutical residue wastewater by advanced oxidation processes and its combination with nanocatalysts: A review. *Journal of Water Process Engineering*, *42*, 102122

110. Kumar, V., & Shah, M. P. (2021). Advanced oxidation processes for complex wastewater treatment. In *Advanced oxidation processes for effluent treatment plants* (pp. 1-31). Elsevier

111. Magana-Arachchi, D. N., & Wanigatunge, R. P. (2020). Ubiquitous waterborne pathogens. In *Waterborne pathogens* (pp. 15-42). Butterworth-Heinemann

112. Antai, S. P. (1987). Incidence of Staphylococcus aureus, coliforms and antibiotic-resistant strains of Escherichia coli in rural water supplies in Port Harcourt. *Journal of Applied Bacteriology*, *62*(4), 371-375

113. Otto, M. (2018). Staphylococcal biofilms. *Microbiology spectrum*, *6*(4), 6-4

114. Boles, B. R., Thoendel, M., Roth, A. J., & Horswill, A. R. (2010). Identification of genes involved in polysaccharide-independent Staphylococcus aureus biofilm formation. *PloS one*, *5*(4), e10146

115. World Health Organization 2017a Guidelines for Drinking-Water Quality: Incorporating First Addendum. World Health Organization, Geneva, Switzerland.

116. Simoes, L. C., & Simões, M. (2013). Biofilms in drinking water: problems and solutions. *Rsc Advances*, *3*(8), 2520-2533

117. Luppens, S. B., Reij, M. W., van der Heijden, R. W., Rombouts, F. M., & Abee, T. (2002). Development of a standard test to assess the resistance of Staphylococcus aureus biofilm cells to disinfectants. *Applied and Environmental Microbiology*, *68*(9), 4194-4200

118. Vercellino, T., Morse, A., Tran, P., Hamood, A., Reid, T., Song, L., & Moseley, T. (2013). The use of covalently attached organo-selenium to inhibit S. aureus and E. coli biofilms on RO membranes and feed spacers. *Desalination*, *317*, 142-151

119. Spallholz, J. E. (1994). On the nature of selenium toxicity and carcinostatic activity. *Free Radical Biology and Medicine*, *17*(1), 45-64.

120. Misra, S., Boylan, M., Selvam, A., Spallholz, J. E., & Björnstedt, M. (2015). Redox-active selenium compounds—From toxicity and cell death to cancer treatment. *Nutrients*, *7*(5), 3536-3556

121. Dupont, J., & Scholten, J. D. (2010). On the structural and surface properties of transition-metal nanoparticles in ionic liquids. *Chemical Society Reviews*, *39*(5), 1780-1804.

122. Sugunan, A., Thanachayanont, C., Dutta, J., & Hilborn, J. G. (2005). Heavy-metal ion sensors using chitosan-capped gold nanoparticles. *Science and Technology of Advanced Materials*, *6*(3-4), 335

123. Sengan, M., Kamlekar, R. K., & Veerappan, A. (2020). Highly selective rapid colorimetric sensing of Pb2+ ion in water samples and paint based on metal induced

aggregation of N-decanoyltromethamine capped gold nanoparticles. *Spectrochimica Acta Part A: Molecular and Biomolecular Spectroscopy*, *239*, 118485

124. Ghodake, G., Vassiliadis, V. S., Choi, J. H., Jang, J., & Lee, D. S. (2015). Facile synthesis of gold nanoparticles by amino acid asparagine: selective sensing of arsenic. *Journal of nanoscience and nanotechnology*, *15*(9), 7235-7239.

125. Zohora, N., Kumar, D., Yazdani, M., Rotello, V. M., Ramanathan, R., & Bansal, V. (2017). Rapid colorimetric detection of mercury using biosynthesized gold nanoparticles. *Colloids and Surfaces A: Physicochemical and Engineering Aspects*, *532*, 451-457.

126. Avan, A. A., Filik, H., & Demirata, B. (2021). Solid-phase extraction of Cr (VI) with magnetic melamine–formaldehyde resins, followed by its colorimetric sensing using gold nanoparticles modified with p-amino hippuric acid. *Microchemical Journal*, *164*, 105962

127. Ha, W., Yu, J., Wang, R., Chen, J., & Shi, Y. P. (2014). "Green" colorimetric assay for the selective detection of trivalent chromium based on Xanthoceras sorbifolia tannin attached to gold nanoparticles. *Analytical Methods*, *6*(15), 5720-5726

128. Shrivas, K., Shankar, R., & Dewangan, K. (2015). Gold nanoparticles as a localized surface plasmon resonance based chemical sensor for on-site colorimetric detection of arsenic in water samples. *Sensors and Actuators B: Chemical*, *220*, 1376-1383

129. Ullah, N., Mansha, M., Khan, I., & Qurashi, A. (2018). Nanomaterial-based optical chemical sensors for the detection of heavy metals in water: Recent advances and challenges. *TrAC Trends in Analytical Chemistry*, *100*, 155-166

130. Zhu, L., Peng, X., Li, H., Zhang, Y., & Yao, S. (2017). On–off–on fluorescent silicon nanoparticles for recognition of chromium (VI) and hydrogen sulfide based on the inner filter effect. *Sensors and Actuators B: Chemical*, *238*, 196-203

131. Wang, P., Li, L., Pang, X., Zhang, Y., Zhang, Y., Dong, W. F., & Yan, R. (2021). Chitosan-based carbon nanoparticles as a heavy metal indicator and for wastewater treatment. *RSC Advances*, *11*(20), 12015-12021

132. Haque, F., Daeneke, T., Kalantar-Zadeh, K., & Ou, J. Z. (2018). Two-dimensional transition metal oxide and chalcogenide-based photocatalysts. *Nano-micro letters*, *10*(2), 1-27

133. Lan, Y., Lu, Y., & Ren, Z. (2013). Mini review on photocatalysis of titanium dioxide nanoparticles and their solar applications. *Nano energy*, *2*(5), 1031-1045

134. De, M., Ghosh, P. S., & Rotello, V. M. (2008). Applications of nanoparticles in biology. *Advanced Materials*, *20*(22), 4225-4241

135. Salata, O. V. (2004). Applications of nanoparticles in biology and medicine. *Journal of nanobiotechnology*, *2*(1), 1-6

136. Murphy, C. J., Gole, A. M., Stone, J. W., Sisco, P. N., Alkilany, A. M., Goldsmith, E. C., & Baxter, S. C. (2008). Gold nanoparticles in biology: beyond toxicity to cellular imaging. *Accounts of chemical research*, *41*(12), 1721-1730

137. Moreno-Vega, A. I., Gomez-Quintero, T., Nunez-Anita, R. E., Acosta-Torres, L. S., & Castaño, V. (2012). Polymeric and ceramic nanoparticles in biomedical applications. *Journal of Nanotechnology*, *2012*.].

138. Zhao, Y., Tian, Y., Cui, Y., Liu, W., Ma, W., & Jiang, X. (2010). Small molecule-capped gold nanoparticles as potent antibacterial agents that target gram-negative bacteria. *Journal of the American Chemical Society*, *132*(35), 12349-12356

139. Ranjan, S., & Ramalingam, C. (2016). Titanium dioxide nanoparticles induce bacterial membrane rupture by reactive oxygen species generation. *Environmental Chemistry Letters*, *14*, 487-494

140. Cheng, R., Meng, F., Deng, C., Klok, H. A., & Zhong, Z. (2013). Dual and multi-stimuli responsive polymeric nanoparticles for programmed site-specific drug delivery. *Biomaterials*, *34*(14), 3647-3657

141. Polyak, B., & Friedman, G. (2009). Magnetic targeting for site-specific drug delivery: applications and clinical potential. *Expert opinion on drug delivery*, *6*(1), 53-70

142. Nga, N. K., Chau, N. T. T., & Viet, P. H. (2018). Facile synthesis of hydroxyapatite nanoparticles mimicking biological apatite from eggshells for bone-tissue engineering. *Colloids and Surfaces B: Biointerfaces*, *172*, 769-778

143. Zor, E., Mollarasouli, F., Karadurmus, L., Ozcelikay, G., & Ozkan, S. A. (2022). Carbon dots in the detection of pathogenic bacteria and viruses. *Critical Reviews in Analytical Chemistry*, 1-28

144. Pirsaheb, M., Mohammadi, S., & Salimi, A. (2019). Current advances of carbon dots based biosensors for tumor marker detection, cancer cells analysis and bioimaging. *TrAC Trends in Analytical Chemistry*, *115*, 83-99

145. Couleaud, P., Morosini, V., Frochot, C., Richeter, S., Raehm, L., & Durand, J. O. (2010). Silica-based nanoparticles for photodynamic therapy applications. *Nanoscale*, *2*(7), 1083-1095

146. Chatterjee, D. K., Fong, L. S., & Zhang, Y. (2008). Nanoparticles in photodynamic therapy: an emerging paradigm. *Advanced drug delivery reviews*, *60*(15), 1627-1637

147. Dutta, A. K., Maji, S. K., & Adhikary, B. (2014). γ-Fe2O3 nanoparticles: an easily recoverable effective photo-catalyst for the degradation of rose bengal and methylene blue dyes in the waste-water treatment plant. *Materials Research Bulletin*, *49*, 28-34

148. Hu, H., & Zhang, W. (2006). Synthesis and properties of transition metals and rare-earth metals doped ZnS nanoparticles. *Optical materials*, *28*(5), 536-550.

149. Prakash, S., Sahu, S., Patra, B., & Mishra, A. K. (2023). Understanding the aggregation of excitation wavelength independent emission of amphiphilic carbon dots for bioimaging and organic acid sensing. *Spectrochimica Acta Part A: Molecular and Biomolecular Spectroscopy*, *290*, 122257

150. Huang, Z., Han, F., Li, M., Zhou, Z., Guan, X., & Guo, L. (2019). Which phase of iron oxyhydroxides (FeOOH) is more competent in overall water splitting as a photocatalyst, goethite, akaganeite or lepidocrocite? A DFT-based investigation. *Computational Materials Science*, *169*, 109110.

151. Novin, D., van der Wel, J., Seifan, M., Ebrahiminezhad, A., Ghasemi, Y., & Berenjian, A. (2020). A functional dairy product rich in Menaquinone-7 and FeOOH nanoparticles. *LWT*, *129*, 109564

152. Ayodhya, D., & Veerabhadram, G. (2019). Influence of g-C3N4 and g-C3N4 nanosheets supported CuS coupled system with effect of pH on the catalytic activity of 4-NP reduction using NaBH4. *FlatChem*, *14*, 100088

153. Chandio, A. A., Memon, S., Memon, A. A., Balouch, A., Memon, R., Thebo, K. H., ... & Otho, A. A. (2022). Eco-Friendly Conversion of p-Nitrophenol into p-Aminophenol Using Calix [4] arene Derived CuO Nanoparticles: An Excellent Catalytic Agent. *Polycyclic Aromatic Compounds*, 1-13

154. 154.Smyth, M. S., & Martin, J. H. (2000). x ray crystallography. *Molecular pathologMP*, *53*(1), 8–14.

155. 155.B. D. Cullity and S. R. Stock; "Elements of X -Ray Diffraction", 3rd edition, Addison-Wesley Publishing Co. Inc., (**2001**).

156. Miao, J., Charalambous, P., Kirz, J., & Sayre, D. (1999). Extending the methodology of X-ray crystallography to allow imaging of micrometre-sized non-crystalline specimens. *Nature*, *400*(6742), 342-344.

157. 157.Pope, C. G. (1997). X-ray diffraction and the Bragg equation. *Journal of chemical education*, *74*(1), 129.

158. 158.Evans, J. S., & Evans, I. R. (2020). Structure analysis from powder diffraction data: Rietveld refinement in excel. *Journal of Chemical Education*, *98*(2), 495-505.

159. 159.Fahami, A., Nasiri-Tabrizi, B., Beall, G. W., & Basirun, W. J. (2017). Structural insights of mechanically induced aluminum-doped hydroxyapatite nanoparticles by Rietveld refinement. *Chinese journal of chemical engineering*, *25*(2), 238-247.

160. 160.Petit, S. (2006). Fourier transform infrared spectroscopy. *Developments in Clay Science*, *1*, 909-918.

161. 161.Ismail, A. A., van de Voort, F. R., & Sedman, J. (1997). Fourier transform infrared spectroscopy: principles and applications. In *Techniques and instrumentation in analytical chemistry* (Vol. 18, pp. 93-139). Elsevier.

162. 162.Dutta, A. (2017). Fourier transform infrared spectroscopy. *Spectroscopic methods for nanomaterials characterization*, 73-93.

163. 163.Ayers, G. P., & Pullin, A. (1976). The ir spectra of matrix isolated water species—I. Assignment of bands to (H2O) 2,(D2O) 2 and HDO dimer species in argon matrices. *Spectrochimica Acta Part A: Molecular Spectroscopy*, *32*(10), 1629-1639.

164. 164.Pavia, D. L., Lampman, G. M., Kriz, G. S., & Vyvyan, J. A. (2008). Introduction to Spectroscopy (p. 38). *Belmont: Brooks/Cole, Cengage Learning*.

165. 165.Griffiths, P. R. (1983). Fourier transform infrared spectrometry. *Science*, *222*(4621), 297-302.

166. 166.Faix, O. (1992). Fourier transform infrared spectroscopy. In *Methods in lignin chemistry* (pp. 83-109). Springer, Berlin, Heidelberg.

167. 167.Herzberg, G. (1945). Infrared and Raman Spectra of Polyatomic Molecules, *Vol. 2 of Molecular Spectra and Molecular Structure*.

168. 168.Smith, E., & Dent, G. (2019). *Modern Raman spectroscopy: a practical approach*. John Wiley & Sons.

169. 169.Das, R. S., & Agrawal, Y. K. (2011). Raman spectroscopy: recent advancements, techniques and applications. *Vibrational spectroscopy*, *57*(2), 163-176.

170. 170.Schmitt, R. (2014). Scanning Electron Microscope. In: Laperrière, L., Reinhart, G. (eds) *CIRP Encyclopedia of Production Engineering*. Springer, Berlin, Heidelberg.

171. 171Lee, M. R., & Smith, C. L. (2006). Scanning transmission electron microscopy using a SEM: Applications to mineralogy and petrology. *Mineralogical Magazine*, *70*(5), 579-590.

172. 172.Novikov, Y. A. (2015). Virtual scanning electron microscope. 5. Application in nanotechnology and in micro-and nanoelectronics. *Russian Microelectronics*, *44*(4), 269-282.

173. 173.Modena, M. M., Rühle, B., Burg, T. P., & Wuttke, S. (2019). Nanoparticle characterization: what to measure?. *Advanced Materials*, *31*(32), 1901556.

174. 174.Zhao, M., Ming, B., Kim, J. W., Gibbons, L. J., Gu, X., Nguyen, T., ... & Liddle, J. A. (2015). New insights into subsurface imaging of carbon nanotubes in polymer composites via scanning electron microscopy. *Nanotechnology*, *26*(8), 085703.

175. 175.Lüders, A., Müller, C., Boonrod, K., Krczal, G., & Ziegler, C. (2012). Tomato bushy stunt viruses (TBSV) in nanotechnology investigated by scanning force and scanning electron microscopy. *Colloids and Surfaces B: Biointerfaces*, *91*, 154-161.

176. 176.Wu, J. S., Kim, A. M., Bleher, R., Myers, B. D., Marvin, R. G., Inada, H., ... & Dravid, V. P. (2013). Imaging and elemental mapping of biological specimens with a dual-EDS dedicated scanning transmission electron microscope. *Ultramicroscopy*, *128*, 24-31.

177. 177.Akhtar, K., Khan, S.A., Khan, S.B., Asiri, A.M. (2018). Scanning Electron Microscopy: Principle and Applications in Nanomaterials Characterization. In: *Sharma, S. (eds) Handbook of Materials Characterization. Springer, Cham.*

178. 178.Amidon, G. E., Secreast, P. J., & Mudie, D. (2009). Particle, powder, and compact characterization. In *Developing solid oral dosage forms* (pp. 163-186). Academic press.

179. 179.Cazaux, J. (2005). Recent developments and new strategies in scanning electron microscopy. *Journal of microscopy*, *217*(1), 16-35.

180. 180.Fultz, B., & Howe, J. M. (2012). *Transmission electron microscopy and diffractometry of materials*. Springer Science & Business Media.

181. 181.Bendersky, L. A., & Gayle, F. W. (2001). Electron diffraction using transmission electron microscopy. *Journal of research of the National Institute of Standards and Technology*, *106*(6), 997.

182. Saadatkhah, N., Carillo Garcia, A., Ackermann, S., Leclerc, P., Latifi, M., Samih, S., ... & Chaouki, J. (2020). Experimental methods in chemical engineering: Thermogravimetric analysis—TGA. *The Canadian Journal of Chemical Engineering*, *98*(1), 34-43.

183. Coats, A. W., & Redfern, J. P. (1963). Thermogravimetric analysis. A review. *Analyst*, *88*(1053), 906-924.

184. Joudeh, N., & Linke, D. (2022). Nanoparticle classification, physicochemical properties, characterization, and applications: a comprehensive review for biologists. *Journal of Nanobiotechnology*, *20*(1), 262.

Cr (VI) SENSING BY *IN SITU* SYNTHESIZED FeOOH @C-DOT NANOPARTICLES
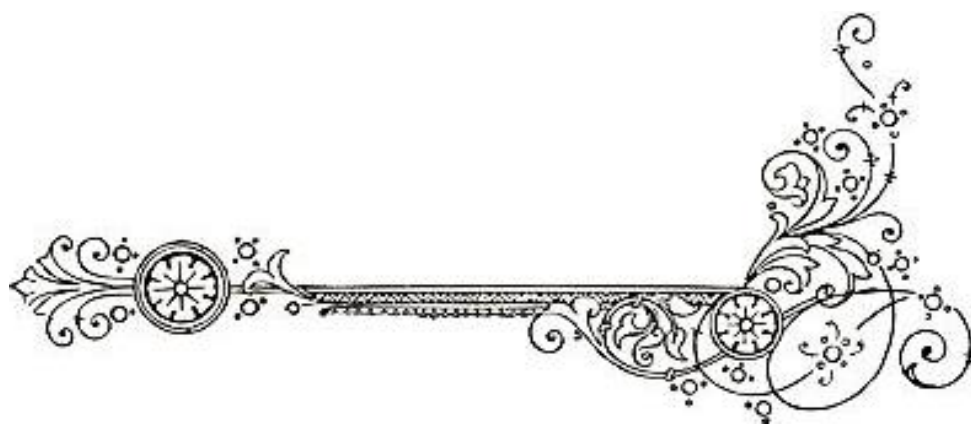
CHAPTER 2

2.1 OVERVIEW

The rapid increase in population and industrialization have introduced several potentially toxic substances into the environment. The accumulation of the effluents released from the industries poses detrimental effects to living organisms and thus becomes a challenge for sustenance. Apart from various organic compounds, these xenobiotics encompass many metals that, at low concentrations, may impact air and soil and subsequently percolate into water bodies disturbing flora and fauna of the aquatic system. [1]. The efflux of toxic wastes into the marine realm needs thorough monitoring, and advanced technologies are much in vogue to reclaim the water for further use as globally, it has been observed that the supply of ground drinking water is under the severe challenge of depletion [2,3]. Wastewater ruefully contains in galore several drugs, organic compounds, organic dyes and, most importantly, a large spectrum of heavy metals which are non-biodegradable. Heavy metal contamination poses marked toxic effects to the ecological as well as to the environment. [4,5]. At this point of agony, there are several initiatives undertaken with the introduction of newer technologies to recycle water and replenish the quantity and quality of the same. Even before the rightful approach to reclaiming water, the priority is to ascertain the presence of heavy metals in water. Several sensing probes have been developed so far, which are based upon several techniques like Atomic Absorption Spectroscopy (AAS) [6-8], capillary electrophoresis [9,10], colorimetric [11-13] electrochemical, and fluorometry, which are employed for the presence of trace amounts of heavy metals in water [14-16] The choice of the sensor comes forth as a pivotal factor as there always been a search of sensors which would be easily procured, economically accessible along with meeting the criteria of biocompatibility.

This chapter focuses on preparing a fluorescent nano-sensor via facile hydrothermal techniques. Several fluorescent probes are used in sensor devices which most of the time suffer from toxicity, given the examples of semi-conductor nanomaterials [17-19], rare earth dopants [20-22], and fluorescent organic dyes [23-26]. The majority of these conjugating compounds are toxic and difficult to handle [27-29], and may cause several pathophysiological reactions in the body. In this chapter, the sensing device

has been tailored using Carbon dots on the goethite (α-FeOOH) matrix. The carbon quantum dots are of tremendous advantage as they can be procured naturally [30-35] and do not suffer from the problem of solubility in the aqueous media as the fluorophores mentioned earlier do. Owing to their small size and the advantage of tuning the sp2 domains, these nanomaterials serve an excellent function in the sensing arena. The C-dots chosen here as a fluorescent probe often suffer from the disadvantages of aggregation, and several matrices were selected to prevent aggregation and subsequent loss in fluorescence [36]. Several well-known matrices like mesoporous silica [37,38] and boehmite nanoparticles [36] were chosen to avoid it. Still, these materials are not refrained from being toxic as they adversely affect the human body [39-43]. So here, we fabricate α-FeOOH nanoparticles, which have already been reported to be biocompatible for their use as food supplements [44]. This nano-material is conjugated with C-dots via an in-situ technique and is checked for its potential to detect hexavalent Cr (VI) in water.

2.2 METHODOLOGY

2.2.1 Materials Required:

Pure salt of Ferric nitrate [Fe $(NO3)_3$] (ACS grade), anhydrous citric acid and Ethylene Diamine (HPLC grade) were purchased from Merck, India. To perform the selectivity analysis of cations and anions in water, the salts of $CaCl_2.2H_2O$, NaCl, $HgCl_2$, $MgCl_2$, $CdCl_2$, $NaNO_3$, Na_2SO_4. $CaCO_3$, Ca $(OH)_2$, Pb $(NO_3)_2$, KCl, Na_2S, $K_2Cr_2O_7$ were purchased from Merck, Germany and As_2O_3 from Sigma Aldrich. For the experiment, washing throughout was carried out with Ultra-pure Millipore water having resistivity ~18.2 MΩ-cm. Further, aqua regia was used to clean all the apparatus, including the sample holders.

2.2.2 Synthesis of the Fluorescent nano probe

The synthesis process of the fluorescent nanoprobe was carried out following the protocol of Roy et al. 2020 [36] with few modifications. A one-pot facile hydrothermal technique prepared the in situ nitrogenous carbon dot decorated α-FeOOH nanoparticles. At room temperature to 160ml of ultra-pure Milli Q water, 0.323g of citric acid was dissolved thoroughly using a magnetic stirrer. As a nitrogen

source, ethylene diamine was added to make the solution alkaline and pH was maintained at 12 at stirring for about a couple of hours.

This entire solution next is transferred next to a Teflon-lined stainless- steel autoclave and was heated for about 12hrs at a temperature of 180°C. The setup was brought to room temperature and subjected to centrifugation at 8000rpm, and the red brick precipitate was obtained. Repeated washing of the residue with ultra-pure Millipore water was done, and the red brick precipitate was dried in vacuum desiccator for a day. The fine powder was made using agate mortar, The obtained fine powder was labelled as FCD and was kept in an air-tight Eppendorf tube for subsequent characterizations.
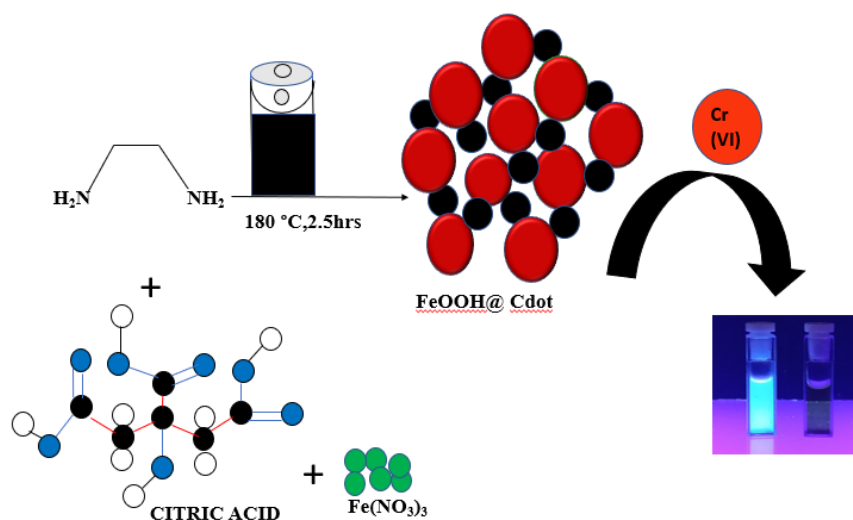
Fig 2.1 : A schematic diagram to explain the formation of FeOOH@Cdot nanostructures

2.3 RESULTS & DISCUSSIONS

2.3.1 Material Characterization and Morphological analyses

The impregnation of the nitrogen-doped carbon dots into the goethite structure needs to be confirmed. For this purpose, the XRD analysis was carried out to determine the crystallographic parameter of the synthesized samples. The diffractogram depicting the h k l planes indicates the successful orthorhombic oxyhydroxide phase of the α-FeOOH. Obtained diffractogram well corroborated with the JCPDS data. The purity of the samples was confirmed by the absence of any residual diffraction planes. As depicted in the figure, the microstrain value was significantly high, which can be

assumed due to the doping introduction of the C dot into the goethite matrix [36]. To develop an idea about crystalline nature, bond length and other parameters of anisotropic growth, Rietveld refinement has been performed using Maud v.299 (Material Analysis using Diffraction) and VESTA v3.0 (Visualisation for Electronic Structural Analyses) for elucidating the finer structures.

PARAMETERS	FCD
a (Å)	10.00903
b (Å)	2.9612691
c (Å)	4.510796
V (Å^3)	133.697
Size (Å)	598.5741
Microstrain	1.25×10^{-3}
R_P (%)	0.03
R_{wp} (%)	0.04
χ^2	1.33
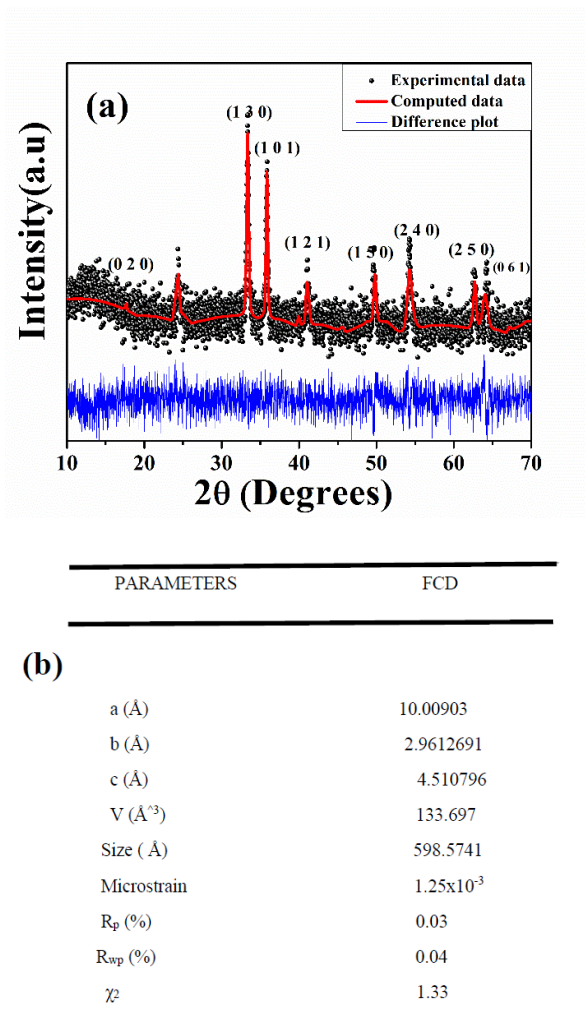
Fig 2.2: (a) Refined X-ray Diffractogram of the sensor sample(FCD),the experimental data has been shown in black, the difference plot in blue and the computed data in red; (b) the microstructural parameters of the prepared sample out of Rietveld measurement.

The presence of dopant nitrogenous carbon dots and surface functional groups in the goethite matrix was determined through FTIR spectroscopy. The vibrational peaks centered at 1035 and 1217 cm^{-1} are attributed to the stretching vibrations of C-C, C-O and C=O bonds, indicating the incorporation of the C dot in the nanomatrix [45]. The

asymmetric stretching vibrations of Fe-CO and Fe-O are assigned to 520 cm^{-1} and 675 cm^{-1} [46,47]. The presence of moisture absorbed by the sample is well established by the absorption bands located at 774 cm^{-1}, 900 cm^{-1} and 1635 cm^{-1}, mainly through O-H stretching vibrations and CO-NH vibrations [47,48] and N-H bending sourcing out of nitrogenous C dot are attributed to a slight vibration at 1525 cm^{-1} [36].

The surface morphology and the particle size of the synthesized nanomaterial were judged through FESEM, and further confirmation of the rightful doping of the C dot was inferred through TEM. Images of FESEM Fig 2.3 (b) and (c) show agglomerated nature of the C dot in the FeOOH nanoparticles, which are a mix of both spherical and hexagonal particles. The TEM images confirmed the particle size of the nanosensor to be ranging in an average diameter of 30-50nm, into which the impregnation of C dots is seen as dark spots.
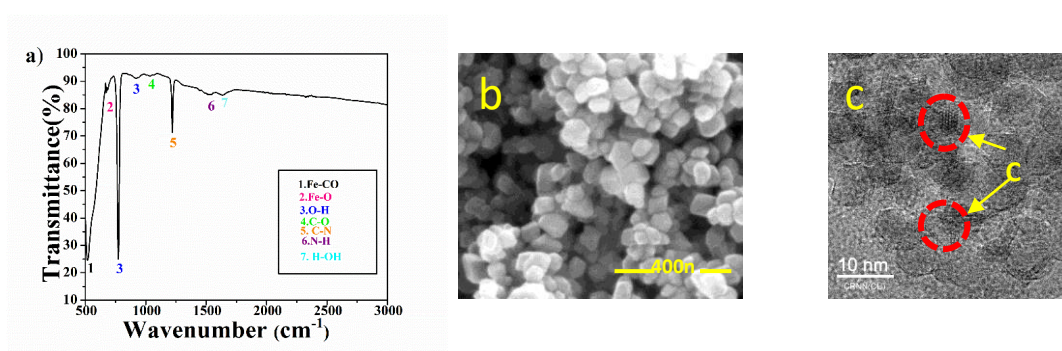
Fig 2.3: (a) FTIR Spectrum of the synthesized nanoprobe; (b) and (c) FESEM and TEM images of the nano sensor

2.3.2 Optical Quality Assessment:

As the present work aims at developing a fluorescent nano-sensor, it inevitably counts for determining the optical ability of the tailored nanoparticle. The optical performance was recorded using UV Vis Spectroscopy. The excitation energy spectrum showed an absorption maximum at 240nm, sourcing out of the π-π* transition of the sp2 hybridization present in the carbon dot [49]. The functionalization of the surface molecules by the – NH$_2$ groups by ethylene diamine resulted in a relatively strong absorption of the nanomaterial at 342nm, which can be inferred by sourcing out of the n-π* transitions [50-52]. The Fe-Fe vibration of the synthesized nanoprobe has been ascribed to 450nm and 572nm, which corroborates with the data of Sherman et al. in a report published in 1985 [53].

The prepared sample is a nano-sensor designed to sense Cr (VI) in water fluorometrically. Thus, apart from the optical activity, the fluorometric ability was also assessed. The nanomaterial exhibited an excitation peak at 345nm. It is also excited at a series of wavelengths ranging from 300-400nm to probe the actual excitation energy, whereby it was observed optimum fluorescence was exhibited at 345nm. At this excitation wavelength, the sample's emission was 460nm. This particular emission was consistent when the sensor material was subjected to varying excitation wavelengths, as seen in Fig 2.4. The enhanced fluorescence of the probe can be explained by introducing a dopant nitrogenous carbon dot which enables the phenomenon of charge localization [54-57].
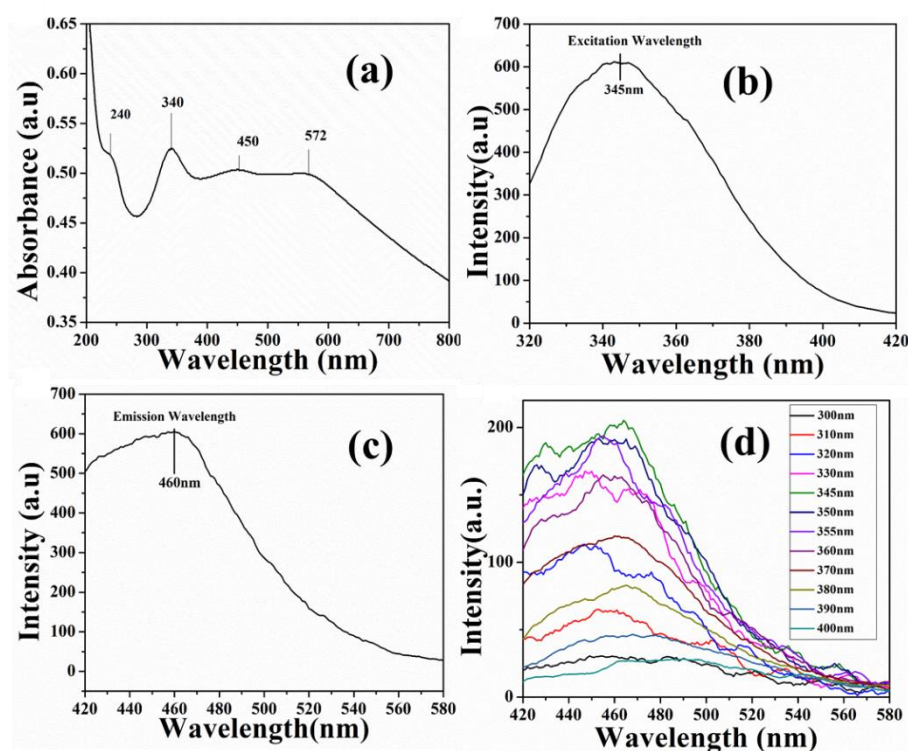
Fig 2.4: (a) UV- Vis Spectra of synthesized FCD nanomaterial; (b) and (c) Fluorescence spectra showing Excitation and Emission spectra of the same sample (d) Emission of the sample with varying wavelengths of excitation energies

The thermogravimetric analysis (DTA-TGA) graph (Fig 2.5) hinted at an endothermic change followed by an exotherm which may be assumed for the loss of moisture in this region. Nevertheless, at a given temperature range, no mass change was observed. Further, a sensor must show stability at different environmental parameters of temperature, time, and varying pH conditions. The synthesized probe functions best at

room temperature (shown in Fig 2.6) when subjected to a temperature range of 30°-50°C.
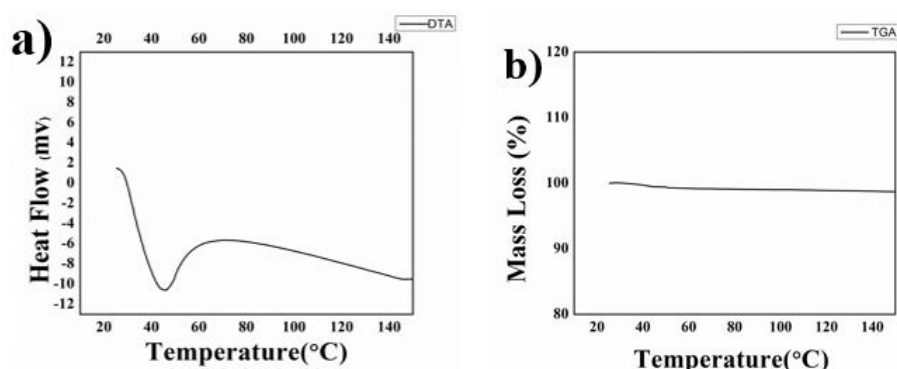
Fig 2.5: a) and b) DTA-TGA graph of the synthesized nano sensor

Through the exposure of the nano-sensor to varying pH ranges of extremely acidic to alkaline conditions, it was found that the fluorophores in the synthesized sample remained relatively stable under all conditions. The fluorescent performance was investigated over time at 10min for 2 hrs. No decline in fluorophore intensity occurred during this period, confirming the stability of the sensor for further applications.
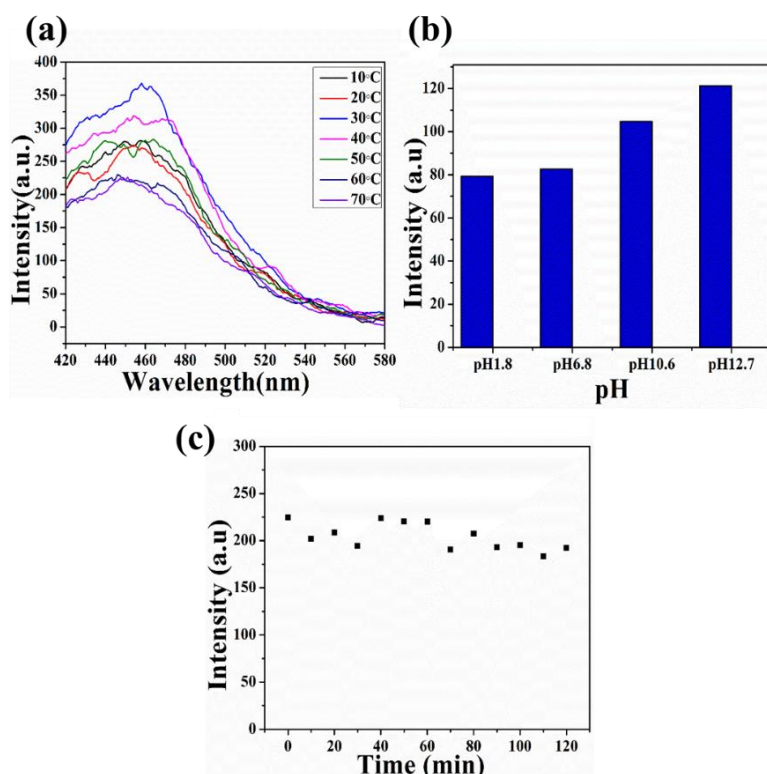
Fig 2.6: Graphs showing the stability of fluorescence when the sensor was subjected to varying (a) Temperature (b) pH conditions and (c) Time

2.3.3 FCD: An efficient Fluorescent sensor of Hexavalent Chromium (Cr (VI))

The sensing repertoire of a probe rests on its ability to detect a specific molecule in the medium. This counts for two cardinal parameters of selectivity besides the sensitivity of the sensing probe. Thus, the prepared sensor was tested against a wide array of ions having a concentration of 500µM. These wide variety of cations and ions include As+, K+, Ca^{2+} Mg^{2+}, Pb^{2+}, Hg^{2+}, Cd^{2+}, Cr^{6+}, OH$^-$, Cl$^-$, S^{2-}, CO$_3$$^{2-}$, SO$_4$$^{2-}$, NO$_3$$^-$. The sensor material was added to the mentioned concentration of each of these ions. A marked decrease in fluorescence intensity was observed due to the binding of Cr (VI) with the sensor material, whereas no change was observed for other ions (Fig 2.7). The result thus hints that the sensor can detect the presence of Cr (VI).

The colorimetric analysis of the sample was validated by the CIE-1931 plot, which depicted that the colour coordinate of the pure sensor sample is x= 0.15504 and y = 0.1344, whereas for a sensor with spiked Cr (VI) is found to have a slight deflection in the blue region. Here the colour coordinates were x= 0.21875 and y= 0.1888.

Fig 2.7: (a) Sensing activity of the probe against a range of cations and anions; (b) CIE-1931 showing colour analysis of the sensor material

The quenching ability of the probe as seen above is determined quantitatively for varying concentration of chromium ions that ranges from 0-23.8µM. It was found that there is a gradual decrease in the intensity of the quencher ions that shows an exponential decay in fluorescence with varying concentration of Cr (VI). The obtained sensitivity was calculated by plotting linear as well as linear Stern Volmer equations [58, 59]

The quenching efficiency was calculated from the SV plots by using the following equations:

$$I_0/I = 1 + K_{SV}[M] \qquad \ldots\ldots \text{ eq (i)}$$

$$I_0/I = A\exp(k_{SV}[M]) \qquad \ldots\ldots\ldots\text{eq (ii)}$$

Where I_0 and I are the fluorescent intensities of the sensor material recorded initially and after the addition of Cr (VI) and [M] stands for the concentration of the hexavalent chromium species, A is constant and SV constant is denoted by k_{SV}. The linearity of the plot was seen up to a concentration of 10μM of Cr (VI) beyond which the exponential decay of fluorescence was observed (Fig 2.8)

Fig 2.8 (a) Fluorescent quenching of the probe upon gradual increase in concentration of Cr (VI); (b) Linear Plot (c) Exponential SV plot

Furthermore, the limit of detection (LOD) and limit of quantification (LOQ) was calculated from the following equations:

$$LOD = 3\sigma/k_{SV} \qquad \text{eq}\ldots\text{ (iii)}$$

$$LOQ = 10\sigma/k_{SV} \qquad \text{eq }\ldots\text{.(iv)}$$
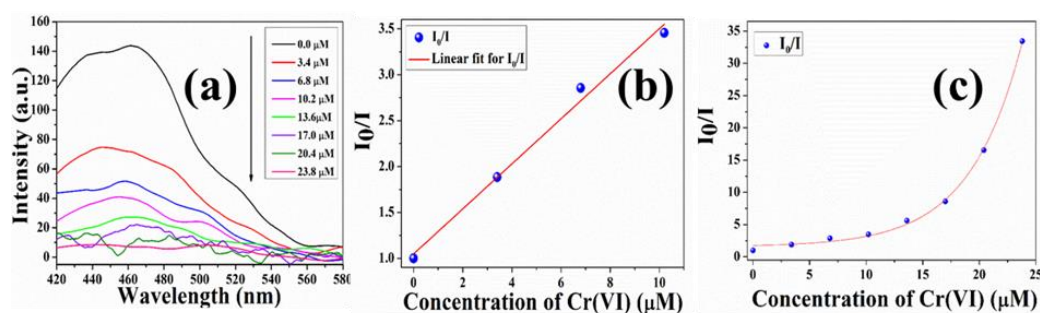
where σ is the standard deviation of the sensor calculated from at least ten separate experiments in the absence of the quenching molecule. The LOD and LOQ calculated using the above equation were found to be respectively 81nM and 269.73nM.

2.3.4 Validation of the sensing mechanism of the nanoprobe

The SV plot and the fluorescence life time data (Fig 2.9) show that the quenching phenomenon occurs when the fluorophores are in the excited state. There is photoinduced electron transfer that occurs from fluorophores of the sensor molecule. Quenching of a chemical moiety can source from a number of factors which includes Inner Filter Effect, Forster Resonance Energy Transfer (FRET), static and dynamic

quenching, Photoinduced electron transfer (PET) [60]. In this sensor based quenching phenomenon PET phenomenon the electron transfer occurs from the fluorescent molecule to the quencher molecule and further due to inadequate number of ions no HOMO-LUMO transition has been observed. This qualifies photoinduced electron transfer as has been explained by Roy *et* al 2020 [36].
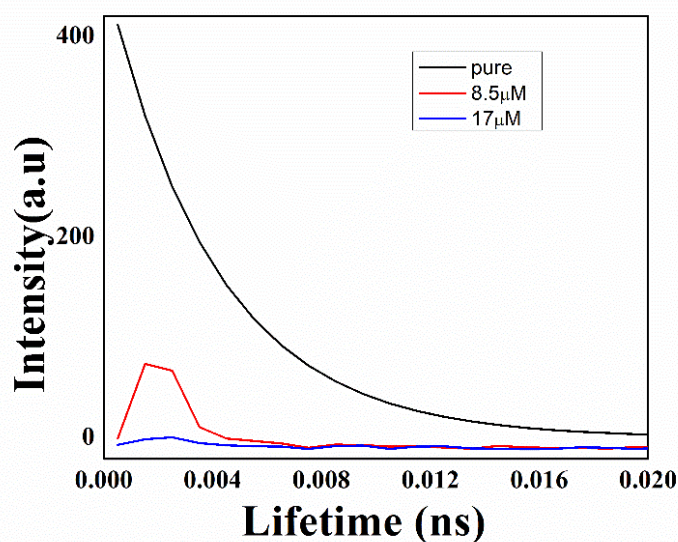
Fig 2.9: Fluorescence Life time data of the sensor material

Moreover, while probing the efficacy of the sensor material it was seen at >10μM concentration the radiative pathway of the fluorophore is blocked by the quencher ions thus establishing the idea of Inner Filter Effect (IFE) which is evident from Fig 2.8 (c) [61,62, 63]. Thus, it can be assumed that the sensing ability of the material is the joined collaboration of the Photoinduced Electron transfer and Inner Filter Effect.

2.3.5 Real life sensing application of FCD

The ultimate applicability of the sensor material was tested in real-life water samples. Different potable water samples were collected from a water purifier, a nearby pond within our university campus and drainage wastewater was collected from Jadavpur, Kolkata. After collecting in sterile tubes, the water was passed through a 0.45μM membrane filter, and two aliquots were made. One of the aliquots was kept as a control, and the other was spiked with 50μM Cr (VI). Also, the sensing efficacy was judged against wastewater collected from a nearby tannery factory. The ICP-AES data showed an alarming concentration of 16.53 ppm of Cr (VI) with other toxic heavy metals. The fluorescent intensity of the FCD sensor material was found to decrease

drastically here too. As depicted in Fig 2.10, it is revealed that the sensing probe is capable enough for application as a sensor for Cr (VI) contaminated wastewater.
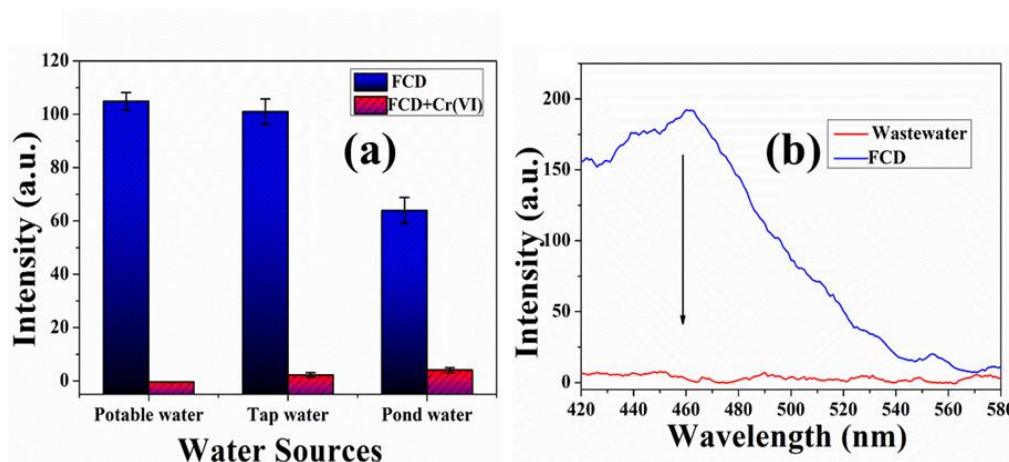
Fig 2.10: (a) Detection ability of Cr (VI) in various water samples (b) Radical decline in fluorescence intensity of sensor in waste water collected from tannery

2.4 SUMMARY

This experimental work provided a strategy to employ a biocompatible matrix tailored with nitrogenous carbon dots for rendering additional features of fluorescence. The characterizations of the nanomaterial via X-ray crystallography and elemental analysis by FTIR confirmed the successful synthesis of the nanomaterial. This nano complex exhibited its functionality as a sensor material by virtue of its efficiency in detecting the presence of hexavalent heavy metal chromium (VI) in water. The sensitivity of the sensor material does not get hindered when exposed to variable parameters of temperature, pH and time and all throughout, has been seen to show adequate stability. The mechanism of sensing can be attributed to the photoinduced electron transfer.

Additionally, it was seen that at a higher concentration of Cr (VI), the phenomenon of the Inner filter effect had been seen to bring about quenching, as evident from the Stern-Volmer plot. The sensor capability of the material was tested against real-life water samples collected from a tannery industry, and marked sensitivity was achieved. Thus, this nanomaterial is seen as a potent nano-sensor, whose effectivity in the biological cells will be elucidated in the next chapter.

REFERENCES

1. Rajendran, S., Priya, T. A. K., Khoo, K. S., Hoang, T. K., Ng, H. S., Munawaroh, H. S. H., ... & Show, P. L. (2022). A critical review on various remediation approaches for heavy metal contaminants removal from contaminated soils. *Chemosphere*, *287*, 132369.

2. Mays, L. W. (2013). Groundwater resources sustainability: past, present, and future. *Water Resources Management*, *27*(13), 4409-4424.

3. Jia, X., Hou, D., Wang, L., O'Connor, D., & Luo, J. (2020). The development of groundwater research in the past 40 years: A burgeoning trend in groundwater depletion and sustainable management. *Journal of Hydrology*, *587*, 125006.

4. Tchounwou, P. B., Yedjou, C. G., Patlolla, A. K., & Sutton, D. J. (2012). Heavy metal toxicity and the environment. *Experientia supplementum (2012)*, *101*, 133–164

5. Wu, X., Cobbina, S. J., Mao, G., Xu, H., Zhang, Z., & Yang, L. (2016). A review of toxicity and mechanisms of individual and mixtures of heavy metals in the environment. *Environmental Science and Pollution Research*, *23*(9), 8244-8259.

6. Porento, M., Sutinen, V., Julku, T., & Oikari, R. (2011). Detection of copper in water using on-line plasma-excited atomic absorption spectroscopy (AAS). *Applied Spectroscopy*, *65*(6), 678-683.

7. Ghaedi, M., Reza Fathi, M., Shokrollahi, A., & Shajarat, F. (2006). Highly selective and sensitive preconcentration of mercury ion and determination by cold vapor atomic absorption spectroscopy. *Analytical Letters*, *39*(6), 1171-1185.

8. Behbahani, M., Tapeh, N. A. G., Mahyari, M., Pourali, A. R., Amin, B. G., & Shaabani, A. (2014). Monitoring of trace amounts of heavy metals in different food and water samples by flame atomic absorption spectrophotometer after preconcentration by amine-functionalized graphene nanosheet. *Environmental monitoring and assessment*, *186*(11), 7245-7257.

9. Tanyanyiwa, J., & Hauser, P. C. (2002). High-voltage contactless conductivity detection of metal ions in capillary electrophoresis. *Electrophoresis*, *23*(21), 3781-3786.

10. Yang, M., Yu, Y., Shen, F., Dierks, K., Fang, W., & Li, Q. (2010). Detection of copper ion with laser-induced fluorescence in a capillary electrophoresis microchip. *Analytical letters*, *43*(18), 2883-2891.

11. Yu, L., Pang, Y., Mo, Z., Huang, Y., & Shen, X. (2021). Coordination array for accurate colorimetric sensing of multiple heavy metal ions. *Talanta*, *231*, 122357.

12. Sengan, M., Kamlekar, R. K., & Veerappan, A. (2020). Highly selective rapid colorimetric sensing of Pb2+ ion in water samples and paint based on metal induced aggregation of N-decanoyltromethamine capped gold nanoparticles. *Spectrochimica Acta Part A: Molecular and Biomolecular Spectroscopy*, *239*, 118485.

13. Karthiga, D., & Anthony, S. P. (2013). Selective colorimetric sensing of toxic metal cations by green synthesized silver nanoparticles over a wide pH range. *RSC Advances*, *3*(37), 16765-16774.

14. Sari, T. K., Takahashi, F., Jin, J., Zein, R., & Munaf, E. (2018). Electrochemical determination of chromium (VI) in river water with gold nanoparticles–graphene nanocomposites modified electrodes. *Analytical Sciences*, *34*(2), 155-160.

15. Fan, C., Chen, L., Jiang, R., Ye, J., Li, H., Shi, Y., ... & Guo, X. (2021). ZnFe2O4 nanoparticles for electrochemical determination of trace Hg (II), Pb (II), Cu (II), and glucose. *ACS Applied Nano Materials*, *4*(4), 4026-4036.

16. Di Masi, S., Garcia Cruz, A., Canfarotta, F., Cowen, T., Marote, P., Malitesta, C., & Piletsky, S. A. (2019). Synthesis and Application of Ion-Imprinted Nanoparticles in Electrochemical Sensors for Copper (II) Determination. *ChemNanoMat*, *5*(6), 754-760.

17. Kaur, J., Kumar, V., Tikoo, K. B., Bansal, S., Kaushik, A., & Singhal, S. (2020). Glutathione modified fluorescent CdS QDs synthesized using environmentally Benign pathway for detection of mercury ions in aqueous phase. *Journal of Fluorescence*, *30*(4), 773-785.

18. Chowdhury, P. (2021). Functionalized CdTe fluorescence nanosensor for the sensitive detection of water borne environmentally hazardous metal ions. *Optical Materials*, *111*, 110584.

19. Faraz, M., Abbasi, A., Naqvi, F. K., Khare, N., Prasad, R., Barman, I., & Pandey, R. (2018). Polyindole/cadmium sulphide nanocomposite based turn-on, multi-ion fluorescence sensor for detection of Cr3+, Fe3+ and Sn2+ ions. *Sensors and Actuators B: Chemical*, *269*, 195-202.

20. Tashi, L., Kumar, M., ul Nisa, Z., Nelofar, N., & Sheikh, H. N. (2020). An efficient down conversion luminescencent probe based on a NaGdF 4: Eu 3+/Ce 3+ nanophosphor for chemical sensing of heavy metal ions (Cd 2+, Pb 2+ and Cr 3+) in waste water. *New Journal of Chemistry*, *44*(3), 1009-1020.

21. Chaudhary, S., Kumar, S., Umar, A., Singh, J., Rawat, M., & Mehta, S. K. (2017). Europium-doped gadolinium oxide nanoparticles: A potential photoluminescencent probe for highly selective and sensitive detection of Fe3+ and Cr3+ ions. *Sensors and Actuators B: Chemical*, *243*, 579-588.

22. Roy, S., Pal, K., Bardhan, S., Maity, S., Chanda, D. K., Ghosh, S., ... & Das, S. (2019). Gd (III)-doped boehmite nanoparticle: an emergent material for the fluorescent sensing of Cr (VI) in wastewater and live cells. *Inorganic Chemistry*, *58*(13), 8369-8378.

23. Nishiyabu, R., Ushikubo, S., Kamiya, Y., & Kubo, Y. (2014). A boronate hydrogel film containing organized two-component dyes as a multicolor fluorescent sensor for heavy metal ions in water. *Journal of Materials Chemistry A*, *2*(38), 15846-15852.

24. Zhu, S., Zhang, J., Janjanam, J., Vegesna, G., Luo, F. T., Tiwari, A., & Liu, H. (2013). Highly water-soluble BODIPY-based fluorescent probes for sensitive fluorescent sensing of zinc (II). *Journal of Materials Chemistry B*, *1*(12), 1722-1728.

25. Maity, A., Ghosh, U., Giri, D., Mukherjee, D., Maiti, T. K., & Patra, S. K. (2019). A water-soluble BODIPY based 'OFF/ON' fluorescent probe for the detection of Cd 2+ ions with high selectivity and sensitivity. *Dalton Transactions*, *48*(6), 2108-2117.

26. Hadar, H. A., Bulatov, V., Dolgin, B., & Schechter, I. (2013). Detection of heavy metals in water using dye nano-complexants and a polymeric film. *Journal of hazardous materials*, *260*, 652-659.

27. Yan, M., Zhang, Y., Xu, K., Fu, T., Qin, H., & Zheng, X. (2011). An in vitro study of vascular endothelial toxicity of CdTe quantum dots. *Toxicology*, *282*(3), 94-103.

28. Paesano, L., Marmiroli, M., Bianchi, M. G., White, J. C., Bussolati, O., Zappettini, A., ... & Marmiroli, N. (2020). Differences in toxicity, mitochondrial function and miRNome in human cells exposed in vitro to Cd as CdS quantum dots or ionic Cd. *Journal of hazardous materials*, *393*, 122430.

29. Semelka, R. C., Ramalho, J., Vakharia, A., AlObaidy, M., Burke, L. M., Jay, M., & Ramalho, M. (2016). Gadolinium deposition disease: Initial description of a disease that has been around for a while. *Magnetic resonance imaging*, *34*(10), 1383-1390.

30. Sachdev, A., & Gopinath, P. (2015). Green synthesis of multifunctional carbon dots from coriander leaves and their potential application as antioxidants, sensors and bioimaging agents. *Analyst*, *140*(12), 4260-4269.

31. Bhatt, S., Bhatt, M., Kumar, A., Vyas, G., Gajaria, T., & Paul, P. (2018). Green route for synthesis of multifunctional fluorescent carbon dots from Tulsi leaves and its application as Cr (VI) sensors, bio-imaging and patterning agents. *Colloids and Surfaces B: Biointerfaces*, *167*, 126-133.

32. Wang, M., Wan, Y., Zhang, K., Fu, Q., Wang, L., Zeng, J., ... & Gao, D. (2019). Green synthesis of carbon dots using the flowers of *Osmanthus fragrans* (Thunb.) Lour. as precursors: application in Fe3+ and ascorbic acid determination and cell imaging. *Analytical and bioanalytical chemistry*, *411*(12), 2715-2727.

33. Huang, K., He, Q., Sun, R., Fang, L., Song, H., Li, L., ... & Zhang, J. (2019). Preparation and application of carbon dots derived from cherry blossom flowers. *Chemical Physics Letters*, *731*, 136586.

34. Nguyen, T. N., Le, P. A., & Phung, V. B. T. (2020). Facile green synthesis of carbon quantum dots and biomass-derived activated carbon from banana peels: synthesis and investigation. *Biomass Conversion and Biorefinery*, 1-10.

35. Shan, F., Xia, H., Xie, X., Fu, L., Yang, H., Zhou, Q., ... & Yu, X. (2021). Novel N-doped carbon dots prepared via citric acid and benzoylurea by green synthesis for high selectivity Fe (III) sensing and imaging in living cells. *Microchemical Journal*, *167*, 106273.

36. Roy, S., Bardhan, S., Chanda, D. K., Roy, J., Mondal, D., & Das, S. (2020). In situ-grown Cdot-wrapped Boehmite nanoparticles for Cr (VI) sensing in wastewater and a theoretical probe for chromium-induced carcinogen detection. *ACS Applied Materials & Interfaces*, *12*(39), 43833-43843.

37. 37.Wang, M., Ren, X., Zhu, L., Xia, Y., & Qiu, J. (2019). Preparation of mesoporous silica/carbon quantum dots composite and its application in selective and sensitive Hg2+ detection. *Microporous and Mesoporous Materials*, *284*, 378-384.

38. Liu, M., Li, T., Zhang, C., Zheng, Y., Wu, C., Zhang, J., ... & Zhang, Z. (2021). Fluorescent carbon dots embedded in mesoporous silica nanospheres: A simple

platform for Cr (VI) detection in environmental water. *Journal of Hazardous Materials*, *415*, 125699.

39. Hamilton Jr, R. F., Thakur, S. A., & Holian, A. (2008). Silica binding and toxicity in alveolar macrophages. *Free Radical Biology and Medicine*, *44*(7), 1246-1258.

40. 40.Yu, T., Malugin, A., & Ghandehari, H. (2011). Impact of silica nanoparticle design on cellular toxicity and hemolytic activity. *ACS nano*, *5*(7), 5717-5728.

41. 41.Chen, L., Liu, J., Zhang, Y., Zhang, G., Kang, Y., Chen, A., ... & Shao, L. (2018). The toxicity of silica nanoparticles to the immune system. *Nanomedicine*, *13*(15), 1939-1962.

42. Khare, T., Dange, D., Jadhav, A., Shriram, V., Gosavi, S., & Kumar, V. (2022). Nano-Boehmite Induced Oxidative and Nitrosative Stress Responses in Vigna radiata L. *Journal of Plant Growth Regulation*, *41*(1), 327-343.

43. 43.Forest, V., Pailleux, M., Pourchez, J., Boudard, D., Tomatis, M., Fubini, B., ... & Cottier, M. (2014). Toxicity of boehmite nanoparticles: impact of the ultrafine fraction and of the agglomerates size on cytotoxicity and pro-inflammatory response. *Inhalation Toxicology*, *26*(9), 545-553.

44. 44.Novin, D., van der Wel, J., Seifan, M., Ebrahiminezhad, A., Ghasemi, Y., & Berenjian, A. (2020). A functional dairy product rich in Menaquinone-7 and FeOOH nanoparticles. *LWT*, *129*, 109564.

45. Ji, T. H., Li, X. L., Mao, Y., Mei, Z., & Tian, Y. (2020). Electron/energy co-transfer behavior and reducibility of Cu-chlorophyllin-bonded carbon-dots. *RSC advances*, *10*(52), 31495-31501.

46. Varotsis, C., & Vamvouka, M. (1998). Resonance Raman and FTIR Studies of Carbon Monoxide-Bound Cytochrome aa 3-600 Oxidase of Bacillus Subtilis. *The Journal of Physical Chemistry B*, *102*(39), 7670-7673.

47. Vernekar, D., & Jagadeesan, D. (2015). Tunable acid–base bifunctional catalytic activity of FeOOH in an orthogonal tandem reaction. *Catalysis Science & Technology*, *5*(8), 4029-4038.

48. Su, Y., Zhou, X., Long, Y., & Li, W. (2018). Immobilization of horseradish peroxidase on amino-functionalized carbon dots for the sensitive detection of hydrogen peroxide. *Microchimica Acta*, *185*(2), 1-8.

49. Wu, Y., & Remcho, V. T. (2016). A capillary electrophoretic method for separation and characterization of carbon dots and carbon dot-antibody bioconjugates. *Talanta*, *161*, 854-859.

50. Tall, A., Cunha, F. A., Kaboré, B., do ES Barbosa, C. D. A., Rocha, U., Sales, T. O., ... & Santos, J. C. C. (2021). Green emitting N, P-doped carbon dots as efficient fluorescent nanoprobes for determination of Cr (VI) in water and soil samples. *Microchemical Journal*, *166*, 106219.

51. Zhao, Y., Liu, X., Yang, Y., Kang, L., Yang, Z., Liu, W., & Chen, L. (2015). Carbon dots: from intense absorption in visible range to excitation-independent and excitation-dependent photoluminescence. *Fullerenes, Nanotubes and Carbon Nanostructures*, *23*(11), 922-929.

52. Tadesse, A., Hagos, M., RamaDevi, D., Basavaiah, K., & Belachew, N. (2020). Fluorescent-nitrogen-doped carbon quantum dots derived from citrus lemon juice: green synthesis, mercury (II) ion sensing, and live cell imaging. *ACS omega*, *5*(8), 3889-3898.

53. Sherman, D. M., & Waite, T. D. (1985). Electronic spectra of Fe3+ oxides and oxide hydroxides in the near IR to near UV. *American Mineralogist*, *70*(11-12), 1262-1269.

54. Tang, X., Yu, H., Bui, B., Wang, L., Xing, C., Wang, S., ... & Chen, W. (2021). Nitrogen-doped fluorescence carbon dots as multi-mechanism detection for iodide and curcumin in biological and food samples. *Bioactive materials*, *6*(6), 1541-1554.

55. Yan, F., Sun, Z., Zhang, H., Sun, X., Jiang, Y., & Bai, Z. (2019). The fluorescence mechanism of carbon dots, and methods for tuning their emission color: A review. *Microchimica Acta*, *186*(8), 1-37.

56. Lu, F., Song, Y., Huang, H., Liu, Y., Fu, Y., Huang, J., ... & Kang, Z. (2017). Fluorescent carbon dots with tunable negative charges for bio-imaging in bacterial viability assessment. *Carbon*, *120*, 95-102.

57. Bardhan, S., Roy, S., Chanda, D. K., Ghosh, S., Mondal, D., Das, S., & Das, S. (2020). Nitrogenous carbon dot decorated natural microcline: an ameliorative dual fluorometric probe for Fe 3+ and Cr 6+ detection. *Dalton Transactions*, *49*(30), 10554-10566.

58. Roy, S., Pal, K., Bardhan, S., Maity, S., Chanda, D. K., Ghosh, S., ... & Das, S. (2019). Gd (III)-doped boehmite nanoparticle: an emergent material for the fluorescent sensing of Cr (VI) in wastewater and live cells. *Inorganic Chemistry*, *58*(13), 8369-8378.

59. Malkondu, S. (2014). A highly selective and sensitive perylenebisimide-based fluorescent PET sensor for Al3+ determination in MeCN. *Tetrahedron*, *70*(35), 5580-5584.

60. Zu, F., Yan, F., Bai, Z., Xu, J., Wang, Y., Huang, Y., & Zhou, X. (2017). The quenching of the fluorescence of carbon dots: a review on mechanisms and applications. *Microchimica Acta*, *184*(7), 1899-1914.

61. Bhatt S et al (2018) Green route for synthesis of multifunctional fluorescent carbon dots from Tulsi leaves and its application as Cr (VI) sensors, bioimaging and patterning agents. Colloids Surf, B167:126–133

62. Mao M et al (2018) Inner filter effect based fluorometric determination of the activity of alkaline phosphatase by using carbon dots codoped with boron and nitrogen. Microchim Acta 185(1):1–6

63. Huang D et al (2021) Fluorescent Nitrogen doped Ti3C2 Mxene quantum dots as unique on off on nanoprobe for chromium (VI) and ascorbic acid based on inner filter effect. Sensors and Actuators B: Chemistry 342

.

BIOSENSING POTENTIAL OF FeOOH @C-DOT IN LIVING CELLS
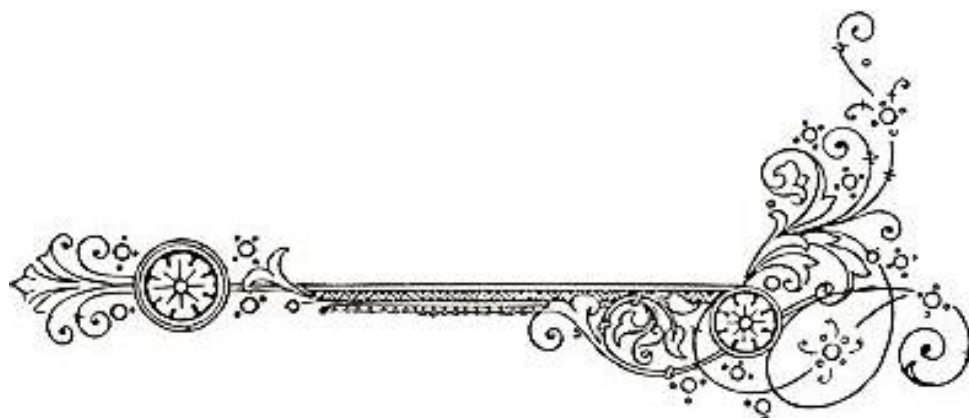
CHAPTER 3

3.1 OVERVIEW

Iron nanoparticles and their various forms have long been in vogue for their widespread applications in various avenues of science, right from heavy metals remediation [1-3] organic dye removal [4-7], electrical and magnetic properties [8-10] to their various sensing applications [11-13]. Besides, iron nanoparticles are valued for their excellent biocompatibility and their role encompasses the various fields of medical research right from tissue imaging, drug targeting, magnetic theranostics to list a few. [14-19]. The use of iron nanoparticles for biosensing is well established and there has been a lot of experimental work regarding the same and owing to the small size regime, iron nanoparticles conjugated with fluorescent probes are pretty much being utilized for sensing in biological cells. The fluorescent probes that have gained prominence for biosensing are mostly prepared through surface functionalization using semi-conductor nanoparticles, fluorescent materials, and polymer coatings [20-23]. As a matter of fact, an ideal fluorescent nanoprobe should be safe for its use in the biological system and the organic dyes and semi-conductor nanomaterials acting as fluorophores render much toxicity and lack stability due to poor solubility in aqueous systems, mostly due to the presence of hydrophobic groups that many organic dyes possess. [24-26]. So, there have been many advancements in the choice of the fluorescent probes [27-29].

The use of carbon dots has acquired considerable momentum in recent times for their safer use in biological systems. In comparison to traditional cadmium and lead quantum dots, carbon dots have acquired widespread popularity due to their dispersibility, almost zero toxicity and marked conductivity and tunable photoluminescent properties sourced from quantum confinement effects [30]. Less than 10nm in diameter, the photoluminescence in carbon dots is mainly due to the dominance of sp3 hybridizations in the amorphous core form that contains small domains of sp2 hybridized carbon [32,33]. Carbon dots, besides their biomedical and bioimaging applications, are finding their relevance in a number of important biological interactions in living cells [34-36]. The use of hetero atoms in synthesizing carbon dots as discussed in Chapter 2 changes the sensing properties of the carbon

dots. It has been found that doping with nitrogen the PL properties drastically alters, which has been attributed to the existence of five electrons in its valence shell [37].

As mentioned earlier, having all the qualities of an ideal sensor, the major conundrum that leads to its instability is its aggregation at high concentration due to an inner filter effect which subsequently causes a reduction in the quantum yield of the carbon dots, thus hampering its sensing capability [38,39]. Thus, the choice of the matrix to avoid aggregation forms a very important factor in reducing agglomeration. Since the preceding chapter has already discussed the usefulness of the goethite matrix, further introduction of this nanomaterial would seem like an exaggeration. But to add to the existing knowledge, the choice of this matrix will provide an additional benefit while performing the biosensing application. Oxides like sulphates of iron, like Fe_3O_4 like ferrous sulphate, are already in prevalence for their use in drug carriers and other applications due to the leakage of iron, and also, these ions in high dosage cause various side effects such as oxidative stress, inflammation and subsequently cell death [40, 41] while FeOOH nanoparticles are been used as iron supplements and are used to treat several haematological parameters [42-44].

So, the same matrix that was used by our group to sense the presence of hexavalent chromium (VI) is now being tested for its additional efficacy in sensing chromium in living cells. Heavy metal detection in living cells rests on the fact of their interactions with several important biological components present inside the cell. Chromate compounds have serious deleterious effects when they enter the cell. These compounds pose cytotoxic and genotoxic effects when they interact with several biomolecules inside the cell. Considered a nephrotoxic compound, Cr (VI) triggers DNA double strand breaks which majorly leads to apoptosis inside the cell via production of intracellular reactive oxygen species (ROS), and alters gene expression by changing histone modification with subsequent miRNA expression [45-47].

Due to the structural similarity, entry of hexavalent chromium into the cell interior via the sulphate ion transporters [48,49]. Cr (VI) undergoes reduction to its lower intermediates like Cr (V), Cr (IV) and Cr (III) by interacting with a number of antioxidants present in the cell like cysteine, ascorbic acid, glutathione, flavoenzymes, cytochrome b5 and cytochrome P450 [50-56]. Such activity culminates in the formation of cancer, the path of which can be traced by probing it with powerful biosensors [57].

Thus, the performance of the C-dot decorated α-FeOOH sensor is judged by its efficacy using fluorescent microscopy techniques using human cervical cancer cells, HeLa cells. Further, a theoretical model for binding of the sensor with the haemoproteins is confirmed through molecular docking techniques.

3.2 METHODOLOGY

3.2.1 Materials Required

Human Cervical Cell Lines (HeLa) were bought from National Centre for Cell Science (NCCS Pune, India), Dulbecco Modified Eagle's Medium (DMEM), Fetal bovine serum was brought from Thermo Fischer Scientific, Waltham, MA, USA, Phosphate Buffer Saline (PBS) was bought from Hi Media, Pvt Ltd, India. The reagents and solvents used entirely in the experiment are of pure analytical grade and were used without further purification. Pure Millipore water having a resistivity of ~18.2MΩ-cm was used for performing the experiment.

3.2.2 *In vitro* sensing and molecular docking experiment

The HeLa cells were cultured in DMEM medium, which was further treated with Foetal Bovine Serum of a concentration of 5% and was kept in an incubator at 37°C for 24hrs in a 5% CO_2 atmosphere. Following incubation, these cells are taken out and subjected to rounds of washing with 1X PBS buffer to dilute the cells and prevent them from getting ruptured due to osmosis. The medium in which the cells were cultured had been constantly changed to avoid nutrient depletion and to maintain confluent growth and the incubation step was repeated again at 5% CO_2 at 37° C in the cell culture incubator.

The cells for the experiment were divided into two equal aliquots and were named IA and IB and accordingly, the sensor material, FCD, was added to the culture plates and was kept at 37° C for incubation at the already mentioned optimum conditions overnight. The next day, the samples were treated with 50μM Cr (VI) solution and were kept at incubation conditions for 2hrs. After that, the samples were checked for any alteration in fluorescence with the help of fluorescent microscopy.

Besides, the intra-cellular biosensing mechanism of the FCD probe was assessed using the molecular docking technique. This technique will hint at the early-stage cancer detection ability of the sensor material. The interaction between the sensitizing

probe and the cellular metabolic proteins cyt b5 and P450, is being theoretically judged with the help of this docking study. With the help of Autodock Tools v.1.5.6, the protein and the C dot decorated α-FeOOH ligand molecule is prepared. For performing, certain modifications were made in which the water molecules are deleted and the addition of the hydrogen bonds and the Kollman charges were made.

3.3 RESULTS AND DISCUSSIONS

Fig 3.1 reveals the sensor-treated material gives out blue fluorescent emission when subjected to UV radiation. This indicates that sensor material has successfully been integrated into the treated HeLa cells. However, with the addition of Cr (VI), the fluorescent intensity is seen to get quenched, which hints that the interaction of the cell with the fluorescent probe and its subsequent attachment with the hexavalent Cr (VI) ion.
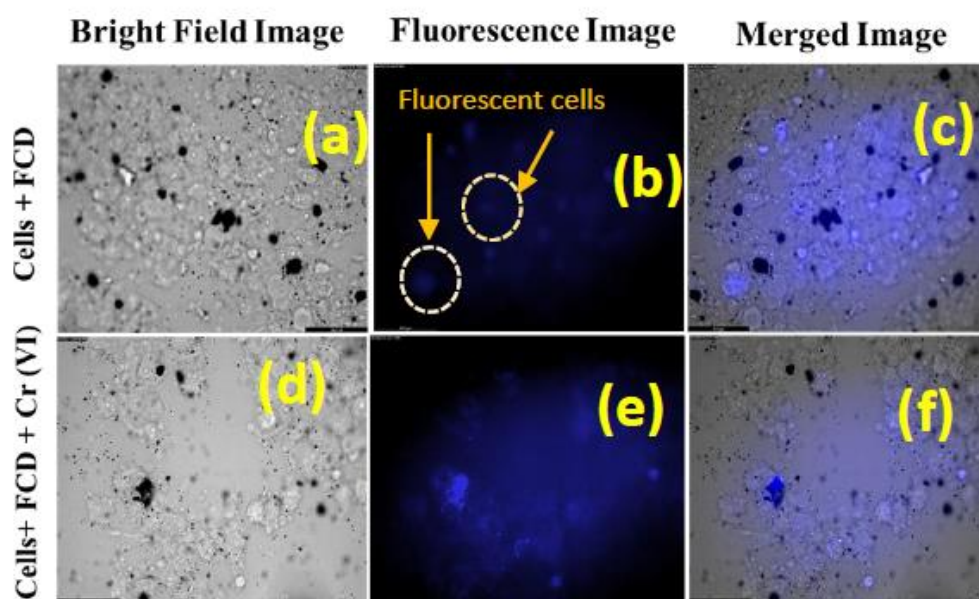
Fig 3.1: Biosensing images of sensor treated and non-treated HeLa cells. (a) and (d) are bright field images (b) and (c) shows fluorescent He la cells where quenching takes place (e) and (f) after Cr (VI) addition.

The result of the binding affinities of the sensitized probe with that of the two different flavoproteins cyt b_5 and cyt P450. In total there had been nine poses obtained out of which the ones having lowest binding energies are chosen. It has been observed that the glycine amino acid present in cyt b5 by virtue of C=O and N-H bonds with the -OH groups of the synthesized sensor material (Fig 3.2). In addition, significant

binding affinity between tyrosine present in the enzyme molecule and the sensor is established which is evident from the binding affinity which was found to be -7.8kcal/mol.

The ligand protein binding was also exhibited while performing docking studies of cyt P450 with the sensor material. As shown in Fig 3.2, it is observed that the terminal nitrogen group in the sensor binds to the carboxyl group of threonine and alanine moiety present in the protein cyt P450 via weak hydrogen bonding and the binding affinity for these two amino acids with the sensor was found to be -8.0kcal/mol.
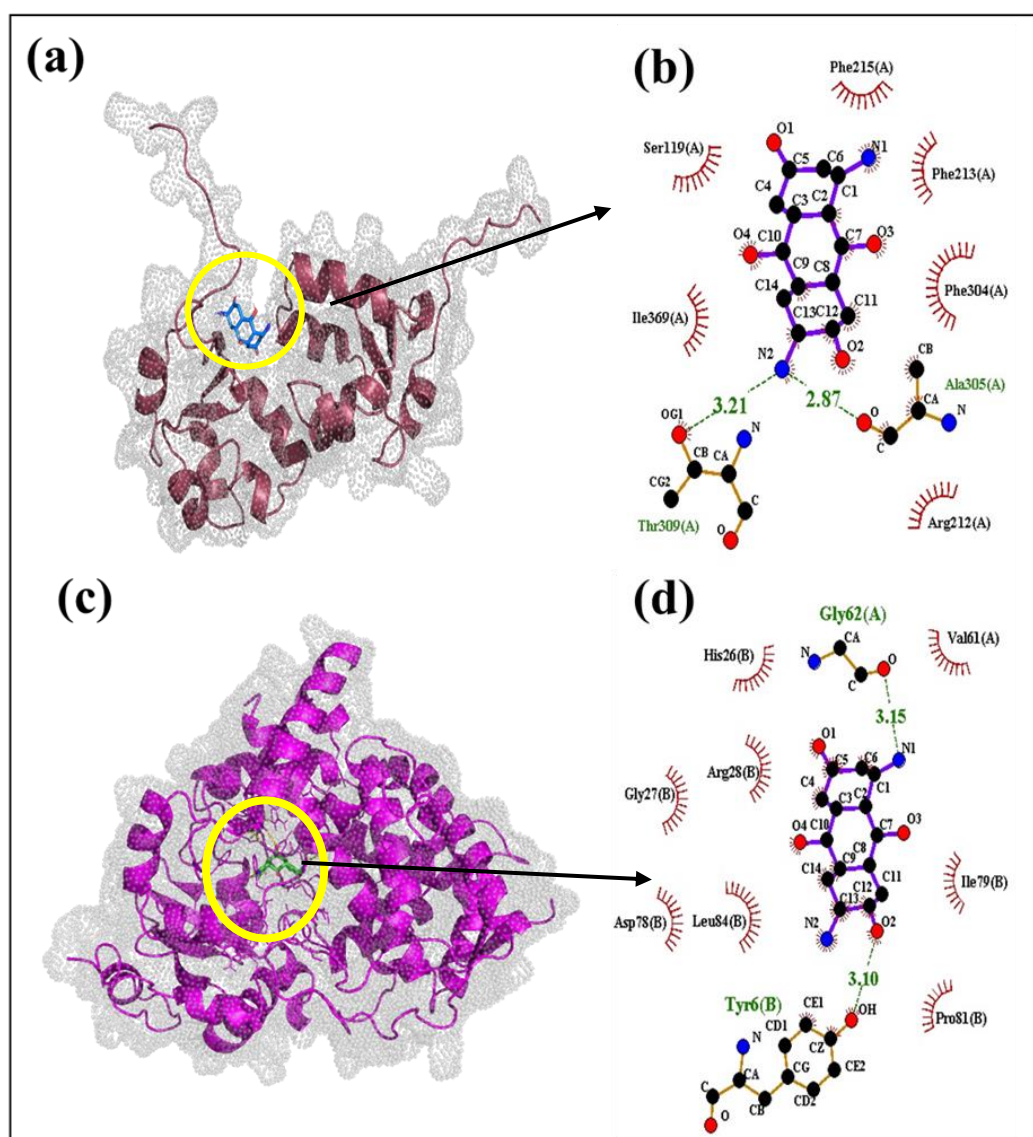
Fig 3.2: Binding of the fluorometric sensor with respective amino acids in cyt b5 (a) and (b) and cyt P450 (c) and (d) is shown

3.4 SUMMARY

This thesis aims at creating nanomaterials for their applications in waste material remediation and also in elucidating their biological activities for being a multifunctional nanomaterial to be harnessed both in industrial as well as in medicinal fields. The successful synthesis of the nanoprobe prepared through facile hydrothermal technique is efficient not only as a waste water sensing device to trace out heavy metal Cr (VI) contaminant, but at the same time, by utilizing its already established biocompatible property, it was substantiated that the sensor material can be used for a stable "On -Off "biosensor device to be used in early- stage cancer detection. The binding affinity of the nanoprobe with the cellular proteins was assessed using molecular docking. Thus, this infers that the sensing probe can have bimodal functions of being utilised both as a chemo sensor as well as a biosensor.

REFERENCES

1. Latif, A., Sheng, D., Sun, K., Si, Y., Azeem, M., Abbas, A., & Bilal, M. (2020). Remediation of heavy metals polluted environment using Fe-based nanoparticles: mechanisms, influencing factors, and environmental implications. *Environmental Pollution*, *264*, 114728.

2. Verma, A., Roy, A., & Bharadvaja, N. (2021). Remediation of heavy metals using nanophytoremediation. In *Advanced oxidation processes for effluent treatment plants* (pp. 273-296). Elsevier.

3. Giraldo, L., Erto, A., & Moreno-Piraján, J. C. (2013). Magnetite nanoparticles for removal of heavy metals from aqueous solutions: synthesis and characterization. *Adsorption*, *19*(2), 465-474.

4. Beheshtkhoo, N., Kouhbanani, M. A. J., Savardashtaki, A., Amani, A. M., & Taghizadeh, S. (2018). Green synthesis of iron oxide nanoparticles by aqueous leaf extract of Daphne mezereum as a novel dye removing material. *Applied Physics A*, *124*(5), 1-7.

5. Radini, I. A., Hasan, N., Malik, M. A., & Khan, Z. (2018). Biosynthesis of iron nanoparticles using Trigonella foenum-graecum seed extract for photocatalytic methyl orange dye degradation and antibacterial applications. *Journal of Photochemistry and Photobiology B: Biology*, *183*, 154-163.

6. Bibi, I., Nazar, N., Ata, S., Sultan, M., Ali, A., Abbas, A., ... & Iqbal, M. (2019). Green synthesis of iron oxide nanoparticles using pomegranate seeds extract and photocatalytic activity evaluation for the degradation of textile dye. *Journal of Materials Research and Technology*, *8*(6), 6115-6124.

7. Bishnoi, S., Kumar, A., & Selvaraj, R. (2018). Facile synthesis of magnetic iron oxide nanoparticles using inedible Cynometra ramiflora fruit extract waste and their

photocatalytic degradation of methylene blue dye. *Materials Research Bulletin*, *97*, 121-127.

8. Lassoued, A., Lassoued, M. S., Dkhil, B., Ammar, S., & Gadri, A. (2018). Synthesis, photoluminescence and Magnetic properties of iron oxide (α-Fe2O3) nanoparticles through precipitation or hydrothermal methods. *Physica E: Low-dimensional Systems and Nanostructures*, *101*, 212-219.

9. Testa-Anta, M., Ramos-Docampo, M. A., Comesaña-Hermo, M., Rivas-Murias, B., & Salgueiriño, V. (2019). Raman spectroscopy to unravel the magnetic properties of iron oxide nanocrystals for bio-related applications. *Nanoscale Advances*, *1*(6), 2086-2103.

10. Khushboo, Sharma, P., Malik, P., & Raina, K. K. (2017). Textural, thermal, optical and electrical properties of Iron nanoparticles dispersed 4′-(Hexyloxy)-4-biphenylcarbonitrile liquid crystal mixture. *Liquid Crystals*, *44*(11), 1717-1726.

11. Bhakta, A. K., Mascarenhas, R. J., D'Souza, O. J., Satpati, A. K., Detriche, S., Mekhalif, Z., & Dalhalle, J. (2015). Iron nanoparticles decorated multi-wall carbon nanotubes modified carbon paste electrode as an electrochemical sensor for the simultaneous determination of uric acid in the presence of ascorbic acid, dopamine and l-tyrosine. *Materials Science and Engineering: C*, *57*, 328-337.

12. Long, N. V., Teranishi, T., Yang, Y., Thi, C. M., Cao, Y., & Nogami, M. (2015). Iron oxide nanoparticles for next generation gas sensors. *Int. J. Metall. Mater. Eng*, *1*(119), 2455-2372.

13. Djebbi, M. A., Allagui, L., El Ayachi, M. S., Boubakri, S., Jaffrezic-Renault, N., Namour, P., & Ben Haj Amara, A. (2022). Zero-Valent Iron Nanoparticles Supported on Biomass-Derived Porous Carbon for Simultaneous Detection of Cd2+ and Pb2+. *ACS Applied Nano Materials*, *5*(1), 546-558.

14. Jain, T. K., Reddy, M. K., Morales, M. A., Leslie-Pelecky, D. L., & Labhasetwar, V. (2008). Biodistribution, clearance, and biocompatibility of iron oxide magnetic nanoparticles in rats. *Molecular pharmaceutics*, *5*(2), 316-327.

15. Ling, D., & Hyeon, T. (2013). Chemical design of biocompatible iron oxide nanoparticles for medical applications. *Small*, *9*(9-10), 1450-1466.

16. Xie, W., Guo, Z., Gao, F., Gao, Q., Wang, D., Liaw, B. S., ... & Zhao, L. (2018). Shape-, size-and structure-controlled synthesis and biocompatibility of iron oxide nanoparticles for magnetic theranostics. *Theranostics*, *8*(12), 3284.

17. Muthiah, M., Park, I. K., & Cho, C. S. (2013). Surface modification of iron oxide nanoparticles by biocompatible polymers for tissue imaging and targeting. *Biotechnology advances*, *31*(8), 1224-1236.

18. Yusefi, M., Shameli, K., Ali, R. R., Pang, S. W., & Teow, S. Y. (2020). Evaluating anticancer activity of plant-mediated synthesized iron oxide nanoparticles using Punica granatum fruit peel extract. *Journal of Molecular Structure*, *1204*, 127539.

19. Yoonus, J., Resmi, R., & Beena, B. (2021). Evaluation of antibacterial and anticancer activity of green synthesized iron oxide (α-Fe2O3) nanoparticles. *Materials Today: Proceedings*, *46*, 2969-2974.

20. Ghasemi, R., Mirahmadi-zare, S.Z., Nasr-Esfahani, M.H. *et al.* Optical biosensing of *Streptococcus agalactiae* based on core/shell magnetic nanoparticle-quantum dot. *Anal Bioanal Chem* **411**, 6733–6743 (2019).

21. Jiang, D., Zhu, P., Jiang, H., Ji, J., Sun, X., Gu, W., & Zhang, G. (2015). Fluorescent magnetic bead-based mast cell biosensor for electrochemical detection of allergens in foodstuffs. *Biosensors and Bioelectronics*, *70*, 482-490.

22. Lee, D. Y., Kang, S., Lee, Y., Kim, J. Y., Yoo, D., Jung, W., ... & Jon, S. (2020). PEGylated bilirubin-coated iron oxide nanoparticles as a biosensor for magnetic relaxation switching-based ROS detection in whole blood. *Theranostics*, *10*(5), 1997.

23. Zhang, W., Li, X., Zou, R., Wu, H., Shi, H., Yu, S., & Liu, Y. (2015). Multifunctional glucose biosensors from Fe3O4 nanoparticles modified chitosan/graphene nanocomposites. *Scientific reports*, *5*(1), 1-9.

24. Zhao, L., Liu, R., Zhao, X., Yang, B., Gao, C., Hao, X., & Wu, Y. (2009). New strategy for the evaluation of CdTe quantum dot toxicity targeted to bovine serum albumin. *Science of the total environment*, *407*(18), 5019-5023.

25. Wang, X., Tian, J., Yong, K. T., Zhu, X., Lin, M. C. M., Jiang, W., ... & Lin, G. (2016). Immunotoxicity assessment of CdSe/ZnS quantum dots in macrophages, lymphocytes and BALB/c mice. *Journal of nanobiotechnology*, *14*(1), 1-12.

26. Mahto, S. K., Yoon, T. H., & Rhee, S. W. (2010). A new perspective on in vitro assessment method for evaluating quantum dot toxicity by using microfluidics technology. *Biomicrofluidics*, *4*(3), 034111.

27. Grimm, J. B., English, B. P., Chen, J., Slaughter, J. P., Zhang, Z., Revyakin, A., Patel, R., Macklin, J. J., Normanno, D., Singer, R. H., Lionnet, T., & Lavis, L. D. (2015). A general method to improve fluorophores for live-cell and single-molecule microscopy. *Nature methods*, *12*(3), 244–250.

28. Wegner, K. D., & Hildebrandt, N. (2015). Quantum dots: bright and versatile in vitro and in vivo fluorescence imaging biosensors. *Chemical Society Reviews*, *44*(14), 4792-4834.

29. Das, A., & Snee, P. T. (2016). Synthetic developments of nontoxic quantum dots. *ChemPhysChem*, *17*(5), 598-617.

30. Liu, Y., Huang, H., Cao, W., Mao, B., Liu, Y., & Kang, Z. (2020). Advances in carbon dots: from the perspective of traditional quantum dots. *Materials Chemistry Frontiers*, *4*(6), 1586-1613.

31. Zheng, X. T., Ananthanarayanan, A., Luo, K. Q., & Chen, P. (2015). Glowing graphene quantum dots and carbon dots: properties, syntheses, and biological applications. *small*, *11*(14), 1620-1636.

32. Chung, S., & Zhang, M. (2021). Microwave-assisted synthesis of carbon dot–iron oxide nanoparticles for fluorescence imaging and therapy. *Frontiers in Bioengineering and Biotechnology*, *9*, 576.

33. Tepliakov, N. V., Kundelev, E. V., Khavlyuk, P. D., Xiong, Y., Leonov, M. Y., Zhu, W., ... & Rukhlenko, I. D. (2019). sp2–sp3-Hybridized atomic domains determine optical features of carbon dots. *ACS nano*, *13*(9), 10737-10744.

34. Yu, Y., Li, C., Chen, C., Huang, H., Liang, C., Lou, Y., ... & Feng, S. (2019). Saccharomyces-derived carbon dots for biosensing pH and vitamin B 12. *Talanta*, *195*, 117-126.

35. Zulfajri, M., Abdelhamid, H. N., Sudewi, S., Dayalan, S., Rasool, A., Habib, A., & Huang, G. G. (2020). Plant part-derived carbon dots for biosensing. *Biosensors*, *10*(6), 68.

36. Yu, Q., Jiang, J., Chen, Z., Han, C., Zhang, X., Yang, S., ... & Yu, C. (2022). A multilevel fluorometric biosensor based on boric acid embedded in carbon dots to detect intracellular and serum glucose. *Sensors and Actuators B: Chemical*, *350*, 130898

37. Shah, H., Xin, Q., Jia, X., & Gong, J. R. (2019). Single precursor-based luminescent nitrogen-doped carbon dots and their application for iron (III) sensing. *Arabian Journal of Chemistry*, *12*(7), 1083-1091.

38. Su, Y., Xie, Z., & Zheng, M. (2020). Carbon dots with concentration-modulated fluorescence: Aggregation-induced multicolor emission. *Journal of colloid and interface science*, *573*, 241-249.

39. Roy, S., Bardhan, S., Chanda, D. K., Roy, J., Mondal, D., & Das, S. (2020). In situ-grown Cdot-wrapped Boehmite nanoparticles for Cr (VI) sensing in wastewater and a theoretical probe for chromium-induced carcinogen detection. *ACS Applied Materials & Interfaces*, *12*(39), 43833-43843.

40. Yarjanli, Z., Ghaedi, K., Esmaeili, A., Rahgozar, S., & Zarrabi, A. (2017). Iron oxide nanoparticles may damage to the neural tissue through iron accumulation, oxidative stress, and protein aggregation. *BMC neuroscience*, *18*(1), 1-12.

41. Kahn, E., Baarine, M., Pelloux, S., Riedinger, J. M., Frouin, F., Tourneur, Y., & Lizard, G. (2010). Iron nanoparticles increase 7-ketocholesterol-induced cell death, inflammation, and oxidation on murine cardiac HL1-NB cells. *International Journal of Nanomedicine*, *5*, 185.

42. He, Z., Su, H., Shen, Y., Shi, W., Liu, X., Liu, Y., ... & Ge, D. (2019). Poly (norepinephrine)-coated FeOOH nanoparticles as carriers of artemisinin for cancer photothermal-chemical combination therapy. *RSC advances*, *9*(18), 9968-9982.

43. Heidari, R., Taghizadeh, S. M., Karami-Darehnaranji, M., Mirzaei, E., Berenjian, A., & Ebrahiminezhad, A. (2022). Application of FeOOH Nano-Ellipsoids as a Novel Nano-Based Iron Supplement: an In Vivo Study. *Biological Trace Element Research*, *200*(5), 2174-2182.

44. Berenjian, A., Karami-Darehnaranji, M., Taghizadeh, S. M., Mirzaei, E., Heidari, R., & Ebrahiminezhad, A. (2020). Bio-assisted synthesis of food-grade FeOOH nanoellipsoids as promising iron supplements for food fortification. *Applied Food Biotechnology*, *8*(1), 71-77.

45. Xie, H., Wise, S. S., & Wise Sr, J. P. (2008). Deficient repair of particulate hexavalent chromium-induced DNA double strand breaks leads to neoplastic transformation. *Mutation Research/Genetic Toxicology and Environmental Mutagenesis*, *649*(1-2), 230-238.

46. Wu, Y. H., Lin, J. C., Wang, T. Y., Lin, T. J., Yen, M. C., Liu, Y. H., ... & Yeh, I. (2020). Hexavalent chromium intoxication induces intrinsic and extrinsic apoptosis in human renal cells. *Molecular Medicine Reports*, *21*(2), 851-857.

47. Sharma, S., Kelly, T. K., & Jones, P. A. (2010). Epigenetics in cancer. *Carcinogenesis*, *31*(1), 27-36.

48. Tang, X., Huang, Y., Li, Y., Wang, L., Pei, X., Zhou, D., ... & Hughes, S. S. (2021). Study on detoxification and removal mechanisms of hexavalent chromium by microorganisms. *Ecotoxicology and Environmental Safety*, *208*, 111699.

49. Zhitkovich, A. (2011). Chromium in drinking water: sources, metabolism, and cancer risks. *Chemical research in toxicology*, *24*(10), 1617-1629.

50. Sugiyama, M. (1992). Role of physiological antioxidants in chromium (VI)-induced cellular injury. *Free Radical Biology and Medicine*, *12*(5), 397-407.

51. Wiegand, H. J., Ottenwälder, H., & Bolt, H. M. (1984). The reduction of chromium (VI) to chromium (III) by glutathione: an intracellular redox pathway in the metabolism of the carcinogen chromate. *Toxicology*, *33*(3-4), 341-348.

52. Suzuki, Y., & Fukuda, K. (1990). Reduction of hexavalent chromium by ascorbic acid and glutathione with special reference to the rat lung. *Archives of toxicology*, *64*(3), 169-176.

53. Kitagawa, S., Seki, H., Kametani, F., & Sakurai, H. (1988). EPR study on the interaction of hexavalent chromium with glutathione or cysteine: production of pentavalent chromium and its stability. *Inorganica chimica acta*, *152*(4), 251-255.

54. Shi, X. (1999). Reduction of chromium (VI) and its relationship to carcinogenesis. *Journal of Toxicology and Environmental Health Part B: Critical Reviews*, *2*(1), 87-104.

55. Borthiry, G. R., Antholine, W. E., Kalyanaraman, B., Myers, J. M., & Myers, C. R. (2007). Reduction of hexavalent chromium by human cytochrome b5: generation of hydroxyl radical and superoxide. *Free Radical Biology and Medicine*, *42*(6), 738-755.

56. Mikalsen, A., Alexander, J., Andersen, R. A., & Daae, H. L. (1989). Reduction of hexavalent chromium in a reconstituted system of cytochrome P-450 and cytochrome b5. *Chemico-biological interactions*, *71*(2-3), 213-221.

57. Roy, S., Bardhan, S., Mondal, D., Saha, I., Roy, J., Das, S., ... & Das, S. (2021). Polymeric carbon dot/boehmite nanocomposite made portable sensing device (Kavach) for non-invasive and selective detection of Cr (VI) in wastewater and living cells. *Sensors and Actuators B: Chemical*, *348*, 130662.

CATALYTIC REDUCTION OF *p*-NITROPHENOL BY BLOCK COPOLYMER STABILIZED CuS NANOPARTICLES
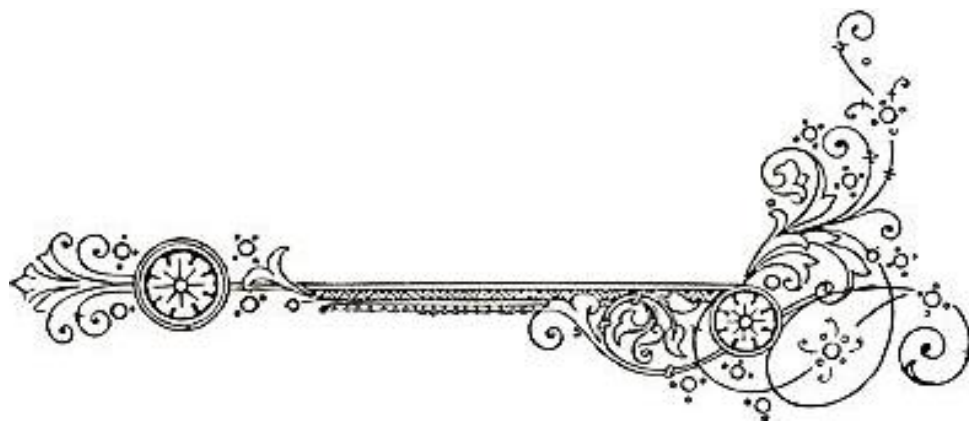
CHAPTER 4

4.1 OVERVIEW

In recent years, d- block transitional metal chalcogenides have gained wider prominence owing to their promising and novel attributes due to their unique properties having shape morphology, compositional and crystalline varieties. Of the various p-type semiconductors known as CuS, a metal chalcogenide has been shown to possess a number of properties encompassing its applications from industry to pharmaceutical fields.

Industrial dyes and organic compounds like phenol are being used indecisively in modern life for a variety of applications [1-3]. The dyes of industrial uses are seen to be toxic, non-biodegradable and can't be degraded by direct sunlight [4] and posing threat to the flora and fauna being exposed to such organic chemicals. The photodegradation of such organic compounds in the presence of photocatalysts can to some extent mitigate the crisis of water pollution. Nitrophenol and phenol are one of those organic pollutants which pose vital threat as they are been extensively used in the pharmaceutical, printing and painting industries [5, 6]. pNP is produced as a byproduct of the production of pesticides, herbicides and synthetic dyes [7]. Photocatalysis is a cost-effective method in photodegradation of organic degradation by chemical oxidation, ozonation [8].

Till recent times, a number of methods have been employed for the successful synthesis of CuS nanoparticles by a number of chemical routes like hydrothermal [9, 10] sol- gel [11, 12], chemical precipitation [13, 14], microwave irradiation [15, 16], chemical vapour deposition [17, 18]. The said methods are robust and the materials used are mostly harsh chemicals and lack traits of biocompatibility. Herein we report a cost-effective low temperature driven colloidal synthetic route of CuS nanoparticles using biocompatible block polymer Pluronic F127.

For use in biological systems, the cardinal point that has to be addressed in the synthesis of nanomaterials is its surface functionalization. The surface functionalization using polymers, ionic and non- ionic detergents further restrict the

disadvantage of aggregations. A wise choice of biocompatible surface functionalization should be made thus for the successful synthesis of the nanomaterials. Of recent advancement, block copolymers have gained profound importance for this particular parameter. Apart from the conventional use of biodegradable homopolymers like starch [19,20] gelatin [21,22] PVA [23,24], PVP [25] PEI [26,27] Block copolymers can act as intriguing alternatives as they allow the use of combinations of various chemical structures without macroscopic phase segregation[28-31] along with additional advantages of increased crystallization [32] and its subsequent applications in stabilization of the nanoparticles by self-assembly and attending myriad of important morphological structures [33,34]. The fundamental idea behind block copolymer-based techniques is that functional groups in one polymer block provide a guided site for the nucleation and development of particles, while the other block functions as a capping ligand to prevent the nanoparticles from aggregating as well the altering the morphological details by adjusting the molecular weight of the polymer used in the block [35] that often employs a hydrophilic and hydrophobic core that stabilizes to form a micellar structure [36,37]. Furthermore, because of varied changes in environmental factors such as changes in solvent properties, concentration, pH fluctuations, and temperature changes, linear block copolymer micelles' sizes and forms are dynamically stable and may deform or entirely disassemble [38].

4.1.1 CuS nanoparticles to CuS nanocatalyst: An apt candidate for catalytic reduction of organic pollutant *p*-nitrophenol

Of all the organic pollutants and dyes, para nitrophenol (*p*NP) is most widely used in fungicide [39,40], in the preparation of the well- known insecticide parathion and paraoxon [41,42] and in leather industries as a fungicide [43] and in various other industrial applications. *p*NP is a derivative of phenol and is highly a skin irritant and can cause extreme levels of water contamination when the influx in water occurs at a concentration of 37.3mg/l [44]. Erstwhile reports about various nitroaromatic rings have thrown much light regarding their genotoxic potential for their propensity of getting converted to arylhydroxy amines or to esters of hydroxyamine via reduction, and this hints at *p*NP also as the cellular DNA contains nucleophilic centres as in the guanine residues which are a bull's eye for electrophiles like nitrogen atoms predominant in the *p*NP ring [45]. Besides, *p*NP is also reported to be one of the

vicious endocrine disrupting agents interacting with various androgen and estrogen receptors and typically binds with androgen co-regulators like FK1 [46].

Thus, it necessitates the search for agents that will either degrade the anthropogenic contaminant or may transform it into a comparatively less toxic product. Photocatalysis is already in vogue for such a phenomenon and the source of light and choice of catalyst have thus become two cardinal factors in meeting such a mammoth challenge. Encompassing right from natural solar light, other visible sources like mercury lamps, halogen lamps and Ultraviolet radiation- the method to degrade the pollutant becomes not just time - consuming but uneconomical. Solar light, though natural, is discrete and discontinuous and degradation ventures will depend largely on the intensity of the solar irradiation. Secondly, the choice of a number of different commercially available catalysts is being used for the possible remediation of the carcinogen. In an approach to convert a contaminant from one particular product to the other there has been the development of Advanced Oxidation Processes (AOPs) which completely degrades or destroys the pollutant [47-49]. In this process of heterogeneous catalysis keeping various adsorbents at bay that serves to work via adsorption, a number of transitional metals are recruited to effectively carry out the function. Moreover, oxides and chalcogenides, by virtue of their band gap under the action of sources of light energy, bring about a series of either oxidation or reduction reactions. Here, an electron hole gets generated when the photonic energy is received when an electron from the valence band gets transferred to the conduction band, initiating a redox reaction [50].

Keeping in mind the above drawbacks of using an external source of light to initiate a catalytic reaction, a reduction process is being carried out using sodium borohydride ($NaBH_4$) which triggers the reaction at room temperature by liberating out H_2 gas which aids in the reduction reaction [51] and consequently it converts the genotoxic *p*NP into Para aminophenol (*p*AP) that has wider applications in the field of sensing and pharmaceutical industries [52, 53].

4.2 METHODOLOGY

4.2.1Materials Required

Block Copolymer Pluronic F127 was purchased from Sigma Aldrich, Copper Chloride dihydrate ($CuCl_2. 2H_2O$), Sodium Sulphide (Na_2S), Sodium Borohydride ($NaBH_4$) and Para Nitrophenol (*p*NP), was obtained from Merck India. The reagents are all of analytical grade and were used throughout the experiment without any further purification. Millipore water (resistivity ~ 18.2 MΩ-cm) was used throughout the experiment.

4.2.2 Preparation of CuS nanoparticles

Colloidal CuS was synthesized via the reflux condensation method using the biocompatible copolymer Pluronic F127. The colloidal solution was prepared by adding 20ml of 0.1ml $CuCl_2$ to previously prepared 60ml of 1% block copolymer solution. The entire solution was heated at 70⁰C for 1hr in a reflux condenser kept in an oil bath. After that, slow addition of the same volume of 0.1ml Na_2S solution was added and reflux was continued by further stirring a magnetic stirrer for 2hrs. A subsequent colour change was noticed from blue to brown and ultimately green sol. The resulting colloidal solution was centrifuged at 18,000rpm and washed repeatedly with deionized water to remove excess impurities and the resulting greenish black precipitate was dried at 60⁰C and grounded in a pestle mortar to obtain fine powder. About 1000mg of the powdered sample was obtained from this batch synthesis.

4.2.3 Characterizations of synthesized Pluronic F-127 Capped CuS NP:

The formation of the chalcogenide nanomaterial was determined through X-ray crystallography, the percentage distribution of the nanoparticles was judged through Dynamic Light Scattering (DLS), the presence of different functional groups was determined via Fluorescence spectroscopy (FTIR) measurements, the optical characterizations as well as the degradation of organic compounds was assessed through UV- Visible spectrophotometry. The morphological structure and the average size of the nanomaterial were confirmed through scanning electron microscopy (SEM) and Transmission electron microscopy (TEM) techniques. Dynamic light Scattering was performed using Nano ZS Zetasizer, Nanoseies Malvern.

4.2.4 Catalytic reduction of *p*NP to *p*AP

For successfully carrying out the reduction of *p*NP in a quartz cuvette to a 150 µL of 15mg/mL of *p*NP solution, about 100 µL of freshly prepared NaBH$_4$ solution at a concentration of 0.1M solution was added dropwise that contains 2.5ml of Millipore water. To initiate the reduction process, CuS nanoparticles at a concentration of 0.5mg were added to initiate the reaction. The variation of different concentrations of catalyst (0.5mg/ml, 1mg/ml, and 2mg/ml) was monitored at a fixed *p*NP concentration of 50mg/ml. The entire reaction was conducted at room temperature.

The intensity of the reaction was monitored through UV-Vis spectrophotometer for the conversion of *p*NP to *p*AP. The conversion percentage was measured using the formula:

$$\% \text{ of Degradation} = (1 - C/C_0) \times 100 \dots \text{ eq (4.1)}$$

Where C_0 is the initial intensity of absorption of *p*NP and C is the intensity of absorption of *p*NP at varying intervals of time.

4.3 RESULTS & DISCUSSIONS

4.3.1 Material Characterization and Morphological Analyses

The successful synthesis of the chalcogenide nanomaterial and its subsequent crystallinity and phase determination was confirmed through X-ray diffraction measurements. The X-ray diffraction pattern in Fig 4.1 showed the major diffraction peaks at 27.85º, 29.51º, 32.17º, 48.07º corresponding to the lattice peaks (101), (102), (006) and (110) which matches with the JCPDS 06-0464 [54] and confirms well indexed and perfect hexagonal covellite nature of CuS nanoparticles. The smaller deflections as shown in the table can be assumed due to the presence of block copolymer functionalization.
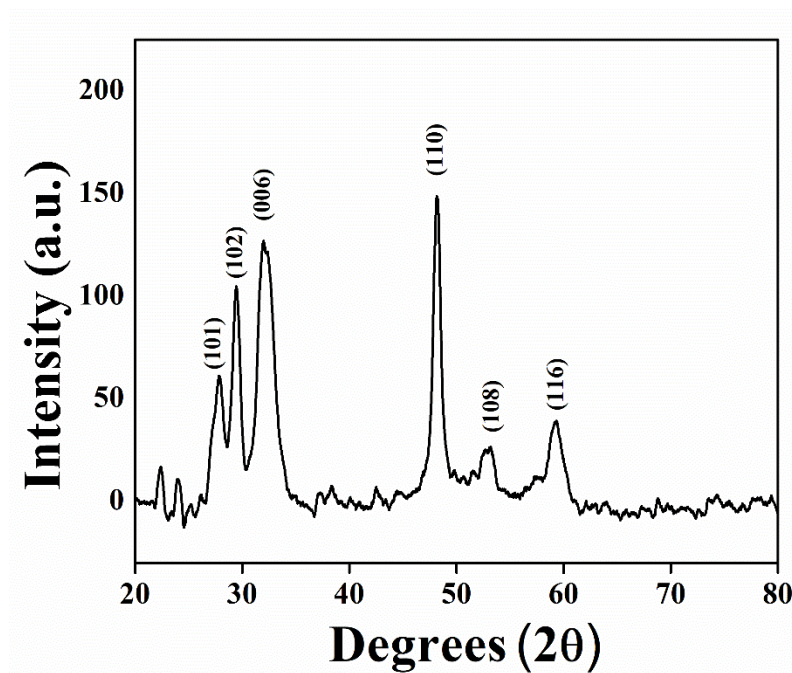
Fig 4.1: XRD spectrum of the synthesized CuS nanoparticles with reference to JCPDS 06-0464 [54]

However, the tentative reaction mechanism as speculated from earlier reports can be deduced as Na_2S is used as a sulphur source. It can be understood that the Na_2S undergoes dissociation between Na+ and S_2- which at once react with the copper ions present as Cu2+ released from Copper Chloride salt ($CuCl_2$. $2H_2O$) to form CuS nanoparticles [55]. This eventually leads to a mixture of nanoplates and complex microstructures [56]. Na_2S being water soluble and used in a 1:1 ratio with and Pluronic F-127 being used as a stabilizer, Na_2S forms a micelle droplet with $CuCl_2$ [57]. The reaction can be presumed as:

$$Cu^{2+} + \text{Pluronic F-127} \longrightarrow [\text{Cu-Pluronic F127}]^{2+} \;\;.... \text{eq (4.2)}$$

$$Na_2S \longrightarrow Na^+ + S^{2-} .... \text{eq (4.3)}$$

$$[\text{Cu-Pluronic F127}]^{2+} + S^{2-} \longrightarrow CuS \;\;.... \text{eq (4.4)}$$
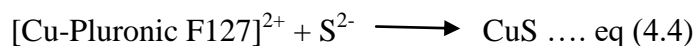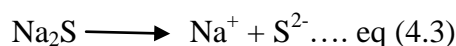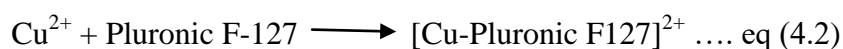
Raman spectroscopy of the nanomaterial was carried out that showed a sharp peak at $468cm^{-1}$ which corroborates with earlier literature reports that point out the fact that the peak arises due to the stretching vibrations of the S-S stretching arising due to the sulphide released out of Na_2S and a feeble band at $263cm^{-1}$ was due to the $A_{1g}TO$ stretching mode [58] conspicuous that can be assumed due to the surface functionalization of the Pluronic F-127.
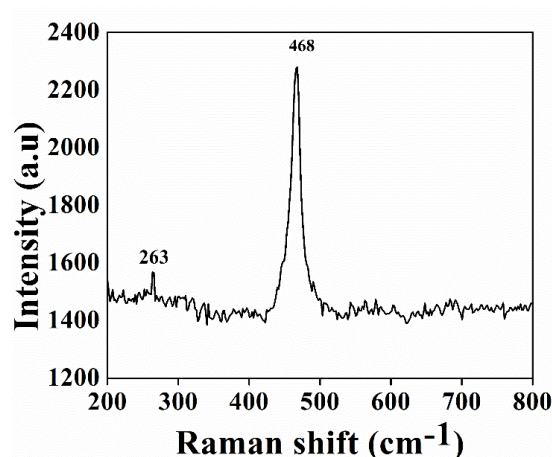
Fig: 4.2: The Raman spectroscopy of the synthesized CuS nanoparticle

The surface morphology of the synthesized nanoparticles was ascertained using FESEM. The nanoparticles show the aggregated nature, most of which are mostly spherical form and range in nano regime and further the tentative size of the nanoparticle was judged through TEM which was found in the range of 10nm when viewed with a JEOL-JEM 2010 Transmission electron microscope when the sample was fixed at a carbon-coated copper grid material.
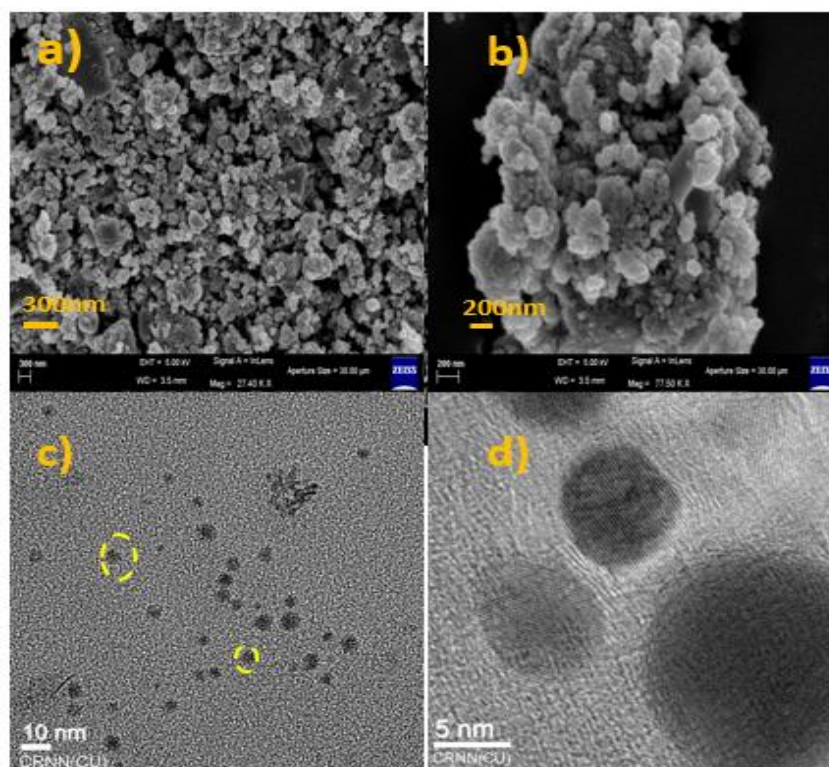
Fig 4.3: a) and b) FESEM photographs of the synthesized CuS nanoparticle; c) and d) TEM and HRTEM micrographs showing the particles are in nano-regime.

The elemental composition of the synthesized nanomaterial was judged through EDAX analysis and the individual atomic percentage of copper was found to be 58.46% whereas the atomic concentration of sulphur was found to be 41.54%. The average hydrodynamic size of the CuS nanomaterial established through Dynamic Light Scattering (DLS) results is revealed to be centring around 7.84 nm.
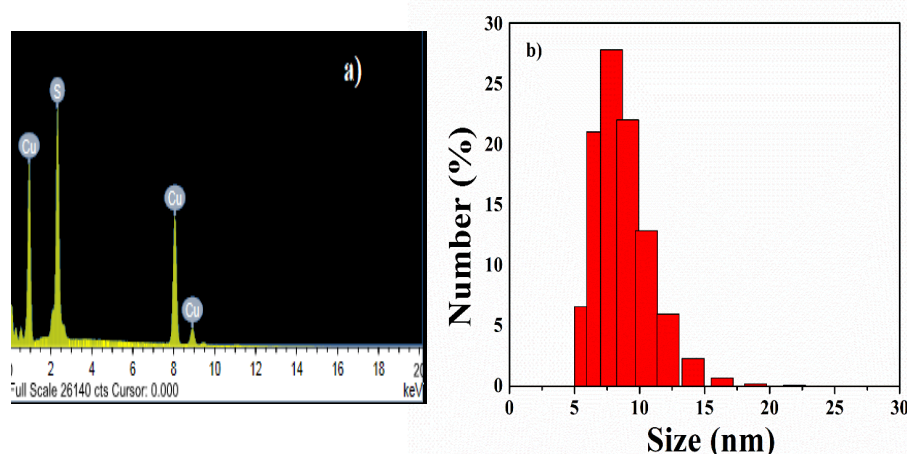
Fig 4.4: a) The EDAX spectrum of the CuS nanoparticles b) Average distribution of CuS nanoparticles as depicted by the Dynamic Light Scattering

4.3.2 Optical Quality Assessment:

The synthesized nanoparticle is primarily aimed at studying the degradation of an organic compound. With this target, the optical quality of the synthesized nanoparticle was recorded using an UV-Vis Spectrophotometer. The spectrum revealed that the synthesized nanomaterial has a small discernible hump between 400-500nm that corroborates with the earlier reports that the CuS nanostructures absorb the wavelength of ultraviolet radiation and consequently the atoms constituting the nanoparticle reach the excitation state [59] while a strong absorption peak was observed at >800nm at the infrared region, which is a typical characteristic of the covellite nature of the CuS nanoparticle. This absorption at greater wavelength is explained by the fact that as the size of the particle gets diminished, the wavelength gets increased, a phenomenon associated with the free electron carriers that undergo considerable scattering effect [60]. Moreover, as reported in earlier texts, the presence of the free electron carriers in metal systems exhibits surface plasmon resonance (SPR) peak [61]. Thus, this phenomenon of absorption at both the visible as well as in

the infrared region makes CuS nanoparticles an excellent candidate for dye degradation and reduction applications.
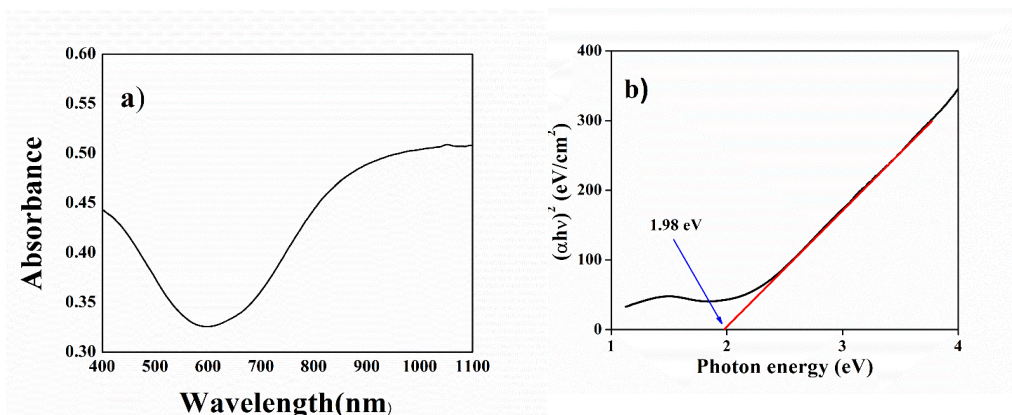
Fig 4.5: a) The UV-Vis spectroscopy and the b) Tauc plot determining the optical band gap of the CuS nanomaterial

The Tauc plot for estimating the band gap of the synthesized semi-conductor nanomaterial was done with photon energy vs a plot of $(\alpha h v)_2$. The calculated direct band gap was found to be 1.98eV. This narrow band gap obtained makes the nanomaterial an efficient candidate for subsequent catalytic reaction.

4.3.3 Reduction of *p*NP to *p*AP

*p*NP when dissolved in water has an absorbance maximum of 317nm. Upon addition of NaBH$_4$ there is generation of *p* nitrophenolate ion and that shifts the absorbance spectra upon deprotonation. This is brought about by a change in pH of the solution and the absorbance peak gets a bathochromic shift to 400nm [62, 63] a characteristic of the *p*-nitrophenolate ion with a concomitant deep yellow colouration of this nitrophenolate ion. The addition of only NaBH$_4$ to the *p*NP solution was made and no reduction in the peak was observed when monitored for 30mins hereby proving that the reduction process is a catalytic dependant reaction. Subsequently the addition of the nano-catalyst caused a reduction in the intensity of the 400nm peak and the emergence of a new peak at 295nm, a characteristic attributed to the formation of *p*AP formation by 15mins there is almost 97% reduction of the *p*NP as shown in Fig 4.6 a. The kinetics of the reaction was seen to follow a pseudo first-order reaction using the following equation:

$$\ln (C_t/C_0)= kt \ \ \dots\dots eq\ (4.5)$$
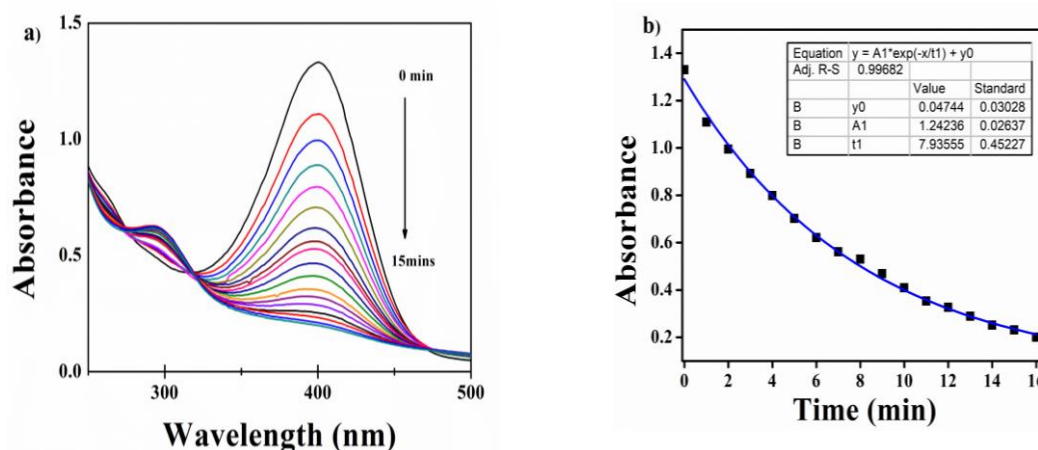
Fig 4.6: a) Catalytic reduction of *p*NP to *p*AP within 15 mins after addition of the nano-catalyst, a decrease in the absorbance peak at 400nm was observed with subsequent addition of the catalyst; b) Absorption kinetics of the nanoparticles depicting the pseudo first order reaction

Where C_t indicates the concentration of *p*NP at a given time t, C_0 denotes the concentration at time 0, i.e when no catalyst was added and the rate constant was given by k which is a reciprocal of t. The value of k can be obtained by the decrease in the intensity of the 400nm peak of the phenolate ion over time. The pseudo first-order reaction kinetics showed that the rate constant k of the reaction is 238×10^{-3} min (Fig 4.6b).
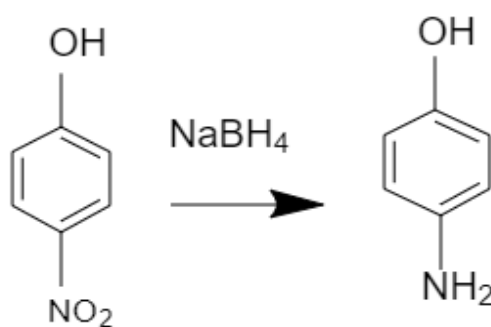
Fig 4.7: Structural representation of conversion of *p* Nitrophenol (*p*NP) to *p*- Aminophenol (*p*AP) under the action of $NaBH_4$ (Structural presentation was drawn through ChemDraw Software)

4.3.4 Effect of varying concentration of the *p*NP, catalyst and pH:

The evaluation of the rate constants was also observed at a fixed lowest nano-catalyst concentration of 0.5mg and a varying concentration of *p*NP (15g/ml, 25mg/ml, 50mg/ml). It was observed the rate of reduction decreased with increased concentration of *p*NP. The plausible explanation for such a phenomenon can be given by the explanation that the active site of the catalyst gets occupied with the increase in the concentration of the *p*NP molecule [64] [Fig 4.7 a)]. The rate constants are all depicted in Table 4.1
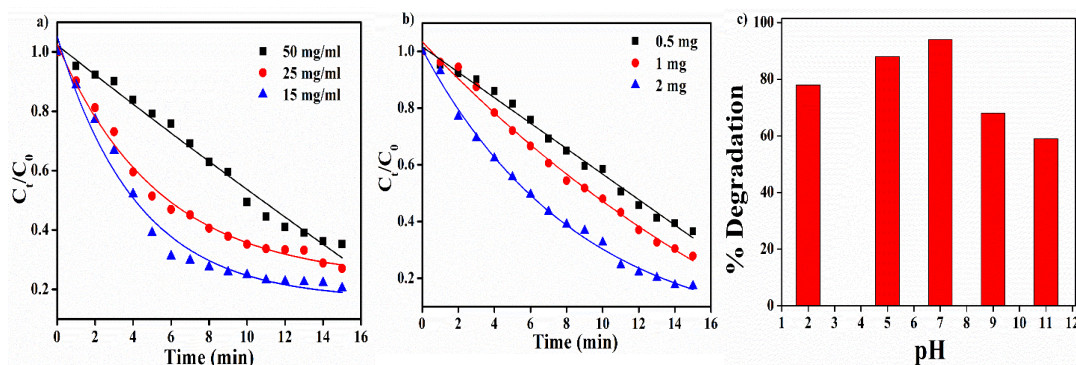
Fig 4.8: a) Kinetics for the reduction of *p*NP with increasing dye concentration at a fixed concentration of the nano-catalyst, b) Kinetics at a fixed concentration of dye at varying concentration of the nano-catalyst c) The percentage of degradation was observed at different pH ranges that shows that stability of CuS nanoparticles to perform at different pH conditions

On the contrary by increasing the concentration of the nano catalyst (0.5mg-2mg) and keeping the highest concentration of the *p*NP (50mg/mL), the rate of reduction as depicted from the dye degradation increases as the accessible nanoparticle catalytic sites becomes exposed for the interaction of dye molecules with more surface to volume ratio of the nanoparticles [65] and hence enhanced rate of degradation was observed which is shown in Fig 4.7 b.

The stability of the nanoparticles to perform as a catalyst was tested under different conditions of pH. At a constant *p*NP concentration of 15mg/ml it was seen that the nanoparticles work best at an alkaline pH (Fig 4.7 c). Previous reports have hinted, about this phenomenon, that the deprotonation of the *p*NP is reduced when the pH of the medium is increased above pH 10 [66].

Table 4.1: *p*NP degradation and rate constants at varying conditions

a) **Varying concentration of *p*NP**

Concentration (mg/ml)	Rate Constant(k) (min^{-1})
15	238 x 10^{-3}
25	185 x 10^{-3}
50	7.54 x 10^{-3}

b) **Varying concentration of the catalyst**

Concentration (mg)	Rate Constant (k) (min^{-1})
0.5	7.54 x10^{-3}
1	38.47 x 10^{-3}
2	115 x 10^{-3}

4.3.5 Possible Reaction Mechanism:

The putative reaction mechanism of the reduction process can be explained through the Langmuir Hinshelwood model. The NaBH$_4$ acts as a hydrogen source and participates in the process of transferring the hydrogen to *p*NP and thereby converting it into a para- nitrophenolate ion. There occurs. The BH$_4$ ion serves as an electron donor where it transfers electrons to *p*NP. The CuS nano-catalyst has on its surface the absorbed [67]. It is seen that the catalytic action is best at low pH values, the BH$_4$ ions are negatively charged and it gets adsorbed on the surface of the nano-catalyst. The porous structure of the CuS nanoparticles further facilitates the transfer of electrons that readily aids in the formation of *p* amino phenol (*p*AP) from *p*NP.

4.3.6 Recyclability of the nano-catalyst:

Recyclability counts as one of the most important parameters to judge the efficacy of the nanoparticle in performing the catalytic reaction. Our synthesized nanomaterial was tested for its catalytic stability. After one round of catalytic action, the nanomaterial was separated out of the reaction mixture, washed thoroughly with Millipore water and was centrifuged at about 8,000rpm to remove residual impurities and then dried in vacuum. After drying in vacuum, the sample was further pestled and mortared and then a second round of catalytic performance was done. There was no significant change in catalytic efficiency observed and it was about 80 %, but in the 3rd and 4th cycles the reduction efficiency was 76% and 72% respectively, as depicted in Fig 4. This gradual decrease can be explained by the fact that some reduced product of the contaminant has blocked the catalytic sites of the nanomaterial, yet even after this, much of the catalytic efficiency has been retained.
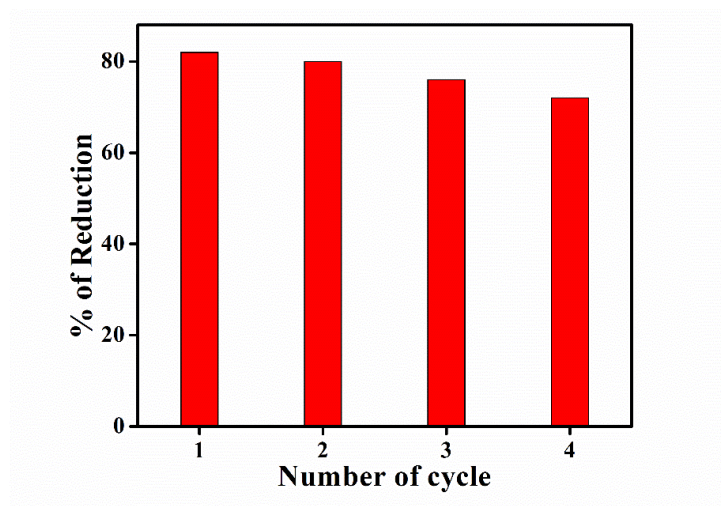
Fig 4.9: Recyclability of the Pluronic F127 capped CuS nanocatalyst against *p*NP after 4 cycles.

4.4 SUMMARY:

This experimental work deals with the synthesis of a biocompatible block copolymer-based chalcogenide nanoparticle via low temperature reflux condensation method. The characterization of the synthesized nanomaterial with the help of X-ray Crystallography, Raman Spectroscopy and morphology analysis via SEM and TEM has been successful in establishing the successful synthesis of the nanomaterial. The polymer-based nanomaterial has been harnessed in the process of catalytic reduction

of an organic pollutant *p*NP. A spectrophotometric monitoring of its reduction was observed that the nanomaterial is efficient enough in reducing anthropogenic carcinogens, thereby proving itself to have a significant candidate in water remediation strategies. Though earlier reports have thrown a lot of light regarding the potential of the nanomaterial in reducing the mentioned, contaminant, this work mainly focus on the multifaceted ability of the nanomaterial where the synthesis has been via use of cheap and harmless precursors at low temperatures and also the functionalization of a biocompatible polymer will further facilitate its use in biological applications which will be discussed in the next chapter.

REFERENCES:

1. McMullan, G., Meehan, C., Conneely, A., Kirby, N., Robinson, T., Nigam, P., ... & Smyth, W. F. (2001). Microbial decolourisation and degradation of textile dyes. *Applied microbiology and biotechnology*, *56*(1), 81-87.

2. Pereira, L., & Alves, M. (2012). Dyes—environmental impact and remediation. In *Environmental protection strategies for sustainable development* (pp. 111-162). Springer, Dordrecht.

3. Yusuf, M. (2019). Synthetic dyes: a threat to the environment and water ecosystem. *Textiles and clothing*, 11-26.

4. Ayodhya, D., Venkatesham, M., Santoshi Kumari, A., Reddy, G. B., Ramakrishna, D., & Veerabhadram, G. (2016). Photocatalytic degradation of dye pollutants under solar, visible and UV lights using green synthesised CuS nanoparticles. *Journal of Experimental Nanoscience*, *11*(6), 418-432.

5. Jadhav, R. S., Mane, V., Bagle, A. V., Hundiwale, D. G., Mahulikar, P. P., & Waghoo, G. (2013). Synthesis of multicore phenol formaldehyde microcapsules and their application in polyurethane paint formulation for self-healing anticorrosive coating. *International Journal of Industrial Chemistry*, *4*(1), 1-9.

6. Koli, P. B., Kapadnis, K. H., & Deshpande, U. G. (2018). Study of physico-chemical properties, detection and toxicity study of organic compounds from effluent of MIDC Thane and GIDC Ankleshwar industrial zone. *Applied Water Science*, *8*(7), 1-9.

7. Pozun, Z. D., Rodenbusch, S. E., Keller, E., Tran, K., Tang, W., Stevenson, K. J., & Henkelman, G. (2013). A systematic investigation of p-nitrophenol reduction by bimetallic dendrimer encapsulated nanoparticles. *The Journal of Physical Chemistry C*, *117*(15), 7598-7604.

8. San, N., Hatipoğlu, A., Koçtürk, G., & Çınar, Z. (2002). Photocatalytic degradation of 4-nitrophenol in aqueous TiO2 suspensions: theoretical prediction of the intermediates. *Journal of Photochemistry and Photobiology A: Chemistry*, *146*(3), 189-197.

9.   Saranya, M., Santhosh, C., Augustine, S. P., & Grace, A. N. (2014). Synthesis and characterisation of CuS nanomaterials using hydrothermal route. *Journal of Experimental Nanoscience*, *9*(4), 329-336.

10. Selvi, S. S. T., Linet, J. M., & Sagadevan, S. (2018). Influence of CTAB surfactant on structural and optical properties of CuS and CdS nanoparticles by hydrothermal route. *Journal of Experimental Nanoscience*, *13*(1), 130-143.

11. Riyaz, S., Parveen, A., & Azam, A. (2016). Microstructural and optical properties of CuS nanoparticles prepared by sol–gel route. *Perspectives in Science*, *8*, 632-635.

12. Rahman, M. M., Ahmed, J., & Asiri, A. M. (2022). Ultra-sensitive, selective, and rapid carcinogenic 1, 2-diaminobenzene chemical determination using sol–gel coating low-dimensional facile CuS modified-CNT nanocomposites by electrochemical approach. *Microchemical Journal*, *175*, 107230.

13. Freeda, A. M., Madhav, R. N., Mahadevan, C. K., & Ramalingom, S. (2010). Synthesis and characterization of nano-structured materials CuS (Covellite) for their applications. *Nanotechnol. Nanosci*, *1*, 976-7630.

14. Subramanyam, K., Sreelekha, N., Reddy, D. A., Murali, G., Varma, K. R., & Vijayalakshmi, R. P. (2017). Chemical synthesis, structural, optical, magnetic characteristics and enhanced visible light active photocatalysis of Ni doped CuS nanoparticles. *Solid State Sciences*, *65*, 68-78.

15. Nafees, M., Ali, S., Idrees, S., Rashid, K., & Shafique, M. A. (2013). A simple microwave assists aqueous route to synthesis CuS nanoparticles and further aggregation to spherical shape. *Applied Nanoscience*, *3*, 119-124.

16. Nethravathi, C., Rajamathi, J. T., & Rajamathi, M. (2019). Microwave-assisted synthesis of porous aggregates of CuS nanoparticles for sunlight photocatalysis. *ACS omega*, *4*(3), 4825-4831.

17. Saeed, S., Rashid, N., Hussain, R., Malik, M. A., O'Brien, P., & Wong, W. T. (2013). Semiconducting nanostructured copper sulfide thin films from bidentate copper (ii) complexes of N-(dialkylcarbamothioyl)-nitrosubstituted benzamides by chemical vapour deposition. *New Journal of Chemistry*, *37*(10), 3214-3221.

18. Khan, M. D., Malik, M. A., Akhtar, J., Mlowe, S., & Revaprasadu, N. (2017). Phase pure deposition of flower-like thin films by aerosol assisted chemical vapor deposition and solvent mediated structural transformation in copper sulfide nanostructures. *Thin Solid Films*, *638*, 338-344.

19. Mohanty, S., Mishra, S., Jena, P., Jacob, B., Sarkar, B., & Sonawane, A. (2012). An investigation on the antibacterial, cytotoxic, and antibiofilm efficacy of starch-stabilized silver nanoparticles. *Nanomedicine: Nanotechnology, Biology and Medicine*, *8*(6), 916-924.

20. Kumar, S. V., Bafana, A. P., Pawar, P., Rahman, A., Dahoumane, S. A., & Jeffryes, C. S. (2018). High conversion synthesis of< 10 nm starch-stabilized silver nanoparticles using microwave technology. *Scientific reports*, *8*(1), 1-10.

21. Zhang, D., & Yang, H. (2013). Gelatin-stabilized copper nanoparticles: synthesis, morphology, and their surface-enhanced Raman scattering properties. *Physica B: Condensed Matter*, *415*, 44-48.

22. Gvozdenko, A. A., Siddiqui, S. A., Blinov, A. V., Golik, A. B., Nagdalian, A. A., Maglakelidze, D. G., ... & Ibrahim, S. A. (2022). Synthesis of CuO nanoparticles stabilized with gelatin for potential use in food packaging applications. *Scientific reports*, *12*(1), 1-24.

23. Wang, X., Yu, F., Xie, C., & Yu, S. (2018). Highly selective hydrogenation of α-pinene in aqueous medium using PVA-stabilized Ru nanoparticles. *Molecular Catalysis*, *444*, 62-69.

24. Ali, Z. I., Ghazy, O. A., Meligi, G., Saleh, H. H., & Bekhit, M. J. J. O. I. (2018). Copper nanoparticles: Synthesis, characterization and its application as catalyst for p-nitrophenol reduction. *Journal of Inorganic and Organometallic Polymers and Materials*, *28*(3), 1195-1205.

25. Kale, R. D., & Kane, P. B. (2018). Synthesis of PVP stabilized bimetallic nanoparticles for removal of azo based reactive dye from aqueous solution. *Sustainable Chemistry and Pharmacy*, *10*, 153-162.

26. Kamburova, K., Boshkova, N., Boshkov, N., & Radeva, T. (2021). Composite coatings with polymeric modified ZnO nanoparticles and nanocontainers with inhibitor for corrosion protection of low carbon steel. *Colloids and Surfaces A: Physicochemical and Engineering Aspects*, *609*, 125741.

27. Raja, D. A., Shah, M. R., & Malik, M. I. (2022). Polyethyleneimine stabilized silver nanoparticles as an efficient and selective colorimetric assay for promethazine. *Analytica Chimica Acta*, *1223*, 340216.

28. Blanazs, A., Warren, N. J., Lewis, A. L., Armes, S. P., & Ryan, A. J. (2011). Self-assembly of double hydrophilic block copolymers in concentrated aqueous solution. *Soft Matter*, *7*(14), 6399-6403.

29. Huang, S., & Jiang, S. (2014). Structures and morphologies of biocompatible and biodegradable block copolymers. *RSC Advances*, *4*(47), 24566-24583.

30. Hiraguchi, Y., Kushiro, K., & Takai, M. (2016). Formation of reversed nanoscale phase-separated structures using poly (2-methacryloyloxyethyl phosphorylcholine)-based amphiphilic block copolymers. *Polymer*, *99*, 166-172.

31. Schmidt, B. V. (2018). Double Hydrophilic Block Copolymer Self-Assembly in Aqueous Solution. *Macromolecular Chemistry and Physics*, *219*(7), 1700494.

32. Jiang, S., He, C., An, L., Chen, X., & Jiang, B. (2004). Crystallization and Ring-Banded Spherulite Morphology of Poly (ethylene oxide)-block-Poly (ε-caprolactone) Diblock Copolymer. *Macromolecular Chemistry and Physics*, *205*(16), 2229-2234.

33. Ray, D., Aswal, V. K., & Kohlbrecher, J. (2011). Synthesis and characterization of high concentration block copolymer-mediated gold nanoparticles. *Langmuir*, *27*(7), 4048-4056.

34. Li, X., Iocozzia, J., Chen, Y., Zhao, S., Cui, X., Wang, W., ... & Lin, Z. (2018). From precision synthesis of block copolymers to properties and applications of nanoparticles. *Angewandte Chemie International Edition*, *57*(8), 2046-2070.

35. Chai, J., Wang, D., Fan, X., & Buriak, J. M. (2007). Assembly of aligned linear metallic patterns on silicon. *Nature Nanotechnology*, *2*(8), 500-506.

36. Jeong, Y. I., Nah, J. W., Lee, H. C., Kim, S. H., & Cho, C. S. (1999). Adriamycin release from flower-type polymeric micelle based on star-block copolymer composed of poly (γ-benzyl l-glutamate) as the hydrophobic part and poly (ethylene oxide) as the hydrophilic part. *International journal of pharmaceutics*, *188*(1), 49-58.

37. Feng, Z., Lin, L., Yan, Z., & Yu, Y. (2010). Dual responsive block copolymer micelles functionalized by NIPAM and azobenzene. *Macromolecular rapid communications*, *31*(7), 640-644.

38. Bakshi, M. S. (2014). Colloidal micelles of block copolymers as nanoreactors, templates for gold nanoparticles, and vehicles for biomedical applications. *Advances in colloid and interface science*, *213*, 1-20.

39. Berk, S. (1948). Fungicides for Fungus-Proofing Glue-Glycerol-Bonded Cork Gaskets. *Industrial & Engineering Chemistry*, *40*(2), 262-267.

40. Bhatti, Z. I., Toda, H., & Furukawa, K. (2002). p-Nitrophenol degradation by activated sludge attached on nonwovens. *Water Research*, *36*(5), 1135-1142.

41. Ketelaar, J. A. A., & Hellingman, J. E. (1951). Chemical studies on insecticides. Determination of parathion and dimethylparathion. *Analytical Chemistry*, *23*(4), 646-650.

42. Hostert, L., Blanc, C., Zarbin, A. J., Anglaret, E., & Orth, E. S. (2021). SERS detection and comprehensive study of p-nitrophenol: towards pesticide sensing. *New Journal of Chemistry*, *45*(8), 3886-3891

43. Yin, H., Zhou, Y., Ai, S., Liu, X., Zhu, L., & Lu, L. (2010). Electrochemical oxidative determination of 4-nitrophenol based on a glassy carbon electrode modified with a hydroxyapatite nanopowder. *Microchimica acta*, *169*(1), 87-92.

44. Muniz-Lopez, C., Duconge, J., & Roque-Malherbe, R. (2009). Paranitrophenol liquid-phase adsorption in dealuminated Y zeolite. *Journal of colloid and interface science*, *329*(1), 11-16.

45. Eichenbaum, G., Johnson, M., Kirkland, D., O'neill, P., Stellar, S., Bielawne, J., ... & Tonelli, A. (2009). Assessment of the genotoxic and carcinogenic risks of p-nitrophenol when it is present as an impurity in a drug product. *Regulatory Toxicology and Pharmacology*, *55*(1), 33-42.

46. Wu, D., Tao, X., Chen, Z. P., Han, J. T., Jia, W. J., Zhu, N., ... & He, Y. X. (2016). The environmental endocrine disruptor p-nitrophenol interacts with FKBP51, a positive regulator of androgen receptor and inhibits androgen receptor signaling in human cells. *Journal of hazardous materials*, *307*, 193-201.

47. Zhou, M., & He, J. (2007). Degradation of azo dye by three clean advanced oxidation processes: wet oxidation, electrochemical oxidation and wet electrochemical oxidation—a comparative study. *Electrochimica Acta*, *53*(4), 1902-1910.

48. Wang, J. L., & Xu, L. J. (2012). Advanced oxidation processes for wastewater treatment: formation of hydroxyl radical and application. *Critical reviews in environmental science and technology*, *42*(3), 251-325.

49. Khakyzadeh, V., Rezaei-Vahidian, H., Sheikhaleslami, S., & Azimi, S. B. (2021). Modelling and optimisation of p-nitrophenol removal process using homogeneous photo-periodate (UV/KPI) advanced oxidation process. *International Journal of Environmental Analytical Chemistry*, 1-12.

50. Litter, M. I. (1999). Heterogeneous photocatalysis: transition metal ions in photocatalytic systems. *Applied catalysis B: environmental*, *23*(2-3), 89-114.

51. Rakap, M., & Özkar, S. (2012). Hydroxyapatite-supported cobalt (0) nanoclusters as efficient and cost-effective catalyst for hydrogen generation from the hydrolysis of both sodium borohydride and ammonia-borane. *Catalysis today*, *183s*(1), 17-25.

52. Ekinci, E., Karagözler, A. A., & Karagözler, A. E. (1996). The preparation and sensor application of poly (p-aminophenol). *Electroanalysis*, *8*(6), 571-574.

53. Mohamed, F. A., AbdAllah, M. A., & Shammat, S. M. (1997). Selective spectrophotometric determination of p-aminophenol and acetaminophen. *Talanta*, *44*(1), 61-68.

54. Raj, S. I., Jaiswal, A., & Uddin, I. (2020). Ultrasmall aqueous starch-capped CuS quantum dots with tunable localized surface plasmon resonance and composition for the selective and sensitive detection of mercury (ii) ions. *RSC advances*, *10*(24), 14050-14059

55. Mageshwari, K., Mali, S. S., Hemalatha, T., Sathyamoorthy, R., & Patil, P. S. (2011). Low temperature growth of CuS nanoparticles by reflux condensation method. *Progress in Solid State Chemistry*, *39*(3-4), 108-113.

56. Zhang, Y. Q., Zhang, B. P., Ge, Z. H., Zhu, L. F., & Li, Y. (2014). Preparation by solvothermal synthesis, growth mechanism, and photocatalytic performance of CuS nanopowders. *European Journal of Inorganic Chemistry*, *2014*(14), 2368-2375

57. Yu, X. L., Cao, C. B., Zhu, H. S., Li, Q. S., Liu, C. L., & Gong, Q. H. (2007). Nanometer-sized copper sulfide hollow spheres with strong optical-limiting properties. *Advanced Functional Materials*, *17*(8), 1397-1401.

58. Pal, M., Mathews, N. R., Sanchez-Mora, E., Pal, U., Paraguay-Delgado, F., & Mathew, X. (2015). Synthesis of CuS nanoparticles by a wet chemical route and their photocatalytic activity. *Journal of Nanoparticle Research*, *17*, 1-12.

59. Ahmed, H. M. (2016). Shujahadeen B. Aziz, Rebar T. Abdulwahid, Hazhar A. Rsaul &. *J Mater Sci: Mater Electron*, *27*, 4163-4171

60. Saranya, M., Santhosh, C., Ramachandran, R., & Nirmala Grace, A. (2014). Growth of CuS nanostructures by hydrothermal route and its optical properties. *Journal of Nanotechnology*, *2014*.

61. Aziz, S. B., Abdulwahid, R. T., Rsaul, H. A., & Ahmed, H. M. (2016). In situ synthesis of CuS nanoparticle with a distinguishable SPR peak in NIR region. *Journal of Materials Science: Materials in Electronics*, *27*, 4163-4171.

62. Zhang, W., Tan, F., Wang, W., Qiu, X., Qiao, X., & Chen, J. (2012). Facile, template-free synthesis of silver nanodendrites with high catalytic activity for the reduction of p-nitrophenol. *Journal of Hazardous materials*, *217*, 36-42.

63. Arshad, M., Wang, Z., Nasir, J. A., Amador, E., Jin, M., Li, H., ... & Chen, W. (2021). Single source precursor synthesized CuS nanoparticles for NIR phototherapy of cancer and photodegradation of organic carcinogen. *Journal of Photochemistry and Photobiology B: Biology*, *214*, 112084.

64. Samai, B., & Bhattacharya, S. C. (2018). Conducting polymer supported cerium oxide nanoparticle: Enhanced photocatalytic activity for waste water treatment. *Materials Chemistry and Physics*, *220*, 171-181.

65. Comparelli, R., Fanizza, E., Curri, M. L., Cozzoli, P. D., Mascolo, G., & Agostiano, A. (2005). UV-induced photocatalytic degradation of azo dyes by organic-capped ZnO nanocrystals immobilized onto substrates. *Applied Catalysis B: Environmental*, *60*(1-2), 1-11.

66. Mondal, A., Mondal, A., Adhikary, B., & Mukherjee, D. K. (2017). Cobalt nanoparticles as reusable catalysts for reduction of 4-nitrophenol under mild conditions. *Bulletin of Materials Science*, *40*(2), 321-328.

67. Filiz, B. C. (2020). The role of catalyst support on activity of copper oxide nanoparticles for reduction of 4-nitrophenol. *Advanced Powder Technology*, *31*(9), 3845-3859.

UNRAVELLING THE ANTIMICROBIAL, ANTIOXIDANT POTENCY & CYTOCOMPATIBILITY OF PLURONIC F-127 CAPPED CuS NANOPARTICLES
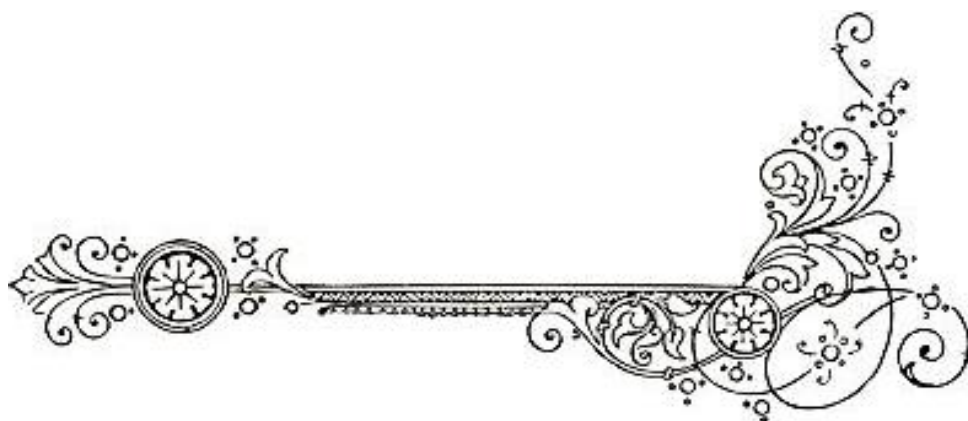
CHAPTER 5

5.1 OVERVIEW:

Nanoparticles are almost always abundant in their applications in the field of biological sciences. From their omnipresence in the field of being potent antimicrobials and drugs in cancer cell remediation semiconductor nanoparticles have made their significant contributions in pharmaceutical industries. Due to the persistence of high multidrug resistance, there is a search of new antimicrobials to meet the conundrum of the resistance. Antibiotics in vogue are currently target three cardinal "bull's eye" related to the bacterial growth - cell wall synthesis, interfering with enzymes of translation and DNA replication. But a matter of fact fatefully none of them can efficiently carry out the function as resistance pattern further resurrect [1]. Nanoparticles because of their large surface to volume ratio has now been chosen as a drug by researchers as there is close immediate contact of bacterial cell wall to that of the nanoparticles without having the need for it to enter into the cell's interior [1]. Of late, an array of transition metals has been utilized in the form of their oxides and sulphides that are used for antimicrobial activity as well as for drug delivery applications [2-4].

Transition metal chalcogenides in contrast to their oxide counterparts have a low band gap by virtue of the sulphide anion having larger radius and their well dispersed 3p orbits. This desirable band energy forms a Trojan horse in its application for photodynamic damage to bacteria [5]. Copper is used as a nutritional supplement [6] in diet, besides copper nanoparticles have wide gained popularity for their vast arena of biological applications [7-10]. Thus, the green covellite form of CuS nanoparticles are long been a preferable choice as antimicrobial agent unlike cadmium sulphide (CdS) of their low toxicity. Additionally, its absorption in the near infrared region CuS nanoparticles form good candidates in photothermal ablation of tumor cells [11]. In the previous chapter, we have seen the performance of the synthesized nanomaterial as a catalyst against waste water remediation from organic phenol derivatives. The nanoparticle is also been judged for its used in filtration purpose by testing against a Gram- negative faecal coliform, *Escherichia coli (E. coli)* and a notorious biofilm

forming Gram positive bacteria *Staphylococcus aureus* (*S.aureus*). The nanoparticle potency against the latter one may further augment its application in topical purpose and wound healing as an alternative to noble nanoparticles like silver and gold [12,13].

With this knowledge there also begins a hunt for exploring antioxidants so that from performing as a good antimicrobial the nanodrug can also behave as a good antioxidant. Before delving into the details of the antioxidant nature of the nanoparticles a brief overview is required about the free radical prevalence arising out of metabolism. Cytochrome oxidase forms the terminal electron acceptor in the electron transport chain where it readily transports the reducing equivalents produced during aerobic oxidation for successful electron transport chain to function with the concomitant production of energy in the form of ATP. In the course of such a reaction an electron is been accepted by the oxygen that should get accepted by an electron carrier in the transport chain, the iron-sulphur centers being the central position for such a catastrophe resulting in the production of a free radical of oxygen ($O_2^{\cdot -}$) [14]. Out of cellular respiration the highly reactive endogenous species that are produced in the body are reactive oxygen species (ROS) like hydroxyl radicals ($OH^{\cdot}$), hydrogen peroxide (H_2O_2) and several reactive nitrogen species (RNS) ($NO_x^{\cdot}$) like nitric oxide radical ($NO^{\cdot}$), nitrogen dioxide radical ($NO_2^{\cdot}$) [15]. The generation of these free radicals that takes place in the body of the organism may initially augment cellular ageing [16,17] and consequently may lead to serious consequences like neuro-degenerative disorders [18,19] culminating in cancer [20].

To combat these oxidative challenges inside the cells a number of antioxidants are available which are in taken in the form of food materials and supplements that protects the cells against lipid peroxidation [21,22]. These antioxidants may trigger in the generation of certain cell signalling pathways or releases enzymes that degrades the production of ROS [23]. For the annihilation of different abnormalities inside the cells an alternative of medicines in the form of nanodrugs has been formulated [24]. A wide array of nanoparticles besides there antimicrobial and anticancer activities as now been harnessed for their broader application as antioxidants. Noble nanomaterials like gold, silver and platinum are been utilized for their use as antioxidants [25, 26].

Our quest in designing a nanodrug that will have multifaceted properties with ancillary properties of biocompatibility is being accomplished by fabricating the CuS nanoparticles with Pluronic F- 127 block copolymer. Pluronics block copolymers are used invariably for their biocompatibility and moreover to mitigate the drawbacks of insolubility of hydrophobic drugs [27]. The Pluronic coated CuS nanoparticles is thus being assessed for scavenging free radicals using 1,1,Diphenyl 2picrylhydrazyl (DPPH).

Lastly *in vitro* investigations of the cytocompatibility of the nanoparticles for its use in the living system was evaluated through haemolytic prevention assay. The percent haemolysis will provide information about the toxicity profile of the nanoparticles but also will give an idea about the extent of the concentrations of the nanoparticle to be used for the above biological applications.

5.2 METHODOLOGY

5.2.1 Materials Required:

Luria- Bertani (LB) media, anhydrous Dextrose ,L-Ascorbic acid, Tris Base, Sodium Chloride (NaCl), Potassium Chloride (KCl) and Magnesium sulphate (MgSO$_4$) was purchased from HiMedia Pvt Ltd, Na-citrate, Citric Acid and 1,1,Diphenyl 2picrylhydrazyl (DPPH) was purchased from Sigma- Aldrich, absolute ethanol (99.9%) was purchased from Merck Germany, Triton X-100 was purchased from Sigma Aldrich, for the preparation of phosphate Buffer saline (PBS) [prepared using disodium hydrogen phosphate (Na$_2$HPO$_4$) and sodium dihydrogen phosphate (NaH$_2$PO$_4$) was purchased from Merck Germany] bacterial strains used for the investigation of antimicrobial testing were *E. coli* (ATCC 25922) and *Staphylococcus aureus* (ATCC 25923). The reagents that were used for the assessing the different biological aspects of the block copolymer capped nanoparticle was thoroughly used of analytical grade. The entire biological experiments were performed using Millipore water of resistivity ~18.2 MΩ-cm. For to maintain aseptic conditions throughout the experiment in case of antimicrobial experiments, glass apparatus including water was autoclaved.

5.2.2 Preparation of starting stock solutions and buffers for biological experimentations:

a) Preparation of PBS saline:

Phosphate Buffer Saline (PBS) being a physiological buffer needs to be prepared for to maintain a stable pH and to aid to carry out different biological experiments. A PBS buffer at a pH of 7.4 was prepared for cytocompatibility testing of the nanoparticles against erythrocytes.

For this 35.6g Na_2HPO_4 (0.2M) was dissolved in 500mL water and 0.85% NaCl was added to it and the pH was adjusted with 31.2g $Na_2H_2PO_4$ (0.2M) to pH 6.8, and the final volume was then made up to 1L (it was observed that addition of NaCl changes the pH slightly so it was added before) the solution was diluted to 1X checked for pH (7.2-7.4) and stored at 4°C.

b) Preparation of DPPH solution

3.3mM of standard DPPH solution was prepared in absolute ethanol using a weighing balance and kept in a coloured bottle in dark.

c) Preparation of Alsever's Solution:

To test for the cytocompatibility of the nanoparticle's haemolysis assay was checked and for that Alsever's solution is required as an anticoagulant. Alsever's solution besides other available anti-coagulants. Alsever's solution is an isotonic solution and has been routinely used for the preservation of red blood cells [28]. Alsever's solution is prepared with slightest modifications using 2.05% dextrose, 0.18% Na-citrate, 0.055% citric acid an 0.42% sodium chloride. About 50mL of Alsever's solution was prepared and was stored in the refrigerator.

5.2.3 Determination of Antimicrobial Activity of the nanoparticles

In an aim to the determine of antibacterial activity of the synthesized nanomaterial, one Gram- negative *Escherichia. coli* ATCC 25922 and another Gram-positive *Staphylococcus aureus* ATCC 25923 was taken. Prior the start of the experiment, all the glass apparatus and the media were thoroughly autoclaved to ensure sterilization. The bacterial cells were first synchronized before the beginning of the antimicrobial assay. For that purpose, test bacteria were grown in a synchronized Luria Broth

Medium and synchronization of the cells were done by a method proposed by Chakraborty *et* al 2015 [29]. The Luria Broth medium was separately inoculated with the said Gram positive and Gram-negative bacterial cells overnight at 37°C. The very next day, the cells were diluted in freshly prepared LB medium and was placed in a rotatory shaker at 37°C and growth of the culture was monitored spectrophotometrically until the optical density (O.D$_{600nm}$) reaches 0.2. The cells were diluted to reach a McFarland standard of 0.5 that corresponds to about 10^8 cells /mL. These cells were washed and centrifuged using 1M starvation buffer at pH 8.0 (prepared through adding KCl, NaCl, Tris Base, $MgSO_4$ and $CaCl_2$ in 1000mL of Millipore water).

An initial stock solution of 1mg/ml CuS nanoparticle was prepared and different concentrations of the nanomaterial starting from, 5µg/ml 15µg/ml, 25µg/ml,35µg/ml,50µg/ml and 100µg/ml for both the bacterial cultures were made. The nanoparticles of the above varying concentrations were added to test tubes containing 3mL of the inoculum containing synchronized broth cultures. A control tube was also kept as a reference which only contains the respective inoculum without the nanomaterial. The tubes containing the broth cultures with the treated and control tubes were incubated overnight in a rotatory shaker. This was also done in an aim to ensure proper mixing of the nanoparticle with the inoculum. The O.D value of each of the samples were taken in triplicate to obtain the standard error. The IC $_{50}$ The viable number of cells was counted using the formula below:

$$\text{\% of Viable bacterial Cells} = (C-T) \times 100 \qquad \ldots \text{eq 5.1}$$

where C is the mean of the control samples and T denotes the mean of the treated samples.

5.2.4 DPPH Free Radical Scavenging Assay by CuS nanoparticles:

For antioxidant assay of the synthesized nanomaterial, DPPH an artificial free radical has been utilized to study about the scavenging activity of the synthesized nanomaterial. DPPH is categorized as a stable free radical due to the delocalization of the electron throughout the molecule [30]. A purple colour is yielded when DPPH reacts with either absolute ethanol or methanol. There will be a reduction in the purple colour when DPPH in its oxidized gets scavenged by any polyphenols or flavonoids or nanoparticles.

Ascorbic acid (Vitamin C) is taken as the positive control for the DPPH free radical scavenging assay.
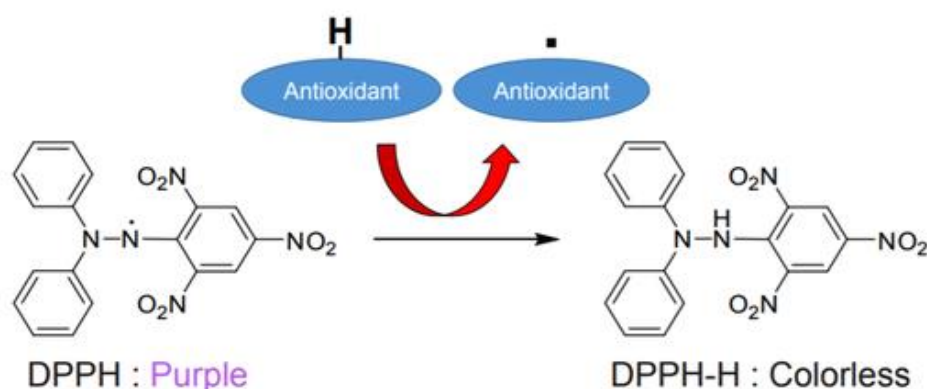
Fig 5.1: DPPH free radical reacting with antioxidants [31]

- *Radical scavenging Assay of DPPH with Pluronic F127 stabilized CuS nanoparticles*

For the assay procedure Ascorbic acid was taken in a test tube and is used as a positive control for the entire experiment following the protocol of Bhattacharya *et al* 2014 with slightest modifications. Varying concentrations of the CuS nanoparticles labelled as test samples (0.5,1mg, 3mg, 5mg, 10mg, 15mg,20mg) were added to 3mL solution of 3.3mM DPPH containing tubes. The entire mixture was thoroughly vortexed for 10-15secs. The tubes are then incubated at room temperature for 30mins in the dark. Meanwhile the spectrophotometer was set up at 517nm and the after proper incubation at the stipulated time the absorbance was read.

The percentage scavenging activity or Inhibition ratio (%) was recorded using the formula below:

% Scavenging Activity/ Inhibition Ratio (%) =   (Absorbance of Control-Absorbance of Test Samples/ Absorbance of Control) x 100 …. eq (5.2)

- *Determination of the* IC_{50} *of the test samples*

The IC_{50} of the test samples was calculated following the method of Xiao F *et al* 2020[31]. A regression line was drawn using the graph plotted using inhibition ratio against the sample concentrations. The IC_{50} value was determined using the regression line plotted using the regression line equation $y= ax + b$ where by

substituting the value of y with 50 the unknown IC $_{50}$ concentration of the test sample can be traced out.

5.2.5 Cytotoxicity assessment of nanoparticles by Haemolysis Assay:

The principle of haemolysis is rested on the release of haemoglobin from the damaged mammalian erythrocyte membranes by the action of a haemolytic agent. In this experiment to judge the efficacy of the nanoparticles to be used as an antimicrobial agent the synthesized nanoparticles are been subjected to haemolytic assay.

The haemolysis experimental protocol was followed as reported by Bhattacharya K *et al* 2014 [32]. In a typical experiment sheep blood was collected using new sterilized syringe. To 9mL of blood sample collected in a sterilized container, 1mL of freshly prepared Alsever's solution was added and was thoroughly mixed to prevent coagulation of blood. The anticoagulant containing collected blood samples were immediately transferred into ice for storage until further use.

The blood sample was then centrifuged at 3,000 rpm for 5mins at 4°C after which the supernatant was discarded and the cell pellet was resuspended in already prepared PBS buffer maintained at a pH of 7.4. It was washed twice or thrice with the PBS buffer and ultimately kept in the 30mL of the same. 100uL of nanoparticle solution of different concentrations (500 μg/mL,1mg/mL, 2mg/mL, 5mg/mL) along with 1900μL of erythrocyte suspension was tested for haemolytic activity. In mild shaking condition the entire mixture was kept in a rotatory shaker at 37°C for 90 mins. For the purpose of comparison positive and negative controls were taken by mixing respectively the same amount of erythrocyte suspension to 5% Triton X 100 that serves as the positive control and PBS buffer kept at a pH 7.4.

After the required incubation time the samples were again subjected to centrifugation at 3,000rpm for 5mins which will pellet out the RBC cells. The supernatant after being carefully separated out was used to check absorbance at 540nm in a UV Vis Spectrophotometer using PBS buffer solution as blank.

The percentage of haemolysis or in other words the haemolytic index was calculated by

Haemolysis (%) = (Abs $_{Test}$ − Abs $_{Negative\ Control}$ / Abs $_{Positive\ Control}$ -- Abs $_{Negative\ Control}$) x 100 …… eq (5.3) [32]

5.3 RESULTS & DISCUSSION

5.3.1 The antimicrobial potential analyses of the synthesized nanomaterial

The antimicrobial activity of the test sample was evaluated statistically using one way ANOVA (Post Hoc Tukey HSD) using SPSS 11 software package. The HSD test allows us to find pairwise comparison, to be precise to have an idea about any significant difference present within the given ANOVA data. The *p* value chosen is *<.05* indicates about any significant difference exists between the control samples and the test samples.

Table 5.1 indicates the result obtained after the analysis, suggested that there is a significant difference ($p < .05.$) in between the mean value of control set (C) and the treatment set 5 ug/ml concentration of nano-particle. Further data obtained from the analysis (compared mean between control and others treatment sets 15μg/mL, 25μg/mL, 35μg/mL, 50μg/mL, 75μg/mL and 100μg/mL) revealed that the decrease in bacterial growth after the treatment with these subsequent concentrations of nano-particle, suggesting the significant changes ($p < .05$) in the growth pattern of *E.coli* ATCC 25922.

Table 5.1: *p* values and comparison chart of the level of significance between Control and CuS Nanoparticle Treated Samples containing *E.coli* ATCC 25922

Control (C) vs Treatment Concentrations	*P* value (taken <.05)	Remarks for level of significance
C vs 5μg/mL	*P* value is <.00001	The result was found significant at p<0.5
C vs 15μg/ml	*P* value is <.00001	The result was found significant at p<0.5
C vs 25μg/ml	*P* value is <.00001	The result was found significant at p<0.5
C vs 35μg/ml	*P* value is <.00001	The result was found significant at p<0.5
C vs 50μg/ml	*P* value is <.00001	The result was found significant at p<0.5
C vs 75μg/ml	*P* value is <.00001	The result was found significant at p<0.5
C vs 100μg/ml	*P* value is <.00001	The result was found significant at p<0.5

Another analysis was also performed using the one-way ANOVA where two subsequent data sets were taken into consideration. Table 5.2 gives us the idea that that 5 ug/ml concentration of nano-material was sufficient to significantly reduce the bacterial growth. Similarly, significant variation was also observed in case of further treatment sets, i.e 15µg/mL, 25µg/mL, 35µg/mL,50µg/mL,75µg/mL and 100µg/mL On the contrary, there was no significant variation observed in between 35µg/mL and 50µg/ml. This indicates that the changes in the treatment regime, particularly, after the treatment with 35 ug/ml of nano-material was found to be insignificant decrease in bacterial growth. This value can be rightfully chosen as the Minimum Inhibitory Concentration (MIC) of the sample. Further the test of significance was checked up to the concentration of 100µg/mL and the results indicate that there are no level of significance observed in these values. The statistical values are further plotted in Fig 5.2 a) points out the cell viability pattern of the nanoparticle against *E.coli* ATCC 25922 whereas from Fig 5.2 b) the IC_{50} value can be found out using intercept equation which was found to be 24.92µg/mL that can be roughly translated to the concentration of 25µg/mL.

Table 5.2: Comparison between different concentrations of nanoparticles treated sets containing *E.coli* ATCC 25922

Comparison between treatment sets	*P value*	Remarks
C vs 5µg/ml	*P-value* is < 0.00001.	Result is significant at p<0.05
5µg/ml vs 15µg/ml	*P-value* is < 0.00001.	Result is significant at p<0.05
15µg/ml vs 25µg/ml	*P-value* is < 0.00001.	Result is significant at p<0.05
25µg/ml vs 35µg/ml	*P-value* is < 0.00001.	Result is significant at p<0.05
35µg/ml vs 50µg/ml	*P-value* = 0.579584	**Result is not significant**
50µg/ml vs 75µg/ml	*P-value*=0.095452.	**Result is not significant**
75µg/ml vs 100µg/ml	*P-value* =0.397204	**Result is not significant**
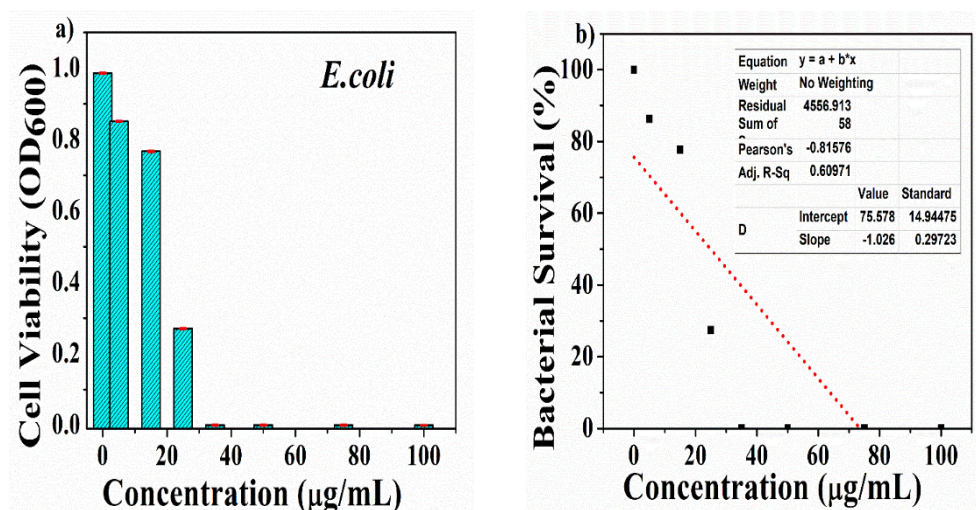
Fig 5.2 a) Cell viability of the *E.Coli* ATCC 25922 cells when treated with nanoparticles; b) Determination of IC$_{50}$ value from a scatter graph

The antimicrobial efficacy against Gram positive bacterial strain *S.aureus* ATCC 25923. Similar to *E.coli* ATCC 25922 the statistical analysis was done through one way ANOVA Post Hoc Tukey HSD where levels of significance was determined first through comparison with control sets and then with individual treated samples were tested according to their increasing concentrations. The results for comparison for the levels of significance of the control samples with the treated samples are abridged in Table 5.3.

Table 5.3: Comparison of the *p* values of Control with nanoparticle treated samples containing *S.aureus* ATCC 25923

Control vs Treatment Concentrations	*P* value (taken <.05)	Remarks for level of significance
C vs 5µg/mL	*P* value is <.00001	Result found significant at *P*<0.05
C vs 15µg/ml	*P* value is <.00001	Result found significant at *P*<0.05
C vs 25µg/ml	*P* value is <.00001	Result found significant at *P*<0.05
C vs 35µg/ml	*P* value is <.00001	Result found significant at *P*<0.05
C vs 50µg/ml	*P* value is <.00001	Result found significant at *P*<0.05
C vs 75µg/ml	*P* value is <.00001	Result found significant at *P*<0.05
C vs 100µg/ml	*P* value is <.00001	Result found significant at *P*<0.05

The result of synthesized nanoparticle treated *S. aureus* ATCC 25923 showed that when compared with the control sample all the treated concentrations (5µg/mL, 15µg/mL, 25µg/mL,35µg/mL,50µg/mL,75µg/mL and 100µg/mL) there is a significant difference between the control mean to that of the nanoparticle treatment concentrations which is also evident from Fig 5.3 a). The IC_{50} value of the nanomaterial against the Gram positive bacteria was obtained from Fig 5.3 b) which was found to be 40.2 µg/mL.

Just like the Gram- negative bacteria a second set of analyses was also performed where gradual treatment concentrations were compared against Gram positive *S. aureus*. This will clearly hint at the Minimum Inhibitory Concentration (MIC) of the synthesized sample. As depicted in Table 5.4 it was found that p value is not significant after 75 µg/mL. Thus from the level of significance 75µg/mL was chosen as the MIC of the CuS nanoparticles against *S.aureus* ATCC 25923.

Table 5.4: Comparison between nanoparticles treated sets containing *S.aureus* ATCC 25923

Comparison between treatment sets	*P value*	Remarks
C vs 5µg/ml	*P-value* is < 0.00001.	Result is significant at *P*<0.05
5µg/ml vs 15µg/ml	*P-value* is < 0.00001.	Result is significant at *P*<0.05
15µg/ml vs 25µg/ml	*P-value* is < 0.00001.	Result is significant at *P*<0.05
25µg/ml vs 35µg/ml	*P-value* is < 0.00001.	Result is significant at *P*<0.05
35µg/ml vs 50µg/ml	*P-value* is < 0.00001.	Result is significant at *P*<0.05
50µg/ml vs 75µg/ml	*P-value* is < 0.00001.	Result is significant at *P*<0.05
75µg/ml vs 100 µg/ml	*P-value* =0.331909	**Result is not found significant at *P* <0.05**
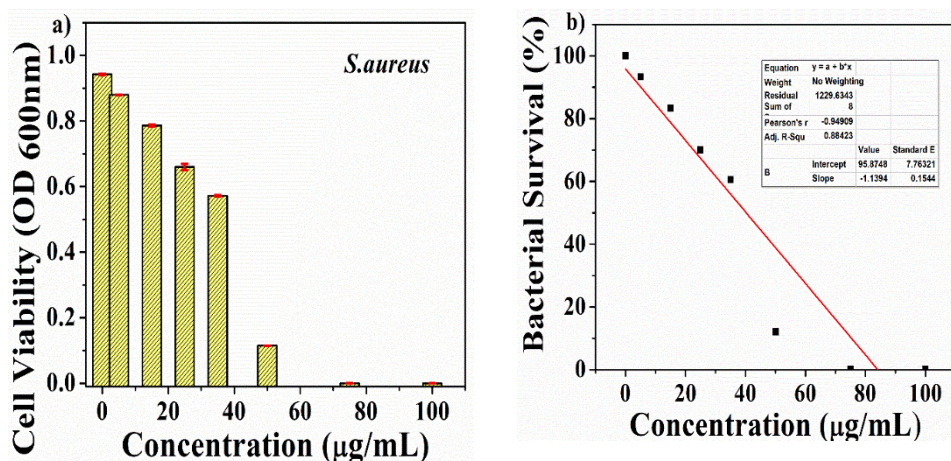
Fig 5.3 a) Plot of Cell viability of *S.aureus* ATCC 25923 when treated with varying concentrations of nanomaterial; b) Determination of IC_{50} value of the nanomaterial against the same.

- **Probable mode of action of the nanoparticle with the bacteria**

The suggested mechanism of action of the nanodrug with that metal nanoparticles initially interact with the bacterial cell wall upon attachment and consequently disrupts the cell membrane via pit formation [33,34]. The cell wall surface of both the Gram positive and Gram- negative bacteria is also inhabited with a number of anionic species' Literature reports hints at the larger concentrations of nanoparticle binding with these negatively charged species increases the repertoire of cidal activity of the nanoparticles [35].

The justification of the MIC value of the Gram- positive bacteria being higher than the Gram- negative bacteria found in the experimental data can be explained by the fact that the differential inhibition arises from the discrepancies in the cell wall thickness. The Gram-positive bacterial cell has a thick peptidoglycan layer compared to that of a Gram-negative bacterium that is refractory to most of the bacterial targets [33].

5.3.2 Antioxidant Activity of the nanoparticles against DPPH free radical

Pluronic F127 stabilized CuS nanoparticles when tested for the unbound DPPH free radical scavenging assay it was found that the nanoparticle has strong antioxidant activity. The nanoparticles were judged for their scavenging activity against Ascorbic Acid taken as the positive control. Fig 5.4 shows that the scavenging activity between

15-20mg of the nanoparticle. After 15mg almost there is a plateau reached and thus no notable change is not observed.
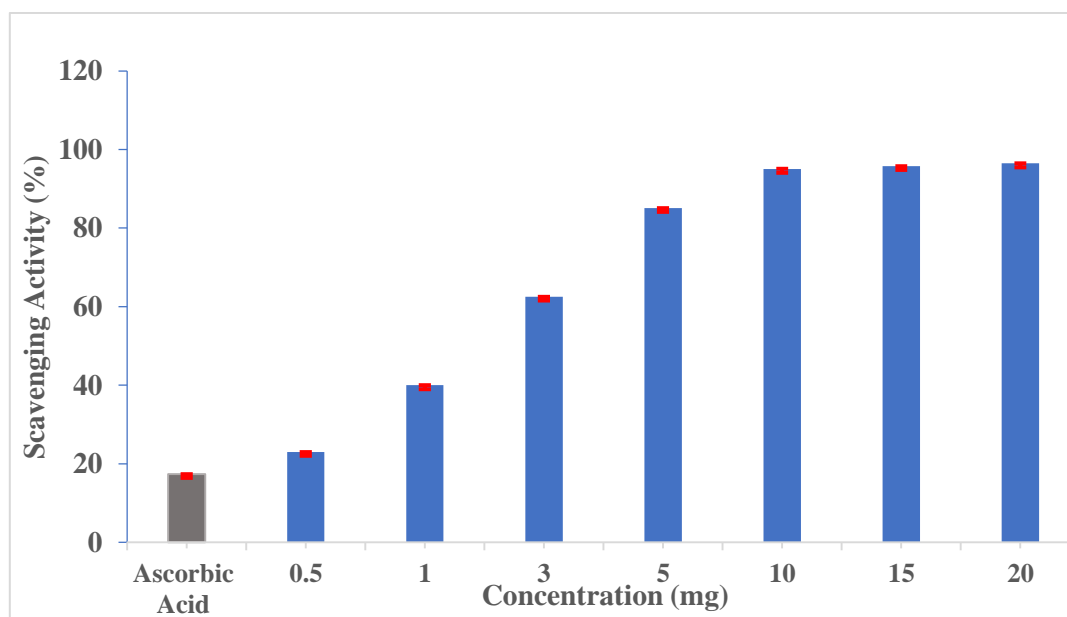
Fig: 5.4 Dose dependant scavenging activity of nanoparticles against DPPH

The IC$_{50}$ value of the scavenging activity was also estimated from the regression line equation was found to be 1.356 mg shown in Fig 5.5.

Equation	y = a + b*x		
Weight	No Weighting		
Residual Sum of	1746.40222		
Pearson's r	0.82174		
Adj. R-Squar	0.6103		
		Value	Standard Err
B	Intercept	45.5406	10.62656
	Slope	3.28781	1.01968
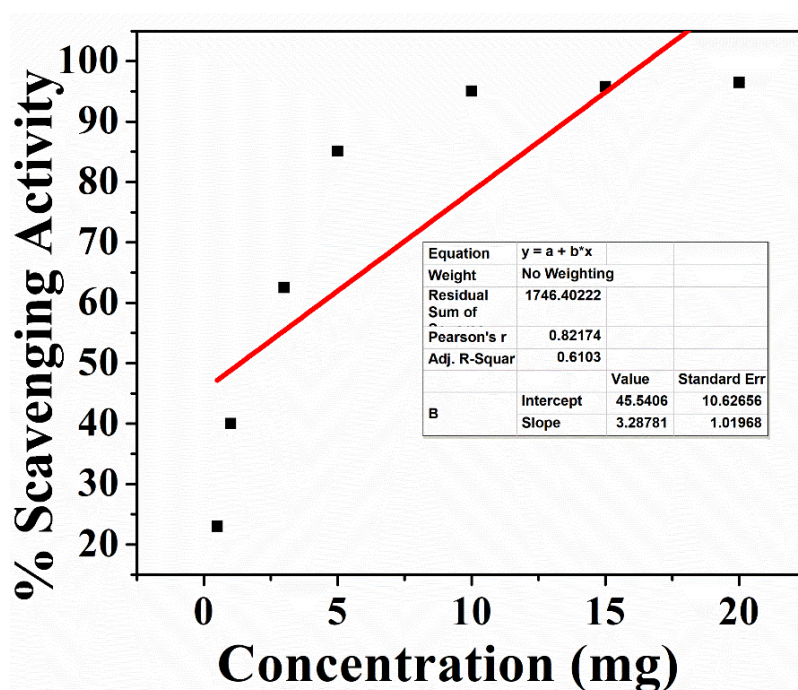
Fig 5.5: The IC$_{50}$ scavenging activity of Pluronic F127 capped CuS nanoparticles against DPPH free radical

With increasing in the concentration of the nanoparticles the purple-coloured solution of the DPPH free radical is found to fade slowly DPPH molecule gets reduced to a diamagnetic molecule due to pairing of the lone pair of electrons [32].

5.3.3 Evaluation of cytocompatibility through Haemolysis Assay

The toxicity of the nanoparticles assessed through haemolysis assay. The results evaluated from Eq 5.3 indicated that the nanoparticle can be safely used up to a concentration of 5.0mg/mL (Fig 5.6) after which there is considerable release of haemoglobin from the erythrocytic cells since 5% haemolysis is considered as the acceptable haemolytic index [36,37]. Thus, the synthesized nanomaterial can be used safely for biological applications as an antimicrobial and as an antioxidant.
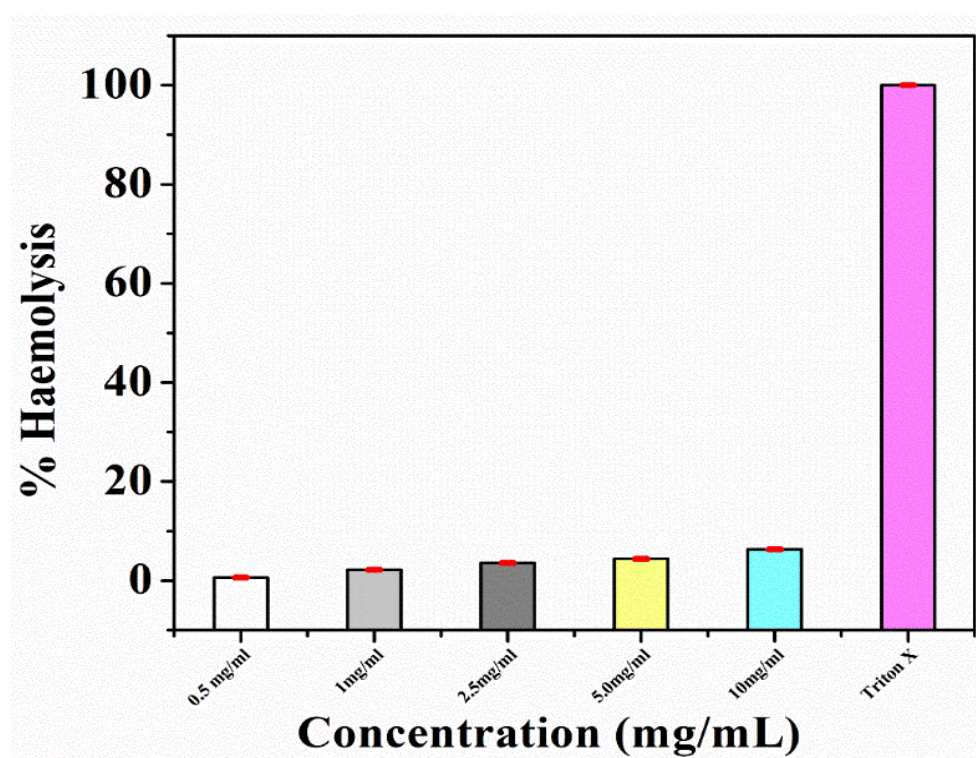
Fig 5.6 Haemocompatibility assessment of synthesized nanoparticle by haemolysis assay

5.4 SUMMARY

This chapter focusses on further utilizing the synthesized transitional metal chalcogenide for biological application. This apart from its catalytic nature in waste water treatment may simultaneously broaden the opportunity of using it in treating faecal coliforms as the nanomaterial has proved itself to be a good candidate in inhibiting Gram negative *E.coli* ATCC 25922. Additionally, the synthesized

nanoparticle can also be used as an alternative to conventional antibiotics and other remedials. It has proved itself to be a broad- spectrum antibiotic and can be applied topically in treating wounds as it can combat against Gram positive *S.aureus* ATCC 25923 which is also supported by the biocompatible nature of the nanoparticle when tested in mammalian erythrocyte cells.

REFERENCES

1. Wang, L., Hu, C., & Shao, L. (2017). The antimicrobial activity of nanoparticles: present situation and prospects for the future. *International journal of nanomedicine*, *12*, 1227.

2. Wang, Z., Lee, Y. H., Wu, B., Horst, A., Kang, Y., Tang, Y. J., & Chen, D. R. (2010). Anti-microbial activities of aerosolized transition metal oxide nanoparticles. *Chemosphere*, *80*(5), 525-529.

3. Feng, Y., Marusak, K. E., You, L., & Zauscher, S. (2018). Biosynthetic transition metal chalcogenide semiconductor nanoparticles: progress in synthesis, property control and applications. *Current Opinion in Colloid & Interface Science*, *38*, 190-203.

4. Trchounian, A., Gabrielyan, L., & Mnatsakanyan, N. (2018). Nanoparticles of various transition metals and their applications as antimicrobial agents. *Saylor Y, IrbyV, Editors. Metal Nanoparticles: Properties, Synthesis and Applications*, 161-211.

5. Han, H., Yang, J., Li, X., Qi, Y., Yang, Z., Han, Z., ... & Wang, F. (2021). Shining light on transition metal sulfides: New choices as highly efficient antibacterial agents. *Nano Research*, *14*(8), 2512-2534.

6. Bost, M., Houdart, S., Oberli, M., Kalonji, E., Huneau, J. F., & Margaritis, I. (2016). Dietary copper and human health: Current evidence and unresolved issues. *Journal of Trace Elements in Medicine and Biology*, *35*, 107-115.

7. Bogdanović, U., Lazić, V., Vodnik, V., Budimir, M., Marković, Z., & Dimitrijević, S. (2014). Copper nanoparticles with high antimicrobial activity. *Materials Letters*, *128*, 75-78.

8. Sankar, R., Maheswari, R., Karthik, S., Shivashangari, K. S., & Ravikumar, V. (2014). Anticancer activity of Ficus religiosa engineered copper oxide nanoparticles. *Materials Science and Engineering: C*, *44*, 234-239.

9. Sivaraj, R., Rahman, P. K., Rajiv, P., Narendhran, S., & Venckatesh, R. (2014). Biosynthesis and characterization of Acalypha indica mediated copper oxide nanoparticles and evaluation of its antimicrobial and anticancer activity. *Spectrochimica Acta Part A: Molecular and Biomolecular Spectroscopy*, *129*, 255-258.

10. Bezza, F. A., Tichapondwa, S. M., & Chirwa, E. (2020). Fabrication of monodispersed copper oxide nanoparticles with potential application as antimicrobial agents. *Scientific reports*, *10*(1), 1-18.

11. Wang, L. (2016). Synthetic methods of CuS nanoparticles and their applications for imaging and cancer therapy. *RSC advances*, *6*(86), 82596-82615.

12. Adibhesami, M., Ahmadi, M., Farshid, A. A., Sarrafzadeh-Rezaei, F., & Dalir-Naghadeh, B. (2017). Effects of silver nanoparticles on Staphylococcus aureus contaminated open wounds healing in mice: An experimental study. In *Veterinary Research Forum* (Vol. 8, No. 1, p. 23). Faculty of Veterinary Medicine, Urmia University, Urmia, Iran.

13. Arafa, M. G., El-Kased, R. F., & Elmazar, M. M. (2018). Thermoresponsive gels containing gold nanoparticles as smart antibacterial and wound healing agents. *Scientific reports*, *8*(1), 1-16.

14. Cadenas, E., & Davies, K. J. (2000). Mitochondrial free radical generation, oxidative stress, and aging. *Free radical biology and medicine*, *29*(3-4), 222-230.

15. Krumova, K., & Cosa, G. (2016). Overview of reactive oxygen species.

16. Dröge, W. (2002). Free radicals in the physiological control of cell function. *Physiological reviews*.

17. Lagouge, M., & Larsson, N. G. (2013). The role of mitochondrial DNA mutations and free radicals in disease and ageing. *Journal of internal medicine*, *273*(6), 529-543.

18. Knight, J. A. (1997). Reactive oxygen species and the neurodegenerative disorders. *Annals of Clinical & Laboratory Science*, *27*(1), 11-25.

19. Mukherjee, S., Pawar, N., Kulkarni, O., Nagarkar, B., Thopte, S., Bhujbal, A., & Pawar, P. (2011). Evaluation of free-radical quenching properties of standard Ayurvedic formulation Vayasthapana Rasayana. *BMC complementary and alternative medicine*, *11*(1), 1-6.

20. Liou, G. Y., & Storz, P. (2010). Reactive oxygen species in cancer. *Free radical research*, *44*(5), 479-496.

21. Wilson, D. W., Nash, P., Buttar, H. S., Griffiths, K., Singh, R., De Meester, F., ... & Takahashi, T. (2017). The role of food antioxidants, benefits of functional foods, and influence of feeding habits on the health of the older person: An overview. *Antioxidants*, *6*(4), 81.

22. 22.Lourenço, S. C., Moldão-Martins, M., & Alves, V. D. (2019). Antioxidants of natural plant origins: From sources to food industry applications. *Molecules*, *24*(22), 4132.

23. Finley, J. W., Kong, A. N., Hintze, K. J., Jeffery, E. H., Ji, L. L., & Lei, X. G. (2011). Antioxidants in foods: state of the science important to the food industry. *Journal of agricultural and food chemistry*, *59*(13), 6837-6846.

24. 24.Thiruvengadam, M., Chung, I. M., Gomathi, T., Ansari, M. A., Gopiesh Khanna, V., Babu, V., & Rajakumar, G. (2019). Synthesis, characterization and pharmacological potential of green synthesized copper nanoparticles. *Bioprocess and biosystems engineering*, *42*(11), 1769-1777.

25. 25.Konwarh, R., Gogoi, B., Philip, R., Laskar, M. A., & Karak, N. (2011). Biomimetic preparation of polymer-supported free radical scavenging, cytocompatible and antimicrobial "green" silver nanoparticles using aqueous extract of Citrus sinensis peel. *Colloids and Surfaces B: Biointerfaces*, *84*(2), 338-345.

26. Dauthal, P., & Mukhopadhyay, M. (2013). In-vitro free radical scavenging activity of biosynthesized gold and silver nanoparticles using Prunus armeniaca (apricot) fruit extract. *Journal of nanoparticle research*, *15*(1), 1-11.

27. Gonzales, M., & Krishnan, K. M. (2007). Phase transfer of highly monodisperse iron oxide nanocrystals with Pluronic F127 for biomedical applications. *Journal of Magnetism and Magnetic Materials*, *311*(1), 59-62.

28. 28.Son, M., Lee, Y. S., Lee, M. J., Park, Y., Bae, H. R., Lee, S. Y., ... & Yang, S. (2021). Effects of osmolality and solutes on the morphology of red blood cells according to three-dimensional refractive index tomography. *PloS one*, *16*(12), e0262106.

29. 29.Chakraborty, R., Sarkar, R. K., Chatterjee, A. K., Manju, U., Chattopadhyay, A. P., & Basu, T. (2015). A simple, fast and cost-effective method of synthesis of cupric oxide nanoparticle with promising antibacterial potency: Unraveling the biological and chemical modes of action. *Biochimica et Biophysica Acta (BBA)-General Subjects*, *1850*(4), 845-856.

30. 30.Kedare, S. B., & Singh, R. P. (2011). Genesis and development of DPPH method of antioxidant assay. *Journal of food science and technology*, *48*(4), 412-422.

31. Xiao, F., Xu, T., Lu, B., & Liu, R. (2020). Guidelines for antioxidant assays for food components. *Food Frontiers*, *1*(1), 60-69.

32. Bhattacharya, K., Gogoi, B., Buragohain, A. K., & Deb, P. (2014). Fe2O3/C nanocomposites having distinctive antioxidant activity and hemolysis prevention efficiency. *Materials Science and Engineering: C*, *42*, 595-600.

33. 33.Martinez de Tejada, G., Sánchez-Gómez, S., Rázquin-Olazaran, I., Kowalski, I., Kaconis, Y., Heinbockel, L., ... & Brandenburg, K. (2012). Bacterial cell wall compounds as promising targets of antimicrobial agents I. Antimicrobial peptides and lipopolyamines. *Current drug targets*, *13*(9), 1121-1130.

34. Nisar, P., Ali, N., Rahman, L., Ali, M., & Shinwari, Z. K. (2019). Antimicrobial activities of biologically synthesized metal nanoparticles: an insight into the mechanism of action. *JBIC Journal of Biological Inorganic Chemistry*, *24*(7), 929-941.

35. Slavin, Y. N., Asnis, J., Häfeli, U. O., & Bach, H. (2017). Metal nanoparticles: understanding the mechanisms behind antibacterial activity. *Journal of nanobiotechnology*, *15*(1), 1-20.

36. Singhal, J. P., & Ray, A. R. (2002). Synthesis of blood compatible polyamide block copolymers. *Biomaterials*, *23*(4), 1139-1145.

37. Das, D., Nath, B. C., Phukon, P., & Dolui, S. K. (2013). Synthesis of ZnO nanoparticles and evaluation of antioxidant and cytotoxic activity. *Colloids and Surfaces B: Biointerfaces*, *111*, 556-560.

CONCLUSION & FUTURE PERSPECTIVES
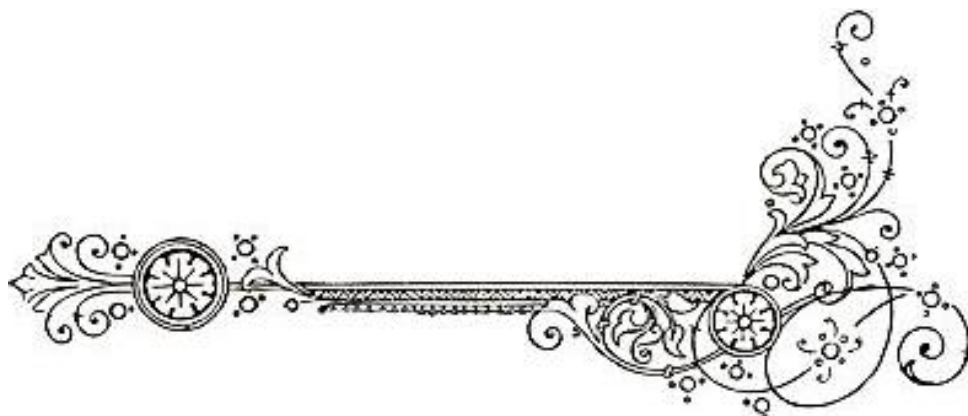
CHAPTER 6

CONCLUSION & FUTURE PERSPECTIVES

Two global predicaments that dwell and interfere with the lives and overall well beings of lives of masses are scarcity of pure drinking water and a new drug that will be an alternative over the existing antibiotics that meets the shortcoming of resistance due to their overuse. The world- wide potable drinking water crisis can be envisioned from two point of view- Primarily various heavy metal contaminants are being dumped into the aqueous milieu that sources out of injudicious anthropogenic activities in turn largely out of rapid industrialization are putting a big question to poise between civilization and its aftermath that is culminating into disastrous side-effects afflicting not only to the human community but to other living aqueous cohorts like phyto-planktons and zooplanktons as well. Of largely contaminating arsenic, chromium, cadmium, mercury etc heavy metals the prime important task lies in estimating their quantity in water and thereby the treatment for reclamation may be devised. Thus, determining the presence of heavy metals in waste water need the requirement of a good sensor that will give one the possible direction of fabricating a material for its further removal. Though a huge number of sensors are available, most of these aren't eco-friendly and are toxic if not handled properly. So, it demands the choice of a good biocompatible material that could be mobilized in the built of a good sensor device for heavy metal detection.

The second major issue apart from heavy metals contamination are organic pollutants which too harbour in the water realm posing serious threats to mankind and piscean communities as well. The removal of organic pollutants through photocatalysis method is one of the most efficient strategies of retrieving potable water.

In this thesis in an aim to deal with heavy metal detection in water and reducing the organic phenol contaminants transitional metal nanoparticles in the form of iron hydroxides and chalcogenide metal sulphide nanoparticles respectively are been chosen. Furthermore, the biological applications in an aim to meet biocompatibility was also assessed.

In a nutshell a navigation to the thesis as an epilogue of the same is resonated below:

Chapter 1 is a briefing regarding water pollution, its various causes like heavy metal pollution, organic pollutant and microorganism mediated pollution along with their sources and a discussion on the transitional metals with the light of application of transitional metal hydroxide nanoparticles in waste water remediation, the sources of heavy metal contamination in the light of chromium contamination along with the discussion of transgenic metal nanoparticles their function as chalcogenides in degradation of organic dyes and phenol derivatives. Since all of these applications are rested upon the proper synthesis of nanomaterial so the basic instrumentation system for qualifying the nanoparticle has also been narrated in detail.

Chapter 2 focuses on the synthesis of a fluorometric nano-sensor via hydrothermal method in which carbon dots are impregnated on a goethite matrix (α- FeOOH), a transitional metal oxyhydroxide, which can be seen as an effective alternative of the conventional fluorophores as well as other nanoprobes of abundant usage that suffer not only from the disadvantage of solubility but also from the major violation of biocompatibility. The synthesized nanomaterial was subjected to sensing of hexavalent chromium, Cr (VI) in waste water after the nanomaterial was thoroughly characterized by X-ray crystallography, FTIR, SEM, TEM. The fabricated sensor material had a LOD of 81nM and a LOQ of 269.73nM. The nanomaterial further has been proved to be unaffected and stable at various parameters of temperature, pH, time. The mechanism that is responsible for such a fluorescence-based system has been seen to be attributed by photo induced mode of electron transfer. Based on low cost and using biocompatible materials this nano sensor can be seen to address one of the alarming issues related to global health which is water pollution.

The central goal of **Chapter 3** is to investigate the biological potential of the nano-sensor that has been discussed in Chapter 2. The sensor apart from its ability to sense Cr (VI) in contaminated water was equally capable in sensing early- stage cancer detection. A theoretical model was established through molecular docking techniques which showed the sensing device to interact with the metabolic proteins like cytochrome b5 (cyt b5) and cytochrome P450 (cyt P450) of the cell. The synthesized nanomaterial thus has dual functions of performing both as a nano chemo-sensor as well as a nano bio-sensor.

Since the focus of the thesis lies on water pollution, so the aim was to identify the pivotal cause of water pollution as well as it is an endeavour to remove the pollutant through the benevolence of transitional metal nanoparticles. Chapter 2 was about designing a transitional metal hydroxide fluoro-sensor fabricated with carbon dots that can be harnessed for heavy metal detection in waste water.

Chapter 4 introduces another important aspect of water pollutant caused due to organic pollutant para nitrophenol (pNP). Here to reclaim the waste water the known water pollutant is removed using transitional metal sulphide (CuS) nanoparticles. This widely used semi-conductor has been prepared via reflux condensation method using biocompatible copolymer Pluronic F-127. The nanoparticle was thoroughly characterized and reduction of pNP was monitored using UV-Vis spectrophotometer that showed rapid reduction of the pNP to para aminophenol (pAP). The rate kinetics for the entire reduction system was also monitored and varying parameters of pNP as well as catalyst concentration and pH varying were studied. This synthesized nanoparticle was thus seen to perform as a chemical catalyst having recyclability sustaining efficient reduction efficiency up to 4th cycles of its use.

Chapter 5 can be seen as a both as a continuation of Chapter 4 as well as a termination of this research work. The nano- catalyst used was further explored for its biological potential of judging antimicrobial efficacy against the most notorious faecal coliform *E.coli* ATCC 25922, a Gram negative bacteria and *Staphylococcus aureus* ATCC 25923, a Gram- positive bacteria. The nanoparticle was seen to perform well as an effective antimicrobial against *E. coli* ATCC 25922 and thus it can be said apart from pNP reduction the nano-system will also combat against the major coliform producing bacteria. The efficient activity of the nanoparticle against *Staphylococcus aureus* ATCC 25923 also proved that the nanomaterial can used as a topical agent fighting against skin infections.

As a part of the biological activity the nanoparticle exhibited excellent antioxidant activity against DPPH free radical. The cyto-compatibility of the nanoparticle towards red blood cells proved further that the nanomaterial is safe and can used both in the aqueous milieu as well as in the living systems.

With these knowledge the future prospects for the application for both the nanomaterials can be addressed herein:

- **Turning nano-sensor into a device**: The transitional metal oxyhydroxide fabricated with C- dots can be tuned in the form of a device and amends can be made to make it potable for detecting heavy metal contamination in water.

- **Enhancing reusability of the nano-sensor through hydrogel entrapment:** The fabricated nano-sensor for its long term usage can be trapped into a biopolymer based hydrogel thereby increasing its sorption activity and enhancing its reusability.

- **Turning nano-catalyst into water filter candles:** The synthesized transitional metal sulphide nanoparticles can be utilized in the preparation of filter candles for waste water remediation in industries as well as for household purposes as an alternative to silver- based filtration systems used nowadays.

- **Using metal sulphide nanoparticles in catheter mediated infections:** The transitional metal sulphide nanoparticles since have the capability to fight against both Gram positive and Gram negative bacteria can be utilized for its use in medical devices that often suffer from the formation of biofilms. The inbuilt nanoparticle coating systems will inhibit formation of biofilms and therefore will prevent several nosocomial infections and increase the shelf life of several medical devices.

ORIGINAL ARTICLE

Biocompatible Carbon Dot Decorated α-FeOOH Nanohybrid for an Effective Fluorometric Sensing of Cr (VI) in Wastewater and Living Cells

Bidisha Ghosh[1] · Shubham Roy[1] · Souravi Bardhan[1] · Dhananjoy Mondal[1] · Ishita Saha[2] · Saheli Ghosh[1] · Ruma Basu[3] · Parimal Karmakar[2] · Kaustuv Das[1] · Sukhen Das[1]

Abstract

This article reports the fluorometric detection of toxic hexavalent chromium Cr (VI)) in wastewater and Cr (VI) contaminated living cells using *in-situ* grown carbon quantum dots into the goethite (α-FeOOH) nano-matrix. The synthesized nano-hybrid shows enormous potential in determining the chromium contamination levels in various types of water samples. This selective fluorometric probe is enormously sensitive (LOD 81 nM) toward hexavalent chromium, which makes it a dedicated chromium sensor. Moreover, the sensing mechanism has been assessed using Stern–Volmer's equation and fluorescence lifetime experiments showing the simultaneous occurrence of photoinduced electron transfer and the inner filter effect. This chromium sensor has also been employed to assess the contamination level in real-life industrial wastewater. The performance of this probe in a real-life wastewater sample is quite commendable. Further, this biocompatible fluorometric probe has been used to demonstrate the in-vitro sensing of Cr (VI) in HeLa cells. The rapid detection mechanism of hexavalent chromium in living cells has been validated using theoretical docking simulations. Henceforth, this fluorometric sensor material could open new avenues not only in wastewater monitoring but also in biomedical applications.

Keywords Hexavalent chromium · Fluorometric sensor · Stern–Volmer plot · Molecular docking

Introduction

Natural sources like weathering of rocks, volcanic eruptions, and mining are counted to be potential sources of heavy metal contamination [1]. Heavy metals are those that have a specific density of 5gm/cm^3 and have the ability to affect the environment and living organisms [2].

Bidisha Ghosh and Shubham Roy are authors contributed equally in this work.

✉ Kaustuv Das
  kaustuv12@gmail.com

✉ Sukhen Das
  sdasphysics@gmail.com

1   Department of Physics, Jadavpur University, Kolkata-700032, India

2   Department of Life Science and Biotechnology, Jadavpur University, Kolkata-700032, India

3   Department of Physics, Jogamaya Devi College, Kolkata- 700026, India

Of all the heavy metals known chromium is one of the most toxic heavy metals, commonly prevalent in nature as trivalent chromium Cr (III) and hexavalent Cr (VI) [3]. Cr (VI) has been regarded as 100-fold toxic and mutagenic than its lower oxidative counterpart Cr (III) [4]. As an effluent, it is often improperly discharged mainly into waterbodies from printing, electroplating, and tanning industries and thereby promoting biomagnification, scale rot, and osmoregulatory dysfunction of fish [5]. Cast iron pipes and ductile iron pipes are mostly lined with cement mortar that contains a considerable amount of chromium and thus chromium leaches out from the cement mortar lining into the drinking water [6]. It has been seen that Cr (VI) exposure to Swiss mice causes a sharp decrease in leucocyte and erythrocytes with an additional deforming of echinocyte formation from erythrocytes [7]. Cr (VI) has been recognized as a group-1 carcinogen by World Health Organization (WHO) as it can disrupt DNA via reactive oxygen species (ROS) generation, a maximum limit of 50 μgL^{-1} has been set by WHO [8, 9].

Considering the toxicity of the numerous organic and inorganic fluorophores and chromophores there is a need

for a cost-effective and biocompatible sensor that can detect Cr (VI) in water samples [10]. Besides, almost all of the methods of preparation were mostly two-step reactions for conjugating the fluorophores and employed robust detection techniques using the electrochemical method. Thus, it necessitates the use of quick, cheaper methods and biocompatible fluorophores that could be procured easily fabricated with the nanoparticle for the detection of chromium.

Herein, α-FeOOH nanoparticle has been modified with in situ grown C-dots to detect hexavalent chromium in wastewater fluorometrically. C-dot has a tendency to form agglomerates and thereby loses its fluorescence property rapidly. Thus, there is a pressing need to restrict such agglomeration for better fluorometric applications. There are earlier reports on C-dot immobilized on oxyhydroxides and mesoporous silica-like matrices for sensing, [11] but those matrices are way too toxic to handle as they can diffuse through the skin and pulmonary routes [12–14]. FeOOH nanoparticles have been approved and used widely as food and iron supplements [15, 16] thereby its bio-safe property makes it advantageous in employing as a heavy metal ion sensor. Further, a molecular docking study has been performed with the probe and two flavoproteins (cytb$_5$ and cyt P450) to estimate the intercellular biosensing pathway of the sensing probe. The theoretical docking studies have been experimentally verified using fluorescence microscopy revealing the early-stage cancer detection property of the probe.

Experimental Section

Materials

The ferric nitrate, anhydrous citric acid and ethylenediamine were purchased from Merck, Germany. The chemicals were all of the pure grades and did not require any further purification. Ultra-pure Millipore water (resistivity ~ 18.2 MΩ-cm) was used throughout the experiments. The glassware and sample holders were cleaned using aqua regia before and after each experiment.

Synthesis C-Dot Doped α-FeOOH (FCD)

In a one-pot synthesis process, 6.464 g of ferric nitrate was taken along with 0.323 g of citric acid in 160 mL of Millipore water and was thoroughly mixed using a magnetic stirrer at room temperature until all the chemical contents were dissolved. To this, ethylenediamine was added dropwise until the pH of the solution reached 12. The mixture was then stirred for another 3 h and then transferred to a Teflon-lined stainless-steel autoclave. The autoclave was then heated at 180 ºC for 12 h and thereafter cooled to room temperature to collect the brick red precipitate through

centrifugation. After proper washing, the precipitate was dried in a vacuum chamber for 24 h and ground in an agate mortar to obtain the fine powder. Finally, the synthesized sample is named FCD and sent for characterization.

Material Characterization

To provide a detailed insight into the crystallographic details of the synthesized materials, X-ray crystallography was employed using X-Ray Diffractometer (Model D8 Advanced, Bruker AXS) with Cu-K$_\alpha$ target (λ = 1.5405 Å) from 10° to 80° in the 2θ range and the scan speed was fixed at 0.02 steps/sec. The operating tube voltage was fixed at 35 kV and 35 mA to generate the X-rays. Further, the refinement of the diffractograms has been done by using the Rietveld-based program MAUD v.2.99 (Material Analysis Using Diffraction) [17] and the refined structures were visualized using VESTA v.3.0 (Visualisation for Electronic Structural Analysis) [18, 19] for better understanding. Additionally, a FTIR-8400S, Shimadzu was employed in the wavenumber ranging between 500 and 3000 cm^{-1} to observe the bonding networks present in the samples. The samples were mixed and homogenized in KBr media in a 1:50 sample to KBr ratio.

The morphological features of the synthesized materials were ascertained by an Inspect-F50, FEI Field Emission Scanning Electron Microscope (FESEM). Very small amounts of samples were placed on carbon-coated grids and used for observing the microscopic details. The accelerating voltage of the electron gun was set in between 10 and 20 kV for taking the micrographs. Further, the size of the nanoparticles was investigated by employing a Jeol-2000FX Transmission Electron Microscope (TEM). A homogenous solution of the sample was prepared by dissolving the sample in acetone and the sample was kept under ultrasonication for 2 h. The solution was then drop-casted to form a thin film over a carbon-coated copper grid (300 mesh) and then dried under a vacuum before microscopy. The TEM micrograph was taken under an excitation of 200 kV.

The optical absorption properties of the samples were analyzed using a 1900i, Shimadzu spectrophotometer. Whereas, all the fluorescence characteristics and fluorescence lifetime of the samples were performed in a Cary Eclipse, Agilent fluorescence spectrophotometer equipped with a Cary single-cell Peltier accessory, Agilent in an excitation wavelength (λ$_{ex}$) 345 nm. The excitation and emission slits were set at 5 nm throughout the experiments.

Biological Experiments and Cell Culture

Autodock Tools v.1.5.6 was used to prepare the proteins and the ligand molecule (cdot). The water molecules of the protein have been removed and polar hydrogen bonds and

Kollman charges were added to the protein structures [20]. Autodock vina v.1.1.2 was used to estimate the binding affinities between the protein–ligand complexes [21, 22]. The binding pockets were identified and visualized using PyMol v.2.0.7 program [23, 24].

A human cervical cancer cell line (HeLa) was purchased from National Centre for Cell Science (NCCS Pune, India). These cells were cultured in DMEM (Dulbecco's Modified Eagle's Medium) medium and treated with 5% FBS (fetal bovine serum) followed by incubation at 37 ℃ in a 5% CO_2 atmosphere for 24 h. Further, the cells were washed with $1 \times PBS$ (phosphate buffer saline) buffer to avoid any contamination. The fresh medium was then added to the washed cells and incubated again at 37 ℃ with a 5% CO_2 atmosphere. HeLa cells were then divided into two parts (namely, IA and IB) and placed over two separate PV/BH@CD membranes, those have already been mounted over cell culture plates and sent for overnight incubation (37 ℃ with 5% CO_2 atmosphere). On the very next day, the IB sample was treated with a small drop of Cr (VI) solution of 50 μM and incubated for another 2 h to interact. After incubation, the samples were sent for microscopy under a fluorescence microscope (Leica, Germany).

Results and Discussion

Structural and Morphological Analyses

The structural information of the synthesized sample has been collected by employing X-ray diffraction (XRD) and Fourier transform infrared spectroscopy (FTIR). The diffractogram show numerous diffraction lines (h k l planes) of the orthorhombic oxy-hydroxide phase of iron (α-FeOOH) corroborating the successful synthesis of the goethite. Figure 1 shows the diffractogram having diffraction maxima located at 17.69°, 33.34°, 35.85°, 40.99°,49.57°, 54.35°,62.82° and 64.18° corresponds to the (h k l) planes of (0 2 0), (1 3 0), (1 0 1), (1 2 1), (1 5 0), (2 4 0), (2 5 0) and (0 6 1) respectively that well matches with the Joint Committee on Powder Diffraction Standards (JCPDS) data card no. 81–0464. The absence of any other diffraction planes suggests the purity of the sample. Further, Rietveld refinement of the diffractogram has been performed in order to estimate the crystallite dimension, microstrain, bond angles, bond lengths, and other phase parameters like anisotropic growth. It is observed that the microstrain value, in this case, is quite high (1.26×10^{-3}), which could arise due to the incorporation of carbon quantum dots. The microstructural parameters have been mentioned in Supplementary Table S1 for better understanding.

The presence of carbon quantum dots in goethite has also been confirmed by using FTIR spectra of the synthesized sample shown in Fig. 1. The C–C, C-O, and C＝O stretching

bands are assigned to the vibrations centered at 1035 and 1217 cm^{-1} respectively depicting the presence of carbon content in the sample [25]. While the absorption bands at 520 and 675 cm^{-1} are attributed to the Fe-CO and Fe–O symmetric stretching vibrations [26, 27]. The vibration maxima between 774 and 900 and 1635 cm^{-1} are ascribed to the O–H bending suggesting the adsorbed moisture and presence of CONH vibrations respectively in the sample [27, 28] A small vibration centered at 1525 cm^{-1} is assigned to the N–H bending arising from the nitrogenous carbon quantum dots [11].

The morphology and particle size of the sample have been estimated by using FESEM and TEM micrographs depicted in Fig. 1. The FESEM image of the sample shows an admixture of spherical and hexagonal particles. The hydrothermally grown carbon dot contained goethite sample (FCD) is quite agglomerated and found to be in the nano regime. In order to estimate the particle size, transmission electron microscopy has been assigned. The TEM micrograph shows 30–50 nm hexagonal/ spherical particles containing 5–7 nm dark spots. These dark spots are assigned as carbon quantum dots as seen in previous characterizations. In reality, the *in-situ* hydrothermal treatment successfully incorporates the carbon dots within the goethite matrix, which is visible in the TEM image.

Optical Properties of the Synthesized Sample

The optical quality of any sample can be verified by using its absorbance and emission properties shown in Fig. 2.

Herein, absorption spectroscopy has been performed to estimate the excitation energy of the nanostructure. It is observed that a small absorption maximum is located at 240 nm, which is usually ascribed to the π-π^* transition of the sp^2- hybridized carbon atoms of the carbon dot moiety [29]. Additionally, a relatively stronger absorbance has been achieved at 342 nm, suggesting the n-π^* transition related to the surface defects of the carbon dots in C-N bonds in sp^3 hybridizations sourcing from the amine (-NH_2) groups from surface functionalization [9, 30, 31]. The broad absorbance bands centered between 450 and 572 nm are sourced from the Fe–Fe transitions. A similar observation has also been made by Sherman et al. in their 1985 work [32]**.** Further, the excitation and emission spectra have been recorded to assess the fluorescence quality of the sample. The excitation spectrum in Fig. 2 shows a significant peak centered at 345 nm, which is in accordance with the absorbance spectrum of the FCD sample. Additionally, the sample has been excited manually with a series of wavelengths ranging between 300–400 nm in order to validate the exact excitation energy. It is found that the energy which corresponds to the 345 nm wavelength is providing the optimum fluorescence emission
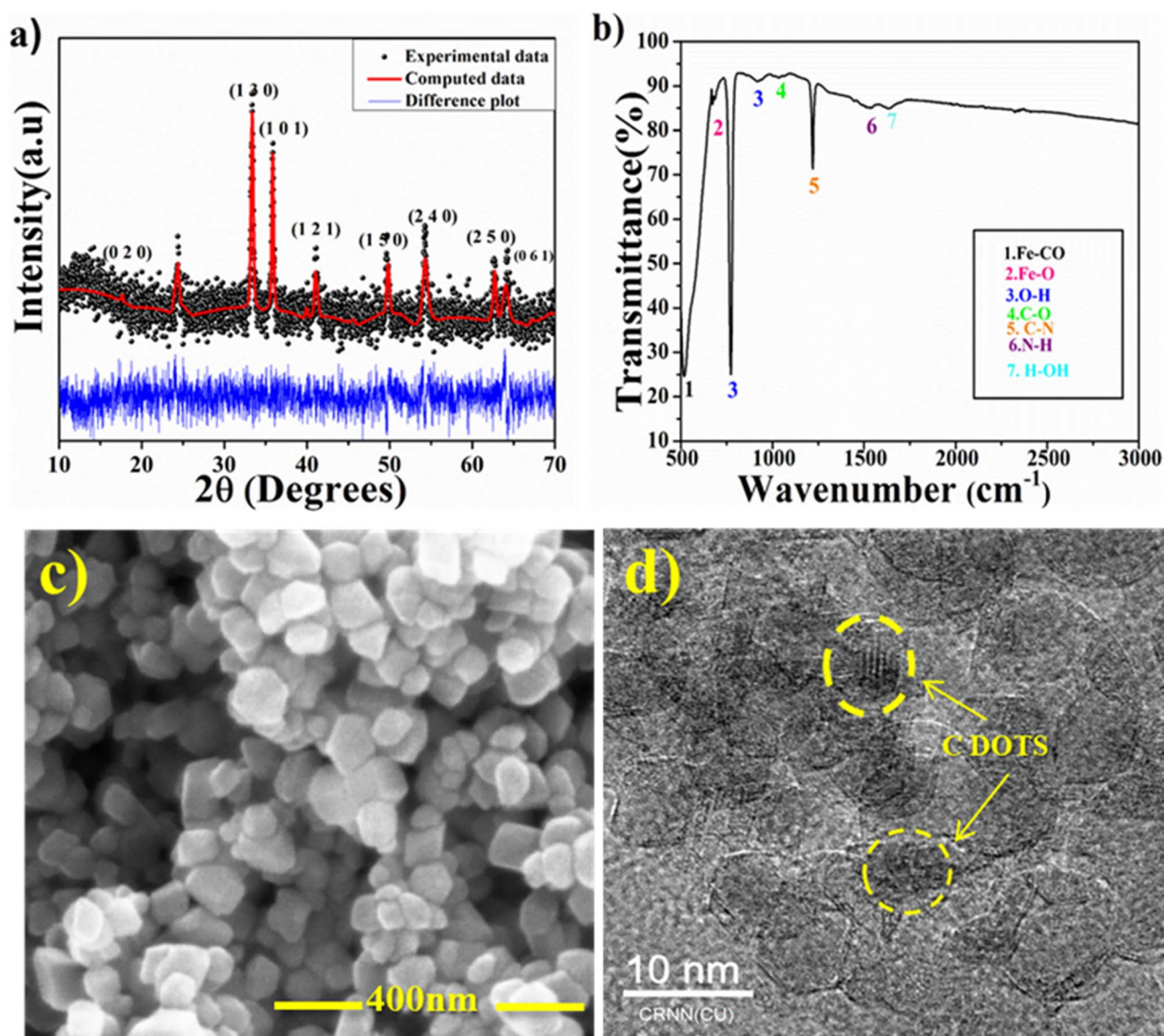
Fig. 1 **a** Refined X-ray diffractogram of the prepared material; **b** FTIR spectrum of the synthesized material; **c** FESEM and **d** TEM images of the synthesized nanostructure

at 460 nm shown in Fig. 2 and thus this wavelength is selected to excite the fluorophores of the sample for further fluorometric experiments. Under the 345 nm excitation, the FCD sample glows with an outstanding blue fluorescence and does not alter the position of the emission peak under varying excitation wavelengths as shown in Fig. 2. In reality, the surface functional groups of the nitrogenous carbon dot introduce new energy levels and control the bandgap causing enhanced fluorescence intensity. The presence of nitrogenous dopant, which in this case has been introduced by using ethylenediamine, causes charge dislocation and efficiently promotes the electron transfer capacity of the carbon quantum dots [33–36]. This

validates the FCD to be a promising fluorescent material in the blue region of the spectrum and could be employed in fluorometric applications.

Dependence of the Fluorescence Quality on Different Ambient Conditions

The fluorescence stability of the nano-engineered sample (FCD) is evaluated against varied ambient conditions to justify its real-life applicability. Initially, the fluorescence stability of the sample has been measured over a period of 2 h at an interval of 10 min to check for any fluorometric decay of the fluorophores. It is evident that no noticeable
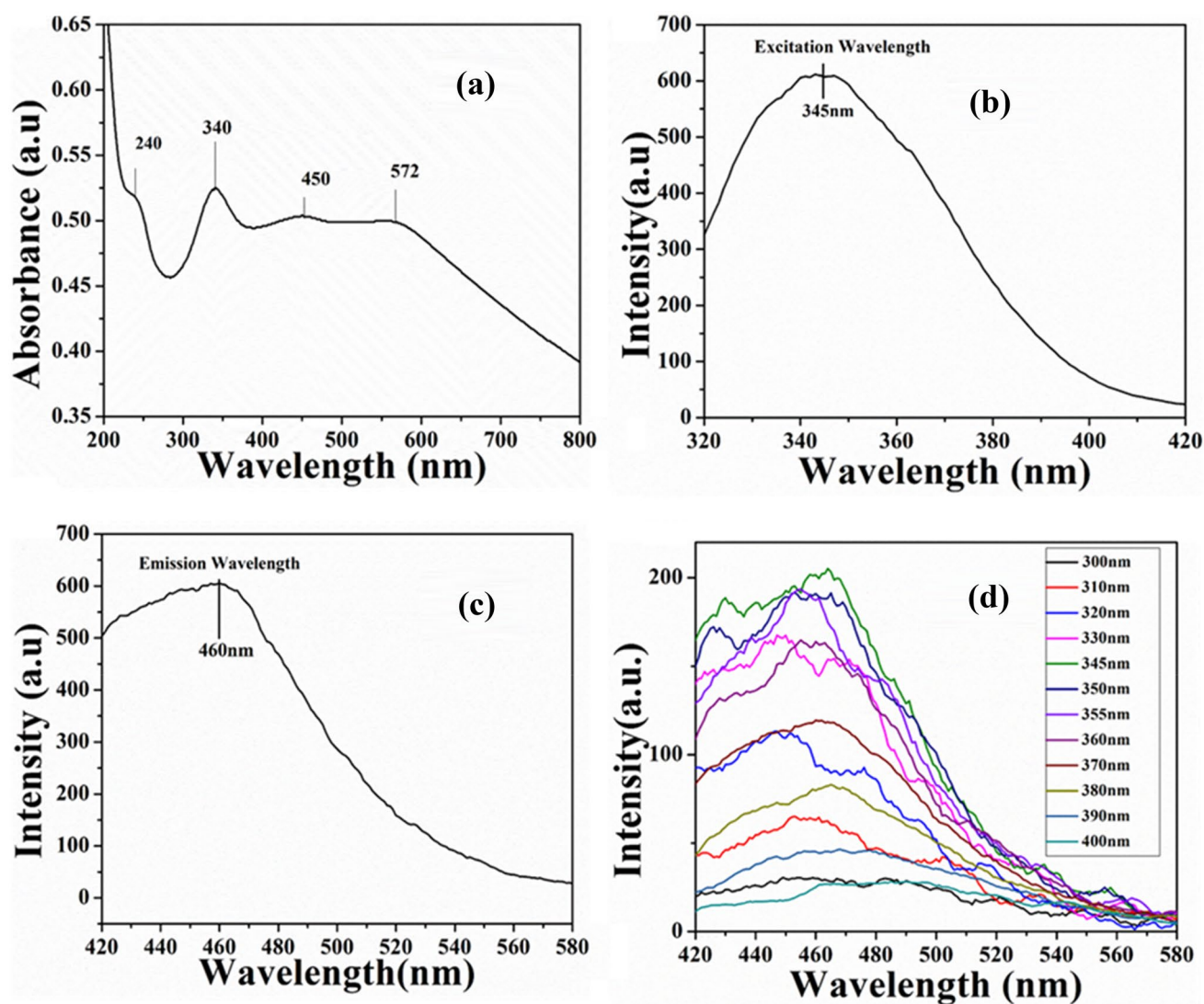
Fig. 2 **a** UV–Vis absorption spectrum of the synthesized probe; **b** excitation and **c** emission spectra of the synthesized material; **d** emission of the sample with respect to different excitation energies

alteration has occurred in the fluorescence intensity inferring the photo-stability of the sample (Fig. 3). The FCD sample has been exposed to a varying pH environment, ranging from extreme acidic 1.8 to extreme alkaline 12.7 conditions as seen in Fig. 3. The fluorescence quenching intensity of the synthesized FCD takes place when subjected to different pH conditions. This suggests the fluorophores of the FCD sample are highly stable at these varying pH conditions.

Additionally, in Fig. 3 the thermal response to the photo-stability has been assessed by varying the working temperature (10–70 ºC) of the FCD sample while measuring the fluorescence level. The fluorescence intensity does not seem to fluctuate much, but it turned out that room temperature conditions (at about 30–50 °C) are the best working temperature for the fluorescent FCD sample. The DTA-TGA (Fig. S1) results revealed there is almost no mass change

over the entire range of temperature. However, the DTA results that at 40 °C there is an endotherm followed by an exotherm. The possible explanation for this can be due to the release of the adsorbed moisture in this region.

FCD as a Fluorometric Sensing Probe for Hexavalent Chromium (Cr (VI))

Selectivity and Sensitivity Assays of the Synthesized Probe

Selectivity and sensitivity are the utmost important parameters to rationalize the sensing efficacy of a probe. Figure 4 shows that the synthesized fluorometric probe (FCD) has been exposed to a wide range of cations and anions (As^+, Ca^{2+}, Cd^{2+}, Mg^{2+}, Pb^{2+}, Hg^{2+}, K^+, Cr^{6+}, Cl^-, CO_3^{2-}, SO_4^{2-}, OH^-, S^{2-}, NO_3^-) in order to assess its selectivity.

(a)

(b)

(c)
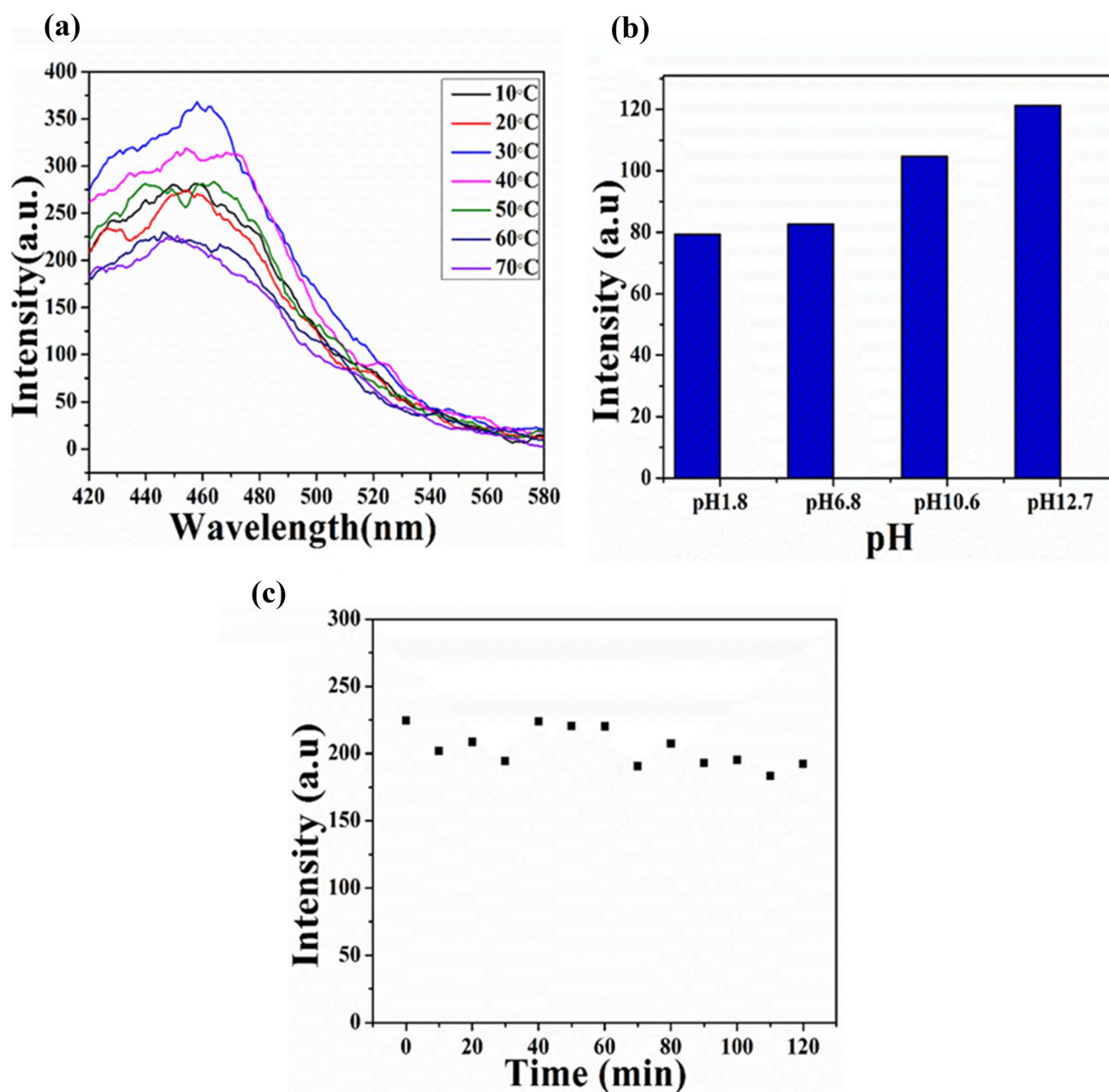
Fig. 3 Fluorescence stability experiments of the sensing probe varying the **a** temperature, **b** pH and **c** time respectively

Initially, each ionic solution has been separately prepared at 500 µM concentration and added to the sensing probe (FCD) to measure the fluorescence intensity. Although no notable changes have been observed in the fluorescence intensity of the probe for any ionic environment, however in the case of Cr (VI) the fluorescence intensity quenches drastically, which can be visualized even through naked eyes. Additionally, in Fig. 4 the colorimetric analysis of this sensing phenomenon has been validated using the CIE-1931 plot. The fluorometric colour coordinates of the chromium-induced sample are x = 0.21875 and y = 0.1888 whereas it is found

to be x = 0.15504 and y = 0.1344 in the pure sensor material. Such dramatic quenching makes this fluorometric probe (FCD) a potential Cr (VI) sensor.

Alternatively, a quantitative quenching experiment has been conducted to determine the amount of chromium contamination in water. In this experiment, the varying concentration of hexavalent chromium has been added to the fluorometric probe (FCD) separately and the corresponding fluorescence intensities have been measured. It is found that the fluorescence intensity has been gradually quenched upon Cr (VI) addition. Further, the fluorescence intensities
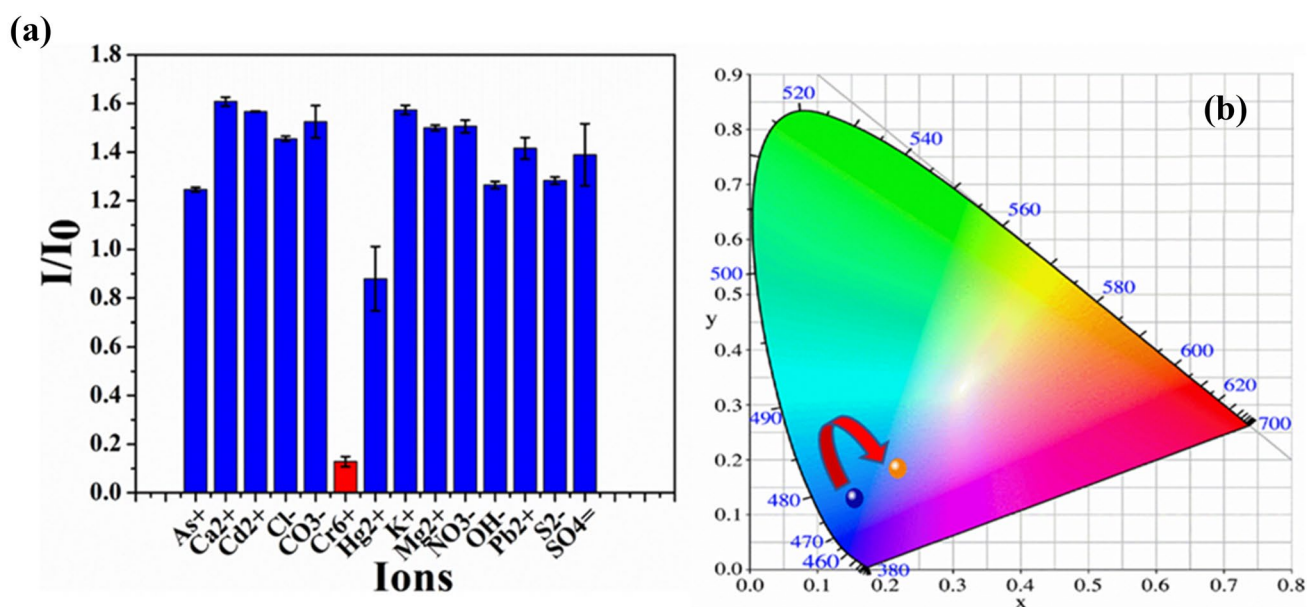
Fig. 4 **a** Selectivity study of the sensor probe against an array of different ions; **b** CIE-1931 plot showing colorimetric analysis of the sensor material

at higher concentrations follow an exponential decay which is quite significant in this type of sensing probe evident in Fig. 5. The concentration-dependent fluorescence intensities have been plotted and further fitted with linear and exponential Stern–Volmer equations [37, 38].

The Stern Volmer plot (S-V) was used to estimate the limit of detection (LOD) and limit of quantitation (LOQ) using the following expressions,

$$I_0/I = 1 + K_{SV}[M] \tag{1}$$

$$I_0/I = A\exp(K_{SV}[M]) \tag{2}$$

where I_0 and I are taken as fluorescent intensities of the probe before and after the Cr (VI) addition, [M] stands for

the concentration of respective ions, A is a constant term and K_{SV} is the Stern–Volmer constant. The linearity of the plot was found up to 10 μM concentration beyond this concentration of Cr (VI) exponential decay of the fluorescence occurred.

The LOD and LOQ of the probe have been estimated using Eqs. 3 and 4 and found to be 81 nM and 269.73 nM respectively.

$$LOD = 3\sigma/K_{SV} \tag{3}$$

$$LOD = 10\sigma/K_{SV} \tag{4}$$

where σ and K_{SV} are the calculated normalized standard deviation of the fluorescence of the sensing probe without
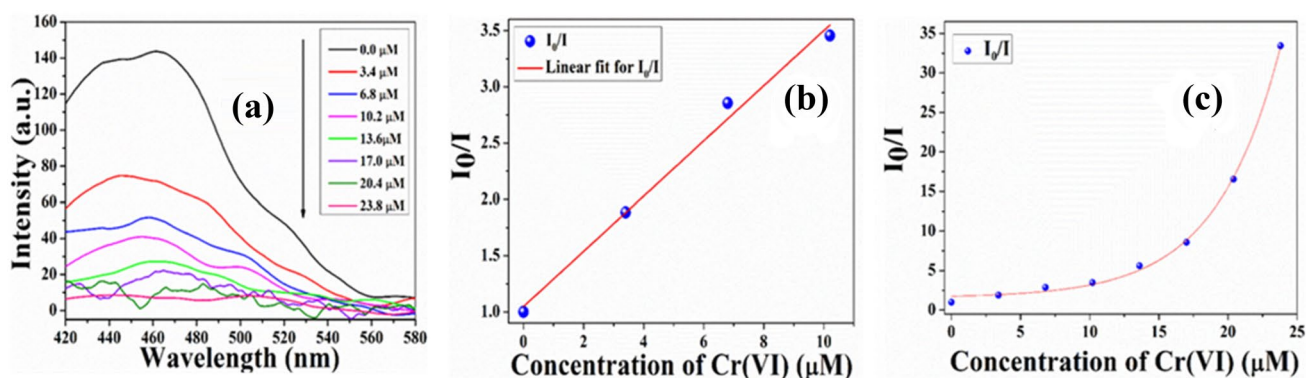
Fig. 5 **a** Concentration-dependent quenching experiment; **b** linear and **c** exponential S-V Plots of the sensing probe upon Cr (VI) addition

any quencher (taking at least ten separate experiments) and S-V quenching constant respectively. Such a competent selectivity and low detection limit (LOD 81 nM) with moderately high K_{SV} values suggest the fluorescent FCD is an effective sensing probe for hexavalent chromium in the aqueous medium (Table S2).

Detection Mechanism of the Sensing Probe

The fluorometric detection of hexavalent chromium is ascertained by using the S-V plots and the fluorescence lifetime data of the sensor material. The simultaneous decay of the steady-state fluorescence (from S-V plots) and fluorescence lifetime upon chromium addition suggests that the fluorescence quenching mechanism takes place in the excited state of the fluorophores. The linear S-V plot (up to 10 µM concentration) in Fig. 5 of the sensor material also validates the photoinduced electron transfer from the fluorophores to the quencher moiety [38–40]. Such electron transfer definitely restricts the radiative transition during the emission of the fluorophore molecule (precisely carbon dot). Thus, no emission occurs during the LUMO–HOMO transition of the fluorophores due to an insufficient number of electrons. This phenomenon has been reported by various other groups in their recent papers [11].

Moreover, at higher quencher concentrations (> 10 µM concentration), the fluorophores are surrounded by the quencher ions, which block the radiative path of the fluorophores causing rapid fluorometric quenching. Such a phenomenon is known as the inner filter effect [41–43]. Herein, the simultaneous occurrence of the photoinduced electron

transfer and inner filter effect is obtained at higher Cr (VI) concentrations, which justifies the exponential S-V plot.

Application of Sensor in Real-life Water Samples

The efficacy of the synthesized probe was analyzed for an array of water samples collected from different sources. Potable drinking water was taken from a water purifier, pond water was collected from a nearby small pond within the Jadavpur University campus and the wastewater was collected from drainage near the Jadavpur area, Kolkata. The water samples were collected in fresh sterile tubes and were further passed through 0.45 µm membrane filters and divided into two parts. One part is treated with 50 µM Cr(VI) and the other remained untreated. The physical parameters of the collected freshwater samples have been assessed using a Hanna-HI991300 portable pH/TDS/Temperature meter prior to the fluorescence assay (Table S3). The fluorescence intensity in all the cases is recorded and depicted in Fig. 6. It is found that the fluorescence intensity of the Cr (VI) treated water samples get quenched irrespective of their source. Such sensing characteristics of the sensing probe in various real-life water samples certainly reveal the real-life applicability of the probe.

The sensing efficacy of the synthesized probe was further tested against real-life tannery wastewater, which was collected from a canal adjacent to a tannery factory. Initially, the elemental analysis was performed by employing an inductively coupled plasma atomic absorption spectroscopy (ICP-AES) showing an alarming amount of chromium (16.53 ppm) (Table S4) besides other toxic heavy metals. Further, the fluorescence intensity of this wastewater sample
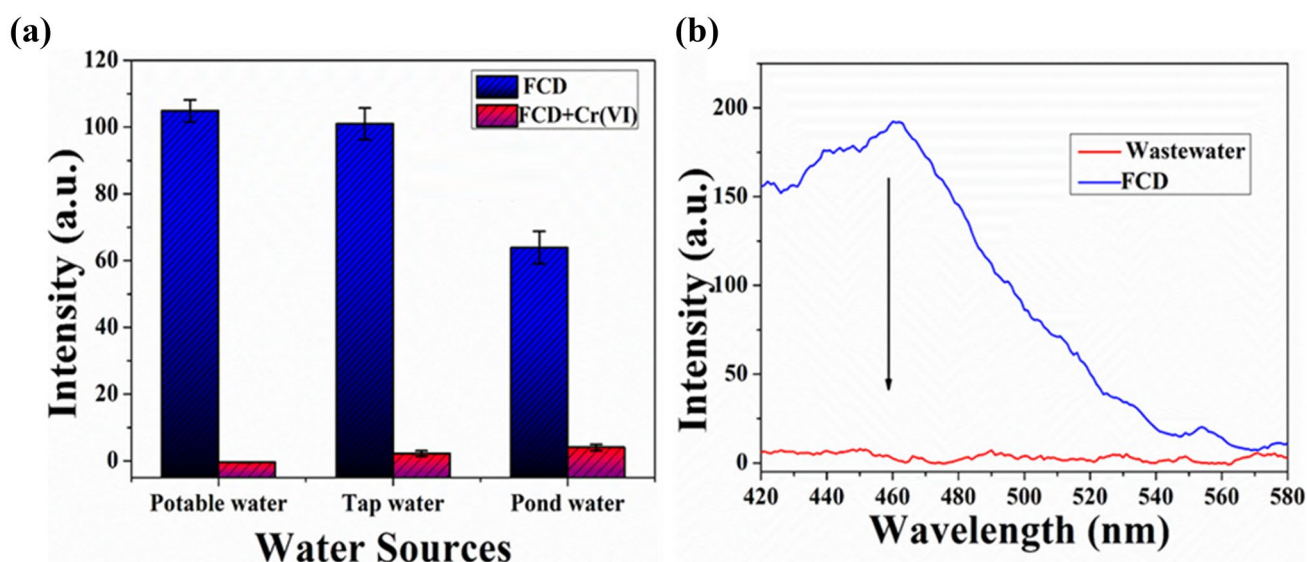
Fig. 6 (a) Detection of hexavalent chromium in different water samples (b); Real-life sensing of Cr (VI) in tannery wastewater

has been experimented with using the synthesized sensing probe (FCD). The fluorescence intensity is found to decrease rapidly after the addition of the wastewater sample into the probe solution. This proves the fact that our synthesized nano-probe can detect Cr (VI) in real-life industrial wastewater samples.

In-Vitro Biosensing of Cr (VI) using the Probe

Hexavalent chromium Cr (VI) enters into the cells via an array of enzyme mediating reactions with the generation of intermediates and free radicals like hydroxyl and peroxide ultimately culminating in the production of Cr (III). This reduction of chromium can be extracellular or intracellular, the latter piles up ultimately in the cell to give rise to genotoxicity, its intercalation within the DNA through Fenton's reaction, causing oxidative stress via p53 generation [44–50]. Thus, it is necessary to detect hexavalent chromium in living cells in order to assess the rate of contamination.

Herein, the experimental verification of the biosensing efficacy of our probe (FCD) has been performed using a simple fluorescence microscopy technique [51–54]. HeLa cells have been used to determine such activity of the sensing probe. Initially, HeLa cells were segregated into two segments. One segment is treated with hexavalent chromium and the other one remained untreated. Both the treated and untreated cells were additionally treated with the sensor material prior to the Cr(VI) treatment. Finally, the cells are seen using a fluorescence microscope and the images are depicted in Fig. 7. The fluorescence microscopy images show a promising blue emission in the untreated sample under UV excitation. This suggests the permeability of the nano-sensor (FCD) through the cell membrane. Whereas, the Cr(VI) treated samples do not show any fluorescence under the UV excitation energy. Such drastic quenching of fluorescence suggests the successful sensing efficacy of Cr(VI) in living cells. In order to validate such biosensing activity, a theoretical molecular docking study was performed involving the probe (FCD) with that of cytochrome-b_5 (cyt b_5) and cytochrome-P450 (cyt P450) as shown in Fig. 8. There is a total of nine poses obtained for both cyt b_5 and cyt P450 separately, among which the initial poses have been selected as they are providing the lowest binding energies. In the case of cyt b_5, there was weak hydrogen bonding resulting from C=O and N–H interaction between the glycine residue and the OH-group of the carbon dot moiety of the sensing probe. Additionally, the tyrosine moiety of the enzyme is well attached to the probe resulting in a binding affinity of -7.8 kcal/mol between the sensor and cyt b_5.
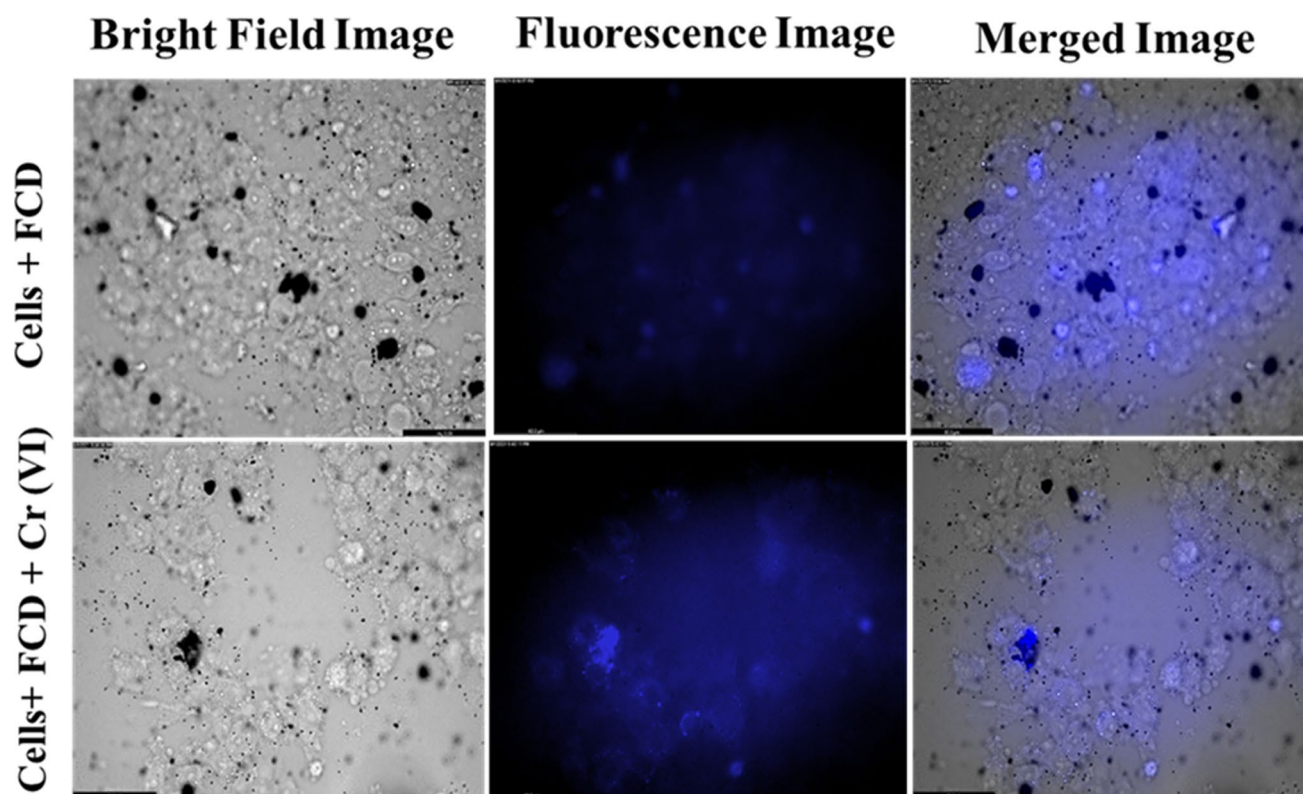
Fig. 7 Bio-imaging of pure and Cr (VI) contained He La cells using the synthesized sensor material
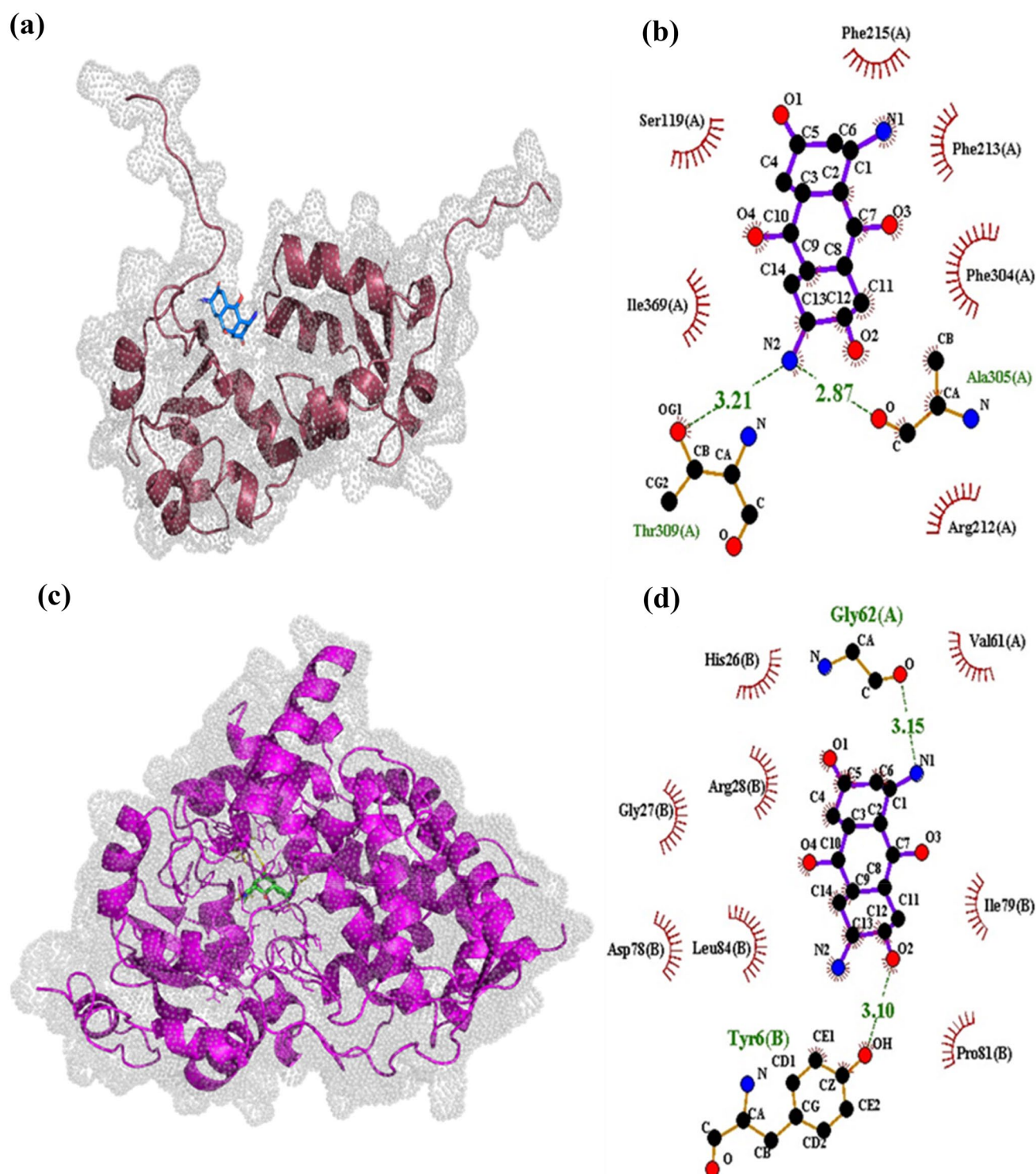
Fig. 8 Molecular docking simulation of Cyt b5 (**a**, **b**) and Cyt P450 (**c**, **d**) respectively showing binding of the fluorophore with the respective amino acids

On the other hand, the carbon dot moiety of the fluorescent probe is attached to the crevices of the cyt P450 by weak hydrogen bonding. This interaction with amino acids like threonine and alanine resulted in a binding affinity of -8.0 kcal/mol between the sensing probe and the enzyme. The terminal nitrogen of the sensor moiety in this case forms weak hydrogen bonds with both the carboxylic groups of the hydrophobic threonine (Thr 309) and aliphatic alanine (Ala 305) for interaction.

Conclusions

In this work, a fluorescent carbon quantum dot incorporated biocompatible α-FeOOH nanoparticle has been synthesized through a facile hydrothermal method. The x-ray crystallographic studies coupled with elemental and morphological analyses infers the successful synthesis of the hybrid nanoparticle. The synthesized nanosystem acts as a selective and sensitive probe for hexavalent chromium ions in wastewater with a pronounced sensitivity (LOD 81 nm). It can be presumed that the fluorescence quenching is taking place at an excited state, which is a case of photoinduced electron transfer, where with the addition of Cr (VI) quenches the fluorophores rapidly. In higher Cr (VI) concentrations, the fluorescence intensity seems to decrease a way faster and can be attributed to the simultaneous possessions of the inner filter effect and photoinduced electron transfer. The efficacy of the probe has been validated by using various types of Cr (VI) contained waters showing uninterrupted sensing efficiency of the probe in all water types. Additionally, a sensing experiment has been conducted in chromium-containing industrial tannery wastewater, which also depicts the successful detection of hexavalent chromium irrespective of other heavy metals present in the sample. Such an efficient and rapid fluorometric probe has been employed in biosensing studies to detect Cr(VI) in living cells. The sensor material shows an excellent blue fluorescence in cells, whereas it gets quenched upon chromium addition. Such sensing activity has been theoretically demonstrated using molecular docking simulations showing that the cyt b_5 and cyt p450 are primarily responsible for such sensing phenomenon in HeLa cells. Such excellent bioimaging capability, especially in the cancer cell line confirms the potentiality of the sensor in early-stage cancer detection. Such natural mineral-based cost-effective but efficient sensor can have the immense possibility as a tumor marker and in biopsy applications as an alternative to the expensive medical techniques. Moreover, this sensor can be useful for tracing the pathway for biomagnification and in bioaccumulation studies. Hence, this fluoro-sensor is a promising candidate in wastewater monitoring systems but also creates an opportunity to evaluate chromium toxicity in living systems.

Data Availability Statement The data will be available at the reasonable request.

Declarations

Ethics Approval Not applicable.

Consent to Participate Not applicable.

Consent for Publication Not applicable.

Competing Interests The authors declare that they have no competing interests.

References

1. Hazrat A, Khan E, Ilahi I (2019) Environmental Chemistry & Ecotoxicology of Hazardous Heavy Metals: Environmental Persistence Toxicity & Bioaccumulation. J Chem 4:1–14
2. Jarup L (2003) Hazards of Heavy Metal Contamination. Br Med Bull 68(1):167–182
3. Jayshankar M et al (2014) Toxicity mechanism and health effects of some heavy metals. Interdiscip Toxicol 7(2):60–72
4. Rahman Z, Singh VP (2019) The relative impact of toxic heavy metals (THMs) arsenic (As), cadmium (Cd), chromium (Cr VI), mercury (Hg) and lead (Pb) on the total environment. Environ Monit Assess 191(7):1–11
5. Mitra S, Sarkar A, Sen S (2017) Removal of Chromium from industrial effluents using nanotechnology: a review. Nanotechnology Environmental Engineering 2(11):1–14
6. Guo Q (1997) Increase of lead and chromium in drinking water from using cement-mortar lined pipes: initial modelling and assessment. J Hazard Mater 56(1–2):181–213
7. Ray RR (2016) Adverse hematological effects of hexavalent chromium: an overview. Interdiscip Toxicol 9(2):55–65
8. Turskewycz AR, Shukla R, Ball AS (2018) Pndhytofabrication of Iron nanoparticles for hexavalent chromium remediation. ACS Omega 3(9):10781–10790
9. Tall A et al (2021) Green emitting N, P- doped Carbon dots as efficient fluorescent nanoprobes for determination of Cr (VI) in water and soil samples. Microchem J 166:1–11
10. Alford R et al (2009) Toxicity of Organic Fluorophores Used in Molecular Imaging: Literature Review. Mol Imaging 8(6):341–354
11. Roy S et al (2020) In situ Grown C-dot Wrapped Boehmite Nanoparticles for Cr (VI) Sensing in Waste water and a Theoretical Probe for Chromium-Induced Carcinogen Detection. ACS Applied Material Interfaces 12(39):43833–43843
12. Ryu HJ et al (2014) Evaluation of silica nanoparticle toxicity after topical exposure for 90 days. Int J Nanomed 9(2):127–136
13. Forest V et al (2014) Toxicity of boehmite nanoparticles: Impact of the ultrafine fraction and of the agglomerates size on cytotoxicity and proinflammatory response. Inhalation Toxicol 26(9):545–553

14. Pauluhn J (2009) Pulmonary Toxicity and Fate of Agglomerated 10 and 40nm Aluminium oxyhydroxides following 4 week Inhalation exposure of Rats: Toxic Effects are Determined by Agglomerated, not primary particle size. Toxicol Sci 109(1):152–167

15. Darehnaranji MK et al (2021) Bio Assisted Food Grade FeOOH Nanoellipsoids as Promising Iron Supplements For Food Fortification. Applied Food Biotechnology 8:71–77

16. Novin D et al (2020) A functional dairy product rich in Menaquinone-7 and FeOOH nanoparticles. Food Sci Technol 129:1–18

17. Saffari F et al (2015) Effects of Co-substitution on the structural and magnetic properties of Ni $Co_xFe_{2-x}O_4$ ferrite nanoparticles. Ceramic International 41(6):7352–7358

18. Momma K, Izumi F (2008) VESTA: A Three-Dimensional Visualization System for Electronic and Structural Analysis. J Appl Crystallogr 41:653–658

19. Siroha P et al (2006) Comparative Study on crystallographic representation of transition metal oxides polymorphs nanomaterials using VESTA software: Case Study of Fe_2O_3 and TiO_2. AIP Conference Proceedings

20. Goodsell DS, Morris GM, Olson AJ (1996) Automated docking of flexible ligands: applications of Auto dock. J Mol Recognit 9(1):1–5

21. Muzio ED, Toti D, Polticelli F (2017) DockingApp: a user-friendly interface for facilitated simulations with Autodock Vina. J Comput Aided Mol Des 31(2):213–218

22. Trott O, Olson AJ (2010) Autodock Vina: Improving the speed and accuracy of docking with a new scoring function, efficient optimization and multithreading. J Comput Chem 31(2):455–461

23. Delano WL et al (2002) An open- source molecular graphics tool. CCP4 Newsletter Protein Crystallography 40:82–92

24. Seeliger D, Groot BL (2010) Ligand Docking and binding site analysis with PyMOL and Autodock/Vina. Computer- Aided Molecular Design 24(5):417–422

25. Ji TH et al (2020) Electron/ energy co-transfer behaviour and reducibility of Cu-Chlorophyllin bonded carbon dots. RSC Advance 10(52):31495–31501

26. Varotsis C, Vamvouka M (1998) Resonance Raman and FTIR studies of Carbon Monoxide-bound Cytochrome aa_3-600 Oxidase of Bacillus subtilis. J Phys Chem B 102(39):7670–7673

27. Verneker D, Jagadeesan D (2015) Tunable acid base bifunctional catalytic activity of FeOOH in an orthogonal tandem reaction. Cat Sci Technol 5(8):4029–4038

28. Su Y et al (2018) Immobilization of horse peroxidase on amino functionalized carbon dots for the sensitive detection of hydrogen peroxide. Microchim Acta 185(2):1–8

29. Wu Y, Remcho VT (2016) A capillary electrophoretic method for separation and characterization of carbon dots and carbon antibody bioconjugates. Talanta 161:854–859

30. Zhao Y et al (2015) Carbon dots: From Intense Absorption in Visible Range to Excitation Independent and Excitation dependant Fluorescence. Fullerene Nanotubes Carbon Nanostructures 23(11):922–929

31. Tadesse A et al (2020) Fluorescent Nitrogen Doped Carbon Quantum dots Derived from Citrus Lemon Juice: Green Synthesis, Mercury (II) Ion Sensing and Live Cell Imaging. ACS Omega 5(8):3889–3898

32. Sherman DM, Waite TD (1985) Electronic spectra of Fe^{3+} oxide and oxide hydroxides in the near IR to UV. Am Miner 70(11–12):1262–1269

33. Tang X, Yu H, Bui B (2021) Nitrogen Doped Fluorescent Carbon dots as multi mechanism detection for iodide and curcumin in biological and food sample. Bioactive Materials 6(6):1541–1554

34. Yan F et al (2019) The fluorescence mechanism of carbon dots and methods for tuning their emission color: a review. Microchim Acta 186(8):1–37

35. Lu F (2017) Fluorescent Carbon dots with tunable negative charges for bioimaging in bacterial viability assessment. Carbon 120:95–102

36. Bardhan S et al (2020) Nitrogenous Carbon dot decorated natural microcline: an ameliorative dual probe for Fe^{3+} and Cr^{6+} detection. Dalton Trans 49(30):10554–10556

37. Roy S et al (2019) Gd (III) Doped Boehmite Nanoparticle: An Emergent Material for Fluorescent sensing of Cr (VI) in Waste Water and Live cells. Inorg Chem 58(13):8369–8378

38. Malkondu S (2014) A highly selective and sensitive perylenebisimide based fluorescent PET sensor for Al^{3+} determination in MeCN. Tetrahedron 70(35):5580–5584

39. Mohandoss S, Stalin T (2017) A new fluorescent PET sensor probe for Co^{2+} ion detection: computational, logic device and living cell imaging applications. RSC Advance 7(27):16581–16593

40. Fegade U, Attarde S, Kuwar A (2013) Fluorescent recognition of Fe^{3+} ion with photoinduced electron transfer (PET) sensor. Chem Phys Lett 584:165–171

41. Bhatt S et al (2018) Green route for synthesis of multifunctional fluorescent carbon dots from Tulsi leaves and its application as Cr (VI) sensors, bioimaging and patterning agents. Colloids Surf, B 167:126–133

42. Mao M et al (2018) Inner filter effect based fluorometric determination of the activity of alkaline phosphatase by using carbon dots codoped with boron and nitrogen. Microchim Acta 185(1):1–6

43. Huang D et al (2021) Fluorescent Nitrogen doped Ti_3C_2 Mxene quantum dots as unique on off on nanoprobe for chromium (VI) and ascorbic acid based on inner filter effect. Sensors and Actuators B: Chemistry 342

44. Mattia GD et al (2004) Impairment of cell and plasma redox state in subjects professionally exposed to chromium. Am J Ind Med 46(2):120–125

45. Chiu A et al (2010) Review of chromium (VI) apoptosis, cell cycle arrest and carcinogenesis. J Environ Sci Health C Environ Carcinog Ecotoxicol Rev 28(3):188–230

46. Wang S et al (2020) The role of hydroxyl radical as a messenger in Cr (VI) induced p53 activation. American Journal of Physiology-Cell- Physiology 279(3):868–875

47. Myers CR (2012) The effect of chromium (VI) on the thioredoxin system: Implications for redox regulation. Free Radical Biol Med 52(10):2091–2107

48. Des Marias TL, Costa DL (2019) Mechanisms of chromium induced toxicity. Curr Opin Toxicol 14:1–7

49. Fang Z et al (2014) Genotoxicity of Tri and Hexavalent Chromium Compounds In Vivo and Their mode of action on DNA damage In Vitro. PLoS ONE 9(8):1–9

50. Zhang XH et al (2011) Chronic occupational exposure to hexavalent chromium causes DNA damage in electroplating workers. BMC Public Health 11:1–8

51. Huang Q et al (2021) Carbon dots derived from Poria cocos polysaccharide as an effective "'on off" fluorescent sensor for chromium (VI) detection. J Pharm Anal p. 1–9

52. Lu KH et al (2019) A fluorometric paper test for chromium (VI) based on the use of N doped carbon dots. Mirochimica Acta 186(227):1–7

53. Gao Y et al (2018) Carbon dots with red emission as a fluorescence and colorimetric dual readout probe for the detection of chromium (VI) and cysteine and its logic gate operation. J Mater Chem B 6(38):6099–6107

54. Sakaew C et al (2020) Green and facile synthesis of water soluble carbon dots from ethanolic shallot extract for chromium ion sensing in milk, fruit juices and waste water samples. RSC Adv 10(35):20638–20645

Publisher's Note Springer Nature remains neutral with regard to jurisdictional claims in published maps and institutional affiliations.

Factors for COVID-19 Infection that Govern the Severity of Illness

Bidisha Ghosh [1†], Soumyadev Sarkar [2†], Nayim Sepay [3], Kaustuv Das [1],

Sukhen Das [1], Sujata Ghosh Dastidar [4*]

[1] *Department of Physics, Jadavpur University, 188, Raja S.C Mullick Road, Kolkata-700032, India.*

[2] *Division of Biology, Kansas State University, Manhattan, Kansas, United States.*

[3] *Department of Chemistry, Lady Brabourne College, Kolkata-700017, India.*

[4] *Department of Microbiology, Herbicure Healthcare Bio-Herbal Research Foundation, Saral Dighi (E), Boral, Kolkata-700154, India.*

Abstract

Coronaviruses have been posing a serious threat to mammals and birds and a new class of SARS-CoV is creating havoc to the world after its first incidence in Wuhan City in China in December 2019. These viruses are mainly responsible for causing serious respiratory tract infections which generally appear initially as the common cold and can be lethal just like SARS-CoV. The problems seem to vary and worsen from one person to another depending on age, gender, ethnicity, blood groups, host genetics, and associated comorbidities. Complications should also arise as this virus keeps mutating and evolving. This review points out the various underlying causes behind the severity of the illness and the mechanisms associated with it. This review will help society to understand the risks and severities associated with COVID-19. Individuals with health complexities and predispositions listed in this review are the most vulnerable in terms of severity and should take every possible measure to protect themselves from getting infected. As a consequence, this will lead to a decrease in mortality rates arising from COVID-19.

Keywords: SARS-CoV-2; COVID-19; Coronavirus; Severity; Comorbidity.

1. Introduction

The newly evolved SARS-CoV-2 that had originated in the Wuhan City, Hubei Province in China in December 2019, has by now affected almost 218 countries of the globe [1]. Initially World Health Organization (WHO) named the disease 2019 novel coronavirus (2019 n-CoV) on 12th January 2020, and on 12th February 2019 they coined the term coronavirus disease 2019 (COVID-19). The name SARS-CoV-2 was finally issued by the Coronavirus Study Group (CSG) and this sudden outbreak was declared by WHO as Public Health Emergency of International concern by January 30th 2020 [2, 3]. As per the reports of WHO of March 20 2021, there are 121,969,223 confirmed cases of COVID infection, 2,694,094 deaths worldwide [4]. The patients were reported to have pneumonia like symptoms with other ancillary clinical SARS-CoV like symptoms such as dry cough, dyspnoea, fever, myalgia, and fewer having symptoms like fatigue, diarrhoea, haemoptysis, abdominal pain [5, 6]. Bilateral pneumonia was recorded in 75% of the patients [5]. In this review, we discuss the newly emerging SARS-CoV-2 virus, its origin, trying to address the

underlying causes of severity due to gender, genetic and molecular differences, existing diseases as well as socio-demographic factors that further exacerbate the disease.

2. Structural, Genomic Composition, And Sequence Homology Of SARS-Cov-2 Virus-Relation To Pathogenesis

Coronaviruses are one of the two genera besides toroviruses of the Coronaviridae family [7, 8]. Coronaviruses and Toroviruses are regarded now as a family in the order of Nidovirales that has an envelope in which the genome is a positive-sense single-stranded RNA. Coronaviruses are considered much more powerful compared to HIV-1 as the infectivity of SARS-CoV is high and remaining viable for 1-4 days compared to MERS-CoV virions which are comparatively fragile than SARS [9]. SARS-CoV-2 is closer to SARS-CoV sharing about 79.5% maximum sequence homology, and 94.4% identity with SARS-CoV in the ORF1ab amino acid sequence carrying seven conserved sequences of replicase [10] and just 50% with MERS CoV [11].

Cats, ferrets [12], rodents [13] can be considered as intermediate host reservoirs for SARS-CoV-2, barring pangolin and Civet cats which cannot serve as direct intermediate host because the full length genomic homology of the pangolin coronavirus is 90.3% with that of SARS-CoV-2 and Spike glycoprotein (S) [SRR10168377] homology about 75% with SARS-CoV [13, 14], and lacking polybasic cleavage site required for ACE2 receptor expressed in human cells [15] On the other hand, the sequence homology of the S protein of Civet cats to that of humans SARS-CoV-2 is 75.4% [13].

The 2019 COVID SARS-CoV-2 has been found to have 14 ORFs encoding 27 proteins as was proposed by Wu *et al*. The four structural proteins for spike surface glycoprotein (S), small envelope protein (I), matrix glycoprotein (M), and nucleocapsid protein (N), along with eight accessory proteins 3a, 3b, p6, 7a, 7b, 8b, 9b and orf 14 is present in the 3' terminus of the genome (Figure 1).
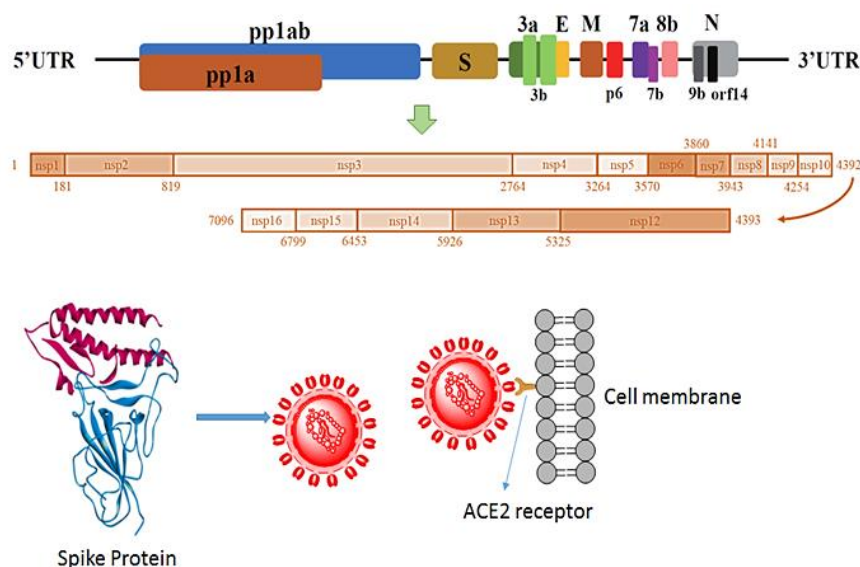
Figure 1. Spike protein development of coronavirus and its binding with ACE2

The 5' terminus of the genome contains orf1ab and orf1b genes encoding pp1ab and pp1a protein respectively. Further phylogenetics and Molecular Evolutionary Genetics analysis (MEGA version 7.0) in their study showed the SARS- CoV-2 2019 virus can be placed in parallel to SARS Bat CoV as almost all encoded protein of pp1ab, pp1a, envelop, accessory protein 7a in the 2019 SARS-CoV-2 have similarity with SARS- CoV along with the spike gene and 3ab and 8b have closest resemblance to SARS-CoVs [16]. However, their study revealed that there are marked differences between SARS-CoV and SARS-CoV-2 (2019) virus in terms of their accessory proteins, their presence, and relative amino acid composition. The 8a protein is present in SARS-CoV and not in SARS-CoV-2, the 8b protein in SARS-CoV-2 is 121 amino acid long but is only composed of 84 amino acids in SARS-CoV. The 3b protein is 154 amino acid long in SARS-CoV while it is only 22 amino acid long in SARS-CoV-2 virus [16]. How this amino acid variation in the accessory protein composition of SARS-CoV-2 contributes to being more virulent than its counterpart SARS-CoV is still needs to be elucidated. However, as it has been seen the degree of binding patterns of the S glycoprotein of the newly evolved SARS-CoV2 with the ACE2 receptor expressed on the lung cells strikingly differ from that of SARS-CoV [17]. Earlier reports suggest spike protein of SARS-CoV contains a receptor-binding domain (RBD) that specifically binds to ACE2 [18]. Joseph Thomas *et al*. proposed via molecular docking techniques that the increased binding capability of the viral spike protein with the ACE2 is due to the several amino acid substitutions in

the RBD domain of the SARS CoV-2. They showed the two longer cappings of the RBD of the SARS-CoV-2 is providing tight binding to the receptor ACE2 [19].

3. Role of ACE2 Receptor in Virus Adherence, Its Presence – A Boon or Bane? Immune Cells Playing a Peekaboo?

ACE2 is a type I glycoprotein [20] which acts as a key component in RAS signalling. In the RAS signalling pathway, Angiotensin I (Ang I) is metabolised by ACE, a dipeptide carboxypeptidase which leads to Angiotensin II (Ang II) which is then metabolised by ACE2 that forms Angiotensin 1-7 [21]. The ACE2 receptor thus regulates the balance of angiotensin II (Ang II) that induces pulmonary vasoconstriction. ACE2 is expressed almost in all types of cells but the presence of it is more in type II alveolar epithelial cells of the lungs, and thus it efficiently facilitates the adhesion, translocation, and replication of the SARS-CoV and the new SARS-CoV-2 responsible for the outbreak in 2019-2020. Therefore, it can be said that heightened ACE2 expression is associated with an enhanced risk in COVID-19 cases [22]. Increased levels of Ang II cause vascular permeability which causes pulmonary oedema [23]. The etiology of the SARS-CoV-2 2019 has been seen to be largely associated with differential ACE2 expression. Jiawei Chen *et al*. performed a study of the ACE2 expression in 30 different tissues among thousand individuals by Gene Tissue Expression (GTEx) and found that high levels at about 100 % of ACE2 expression are seen in East Asian, and >30% in other ethnic groups. Their study further pointed out two important findings: a) higher ACE2 expression is seen in Asian females than in Asian males. It has been related to the secretion of estrogen levels in female, which decline with age and thus decreasing the levels of ACE2 expression and thus making them more prone to infection; b) The study pointed out that transgender males who sought estrogen therapy and androgen therapy for a year show high levels of ACE2 expression and the Sertoli cells of their body showed a large number of ACE2 expressing cells [24]. Zhao *et al*. pointed out via single-cell RNA sequencing that the expression of ACE2 expression in the lung cells is more in the Asian race compared to those belonging to African-American ethnicity [25].

However, Vinciguerra *et al*. put forward a hypothesis that lack of ACE2 expression may be a protective factor against SARS-CoV-2 as the virus enters by binding to the ACE2 receptor and thus they proposed that black people has an advantage over other ethnic groups but also it was concluded that once contracted with the virus it may pose detrimental effects to the host. As it was seen that in the black people, 20 out of 31 individuals by April 2020 was hit hard by the infection due to reduced ACE2 expression and subsequent rise in Ang II levels and thereby contributing to the ancillary risk of comorbidity [22]. However, there emerge contrary explanations that say though the SARS-CoV-2 virus employs the ACE2 as a podium to demonstrate its dramatic effects, the worsening effects are largely contributed due to differences in ACE/ACE2 races among individuals irrespective of gender, and have comorbidities. The ACE/ACE2 expression is downregulated in pathological conditions and also with associated comorbidities like hypertension, diabetes, cardiovascular diseases [26, 27] Alzheimer's disease [28, 29] and is upregulated in cigarette smokers [30]. The three different macrophage population that predominates in the lung cells has got a huge role to play because of its differential activation, and its subsequent response via inflammation varies largely following decreased ACE2 expression once the virus enters the cells further aggravating the predicament [31]. Older age is related to "inflammaging" which is a surge of the proinflammatory cytokines like IL-1 [32], IL-6, and TNF-α [33] COVID-19 patients have been diagnosed with higher number of immune cells like macrophages and also monocytes. Also, the neutrophil-monocyte ratio gets substantially elevated in the course of infection with increased proinflammatory cytokines [33]. A point to be considered here is that the dubious role of ACE2 is directly linked to monocytes and macrophages as they both express ACE2 on their cell surface and both SARS-CoV-1 and SARS-CoV-2 causes downregulation of ACE2 and its reduction with age further flares up the susceptibility of infection [34]. It has been seen that aged monocytes contribute to a proinflammatory phenotypic appearance brought about by reduced mitochondrial functioning [2, 34]. Further aging has been seen to directly impair with the phagocytosis of alveolar macrophage cells and thereby promoting the death of mice when infected with influenza virus by downregulation CD204 responsible for the internalization of apoptotic cells [35]. This has been accompanied by cellular changes in the endoplasmic reticulum which are associated with an increased amount of misfolded or unfolded proteins. Reduced activity of these misfolded protein degradations by unfolded protein response capacity (UPR) and reduced autophagic potential can lead to increase in production of these vicious cytokines, TNF and C-reactive protein [36].

4. Vitamin D can Influence COVID-19 Infection and Severity

Another important aspect that needs to be pointed out in this regard is the disparity of Vitamin D deficiency among different races. Ronald Evans *et al.* pointed out that the deficiency of Vitamin D may fail to activate the Vitamin D Receptor (VDR) that has a role to negatively regulate TGFß signaling by interfering with Smad 3 transcriptional silencing in the hepatic stellate cells (HSC) [37]. Vitamin D plays a key role in suppressing pathologic responses to the virus [38]. Vitamin D has been seen to play effective action in reducing the proinflammatory cytokines by the inhibiting factors of the NFBκB pathway and in turn suppressing immune-mediated injury in the body [39-41]. High levels of TGFß has been seen in COVID-19 patients [42] and thereby initiating several inflammatory cytokine release

(IL-Iß1, IL-6, TNF) which causes alveolar damage [43]. There had been evidence that African people have low circulating 25 (OH) D compared to that of the Caucasians and are at high risk of Vitamin D deficiency [44]. This has led to the connection that SARS-CoV-2 is associated with Acute Respiratory Distress Syndrome (ARDS) individuals with low (27.6nmol/L) to very low (13.7nmol/L) 25(OH) D concentration in their blood levels [45, 46]. In a retrospective cohort study conducted by Eboni G *et al.* it was revealed in Lousiana between March 1 and April 11 2020, 59% of COVID-19 mortality rates was related to the black non-Hispanics though they comprise only 33% of the population besides white non-Hispanics and about 80% received mechanical ventilation [47]. Variations in the genes encoding Vitamin D binding protein, VDBP (GC), vitamin D 25-hydroxylase (CYP2R1), genes encoding enzyme 7-dehydrocholesterol reductase and 1,25-hydroxyvitamin-D3-2 4-hydroxylase (the region around DHCR7 and CYP24A1 respectively) and variance in either of these four genes may result in a total variance of 1.5% in these genes. This may appear insignificant but may largely affect 25 (OH) D levels. A variant of the rs4588A allele has been seen to contribute to low 25 (OH) D in the European population which however is not seen in individuals of African ethnicity. So, to conclude it is clear that COVID-19 incidence has a clear connection to vitamin D deficiency, with a majority of COVID-19 patients are found to be deficient in this particular vitamin [48, 49].

5. Impact of Ethnicity, Gender and Age

There is a differential gender-related epidemiology in the SARS-CoV-2 infection and men can be seen as more affected than females. During earlier times, in case of viral infections like Ebola and Zika, women have been seen to have least affected than males though serving roles as frontline caregivers during 2014-16 Ebola virus outbreak in West Africa [50]. A study carried out with COVID-19 confirmed 1,190 adult patients in Wuhan Infectious Disease Hospital and it was found that 635 (53.4%) patients were male and 555 (46.6%) were females although there had been more female health workers than male. There had been marked differences in not only laboratory reports but also in immunological biomarkers. Male patients had higher leucocyte and neutrophil counts, lower lymphocyte, and platelets count and comparatively lower CD4/CD8 ratio, and high levels of inflammatory cytokines than females [51]. There had been previous reports of "cytokine storm" generated due to high plasma levels containing an array of inflammatory interleukins-IL-1ß, IL-6, IL-7, IL-8, IL-18, Granulocyte Colony Stimulating Factor (GSF), and Tumor Necrosis Factor (TNF-α) which results from macrophage activation ultimately leading to mortality (Figure 2) [52].
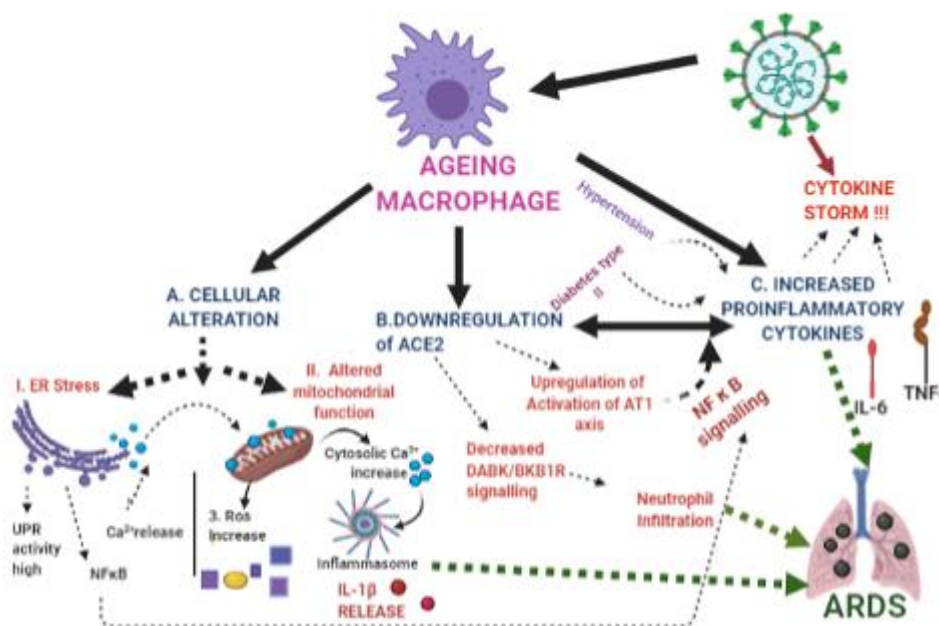
Figure 2. ACE2 downregulation in Aged macrophages: a putative pathway that leads to increased inflammation due to SARS-CoV-2 infection. Cellular pathway alteration leading to defective ER and Mitochondrial dysregulations are important markers in the pathway. The ER releases Ca^{2+} which is taken by mitochondria leading to cytosolic Ca^{2+} pool and ultimate inflammasome formation. Downregulation of ACE2 leads to neutrophil infiltration. Further increased levels in proinflammatory cytokines are consequences of severity of lung distress.

An additional 15 cytokines namely M-CSF, 1L-10, IFN-α2, IL-17,1L-4, IP-10, IL-7, IL-1ra, GSF, IL-2, IFN-γ, IL-1α, IL-2, HGF and PDGF- BB have been identified as biomarkers who increased level causes lung severity when 48 cytokine levels in blood were checked in a case study with 12 COVID-19 patients [53]. In a study conducted by Satis *et al.* with 58 individuals, it was found that the concentrations of Il-8 along with other inflammatory biomarkers had shown to worsen up the situations in SARS- CoV-2. The concentrations of IL-8 along with IL-6 was found to be higher in males than in females [54].

Expression of differential *TMPRSS2*, an androgen-responsive gene, which affects fusion of the viral membrane with the ACE2 receptor has given rise to sexual dimorphisms. It has been seen that TMPRSS2, a transmembrane serine protease 2 cleaves viral S-glycoprotein, and its expression is higher in males than in females. Single nucleotide polymorphisms in the *TMPRSS2* gene play a pivotal role in general population (rs2070788, rs7364083, rs99745890) and gender-related perspective (rs8134378) [55]. This has got a direct relation to the secretion of sex hormones, as estrogen (E2) has been seen to be affected by TMPRSS2 expression, and estrogen in turn, regulates ACE2 expression. E2 treated NHBE cells has been seen to lower ACE2 expression [56, 57]. However, this discrepancy in the infectivity can be attributed to the X-chromosome in humans. The genes for *ACE2* (locus Xp 22.2) and Ang-II receptor Type 2 (*AGTR2*, alias *AT2*, locus Xq23) happens to be located on the X-chromosome. Females have two X chromosomes and are heterozygous than males who have only one chromosome and are hemizygous [58]. One of the X chromosomes in females is inactivated by a process called Lyonization or X-inactivation by which the RNA transcribed from the Xist gene spreads to coat the whole chromosome [59]. The inactivation is however skipped in the Xp22.2 where the *ACE2* gene is located on the X chromosome [60]. The sixteen residue binding of SARS-CoV-2 RBM with 20 residues of ACE2 is somewhat different due to this difference in the X-chromosome inactivation. Out of the two X chromosomes in females, only one X chromosome has the *ACE2* which recognizes the SARS-CoV-2 receptor, the chance for the second X chromosome for binding is low and thus the chance for pulmonary oedema in COVID-19 is lowered. This can be seen as a boon for the females in contrast to males having a single X chromosome [61].

6. Role of Blood Groups in COVID-19 Infection

There had been a correlation with Landsteiner's ABO Blood grouping system with SARS-CoV-2 infection. The ABO blood grouping system is based upon the difference in the carbohydrate residues on the RBC cell surface which is inherited following Mendelian inheritance [62]. A close view of the common ABO blood groupings out of the 29 blood group systems reveal that ABO antigens are oligosaccharides formed of conjugates of carbohydrates and proteins. ABO antigens are biosynthesized when fucose gets attached to the terminal end of galactose via α1→2 linkage, which results in the H antigen that determines the O phenotype. A and B antigens are formed via enzymatic modification of the H epitope when the D isotope of the N-acetylglucosamine or galactose gets attached to the galactosyl residues [63, 64].

The difference in carbohydrate residues can be accounted to the difference in infections caused due to different pathogenic organisms. The RBC cell surface of different carbohydrate residues serve as receptors for toxins produced from the body of the microorganisms, it can be a rich habitat where they can colonize and multiply; pathogens like bacteria stimulate antibodies against RBC antigens [65]. ABO Blood Groupings are based on the surface antigens on the RBC which are either sugars as in the case of the RBC surface markers or proteins as seen in Rh blood group (encoded by the Rh D gene) [66, 67] Some studies indicate there is a high incidence of infection among non-O blood group types [68]. The risk of intubation was highest in B and AB types, and less for individuals with A blood groups, and least for type O individuals [68]. The risk of death was most for AB and less for A and B type individuals [68].

6.1. Role of Adhesion Molecules and Blood Groups

The explanation of the discrepancy of blood groups with COVID infection, however can be attributed to the participation of the adhesion molecules, their binding with the leucocytes, subsequent inflammation [69]. Reduced blood flow results as hemodynamic changes occur due to inflammatory or pathogenic response in the capillaries. This may drive leucocyte adhesion upon activation via chemokines like IL-8, released from the cells of the endothelium which activates neutrophils, MCP-1 and MIP-α that activates Monocytes, leading to their adhesion, subsequent extravasation and diapedesis. Effective receptor- ligand interaction is however mediated by an array of cellular adhesion molecules expressed on the surface of the endothelium cells [70, 71]. Intercellular Adhesion Molecule (ICAM-1) is a transmembrane glycoprotein and member of the immunoglobulin superfamily [72], facilitates immune cell adhesion to the surface of endothelium. ICAM-1 undergoes proteolytic cleavage to form soluble sICAM-1 which inhibits leucocyte-lymphocyte adherence to capillary endothelial wall [73]. ß2 -integrins are expressed largely on the leucocytes and they bind to ICAM-1 in the endothelial cells. ICAM-1 binds to ß integrins like LFA-1 and Mac T expressed on leucocytes that enable them to roll , and the adhesion process is further augmented by a set of selectin molecules like, L-Selectin (expressed on the leucocytes), E-Selectin and P-Selectin (expressed on the endothelial cells) [74, 75]. A1 allele of Blood group A has been seen to have low sICAM-1 and P-selectin levels which is an important biomarker that indicates increased adhesion of leucocytes promoting vascular inflammation [73, 76]. Further glycosylation of sICAM and cellular ICAM-1 is required for P Selectin binding with P-Selectin receptor ligand 1. The glycosylation activity of the A1 allele of Blood group A is seen to be more producing more glycosyltransferases that transfer sugar moieties to H-antigen. This glycosylation process mediates adhesion molecule clearance and the low sICAM1 and P-Selectin concentration in A blood group is strongly indicative of the clearance ability of the A1 allele unlike the O blood group which being devoid of the A and B antigens does not have transferase activity. Low sICAM1 concentration leads to less cellular adhesion of the leucocytes, promote vascular diseases and inflammation [69].

6.2. Difference in the Distribution of Blood Groups in the World

Blood group O considered as "universal donors" are known as the most common type of blood group and the frequencies of their incidence are extremely high among Central & South America, and Australian aborigines. Blood group A is widely distributed in Central Europe and in America. The Asian population is inhabited with Blood group B and Blood group AB which are "universal recipients", is least found in a population and are found in Japan, Korea, and in some regions of China [66, 67].

6.3. Probable Role of Sialic Acids in the Difference in SARS-CoV-2 infection among the Blood Groups

Sialic acids (Sia), are hydrophobic, negatively charged acidic sugars having 9 carbon backbone formed by the acetylation of N-acetyl glucosamine. They are almost ubiquitous in all cells on all cell surfaces and secreted proteins and serve as binding sites for pathogens and toxins. Cell and host-specific interaction by viruses is accomplished by binding with selective sialic acid subtypes [77]. Sialic acids determine half-life of glycoprotein in circulation and its absence causes the glycoprotein to clear away. Besides, Sia regulates cell-cell interactions and immune responses. They are recognized by toxins and pathogens by their specific linkages with the sugar chains thus posing detrimental effects to the host cells. Beta CoVs OC43 CoV, HKU1 CoV use 9-O acetylated sialic acid (9-O-Ac-sialic acid) as the substrate for the haemagglutinin esterases (HFs) which are glycoprotein in the viral envelope that act as receptor destroying enzymes (RDEs) and arise from influenza C like HE fusion protein (HEFs). The O-acetyl residues are detached and that is how viruses are released from host cells and virus aggregation is prevented [78, 79].

The spike protein of coronaviruses responsible for the typical "crown" structure emerges from the viral envelope. Bibliographical review suggests this spike protein yields two subunits S1 and S2 when cleaved by host protease from three equal monomers that compose the spike protein. The subunits are essential for the attachment of the virus with that of the host cell membrane. Prior virus-host interactions indicate that the amino acid bridging the two subunits are cleaved by TMPRSS2 in coronavirus species. However, SARS-CoV-2 virus has an additional furin priming in its spike protein which is a serine endoprotease that can cleave R-X-(R/K/X)-R↓(S)(V/A/L) multi basic protein which is not seen in other coronavirus species like bat coronavirus strain (Bat-RaTG13, Bat -ZXC21 or Bat-ZC45) and SARS-CoV which are not cleaved due to absence of furin [80]. The N- terminal of the S1 monomer has 4ß rich domain A, B, C, D. A or B domain acts as a receptor-binding domain. Coronaviruses use sialic acid residues for binding. Cryo-M studies have revealed a conserved siaglycan binding site in a groove in the A domain that attaches 9-O-acetyl-sialic acid (9-O-Ac-Sia) which is attached to the glycoprotein and gangliosides in the host cell membranes [81].

Expression of 7,9- O- Ac, 9-O-Ac, and Neu5Gc sialic acid are seen in mouse tissues. Sialic acids are predominant in body secretions and it is seen that with age the concentration of sialic acids increases. In the case of diabetes patients the sialic acid concentration has been seen to be more in the retina, iris, and vitreous humour compared to that of normal patients. Case studies have even revealed that tears and ocular fluids contain viral load of SARS-CoV-2 [82-85].

A hypothesis was put forward by José Caetano Silva Filho *et al.* that sialic acid distributions in RBC can be determined by A, B, AB, O antigens, whereby A and B antigens through cis- carbohydrate-carbohydrate interaction can trigger sialoside cluster formation in cells which in turn may promote the SARS-CoV-2 interaction with the ACE2 and CD147 via their RBD and NTD domains [63].

7. Comorbidity

Along with the virus, the associated array of symptoms, and illness, several existing diseases may flare up the severity of COVID-19 requiring absolute hospitalization and intensive care admission. It has been seen though mortality rates resulting from comorbidities are associated with old age and gender, but also significantly younger populations and neonates having pre-existing diseases are highly susceptible to infection. Countries with less economical advantage have received the maximum blow from the pandemic along with healthy realms like USA [86]. According to the recent global epidemiological reports by WHO, as of 22nd November 2020, the African region had an increase of 15% in new cases and about 30% increase in deaths. In India, cumulative deaths as of 22nd Nov 2020 count to almost 1,33,227 according to WHO. Centres for Disease Control and Prevention has enlisted comorbid diseases according to high increased risk and probable chance list of infectivity by COVID-19. In India, however, it has been seen that about 10-20% of patients receive intensive care unit (ICU) admission and 3-10% require intubation and mechanical ventilation [87].

In a retrospective study conducted in the early months in India around April 2020, it was seen that in 206 deaths, diabetes and hypertension tops among other comorbidities, contributing to about 27.8% and 22.1% deaths respectively. Diabetes prevalence is comparatively seen to be highest in India than in any other country [86, 88]. Not only for aged patients, but in fact, children from neonates to up to 16 years of age has been seen to be in the risk zone for COVID-19 complexities who have pre-existing comorbidities. Those include cerebral palsy, Wilson's disease,

dilated cardiomyopathy. Intensive care support and invasive mechanical ventilation have been given to children affected with COVID-19 who had been previously suffering from hydronephrosis, leukemia, and intussusception [89, 90].

Other autoimmune diseases like AITD (Chronic autoimmune thyroid disease) lead to altered immune function as human lymphocytes express nuclear receptors for thyroid hormones. B cell development has been seen to be impaired in the bone marrow of C.RF hyt/hyt mouse where TSHR was defective and TSH production was impaired and mouse was hypothyroidic and subsequent treatment of T4 leads to increase in pro B cells in the S-G2/M phase of the cell cycle [91, 92]. Thyroid gland has been seen to have the highest expression of ACE2 along with other vital organs like the kidney, heart, and small intestine [93]. In a retrospective cohort study conducted on 251 COVID-19 patients who had hypothyroidism as comorbidity, it was seen that 68.1% received hospitalization but not in an increased risk of mechanical ventilation. However, their study indicated that hypothyroidism if well managed will not lead to deleterious extremities like death but the chance of infection remains high for poorly controlled hypothyroidism [94]. Other than this, obese Polycystic ovary syndrome (PCOS) women are also susceptible to higher risk for COVID-19 infection accounted for hypercoagulable state induced due to elevated BMI and insulin resistance.

7.1. Chronic Obstructive Pulmonary Disease (COPD) and COVID-19

A case related study showed that COPD patients who received prescribed inhaled corticosteroids (ICS) were at high risks of COVID-19 infection [95]. In China, patients experienced pneumonia-like symptoms at the onset of December 2019 which was basically the symptoms of the rising COVID-19. It was seen about 7% of patients in China and about 13.7% of patients in Italy who contracted COVID-19, had COPD as pre-existing disease [96]. The expression of ACE2 receptors had been found to increase which contributes a major factor in contracting the disease leading to hyper mucous formation [97]. Tobacco smoking has been correlated with the severity of SARS-CoV-2 when contracted. COPD patients have been recognized by the Global Initiative for Chronic Obstructive Lung Disease (GOLD) as the worst affected individuals who contract COVID-19. Not only current smokers but individuals having a previous history of smoking are equally susceptible to infection. There is differential ACE2 expression like the whole Cigarette smoking largely culminates in upregulation of ACE2 expression while a research group showed that nicotine present in cigarette causes disruption in RAS pathway and both ACE2 and AT1R (Angiotension type 1 receptor) gets downregulated [30, 98, 99]. Second-hand smoking (SHS), use of snuff and air pollution both indoor pollutants like cooking in kerosene and other biomass fuels in village areas, smoke of mosquito coils and exposure to outdoor pollutants like automobile emissions can be other important ancillary causes of COPD [100, 101].

7.2. Cardiovascular Disease, Hypertension and COVID-19

Worldwide about 1.4 million people are affected by hypertension [102]. The 3rd report of Joint National Committee on Detection Evaluation, and Treatment of High Blood Pressure in 1984 (JNC III) proposed that normal bp counts to systolic blood pressure (SBP)<140 mm Hg and diastolic blood pressure (DBP)<90 mm Hg [103]. High cardiovascular risk is seen in patients who have elevated SBP and a low DBP [104]. As per the WHO, in September 2019, it was reported that the African population has the highest incidence of hypertension about 27% while the prevalence is low in America which is about 18%. (World Health Organization, Hypertension (13th September 2019)). It is prognosticated that by 2025 the number of hypertensive patients will increase to 1.56 billion worldwide [105]. Women are seen less to suffer from hypertension compared to males (12% vs 27% respectively). Menopausal women and men are at high risk of cardiovascular diseases can be due to various biological factors like sex hormones, chromosomal differences, behavioural and lifestyle factors like high body mass index (BMI), smoking habits, limited physical activity. Intra-abdominal adiposity has a relationship with high BP and the levels are higher in males compared to females and this relates to increased sympathetic activity in males consequently leading to cardiac arrhythmias, cardiovascular hypertrophy [106-109]. High androgen levels as of testosterone, is associated with noradrenaline synthesis and subsequent vasoconstriction [110]. Low levels of serum androgen promote hypertension and cardiovascular anomalies in males while the reverse is true in females where hypertension and CVD arise from elevated androgen levels. A study conducted on 5α-dihydrosterone (DHT) treated male rats showed intrarenal expression of CYP4A and 20HETE (Hydroxyecosatetraenoic acids) and elevated BP level via NFκB activation and increased production of reactive oxygen species (ROS) and decreased nitric oxide (NO) production paving the way to renal vasoconstriction [111, 112]. Another important factor involves salt levels in the diet, an increased salt consumption leads to an increase in water retention thereby increasing BP levels [113].

SARS-CoV-2 affected patients already having pre-existing cardiovascular diseases are prone to heart attack or myocarditis characterized by high leukocyte count with concomitant IL-6, ferritin levels due to elevated troponin concentration resulting in cytokine storm and in its worst death [114, 115]. Alongside hypertensive patients, contracted with SARS-CoV-2 has been seen to have high sensitivity to CRP compounded with procalcitonin and IL-6 suggesting heightened inflammation [116].

Coronary heart disease is also a major disease of concern in the wake of the COVID-19 pandemic. An imbalance between the ACE2 vasoprotective axis (ACE2-Ang (1-7)- Mas axis) and ACE- Ang II -AngII type 1 Receptor (AT1R axis) leads to pulmonary hypertension-related CHD (CHD-PAH). Though the concentration of ACE2 has been associated with increased inflammatory cytokine levels, however, a new explanation suggests that higher ACE2 expression at baseline can be seen from a vantage point of view as the viral molecules engage in a competition binding with angiotensin II and that maintains angiotensin 1-7 levels which inhibit the proinflammatory action of ACE2. This can be a plausible reason for the disparity of infection and severity across children and young generation with that of adults [117]. In a study conducted with 104 CHD patients (35 men and 69 women) with an age greater than 14 years, it was seen that ACE2 concentration was higher in patients with non-pulmonary hypertension while in patients with pulmonary hypertension ACE2 concentration decreases [118]. But, whether children and new-born with congenital heart disease are least susceptible to COVID-19 remains to be a debatable issue and needs to be further elucidated.

8. Mutations in Virus

Virus mutations are common and the influence of such mutations in the changing facets of SARS-CoV-2 viruses is not a surprise [119-120]. Although, there are more questions than answers at this moment for the mutation(s) that are observed currently, and how it impacts the spreading of the virus. However, there is no denial that already researchers across the world have recorded as many as 12,000 mutations to date (Figure 3).
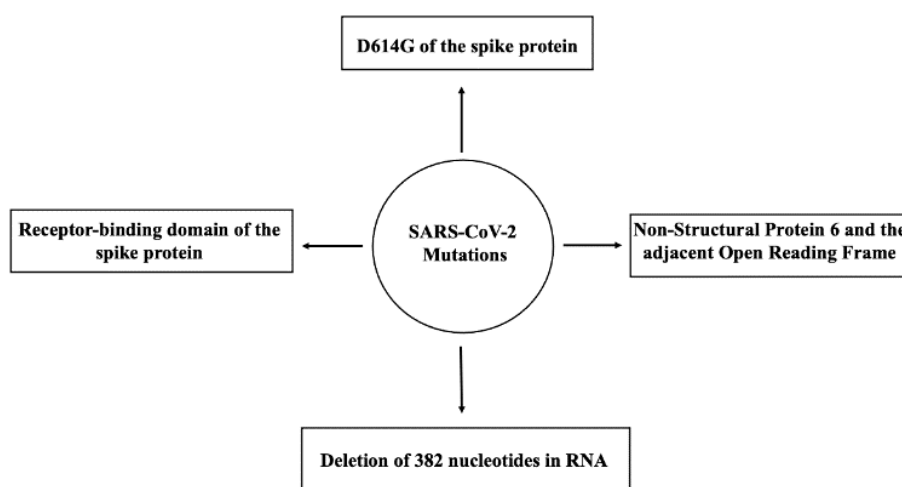
Figure 3. Range of SARS-CoV-2 mutations

It seems that there are no direct correlations between the recorded mutations and faster spreading hitherto [120]. However, the emergence of 12,000 mutations shows how the virus has evolved in the last year (three major variant types – A, B, and C) [121]. On the contrary, it also must be highlighted that this virus is evolving at a slower rate than other RNA viruses due to the presence of a proofreading enzyme which corrects any error(s) during the replication [122]. It is also believed that the virus might have already optimally evolved from the very beginning as it was able to infect such a huge number of people around the world and further mutations may not be so necessary until it faces any resistance from the host.

The most popular mutation that has been recorded for SARS-CoV-2 is the D614G (aspartic acid to glycine) that had incidence from Germany and China [123]. The D614G is reported to change the architecture of the spike protein to a more relaxed structure that might facilitate the chance of infection [124, 125]. Other reports suggest mutations in a receptor-binding domain of the spike protein [126, 127]. Moreover, deletion of 382 nucleotides in RNA has also been studied which potentially reduces the severity of COVID-19 infection [128]. In a separate study, two mutations were detected in the Non-Structural Protein 6 and the adjacent Open Reading Frame, of which one of the mutations might be contributing to the altered intracellular survivability of the virus, but that needs further investigation [129]. So, there must strict vigilance on this and further mutations which might lead to evolution and any alterations in the phenotype. That would ensure successful designing and modifications in upcoming therapeutic strategies.

9. Host Genetics

SARS-CoV-2 infections can exhibit a wide range of consequences in different individuals. Normally, it has more severe outcomes in old individuals with underlying health issues [130]. However, young adults are also prone to varying impacts of disease severity. Patients show grave symptoms like renal and cardiac injury, loss of smell and taste, persistent fever, gastrointestinal malfunctioning, and even hepatitis, among others [131-134]. Others may be

asymptomatic altogether [135]. For many infectious diseases, it is understood that allelic polymorphisms and genetic loci variations have contributed to such differences in disease susceptibility among individuals.

As already discussed in this review, ACE2 is the primary attachment and entry point of SARS-CoV-2. The scientific community thus started to investigate whether any ACE2 polymorphisms impacted viral binding and entry. There were several variants of *ACE2* (S19P, I21V, E23K, K26R, T27A, K31R, N33I, H34R, E35K, E37K, D38V, Y50F, N51S, M62V, N64K, K68E, W69C, F72V, Y83H, T92I, Q102P, G326E, L351V, G352V, D355N, H378R, Q388L, P389H, I468V, D509Y, N720D) that could change the ACE2 conformation thus altering (positively or negatively) interaction with SARS-CoV-2 [136-138]. Again, patients with hypertension, diabetes, and chronic obstructive pulmonary disease (COPD) show a much higher ACE2 expression than healthy counterparts explaining how comorbidity can influence disease severity [139].

TMPRSS2, a serine protease, has a role in viral membrane fusion. There are reports that single nucleotide polymorphism (SNP) results in higher expression of TMPRSS2, which further increases the susceptibility of an individual towards SARS-CoV-2 infection [140].

HLA-typing can be another important factor that determines SARS-Cov-2 infection and disease progression. Research groups have deciphered that HLA-B*46:01 binds to fewest number of peptides of SARS-CoV-2, which suggests that individuals who have this allele can generate a feeble immune response and thus more prone to severe manifestations [141]. On the contrary, individuals with HLA-B*15:03 are more protected from the severity as they have a high capacity to present well-conserved peptides of SARS-CoV-2 and other pathogenic coronaviruses to the immune cells [141].

"Cytokine storm" mediated by increased release of cytokines such as IL-6, TNFα, IL-1β is another complication associated with SARS-CoV-2 infection [138]. Patients with severe clinical symptoms have been associated with hyper-secretion of these cytokines, along with increased levels of C-reactive protein, D-Dimer, ferritin, etc. [138]. The consequence of such a rise in the levels has been related to excessive alveolar damage which ultimately leads to acute respiratory distress syndrome [142]. These events are absent in asymptomatic or patients with milder symptoms. Studies also state that certain immune responsive genes like *AHSG*, *CCL5*, *CCL2*, *IL4* variants have a role in disease severity [143].

10. Natural compounds: Alternatives to Mitigate the Overlooked Side Effects of Common Antivirals in COVID-19

The ever-increasing rates of SARS-CoV-2 pandemic has necessitated the search for effective therapies as no proven appropriate remedy or proper prophylaxis in the form of vaccination is available so far. Nevertheless, to combat the worsening situation, several drugs and antivirals were proposed and administered for treatment. But these drugs have been seen to pose considerable side effects to the body and it calls for urgent need for alternative medical treatment. We discuss certain available chemical drugs used in spite of their known side effects to combat the increasing predicament of the disease.

Antimalarial Drugs: Chloroquine and Hydroxychloroquine – Its mode of action and possible side effects

At the very start of the SARS-CoV-2 pandemic crisis, antimalarial remedial drugs like chloroquine and hydroxychloroquine were used and still in vogue for treatment. Both being 4-aminoquinoline derivatives, chloroquine itself is effective against a spectrum of RNA viruses like Ebola, Zika, polio, influenza A and B viruses, HIV as well as an array of DNA viruses [144]. Chloroquine and its analogue hydroxychloroquine are used as a medicine for lupus erythematous, arthritis, etc. autoimmune diseases and functions by interfering with a) glycosylation of the ACE 2, the receptor for SARS-CoV-2 thereby altering the binding of the virus with the same [145], b) it raises the endosomal pH that blocks viral infection [146], c) a hypothesis suggests possibly the interaction of SARS-CoV-2 with the host cell is interfered with chloroquine treatment that brings about the inhibition of MAPK like kinases and reduces prion inflammatory cytokines [144]. However, via molecular docking studies, it has come to light the enhanced effectivity of hydroxychloroquine. It binds more efficiently to the 32 amino acids present in the four helices of the N-terminal domain (NTD) of the nucleocapsid N protein with a binding energy (-7.28 kcal/mol) much higher than the binding energy of chloroquine (-6.30 kcal/mol) [147]. Hydroxychloroquine causes S protein breakage due to the formation of autophagosomes brought about by the rise in pH of lysosomes and endosomes [145]. Hydroxychloroquine has also been seen to intervene with the antigen processing and presentation brought about by MHC Class II leading to a fall in T-cell production and thereby preventing cytokine storm [148]. Hydroxychloroquine has been reported to block toll-like receptor (TLR9) signalling by binding with nucleic acids and reducing cytokine production [149].

Side effects: Though potentially capable of inhibiting the virus, hydroxychlorine has been reported of inducing fulminant hepatic failure and ventricular arrhythmias [150] and causes more renal toxicity than chloroquine does

[151]. Both these drugs have been associated with delayed action potential in the nerves and prolonged QT interval in myocytes [152].

Antiviral Drugs: Remdesvir, Lopinavir, Ritonavir – A re-evaluation of its effectiveness and toxicity

Chloroquine and hydroxychloroquine are advised not to be used with Remdesvir as the activity of the latter may decrease with the concomitant use of these antimalarial drugs [153]. Remdesvir, an antiviral nucleotide analogue has long been used for a myriad of RNA viruses like MERS-CoV, SARS-CoV, Ebola, Nipah viruses, and other zoonotic viruses [154-157]. Remdesvir is formed by intracellular conversion and its mode of action is competitive binding by mimicking the structure of nucleotides [158]. Also, Remdesvir can halt the inhibition of viral RNA dependant RNA polymerase replication [159]. Remdesvir interestingly has been found to be effective in inhibiting SARS-CoV-2 in human liver cancer Huh 7 cells [160]. Other drugs of choice being a protease inhibitor of SARS-CoV-2 is a combinational therapy of lopinavir-ritonavir that was previously used in the treatment of SARS-CoV and MERS [154, 161]. This therapy targets 3Clpro, a 3chymotrypsin like protease that aid in the processing of viral RNA [162, 163].

Side effects: These antiviral drugs are being complained of serious side effects. Remdesvir is associated with cutaneous side effects [164], hepatocellular injury with increased levels of AST/ALT upon remdesvir [165], cardiac side effects causing hypertension, arterial fibrillation and sinus bradycardia [166]. Lopinavir-ritonavir on the other hand is not refrained from causing adverse effects. Ritonavir induces porphyria, haemophilia and is to be used with much caution for individuals with cardiac ailments [167] and are seen to cause gastrointestinal troubles with ancillary nausea, vomiting and diarrhoea [168, 169].

Natural Compounds: Its beneficiary action – Natural Compounds targeted against 3CLpro, PLpro, Spike protein, ACE2 receptor

With side effects of these practicing remedial soaring high, search necessitates for alternative treatment and natural compounds can be a judicious choice to minimize the exacerbation of the severity brought about by the same as well as providing an economical advantage for the developing countries.

A number of phytochemicals and natural compounds can be used in lieu of these antivirals. Where Lopinavir-Retonavir are targeted against the 3Clpro, molecular docking studies have revealed high receptor binding (docking score S= -16.35) of a phytochemical extracted from *Psorothamnus arborescens* having an isoflavone moiety [5,7,3', 4'- tetrahydroxy-2'-(3,3- dimethylallyl) isoflavone] with that of Cys-145-His-41 catalytic dyad of the 3Clpro much higher than a potent non-competitive inhibitor ML188 (having docking score S= 8.31) when used as a reference. Besides, legume like kidney beans *Phaseolus vulgaris* having 3,5,7,3',4',5'-hexahydroxy flavonone -3-O- beta -D glucopyranoside and Indian gooseberry, *Phallanthus embellica* having (2,S)- Eriodictyol 7-O-(6''-O-gallolyl)-beta D-glucopyranoside, myricitin group from *Myrica cerifera* has been seen to show similar reactivity against the 3Clpro residues of the virus [162]. A variety of potential inhibitors for SARS-CoV-2 are found in the rhizomes of *Zingiber officinale* and galangal (*Alpinia officinarum*) [170]. From earlier reports based on coronavirus inhibition, apart from the chymotrypsin enzyme 3Clpro, there are a number of natural compounds found to be effective against another papain protease, PL[pro], that functions by hampering post-transcriptional modifications of host proteins, cleaving ubiquitin and attenuating interferon that aids largely on innate response of the body and thus the enzyme facilitates in the viral replication by assembling replicase complex for viral replication [171]. A number of natural compounds are seen to have inhibitory action against this Plpro protein. Examples can be cited for Curcumin obtained from *Curcumin longa* which is an easily available medicinal herb and spice, along with tanshinone derivatives obtained from an array of *Salvia sp.*, [172] baicalin from *Scutellaria baicalensis*, and Theaflavin 3,3′-di-O-gallate from *Camellia sinensis* [173]. There are several phytochemicals like Phyllaembillin A, Punigluconin, Punicafolin and Emblicanin A from Indian Gooseberry, *Phyllanthus embilica*, Rutin from Neem, *Azadirichta indica*, Lithospermic acid from *Salvia multiorrhiza*, and Kuwanon X from Mulberry plant , *Morus alba* is considered efficient for simultaneously inhibiting all the three drug targets, that is, PL[pro], 3CL[pro] and IS -spike, a mutational variety of the spike protein of SARS-CoV-2 seen in India [having surface glycoprotein A930V, (24351C>T) [174].

Some common food items, spices, and condiments are seen to be functionally ACE2 inhibitors. A number of flavonoids scutellarin, nicotanamine can be seen as ACE2 inhibitors over conventional ACE2 blockers like telmisartan, losartan[174] as these ACE2 blockers causes upregulation of Angiotensin Type II receptor (AT1R) in diabetic and hypertensive patients thus ramifying further the severity and fatality of infection [175]. Peptide nicotinamine from *Glycine max*, anthraquinone extracted from *Rheum officinale*, apigenin from *Apium graveolus*, Delphinidin and Cyanidin from *Hibiscus sabdariffa* are found effective in ACE2 inhibition [174]. Theaflavin extracted from *Camellia sinensis* of Assamica variety has been seen to inhibit both protein ACE2 and TMPRSS2 expression at 50μg/ml concentration [176].

Besides, essential oils like limonene composed of volatile terpene compounds extracted from lemon and geranium can reduce epithelial ACE2 expression [177]. *In silico* study showed that isothymol, an essential oil extracted from an

annual herb of Western Algeria, *Ammoides verticillate* of the *Apiaceae* family has high binding energy and thus may block ACE2 interfering with the entry of SARS-CoV-2 [178]. Several compounds in the form of essential oils isolated from medicinal plants like basil, cinnamon, thyme, clove contain monoterpenes, terpenoid phenols which can be targeted against Spike S glycoprotein of SARS-CoV-2. Cinnamaldehyde, cinnamyl acetate, these two phenyl terpenoids have been found to show high chemical reactivity with a molecular dipole moment of 4.53 Debye and lower electronegativity of -4.34 that signifies its capability of inhibition [179]. Resveratol found in grape skin along with piceatannol found in berries, grapes are stilbenoids which are a class of phenolic compounds found in grape skin formed a stable complex with the amino acid residues of the S protein ACE2 Receptor complex via hydrophobic, hydrogen and ionic interactions [180, 181]. Taraxerol, Friedlin, Stigmasterol isolated from a perennial herb *Clerodendrum spp.* have high binding capacity with the amino acid residues of the SARS-CoV-2 spike protein. Friedlin interacts with Lys 444, Tyr 449 and Asn 450 while Stigmasterol with Tyr 449 and Phe 490. These compounds can be employed to target the spike protein and inhibit its further interaction with the ACE2 receptor [182]. An unbiased molecular docking study finds potential heparin-binding profiles on coronavirus spike glycoproteins, suggesting the possibility of SARS-CoV-2 interventions through the use of heparins.

Microbial metabolites and compounds from Marine microorganisms targeted against SARS-CoV-2

Recent *in silico* molecular interaction studies have revealed cyanobacterial metabolites like deoxycylindrospermin isolated from *Cylindrospermopsis* interacted with the residues of the main protease 3Clpro/Mpro through hydrophobic and hydrogen bond interactions. Cylindrospermopsin, and eucapsitrione from *Eucapsis sp.* reacts with the Plpro protein [183]. Sulphated polysaccharides from marine microorganisms like sea cucumber *Stichopus japonicus* and Fucoidan from brown algae can have an excellent inhibitory effect on SARS-CoV-2 [184]. Recent reports revealed a T3 terpenoid isolated from marine sponge *Cacospongia mycofinensis* inhibits the action of Mpro via hydrogen bond interactions [185].

Microbial dysbiosis is a common predicament in patients contracted COVID-19 with declining gut bacteria like *Lactobacilli* and *Bifedobacterium* as SARS-CoV-2 disrupts largely the gastrointestinal system where the ACE2 receptor is expressed. Thus treating patients with *Lactobacilli casei* and *Bifedobacterium* can be a suitable way as they are seen to enhance inflammatory signals and promote heightened phagocytosis and increase levels of interferons and immunoglobulins like IgA [186]. A molecular dynamics simulation study predicts an interaction between the secondary fungal metabolite Pyranonigrin A and Mpro, thus proposing this metabolite to have an effective potentiality against the SARS-CoV-2 virus [187].

11. Conclusion

This review entails the factors that lead to severity associated with COVID-19. Coronaviruses can cause a range of manifestations in different individuals – from being asymptomatic, to milder versions, and even resulting in catastrophic symptoms that ultimately leads to the death of an individual. This review explains these fine margins, thus explaining each factor's mechanisms, and how each factor contributes to the severity. Also, this helps to understand which individuals are more prone to infection. Every individual carrying a certain level of these predispositions should be more cautious and should take every step to protect themselves from being exposed to this disease.

12. Declarations

12.1. Author Contributions

12.2. Funding

12.3. Acknowledgements

12.4. Ethical Approval

This review contains no experiments on humans and animals, so ethical approval not required.

12.5. Data Availability Statement

Data sharing is not applicable to this article.

12.6. Conflict of Interest

The authors declare that they have no known competing financial interests or personal relationships that could have appeared to influence the work reported in this paper.

13. References

[1] Noor, A. U., Maqbool, F., Bhatti, Z. A., & Khan, A. U. (2020). Epidemiology of CoViD-19 Pandemic: Recovery and mortality ratio around the globe. Pakistan Journal of Medical Sciences, 36(COVID19-S4). doi:10.12669/pjms.36.covid19-s4.2660.

[2] Liu, Y.-C., Kuo, R.-L., & Shih, S.-R. (2020). COVID-19: The first documented coronavirus pandemic in history. Biomedical Journal, 43(4), 328–333. Doi:10.1016/j.bj.2020.04.007.

[3] Wu, Y., Ho, W., Huang, Y., Jin, D.-Y., Li, S., Liu, S.-L., … Zheng, Z.-M. (2020). SARS-CoV-2 is an appropriate name for the new coronavirus. The Lancet, 395(10228), 949–950. doi:10.1016/s0140-6736(20)30557-2.

[4] World Health Organization: WHO Coronavirus (COVID-19) Dashboard. Available online: https://covid19.who.int/ (accessed on 20 May 2020).

[5] Li, Q., Guan, X., Wu, P., Wang, X., Zhou, L., Tong, Y., … Feng, Z. (2020). Early Transmission Dynamics in Wuhan, China, of Novel Coronavirus–Infected Pneumonia. New England Journal of Medicine, 382(13), 1199–1207. doi:10.1056/nejmoa2001316.

[6] Huang, C., Wang, Y., Li, X., Ren, L., Zhao, J., Hu, Y., … Cao, B. (2020). Clinical features of patients infected with 2019 novel coronavirus in Wuhan, China. The Lancet, 395(10223), 497–506. doi:10.1016/s0140-6736(20)30183-5.

[7] Snijder, E. J., Den Boon, J. A., Horzinek, M. C., & Spaan, W. J. M. (1991). Comparison of the genome organization of toro- and coronaviruses: Evidence for two nonhomologous RNA recombination events during berne virus evolution. Virology, 180(1), 448–452. doi:10.1016/0042-6822(91)90056-h.

[8] Masters, P. S. (2006). The Molecular Biology of Coronaviruses. Advances in Virus Research, 193–292. doi:10.1016/s0065-3527(06)66005-3.

[9] Gundy, P. M., Gerba, C. P., & Pepper, I. L. (2008). Survival of Coronaviruses in Water and Wastewater. Food and Environmental Virology, 1(1). doi:10.1007/s12560-008-9001-6.

[10] Chen, J., Liu, D., Liu, L., Liu, P., Xu, Q., Xia, L., ... & Lu, H. (2020). A pilot study of hydroxychloroquine in treatment of patients with common coronavirus disease-19 (COVID-19). Journal of Zhejiang University (Medical Science), 49(1), 0-0. doi: 10.3785/j.issn.1008-9292.2020.03.03.

[11] Lu, R., Zhao, X., Li, J., Niu, P., Yang, B., Wu, H., … Tan, W. (2020). Genomic characterisation and epidemiology of 2019 novel coronavirus: implications for virus origins and receptor binding. The Lancet, 395(10224), 565–574. doi:10.1016/s0140-6736(20)30251-8.

[12] Liu, J., Xie, W., Wang, Y., Xiong, Y., Chen, S., Han, J., & Wu, Q. (2020). A comparative overview of COVID-19, MERS and SARS: Review article. International Journal of Surgery, 81, 1–8. doi:10.1016/j.ijsu.2020.07.032.

[13] Yuan, S., Jiang, S.-C., & Li, Z.-L. (2020). Analysis of Possible Intermediate Hosts of the New Coronavirus SARS-CoV-2. Frontiers in Veterinary Science, 7. doi:10.3389/fvets.2020.00379.

[14] Liu, Z., Xiao, X., Wei, X., Li, J., Yang, J., Tan, H., ⋯ Liu, L. (2020). Composition and divergence of coronavirus spike proteins and host ACE2 receptors predict potential intermediate hosts of SARS‐CoV‐2. Journal of Medical Virology, 92(6), 595–601. doi:10.1002/jmv.25726.

[15] Zhang, T., Wu, Q., & Zhang, Z. (2020). Probable Pangolin Origin of SARS-CoV-2 Associated with the COVID-19 Outbreak. Current Biology, 30(7), 1346–1351.e2. doi:10.1016/j.cub.2020.03.022.

[16] Wu, A., Peng, Y., Huang, B., Ding, X., Wang, X., Niu, P., … Jiang, T. (2020). Genome Composition and Divergence of the Novel Coronavirus (2019-nCoV) Originating in China. Cell Host & Microbe, 27(3), 325–328. doi:10.1016/j.chom.2020.02.001.

[17] Fani, M., Teimoori, A., & Ghafari, S. (2020). Comparison of the COVID-2019 (SARS-CoV-2) pathogenesis with SARS-CoV and MERS-CoV infections. Future Virology, 15(5), 317–323. doi:10.2217/fvl-2020-0050.

[18] Li, F. (2005). Structure of SARS Coronavirus Spike Receptor-Binding Domain Complexed with Receptor. Science, 309(5742), 1864–1868. doi:10.1126/science.1116480.

[19] Ortega, J. T., Serrano, M. L., Pujol, F. H., & Rangel, H. R. (2020). Role of changes in SARS-CoV-2 spike protein in the interaction with the human ACE2 receptor: An in silico analysis. EXCLI journal, 19, 410. doi: 10.17179/excli2020-1167.

[20] Tipnis, S. R., Hooper, N. M., Hyde, R., Karran, E., Christie, G., & Turner, A. J. (2000). A Human Homolog of Angiotensin-converting Enzyme. Journal of Biological Chemistry, 275(43), 33238–33243. doi:10.1074/jbc.m002615200.

[21] Tikellis, C., & Thomas, M. C. (2012). Angiotensin-Converting Enzyme 2 (ACE2) Is a Key Modulator of the Renin Angiotensin System in Health and Disease. International Journal of Peptides, 2012, 1–8. doi:10.1155/2012/256294.

[22] Vinciguerra, M., & Greco, E. (2020). Sars-CoV-2 and black population: ACE2 as shield or blade? Infection, Genetics and Evolution, 84, 104361. doi:10.1016/j.meegid.2020.104361.

[23] Deng, J., Wang, D., Deng, W., Li, C., & Tong, J. (2012). The Effect of Endogenous Angiotensin II on Alveolar Fluid Clearance in Rats with Acute Lung Injury. Canadian Respiratory Journal, 19(5), 311–318. doi:10.1155/2012/951025.

[24] Chen, J., Jiang, Q., Xia, X., Liu, K., Yu, Z., Tao, W., ⋯ Han, J. J. (2020). Individual variation of the SARS‐CoV‐2 receptor ACE2 gene expression and regulation. Aging Cell, 19(7). doi:10.1111/acel.13168.

[25] Zhao, Y., Zhao, Z., Wang, Y., Zhou, Y., Ma, Y., & Zuo, W. (2020). Single-Cell RNA Expression Profiling of ACE2, the Receptor of SARS-CoV-2. American Journal of Respiratory and Critical Care Medicine, 202(5), 756–759. doi:10.1164/rccm.202001-0179le.

[26] Silhol, F., Sarlon, G., Deharo, J.-C., & Vaïsse, B. (2020). Downregulation of ACE2 induces overstimulation of the renin–angiotensin system in COVID-19: should we block the renin–angiotensin system? Hypertension Research, 43(8), 854–856. doi:10.1038/s41440-020-0476-3.

[27] Verdecchia, P., Cavallini, C., Spanevello, A., & Angeli, F. (2020). The pivotal link between ACE2 deficiency and SARS-CoV-2 infection. European Journal of Internal Medicine, 76, 14–20. doi:10.1016/j.ejim.2020.04.037.

[28] Kehoe, P. G., Wong, S., AL Mulhim, N., Palmer, L. E., & Miners, J. S. (2016). Angiotensin-converting enzyme 2 is reduced in Alzheimer's disease in association with increasing amyloid-β and tau pathology. Alzheimer's Research & Therapy, 8(1). doi:10.1186/s13195-016-0217-7.

[29] Haghighi, M. M., Kakhki, E. G., Sato, C., Ghani, M., & Rogaeva, E. (2020). The Intersection between COVID-19, the Gene Family of ACE2 and Alzheimer's Disease. Neuroscience Insights, 15, 263310552097574. doi:10.1177/2633105520975743.

[30] Smith, J. C., Sausville, E. L., Girish, V., Yuan, M. L., Vasudevan, A., John, K. M., & Sheltzer, J. M. (2020). Cigarette Smoke Exposure and Inflammatory Signaling Increase the Expression of the SARS-CoV-2 Receptor ACE2 in the Respiratory Tract. Developmental Cell, 53(5), 514–529.e3. doi:10.1016/j.devcel.2020.05.012.

[31] Pagliaro, P., & Penna, C. (2020). ACE/ACE2 Ratio: A Key Also in 2019 Coronavirus Disease (Covid-19)? Frontiers in Medicine, 7. doi:10.3389/fmed.2020.00335.

[32] Albright, J. M., Dunn, R. C., Shults, J. A., Boe, D. M., Afshar, M., & Kovacs, E. J. (2016). Advanced Age Alters Monocyte and Macrophage Responses. Antioxidants & Redox Signaling, 25(15), 805–815. doi:10.1089/ars.2016.6691.

[33] Linehan, E., & Fitzgerald, D. (2015). Ageing and the immune system: focus on macrophages. European Journal of Microbiology and Immunology, 5(1), 14–24. doi:10.1556/eujmi-d-14-00035.

[34] Pence, B. D. (2020). Severe COVID-19 and aging: are monocytes the key? GeroScience, 42(4), 1051–1061. doi:10.1007/s11357-020-00213-0.

[35] Wong, C. K., Smith, C. A., Sakamoto, K., Kaminski, N., Koff, J. L., & Goldstein, D. R. (2017). Aging Impairs Alveolar Macrophage Phagocytosis and Increases Influenza-Induced Mortality in Mice. The Journal of Immunology, 199(3), 1060–1068. doi:10.4049/jimmunol.1700397.

[36] Van Beek, A. A., Van den Bossche, J., Mastroberardino, P. G., de Winther, M. P. J., & Leenen, P. J. M. (2019). Metabolic Alterations in Aging Macrophages: Ingredients for Inflammaging? Trends in Immunology, 40(2), 113–127. doi:10.1016/j.it.2018.12.007.

[37] Evans, R. M., & Lippman, S. M. (2020). Shining Light on the COVID-19 Pandemic: A Vitamin D Receptor Checkpoint in Defense of Unregulated Wound Healing. Cell Metabolism, 32(5), 704–709. doi:10.1016/j.cmet.2020.09.007.

[38] Mok, C. K., Ng, Y. L., Ahidjo, B. A., Hua Lee, R. C., Choy Loe, M. W., Liu, J., … Hann Chu, J. J. (2020). Calcitriol, the active form of vitamin D, is a promising candidate for COVID-19 prophylaxis. doi:10.1101/2020.06.21.162396.

[39] Mohan, M., Cherian, J. J., & Sharma, A. (2020). Exploring links between vitamin D deficiency and COVID-19. PLOS Pathogens, 16(9), e1008874. doi:10.1371/journal.ppat.1008874.

[40] Wu, D., & Yang, X. O. (2020). TH17 responses in cytokine storm of COVID-19: An emerging target of JAK2 inhibitor Fedratinib. Journal of Microbiology, Immunology and Infection, 53(3), 368–370. doi:10.1016/j.jmii.2020.03.005.

[41] Chen, Y., Zhang, J., Ge, X., Du, J., Deb, D. K., & Li, Y. C. (2013). Vitamin D Receptor Inhibits Nuclear Factor κB Activation by Interacting with IκB Kinase β Protein. Journal of Biological Chemistry, 288(27), 19450–19458. doi:10.1074/jbc.m113.467670.

[42] George, P. M., Wells, A. U., & Jenkins, R. G. (2020). Pulmonary fibrosis and COVID-19: the potential role for antifibrotic therapy. The Lancet Respiratory Medicine, 8(8), 807–815. doi:10.1016/s2213-2600(20)30225-3.

[43] Gubernatorova, E. O., Gorshkova, E. A., Polinova, A. I., & Drutskaya, M. S. (2020). IL-6: Relevance for immunopathology of SARS-CoV-2. Cytokine & Growth Factor Reviews, 53, 13–24. doi:10.1016/j.cytogfr.2020.05.009.

[44] Saxena, N., & Gutiérrez, O. M. (2013). Fibroblast Growth Factor 23, Vitamin D, and Health Disparities Among African Americans With Chronic Kidney Disease. Seminars in Nephrology, 33(5), 448–456. doi:10.1016/j.semnephrol.2013.07.006.

[45] Dancer, R. C. A., Parekh, D., Lax, S., D'Souza, V., Zheng, S., Bassford, C. R., … Thickett, D. R. (2015). Vitamin D deficiency contributes directly to the acute respiratory distress syndrome (ARDS). Thorax, 70(7), 617–624. doi:10.1136/thoraxjnl-2014-206680.

[46] Biesalski, H. K. (2020). Vitamin D deficiency and co-morbidities in COVID-19 patients – A fatal relationship? NFS Journal, 20, 10–21. doi:10.1016/j.nfs.2020.06.001.

[47] Price-Haywood, E. G., Burton, J., Fort, D., & Seoane, L. (2020). Hospitalization and Mortality among Black Patients and White Patients with Covid-19. New England Journal of Medicine, 382(26), 2534–2543. doi:10.1056/nejmsa2011686.

[48] Kohlmeier, M. (2020). Avoidance of vitamin D deficiency to slow the COVID-19 pandemic. BMJ Nutrition, Prevention & Health, 3(1), 67–73. doi:10.1136/bmjnph-2020-000096.

[49] Azevedo, L. A., Matte, U., Silveira, T. R., Bonfanti, J. W., Bruch, J. P., & Álvares-da-Silva, M. R. (2017). Effect of Vitamin D Serum Levels and GC Gene Polymorphisms in Liver Fibrosis Due to Chronic Hepatitis C. Annals of Hepatology, 16(5), 742–748. doi:10.5604/01.3001.0010.2748.

[50] Davies, S. E., & Bennett, B. (2016). A gendered human rights analysis of Ebola and Zika: locating gender in global health emergencies. International Affairs, 92(5), 1041–1060. doi:10.1111/1468-2346.12704.

[51] Liu, J., Zhang, L., Chen, Y., Wu, Z., Dong, X., Teboul, J.-L., … Chen, D. (2020). Association of sex with clinical outcomes in COVID-19 patients: A retrospective analysis of 1190 cases. Respiratory Medicine, 173, 106159. doi:10.1016/j.rmed.2020.106159.

[52] Tufan, A., Avanoğlu Güler, A., & Matucci-Cerinic, M. (2020). COVID-19, immune system response, hyperinflammation and repurposing antirheumatic drugs. TURKISH JOURNAL OF MEDICAL SCIENCES, 50(SI-1), 620–632. doi:10.3906/sag-2004-168.

[53] Liu, Y., Zhang, C., Huang, F., Yang, Y., Wang, F., Yuan, J., … Jiang, C. (2020). Elevated plasma levels of selective cytokines in COVID-19 patients reflect viral load and lung injury. National Science Review, 7(6), 1003–1011. doi:10.1093/nsr/nwaa037.

[54] Satış, H., Özger, H. S., Aysert Yıldız, P., Hızel, K., Gulbahar, Ö., Erbaş, G., … Tufan, A. (2021). Prognostic value of interleukin-18 and its association with other inflammatory markers and disease severity in COVID-19. Cytokine, 137, 155302. doi:10.1016/j.cyto.2020.155302.

[55] Hashem, N. M., Abdelnour, S. A., Alhimaidi, A. R., & Swelum, A. A. (2021). Potential impacts of COVID-19 on reproductive health: Scientific findings and social dimension. Saudi Journal of Biological Sciences, 28(3), 1702–1712. doi:10.1016/j.sjbs.2020.12.012.

[56] Baena, E., Shao, Z., Linn, D. E., Glass, K., Hamblen, M. J., Fujiwara, Y., … Li, Z. (2013). ETV1 directs androgen metabolism and confers aggressive prostate cancer in targeted mice and patients. Genes & Development, 27(6), 683–698. doi:10.1101/gad.211011.112.

[57] Stelzig, K. E., Canepa-Escaro, F., Schiliro, M., Berdnikovs, S., Prakash, Y. S., & Chiarella, S. E. (2020). Estrogen regulates the expression of SARS-CoV-2 receptor ACE2 in differentiated airway epithelial cells. American Journal of Physiology-Lung Cellular and Molecular Physiology, 318(6), L1280–L1281. doi:10.1152/ajplung.00153.2020.

[58] Gemmati, D., Bramanti, B., Serino, M. L., Secchiero, P., Zauli, G., & Tisato, V. (2020). COVID-19 and Individual Genetic Susceptibility/Receptivity: Role of ACE1/ACE2 Genes, Immunity, Inflammation and Coagulation. Might the Double X-Chromosome in Females Be Protective against SARS-CoV-2 Compared to the Single X-Chromosome in Males? International Journal of Molecular Sciences, 21(10), 3474. doi:10.3390/ijms21103474.

[59] Panning, B. (2008). X-chromosome inactivation: the molecular basis of silencing. Journal of Biology, 7(8), 30. doi:10.1186/jbiol95.

[60] Carrel, L., & Willard, H. F. (2005). X-inactivation profile reveals extensive variability in X-linked gene expression in females. Nature, 434(7031), 400–404. doi:10.1038/nature03479.

[61] Kuba, K., Imai, Y., Rao, S., Gao, H., Guo, F., Guan, B., … Penninger, J. M. (2005). A crucial role of angiotensin converting enzyme 2 (ACE2) in SARS coronavirus–induced lung injury. Nature Medicine, 11(8), 875–879. doi:10.1038/nm1267.

[62] Bangham, J. (2014). Blood groups and human groups: Collecting and calibrating genetic data after World War Two. Studies in History and Philosophy of Science Part C: Studies in History and Philosophy of Biological and Biomedical Sciences, 47, 74–86. doi:10.1016/j.shpsc.2014.05.008.

[63] Silva-Filho, J. C., Melo, C. G. F. de, & Oliveira, J. L. de. (2020). The influence of ABO blood groups on COVID-19 susceptibility and severity: A molecular hypothesis based on carbohydrate-carbohydrate interactions. Medical Hypotheses, 144, 110155. doi:10.1016/j.mehy.2020.110155.

[64] Hosoi, E. (2008). Biological and clinical aspects of ABO blood group system. The Journal of Medical Investigation, 55(3,4), 174–182. doi:10.2152/jmi.55.174.

[65] Cooling, L. (2015). Blood Groups in Infection and Host Susceptibility. Clinical Microbiology Reviews, 28(3), 801–870. doi:10.1128/cmr.00109-14.

[66] Garratty, G., Glynn, S. A., & McEntire, R. (2004). ABO and Rh(D) phenotype frequencies of different racial/ ethnic groups in the United States. Transfusion, 44(5), 703–706. doi:10.1111/j.1537-2995.2004.03338.x.

[67] Daniels, G. L., Fletcher, A., Garratty, G., Henry, S., Jorgensen, J., Judd, W. J., … Zelinski, T. (2004). Blood group terminology 2004: from the International Society of Blood Transfusion committee on terminology for red cell surface antigens. Vox Sanguinis, 87(4), 304–316. doi:10.1111/j.1423-0410.2004.00564.x.

[68] Zietz, M., Zucker, J., & Tatonetti, N. P. (2020). Associations between blood type and COVID-19 infection, intubation, and death. Nature Communications, 11(1). doi:10.1038/s41467-020-19623-x.

[69] Paré, G., Chasman, D. I., Kellogg, M., Zee, R. Y. L., Rifai, N., Badola, S., … Ridker, P. M. (2008). Novel Association of ABO Histo-Blood Group Antigen with Soluble ICAM-1: Results of a Genome-Wide Association Study of 6,578 Women. PLoS Genetics, 4(7), e1000118. doi:10.1371/journal.pgen.1000118.

[70] Muller, W. A. (2013). Getting Leukocytes to the Site of Inflammation. Veterinary Pathology, 50(1), 7–22. doi:10.1177/0300985812469883.

[71] Adams, D. H., & Rlloyd, A. (1997). Chemokines: leucocyte recruitment and activation cytokines. The Lancet, 349(9050), 490–495. doi:10.1016/s0140-6736(96)07524-1.

[72] Staunton, D. E., Marlin, S. D., Stratowa, C., Dustin, M. L., & Springer, T. A. (1988). Primary structure of ICAM-1 demonstrates interaction between members of the immunoglobulin and integrin supergene families. Cell, 52(6), 925–933. doi:10.1016/0092-8674(88)90434-5.

[73] Zhang, W., Xu, Q., Zhuang, Y., & Chen, Y. (2016). Novel association of soluble intercellular adhesion molecule 1 and soluble P-selectin with the ABO blood group in a Chinese population. Experimental and Therapeutic Medicine, 12(2), 909–914. doi:10.3892/etm.2016.3347.

[74] Atarashi, K., Hirata, T., Matsumoto, M., Kanemitsu, N., & Miyasaka, M. (2005). Rolling of Th1 Cells via P-Selectin Glycoprotein Ligand-1 Stimulates LFA-1-Mediated Cell Binding to ICAM-1. The Journal of Immunology, 174(3), 1424–1432. doi:10.4049/jimmunol.174.3.1424.

[75] Beauséjour, Y., & Tremblay, M. J. (2004). Interaction between the Cytoplasmic Domain of ICAM-1 and Pr55Gag Leads to Acquisition of Host ICAM-1 by Human Immunodeficiency Virus Type 1. Journal of Virology, 78(21), 11916–11925. doi:10.1128/jvi.78.21.11916-11925.2004.

[76] Romero, A., San Hipólito‑Luengo, Á., Villalobos, L. A., Vallejo, S., Valencia, I., Michalska, P., ⋯ Peiró, C. (2019). The angiotensin‑(1‑7)/Mas receptor axis protects from endothelial cell senescence via klotho and Nrf2 activation. Aging Cell, 18(3), e12913. doi:10.1111/acel.12913.

[77] Zeng, Q., Langereis, M. A., van Vliet, A. L. W., Huizinga, E. G., & de Groot, R. J. (2008). Structure of coronavirus hemagglutinin-esterase offers insight into corona and influenza virus evolution. Proceedings of the National Academy of Sciences, 105(26), 9065–9069. doi:10.1073/pnas.0800502105.

[78] Varki, A. (2008). Sialic acids in human health and disease. Trends in Molecular Medicine, 14(8), 351–360. doi:10.1016/j.molmed.2008.06.002.

[79] Wielgat, P., Rogowski, K., Godlewska, K., & Car, H. (2020). Coronaviruses: Is Sialic Acid a Gate to the Eye of Cytokine Storm? From the Entry to the Effects. Cells, 9(9), 1963. doi:10.3390/cells9091963.

[80] Barile, E., Baggio, C., Gambini, L., Shiryaev, S. A., Strongin, A. Y., & Pellecchia, M. (2020). Potential Therapeutic Targeting of Coronavirus Spike Glycoprotein Priming. Molecules, 25(10), 2424. doi:10.3390/molecules25102424.

[81] Tortorici, M. A., Walls, A. C., Lang, Y., Wang, C., Li, Z., Koerhuis, D., … Veesler, D. (2019). Structural basis for human coronavirus attachment to sialic acid receptors. Nature Structural & Molecular Biology, 26(6), 481–489. doi:10.1038/s41594-019-0233-y.

[82] Han, H., Luo, Q., Mo, F., Long, L., & Zheng, W. (2020). SARS-CoV-2 RNA more readily detected in induced sputum than in throat swabs of convalescent COVID-19 patients. The Lancet Infectious Diseases, 20(6), 655–656. doi:10.1016/s1473-3099(20)30174-2.

[83] Haddad, H. M. (1964). Sialic Acids in the Eye* *From the Department of Ophthahnology, Washington University School of Medicine. American Journal of Ophthalmology, 58(6), 979–982. doi:10.1016/0002-9394(64)90008-x.

[84] Colavita, F., Lapa, D., Carletti, F., Lalle, E., Bordi, L., Marsella, P., … Castilletti, C. (2020). SARS-CoV-2 Isolation From Ocular Secretions of a Patient With COVID-19 in Italy With Prolonged Viral RNA Detection. Annals of Internal Medicine, 173(3), 242–243. doi:10.7326/m20-1176.

[85] Kaya, H., Çalışkan, A., Okul, M., Sarı, T., & Akbudak, İ. H. (2020). Detection of SARS-CoV-2 in the tears and conjunctival secretions of Coronavirus disease 2019 patients. The Journal of Infection in Developing Countries, 14(09), 977–981. doi:10.3855/jidc.13224.

[86] Singh, A. K., & Misra, A. (2020). Impact of COVID-19 and comorbidities on health and economics: Focus on developing countries and India. Diabetes & Metabolic Syndrome: Clinical Research & Reviews, 14(6), 1625–1630. doi:10.1016/j.dsx.2020.08.032.

[87] Rao, B., Singh, S., Chacko, J., Mani, R., Wattal, C., Khilnani, G., … Tiwary, P. (2020). Critical Care for COVID-19 Affected Patients: Position Statement of the Indian Society of Critical Care Medicine. Indian Journal of Critical Care Medicine, 24(4), 222–241. doi:10.5005/jp-journals-10071-23395.

[88] Majeed, J., Ajmera, P., & Goyal, R. K. (2020). Delineating clinical characteristics and comorbidities among 206 COVID-19 deceased patients in India: Emerging significance of renin angiotensin system derangement. Diabetes Research and Clinical Practice, 167, 108349. doi:10.1016/j.diabres.2020.108349.

[89] Harman, K., Verma, A., Cook, J., Radia, T., Zuckerman, M., Deep, A., … Gupta, A. (2020). Ethnicity and COVID-19 in children with comorbidities. The Lancet Child & Adolescent Health, 4(7), e24–e25. doi:10.1016/s2352-4642(20)30167-x.

[90] Lu, X., Zhang, L., Du, H., Zhang, J., Li, Y. Y., Qu, J., … Wong, G. W. K. (2020). SARS-CoV-2 Infection in Children. New England Journal of Medicine, 382(17), 1663–1665. doi:10.1056/nejmc2005073.

[91] Foster, M. P., Montecino-Rodriguez, E., & Dorshkind, K. (1999). Proliferation of bone marrow pro-B cells is dependent on stimulation by the pituitary/thyroid axis. The Journal of Immunology, 163(11), 5883-5890.

[92] Schoenfeld, P. S., Myers, J. W., Myers, L., & Larocque, J. C. (1995). Suppression of Cell-Mediated Immunity in Hypothyroidism. Southern Medical Journal, 88(3), 347–349. doi:10.1097/00007611-199503000-00019.

[93] Li, M.-Y., Li, L., Zhang, Y., & Wang, X.-S. (2020). Expression of the SARS-CoV-2 cell receptor gene ACE2 in a wide variety of human tissues. Infectious Diseases of Poverty, 9(1). doi:10.1186/s40249-020-00662-x.

[94] Van Gerwen, M., Alsen, M., Little, C., Barlow, J., Naymagon, L., Tremblay, D., … Genden, E. (2020). Outcomes of Patients With Hypothyroidism and COVID-19: A Retrospective Cohort Study. Frontiers in Endocrinology, 11. doi:10.3389/fendo.2020.00565.

[95] Schultze, A., Walker, A. J., MacKenna, B., Morton, C. E., Bhaskaran, K., Brown, J. P., … Goldacre, B. (2020). Risk of COVID-19-related death among patients with chronic obstructive pulmonary disease or asthma prescribed inhaled corticosteroids: an observational cohort study using the OpenSAFELY platform. The Lancet Respiratory Medicine, 8(11), 1106–1120. doi:10.1016/s2213-2600(20)30415-x.

[96] Ejaz, H., Alsrhani, A., Zafar, A., Javed, H., Junaid, K., Abdalla, A. E., … Younas, S. (2020). COVID-19 and comorbidities: Deleterious impact on infected patients. Journal of Infection and Public Health, 13(12), 1833–1839. doi:10.1016/j.jiph.2020.07.014.

[97] Wan, Y., Shang, J., Graham, R., Baric, R. S., & Li, F. (2020). Receptor recognition by the novel coronavirus from Wuhan: an analysis based on decade-long structural studies of SARS coronavirus. Journal of virology, 94(7). doi: 10.1128/JVI.00127-20.

[98] Liu, W., Tao, Z.-W., Wang, L., Yuan, M.-L., Liu, K., Zhou, L., … Hu, Y. (2020). Analysis of factors associated with disease outcomes in hospitalized patients with 2019 novel coronavirus disease. Chinese Medical Journal, 133(9), 1032–1038. doi:10.1097/cm9.0000000000000775.

[99] Oakes, J. M., Fuchs, R. M., Gardner, J. D., Lazartigues, E., & Yue, X. (2018). Nicotine and the renin-angiotensin system. American Journal of Physiology-Regulatory, Integrative and Comparative Physiology, 315(5), R895–R906. doi:10.1152/ajpregu.00099.2018.

[100] Kim, W. J., Song, J. S., Park, D. W., Kwak, H. J., Moon, J.-Y., Kim, S.-H., … Kim, T.-H. (2014). The effects of secondhand smoke on chronic obstructive pulmonary disease in nonsmoking Korean adults. The Korean Journal of Internal Medicine, 29(5), 613. doi:10.3904/kjim.2014.29.5.613.

[101] Ayo-Yusuf, O. A., Reddy, P. S., & van den Borne, B. W. (2008). Association of snuff use with chronic bronchitis among South African women: implications for tobacco harm reduction. Tobacco Control, 17(2), 99–104. doi:10.1136/tc.2007.022608.

[102] Mills, K. T., Bundy, J. D., Kelly, T. N., Reed, J. E., Kearney, P. M., Reynolds, K., … He, J. (2016). Global Disparities of Hypertension Prevalence and Control. Circulation, 134(6), 441–450. doi:10.1161/circulationaha.115.018912.

[103] Carey, R. M. (1984). The 1984 Report of the Joint National Committee on Detection, Evaluation, and Treatment of High Blood Pressure. Archives of Internal Medicine, 144(5), 1045. doi:10.1001/archinte.1984.00350170211032.

[104] Kannel, W. B. (1981). Systolic Blood Pressure, Arterial Rigidity, and Risk of Stroke. JAMA, 245(12), 1225. doi:10.1001/jama.1981.03310370017013.

[105] Kearney, P. M., Whelton, M., Reynolds, K., Muntner, P., Whelton, P. K., & He, J. (2005). Global burden of hypertension: analysis of worldwide data. The Lancet, 365(9455), 217–223. doi:10.1016/s0140-6736(05)17741-1.

[106] Everett, B., & Zajacova, A. (2015). Gender Differences in Hypertension and Hypertension Awareness Among Young Adults. Biodemography and Social Biology, 61(1), 1–17. doi:10.1080/19485565.2014.929488.

[107] Maranon, R., & Reckelhoff, J. F. (2013). Sex and gender differences in control of blood pressure. Clinical Science, 125(7), 311–318. doi:10.1042/cs20130140.

[108] Alvarez, G. E., Beske, S. D., Ballard, T. P., & Davy, K. P. (2002). Sympathetic Neural Activation in Visceral Obesity. Circulation, 106(20), 2533–2536. doi:10.1161/01.cir.0000041244.79165.25.

[109] Esler, M., Lambert, G., & Jennings, G. (1990). Increased regional sympathetic nervous activity in human hypertension: causes and consequences. Journal of hypertension. Supplement: official journal of the International Society of Hypertension, 8(7), S53-7.

[110] Boese, A. C., Kim, S. C., Yin, K.-J., Lee, J.-P., & Hamblin, M. H. (2017). Sex differences in vascular physiology and pathophysiology: estrogen and androgen signaling in health and disease. American Journal of Physiology-Heart and Circulatory Physiology, 313(3), H524–H545. doi:10.1152/ajpheart.00217.2016.

[111] Wu, C.-C., Cheng, J., Zhang, F. F., Gotlinger, K. H., Kelkar, M., Zhang, Y., … Schwartzman, M. L. (2011). Androgen-Dependent Hypertension Is Mediated by 20-Hydroxy-5,8,11,14-Eicosatetraenoic Acid–Induced Vascular Dysfunction. Hypertension, 57(4), 788–794. doi:10.1161/hypertensionaha.110.161570.

[112] Ishizuka, T., Cheng, J., Singh, H., Vitto, M. D., Manthati, V. L., Falck, J. R., & Laniado-Schwartzman, M. (2007). 20-Hydroxyeicosatetraenoic Acid Stimulates Nuclear Factor-κB Activation and the Production of Inflammatory Cytokines in Human Endothelial Cells. Journal of Pharmacology and Experimental Therapeutics, 324(1), 103–110. doi:10.1124/jpet.107.130336.

[113] Girardin, E., Caverzasio, J., Iwai, J., Bonjour, J.-P., Muller, A. F., Montandon, N., & Grandchamp, A. (1980). Pressure natriuresis in isolated kidneys from hypertension-prone and hypertension-resistant rats (Dahl rats). Kidney International, 18(1), 10–19. doi:10.1038/ki.1980.105.

[114] Nishiga, M., Wang, D. W., Han, Y., Lewis, D. B., & Wu, J. C. (2020). COVID-19 and cardiovascular disease: from basic mechanisms to clinical perspectives. Nature Reviews Cardiology, 17(9), 543–558. doi:10.1038/s41569-020-0413-9.

[115] Shi, S., Qin, M., Shen, B., Cai, Y., Liu, T., Yang, F., … Huang, C. (2020). Association of Cardiac Injury With Mortality in Hospitalized Patients With COVID-19 in Wuhan, China. JAMA Cardiology, 5(7), 802. doi:10.1001/jamacardio.2020.0950.

[116] Azevedo, R. B., Botelho, B. G., Hollanda, J. V. G. de, Ferreira, L. V. L., Junqueira de Andrade, L. Z., Oei, S. S. M. L., … Muxfeldt, E. S. (2020). Covid-19 and the cardiovascular system: a comprehensive review. Journal of Human Hypertension, 35(1), 4–11. doi:10.1038/s41371-020-0387-4.

[117] Felsenstein, S., & Hedrich, C. M. (2020). COVID-19 in children and young people. The Lancet Rheumatology, 2(9), e514–e516. doi:10.1016/s2665-9913(20)30212-5.

[118] Dai, H., Guo, Y., Guang, X., Xiao, Z., Zhang, M., & Yin, X. (2013). The Changes of Serum Angiotensin-Converting Enzyme 2 in Patients with Pulmonary Arterial Hypertension due to Congenital Heart Disease. Cardiology, 124(4), 208–212. doi:10.1159/000346884.

[119] Fleischmann Jr, W. R. (1996). Viral genetics. Medical Microbiology. 4th edition. Available online: https://www.ncbi.nlm.nih.gov/books/NBK7627/ (accessed on 20 March 2021).

[120] Grubaugh, N. D., Hanage, W. P., & Rasmussen, A. L. (2020). Making Sense of Mutation: What D614G Means for the COVID-19 Pandemic Remains Unclear. Cell, 182(4), 794–795. doi:10.1016/j.cell.2020.06.040.

[121] Forster, P., Forster, L., Renfrew, C., & Forster, M. (2020). Phylogenetic network analysis of SARS-CoV-2 genomes. Proceedings of the National Academy of Sciences, 117(17), 9241–9243. doi:10.1073/pnas.2004999117.

[122] Robson, F., Khan, K. S., Le, T. K., Paris, C., Demirbag, S., Barfuss, P., … Ng, W.-L. (2020). Coronavirus RNA Proofreading: Molecular Basis and Therapeutic Targeting. Molecular Cell, 79(5), 710–727. doi:10.1016/j.molcel.2020.07.027.

[123] Korber, B., Fischer, W. M., Gnanakaran, S., Yoon, H., Theiler, J., Abfalterer, W., … Wyles, M. D. (2020). Tracking Changes in SARS-CoV-2 Spike: Evidence that D614G Increases Infectivity of the COVID-19 Virus. Cell, 182(4), 812–827.e19. doi:10.1016/j.cell.2020.06.043.

[124] Yurkovetskiy, L., Wang, X., Pascal, K. E., Tomkins-Tinch, C., Nyalile, T. P., Wang, Y., … Luban, J. (2020). Structural and Functional Analysis of the D614G SARS-CoV-2 Spike Protein Variant. Cell, 183(3), 739–751.e8. doi:10.1016/j.cell.2020.09.032.

[125] Mansbach, R. A., Chakraborty, S., Nguyen, K., Montefiori, D. C., Korber, B., & Gnanakaran, S. (2020). The SARS-CoV-2 Spike Variant D614G Favors an Open Conformational State. doi:10.1101/2020.07.26.219741.

[126] Weisblum, Y., Schmidt, F., Zhang, F., DaSilva, J., Poston, D., Lorenzi, J. C., … Bieniasz, P. D. (2020). Escape from neutralizing antibodies by SARS-CoV-2 spike protein variants. eLife, 9. doi:10.7554/elife.61312.

[127] Starr, T. N., Greaney, A. J., Hilton, S. K., Ellis, D., Crawford, K. H. D., Dingens, A. S., … Bloom, J. D. (2020). Deep Mutational Scanning of SARS-CoV-2 Receptor Binding Domain Reveals Constraints on Folding and ACE2 Binding. Cell, 182(5), 1295–1310.e20. doi:10.1016/j.cell.2020.08.012.

[128] Young, B. E., Fong, S.-W., Chan, Y.-H., Mak, T.-M., Ang, L. W., Anderson, D. E., … Ng, L. F. P. (2020). Effects of a major deletion in the SARS-CoV-2 genome on the severity of infection and the inflammatory response: an observational cohort study. The Lancet, 396(10251), 603–611. doi:10.1016/s0140-6736(20)31757-8.

[129] Benvenuto, D., Angeletti, S., Giovanetti, M., Bianchi, M., Pascarella, S., Cauda, R., … Cassone, A. (2020). Evolutionary analysis of SARS-CoV-2: how mutation of Non-Structural Protein 6 (NSP6) could affect viral autophagy. Journal of Infection, 81(1), e24–e27. doi:10.1016/j.jinf.2020.03.058.

[130] Epidemiology Group of Emergency Response Mechanism of Novel Coronavirus Pneumonia, Chinese Center for Disease Control and Prevention. (2020). Analysis of Epidemiological Characteristics of Novel Coronavirus Pneumonia. Chinese Journal of Epidemiology, 41(2): 145-151. doi:10.3760 /cma.j.issn.0254-6450.2020.02.003.

[131] CDC COVID-19 Response Team, CDC COVID-19 Response Team, CDC COVID-19 Response Team, Bialek, S., Boundy, E., Bowen, V., ... & Sauber-Schatz, E. (2020). Severe outcomes among patients with coronavirus disease 2019 (COVID-19)—United States, February 12–March 16, 2020. Morbidity and mortality weekly report, 69(12), 343-346. doi:10.15585/mmwr.mm6912e2.

[132] Kim, I.-C., Kim, J. Y., Kim, H. A., & Han, S. (2020). COVID-19-related myocarditis in a 21-year-old female patient. European Heart Journal, 41(19), 1859–1859. doi:10.1093/eurheartj/ehaa288.

[133] Ottaviano, G., Carecchio, M., Scarpa, B., & Marchese-Ragona, R. (2020). Olfactory and rhinological evaluations in SARS-CoV-2 patients complaining of olfactory loss. Rhinology Journal, 0(0), 0–0. doi:10.4193/rhin20.136.

[134] Xiao, F., Tang, M., Zheng, X., Liu, Y., Li, X., & Shan, H. (2020). Evidence for Gastrointestinal Infection of SARS-CoV-2. Gastroenterology, 158(6), 1831–1833.e3. doi:10.1053/j.gastro.2020.02.055.

[135] Hu, Z., Song, C., Xu, C., Jin, G., Chen, Y., Xu, X., … Shen, H. (2020). Clinical characteristics of 24 asymptomatic infections with COVID-19 screened among close contacts in Nanjing, China. Science China Life Sciences, 63(5), 706–711. doi:10.1007/s11427-020-1661-4.

[136] Benetti, E., Tita, R., Spiga, O., Ciolfi, A., Birolo, G., … Pinto, A. M. (2020). ACE2 gene variants may underlie interindividual variability and susceptibility to COVID-19 in the Italian population. European Journal of Human Genetics, 28(11), 1602–1614. doi:10.1038/s41431-020-0691-z.

[137] Li, Q., Cao, Z., & Rahman, P. (2020). Genetic variability of human angiotensin‐converting enzyme 2 (hACE2) among various ethnic populations. Molecular Genetics & Genomic Medicine, 8(8). doi:10.1002/mgg3.1344.

[138] Ovsyannikova, I. G., Haralambieva, I. H., Crooke, S. N., Poland, G. A., & Kennedy, R. B. (2020). The role of host genetics in the immune response to SARS‐CoV‐2 and COVID‐19 susceptibility and severity. Immunological Reviews, 296(1), 205‐219. doi:10.1111/imr.12897.

[139] Pinto, B. G. G., Oliveira, A. E. R., Singh, Y., Jimenez, L., Gonçalves, A. N. A., … Nakaya, H. I. (2020). ACE2 Expression is Increased in the Lungs of Patients with Comorbidities Associated with Severe COVID-19. doi:10.1101/2020.03.21.20040261.

[140] Russo, R., Andolfo, I., Lasorsa, V. A., Iolascon, A., & Capasso, M. (2020). Genetic analysis of the novel SARS-CoV-2 host receptor TMPRSS2 in different populations. doi:10.1101/2020.04.23.057190.

[141] Zahn, L. M. (2020). HLA genetics and COVID-19. Science, 368(6493), 841.2–841. doi:10.1126/science.368.6493.841-b.

[142] Kadkhoda, K. (2020). COVID-19: an Immunopathological View. mSphere, 5(2). doi:10.1128/msphere.00344-20.

[143] Smatti, M. K., Al-Sarraj, Y. A., Albagha, O., & Yassine, H. M. (2020). Host Genetic Variants Potentially Associated With SARS-CoV-2: A Multi-Population Analysis. Frontiers in Genetics, 11. doi:10.3389/fgene.2020.578523.

[144] Devaux, C. A., Rolain, J.-M., Colson, P., & Raoult, D. (2020). New insights on the antiviral effects of chloroquine against coronavirus: what to expect for COVID-19? International Journal of Antimicrobial Agents, 55(5), 105938. doi:10.1016/j.ijantimicag.2020.105938.

[145] Singh, A. K., Singh, A., Shaikh, A., Singh, R., & Misra, A. (2020). Chloroquine and hydroxychloroquine in the treatment of COVID-19 with or without diabetes: A systematic search and a narrative review with a special reference to India and other developing countries. Diabetes & Metabolic Syndrome: Clinical Research & Reviews, 14(3), 241–246. doi:10.1016/j.dsx.2020.03.011.

[146] Wang, M., Cao, R., Zhang, L., Yang, X., Liu, J., , … Xiao, G. (2020). Remdesivir and chloroquine effectively inhibit the recently emerged novel coronavirus (2019-nCoV) in vitro. Cell Research, 30(3), 269–271. doi:10.1038/s41422-020-0282-0.

[147] Amin, M., & Abbas, G. (2020). Docking study of chloroquine and hydroxychloroquine interaction with RNA binding domain of nucleocapsid phospho-protein – an in silico insight into the comparative efficacy of repurposing antiviral drugs. Journal of Biomolecular Structure and Dynamics, 1–13. doi:10.1080/07391102.2020.1775703.

[148] Fung, K.-L., & Chan, P.-L. (2020). Comment on: COVID-19: a recommendation to examine the effect of hydroxychloroquine in preventing infection and progression. Journal of Antimicrobial Chemotherapy, 75(7), 2016–2017. doi:10.1093/jac/dkaa169.

[149] Tripathy, S., Dassarma, B., Roy, S., Chabalala, H., & Matsabisa, M. G. (2020). A review on possible modes of action of chloroquine/hydroxychloroquine: repurposing against SAR-CoV-2 (COVID-19) pandemic. International Journal of Antimicrobial Agents, 56(2), 106028. doi:10.1016/j.ijantimicag.2020.106028.

[150] Ferner, R. E., & Aronson, J. K. (2020). Chloroquine and hydroxychloroquine in covid-19. BMJ, m1432. doi:10.1136/bmj.m1432.

[151] Finbloom, D. S., Silver, K., Newsome, D. A., & Gunkel, R. (1985). Comparison of hydroxychloroquine and chloroquine use and the development of retinal toxicity. The Journal of rheumatology, 12(4), 692-694.

[152] Zhan, X., Dowell, S., Shen, Y., & Lee, D. L. (2020). Chloroquine to fight COVID-19: A consideration of mechanisms and adverse effects? Heliyon, 6(9), e04900. doi:10.1016/j.heliyon.2020.e04900.

[153] U.S. Food & Drug (FDA), Medical Product Safety Information. Available online: https://www.fda.gov/safety/medical-product-safety-information/remdesivir-gilead-sciences-fda-warns-newly-discovered-potential-drug-interaction-may-reduce (accessed on February 2021).

[154] Sheahan, T. P., Sims, A. C., Leist, S. R., Schäfer, A., Won, J., Brown, A. J., … Baric, R. S. (2020). Comparative therapeutic efficacy of remdesivir and combination lopinavir, ritonavir, and interferon beta against MERS-CoV. Nature Communications, 11(1). doi:10.1038/s41467-019-13940-6.

[155] Pruijssers, A. J., George, A. S., Schäfer, A., Leist, S. R., Gralinksi, L. E., Dinnon, K. H., … Sheahan, T. P. (2020). Remdesivir potently inhibits SARS-CoV-2 in human lung cells and chimeric SARS-CoV expressing the SARS-CoV-2 RNA polymerase in mice. doi:10.1101/2020.04.27.064279.

[156] Tchesnokov, E., Feng, J., Porter, D., & Götte, M. (2019). Mechanism of Inhibition of Ebola Virus RNA-Dependent RNA Polymerase by Remdesivir. Viruses, 11(4), 326. doi:10.3390/v11040326.

[157] Lo, M. K., Feldmann, F., Gary, J. M., Jordan, R., Bannister, R., Cronin, J., … de Wit, E. (2019). Remdesivir (GS-5734) protects African green monkeys from Nipah virus challenge. Science Translational Medicine, 11(494), eaau9242. doi:10.1126/scitranslmed.aau9242.

[158] Malin, J. J., Suárez, I., Priesner, V., Fätkenheuer, G., & Rybniker, J. (2020). Remdesivir against COVID-19 and Other Viral Diseases. Clinical Microbiology Reviews, 34(1). doi:10.1128/cmr.00162-20.

[159] Sreekanth Reddy, O., & Lai, W. (2020). Tackling COVID‐19 Using Remdesivir and Favipiravir as Therapeutic Options. ChemBioChem, 22(6), 939‐948. doi:10.1002/cbic.202000595.

[160] Zhou, P., Yang, X.-L., Wang, X.-G., Hu, B., Zhang, L., Zhang, W., … Shi, Z.-L. (2020). A pneumonia outbreak associated with a new coronavirus of probable bat origin. Nature, 579(7798), 270–273. doi:10.1038/s41586-020-2012-7.

[161] Nukoolkarn, V., Lee, V. S., Malaisree, M., Aruksakulwong, O., & Hannongbua, S. (2008). Molecular dynamic simulations analysis of ritronavir and lopinavir as SARS-CoV 3CLpro inhibitors. Journal of Theoretical Biology, 254(4), 861–867. doi:10.1016/j.jtbi.2008.07.030.

[162] Tahir ul Qamar, M., Alqahtani, S. M., Alamri, M. A., & Chen, L.-L. (2020). Structural basis of SARS-CoV-2 3CLpro and anti-COVID-19 drug discovery from medicinal plants. Journal of Pharmaceutical Analysis, 10(4), 313–319. doi:10.1016/j.jpha.2020.03.009.

[163] Osborne, V., Davies, M., Lane, S., Evans, A., Denyer, J., Dhanda, S., … Shakir, S. (2020). Lopinavir-Ritonavir in the Treatment of COVID-19: A Dynamic Systematic Benefit-Risk Assessment. Drug Safety, 43(8), 809–821. doi:10.1007/s40264-020-00966-9.

[164] Türsen, Ü., Türsen, B., & Lotti, T. (2020). Cutaneous sıde‐effects of the potential COVID-19 drugs. Dermatologic Therapy, 33(4). doi:10.1111/dth.13476.

[165] Zampino, R., Mele, F., Florio, L. L., Bertolino, L., Andini, R., Galdo, M., … Durante-Mangoni, E. (2020). Liver injury in remdesivir-treated COVID-19 patients. Hepatology International, 14(5), 881–883. doi:10.1007/s12072-020-10077-3.

[166] Pendyala, B., & Patras, A. (2020). In silico screening of food bioactive compounds to predict potential inhibitors of COVID-19 main protease (Mpro) and RNA-dependent RNA polymerase (RdRp). ChemRix.

[167] Bharti, S., Malhotra, P., & Hirsch, B. (2016). Acute intermittent porphyria precipitated by atazanavir/ritonavir. International Journal of STD & AIDS, 27(13), 1234–1235. doi:10.1177/0956462416633981.

[168] Owa, A. B., & Owa, O. T. (2020). Lopinavir/ritonavir use in Covid-19 infection: is it completely non-beneficial? Journal of Microbiology, Immunology and Infection, 53(5), 674–675. doi:10.1016/j.jmii.2020.05.014.

[169] Cao, B., Wang, Y., Wen, D., Liu, W., Wang, J., Fan, G., … Wei, M. (2020). A Trial of Lopinavir–Ritonavir in Adults Hospitalized with Severe Covid-19. New England Journal of Medicine, 382(19), 1787–1799. doi:10.1056/nejmoa2001282.

[170] Huang, J., Tao, G., Liu, J., Cai, J., Huang, Z., & Chen, J. (2020). Current Prevention of COVID-19: Natural Products and Herbal Medicine. Frontiers in Pharmacology, 11. doi:10.3389/fphar.2020.588508.

[171] Shin, D., Mukherjee, R., Grewe, D., Bojkova, D., Baek, K., Bhattacharya, A., … Dikic, I. (2020). Papain-like protease regulates SARS-CoV-2 viral spread and innate immunity. Nature, 587(7835), 657–662. doi:10.1038/s41586-020-2601-5.

[172] Boozari, M., & Hosseinzadeh, H. (2020). Natural products for COVID-19 prevention and treatment regarding to previous coronavirus infections and novel studies. Phytotherapy Research, 35(2), 864‐876. doi:10.1002/ptr.6873.

[173] Wu, C., Liu, Y., Yang, Y., Zhang, P., Zhong, W., Wang, Y., … Li, H. (2020). Analysis of therapeutic targets for SARS-CoV-2 and discovery of potential drugs by computational methods. Acta Pharmaceutica Sinica B, 10(5), 766–788. doi:10.1016/j.apsb.2020.02.008.

[174] Muchtaridi, M., Fauzi, M., Khairul Ikram, N. K., Mohd Gazzali, A., & Wahab, H. A. (2020). Natural Flavonoids as Potential Angiotensin-Converting Enzyme 2 Inhibitors for Anti-SARS-CoV-2. Molecules, 25(17), 3980. doi:10.3390/molecules25173980.

[175] Shirazi, F. M., Banerji, S., Nakhaee, S., & Mehrpour, O. (2020). Effect of angiotensin II blockers on the prognosis of COVID-19: a toxicological view. European Journal of Clinical Microbiology & Infectious Diseases, 39(10), 2001–2002. doi:10.1007/s10096-020-03932-6.

[176] Wu, C.-Y., Lin, Y.-S., Yang, Y.-H., Shu, L.-H., Cheng, Y.-C., & Liu, H. T. (2020). GB-2 inhibits ACE2 and TMPRSS2 expression: In vivo and in vitro studies. Biomedicine & Pharmacotherapy, 132, 110816. doi:10.1016/j.biopha.2020.110816.

[177] Senthil Kumar, K. J., Gokila Vani, M., Wang, C.-S., Chen, C.-C., Chen, Y.-C., Lu, L.-P., … Wang, S.-Y. (2020). Geranium and Lemon Essential Oils and Their Active Compounds Downregulate Angiotensin-Converting Enzyme 2 (ACE2), a SARS-CoV-2 Spike Receptor-Binding Domain, in Epithelial Cells. Plants, 9(6), 770. doi:10.3390/plants9060770.

[178] Abdelli, I., Hassani, F., Bekkel Brikci, S., & Ghalem, S. (2020). In silico study the inhibition of angiotensin converting enzyme 2 receptor of COVID-19 by Ammoides verticillata components harvested from Western Algeria. Journal of Biomolecular Structure and Dynamics, 1–14. doi:10.1080/07391102.2020.1763199.

[179] Kulkarni, S. A., Nagarajan, S. K., Ramesh, V., Palaniyandi, V., Selvam, S. P., & Madhavan, T. (2020). Computational evaluation of major components from plant essential oils as potent inhibitors of SARS-CoV-2 spike protein. Journal of Molecular Structure, 1221, 128823. doi:10.1016/j.molstruc.2020.128823.

[180] Teisseyre, A., Uryga, A., & Michalak, K. (2021). Statins as inhibitors of voltage-gated potassium channels Kv1.3 in cancer cells. Journal of Molecular Structure, 1230, 129905. doi:10.1016/j.molstruc.2021.129905.

[181] Seyed, M. A., Jantan, I., Bukhari, S. N. A., & Vijayaraghavan, K. (2016). A Comprehensive Review on the Chemotherapeutic Potential of Piceatannol for Cancer Treatment, with Mechanistic Insights. Journal of Agricultural and Food Chemistry, 64(4), 725–737. doi:10.1021/acs.jafc.5b05993.

[182] Kar, P., Sharma, N. R., Singh, B., Sen, A., & Roy, A. (2020). Natural compounds fromClerodendrumspp. as possible therapeutic candidates against SARS-CoV-2: Anin silicoinvestigation. Journal of Biomolecular Structure and Dynamics, 1–12. doi:10.1080/07391102.2020.1780947.

[183] Naidoo, D., Roy, A., Kar, P., Mutanda, T., & Anandraj, A. (2020). Cyanobacterial metabolites as promising drug leads against the Mproand PLproof SARS-CoV-2: anin silicoanalysis. Journal of Biomolecular Structure and Dynamics, 1–13. doi:10.1080/07391102.2020.1794972.

[184] Song, S., Peng, H., Wang, Q., Liu, Z., Dong, X., Wen, C., … Zhu, B. (2020). Inhibitory activities of marine sulfated polysaccharides against SARS-CoV-2. Food & Function, 11(9), 7415–7420. doi:10.1039/d0fo02017f.

[185] Sepay, N., Sekar, A., Halder, U. C., Alarifi, A., & Afzal, M. (2021). Anti-COVID-19 terpenoid from marine sources: A docking, admet and molecular dynamics study. Journal of Molecular Structure, 1228, 129433. doi:10.1016/j.molstruc.2020.129433.

[186] He, L.-H., Ren, L.-F., Li, J.-F., Wu, Y.-N., Li, X., & Zhang, L. (2020). Intestinal Flora as a Potential Strategy to Fight SARS-CoV-2 Infection. Frontiers in Microbiology, 11. doi:10.3389/fmicb.2020.01388.

[187] Rao, P., Shukla, A., Parmar, P., Rawal, R. M., Patel, B., Saraf, M., & Goswami, D. (2020). Reckoning a fungal metabolite, Pyranonigrin A as a potential Main protease (Mpro) inhibitor of novel SARS-CoV-2 virus identified using docking and molecular dynamics simulation. Biophysical Chemistry, 264, 106425. doi:10.1016/j.bpc.2020.106425.

Short communication

Nitrogen deprivation elicits dimorphism, capsule biosynthesis and autophagy in *Papiliotrema laurentii* strain RY1

Soumyadev Sarkar[a], Avishek Mukherjee[a], Subhadeep Das[a], Bidisha Ghosh[b], Shouvik Chaudhuri[c], Debanjana Bhattacharya[d], Arpita Sarbajna[e], Ratan Gachhui[a],*

[a] *Department of Life Science & Biotechnology, Jadavpur University, 188, Raja S.C. Mallick Road, Kolkata, 700032, India*
[b] *Department of Physics, Jadavpur University, 188, Raja S.C. Mallick Road, Kolkata, 700032, India*
[c] *Department of Mechanical Engineering, Jadavpur University, 188, Raja S.C. Mallick Road, Kolkata, 700032, India*
[d] *School of Nutrition and Food Sciences, Louisiana State University, USA*
[e] *Division of Electron Microscopy, National Institute of Cholera and Enteric Diseases (NICED), P-33, CIT Road, Scheme XM, Beliaghata, Kolkata, 700010, India*

ARTICLE INFO

ABSTRACT

Stress response due to the lack of essential nutrient(s) for an organism has been a focal point of several scientific investigations. The present study investigates the cellular adaptations behind the ability of *Papiliotrema laurentii* strain RY1 to perpetuate without added nitrogen and propagate robustly in growth-limiting amount of nitrogen. We executed phenotypic (using scanning electron microscopy, differential interference contrast microscopy and transmission electron microscopy), microbiological and computational analyses to show multiple responses of dimorphism, capsule formation and autophagy as a survival strategy by the yeast upon nitrogen starvation. The roles of phosphomannose isomerase, phosphomannomutase and several autophagy-related transcripts aiding in such a response have been discussed.

1. Introduction

The essentiality and involvement of nitrogen in metabolic circuits of diverse living organisms has been a subject of active research over the years (Cooper, 1982; Chen et al., 2018; Wiame et al., 1985; Magasanik and Neidhardt, 1987; Magasanik, 1992; Yang et al., 2015). Nitrogen depletion primarily retards the growth rate of cells and promotes cell cycle arrest (Johnston et al., 1977; Brown et al., 2014). Yeast and fungal cells typically exhibit two fundamental responses to deal with nitrogen limitation: (1) morphological modifications such as pseudohyphae generation (2) over-expression of the nitrogen transporters to maintain nitrogen homeostasis within the cells (Montanini et al., 2006).

The basidiomycetous genus *Papiliotrema* (Syn. *Cryptococcus*) has been reported to be isolated from decayed wood inside *Ficus religiosa* tree trunk hollows, avian excreta, tomato rhizosphere and even from soil samples. *Papiliotrema laurentii* is ubiquitous in soil rhizospheres as this yeast can assimilate pentoses, hexoses and organic acids that are present in root secretions. Synergism of *Papiliotrema laurentii* with *Funneliformis mosseae* (arbuscular mycorrhizal fungi), *Agathosma betulina* and *Lupinus angustifolius L.* enhanced uptake of nitrogen, phosphorus and induced photosynthesis in the respective organisms. Therefore, this yeast could have microbiological applications in

rhizospheres by stimulating plant growth (Leguina et al., 2019). *Papiliotrema laurentii* strain RY1, was isolated from Kombucha tea together with strains of nitrogen-fixing bacterial species in the medium that had no combined nitrogen. Probably a small amount of nitrogen in the tea infusion, but the high amount of carbon source will cause it to be exhausted quickly (Dutta and Gachhui, 2006; 2007). Yeasts in their natural habitats typically encounter an environment of low and limiting nitrogen and carbon levels most of the time (Tanghe et al., 2006). So, insights into the alteration of morphology and physiology of yeast under nitrogen depletion could be useful to understand how yeasts respond to such changes in environmental cues.

The yeast showed an ability to perpetuate without nitrogen and propagate robustly in the presence of growth-limiting amount of nitrogen (Chakraborty et al., 2016). The strain has been deposited in the Microbial Type Culture Collection, Chandigarh, India (MTCC 6930). RY1 was understood to adapt to low levels of nitrogen with different mechanisms. Under nitrogen stress, the yeast repressed translation apparatus and up-regulated the expression of transmembrane transporters, fatty-acid oxidation and lipid homeostasis (Sarkar et al., 2018). There was an over-expression of a chitin deacetylase leading to the modification of cell wall in response to nitrogen availability which might be instrumental to provide additional integrity to the cells

Original Article

Distinct Antioxidant Activity of a Common Antidepressant Drug Imipramine

Debalina Sinharoy[1], Debanjan Mukhopadhyay[2], Shauroseni Palchoudhuri[1], Bidisha Ghosh[3], Sukhen Das[3], Sujata G. Dastidar[1*]

[1]Department of Microbiology, Herbicure Healthcare Bio-Herbal Research Foundation, Saraldighi (E), Boral, Kolkata-700154, INDIA.
[2]Department of Molecular Biology, Herbicure Healthcare Bio-Herbal Research Foundation, Saraldighi (E), Boral, Kolkata- 700154, INDIA.
[3]Department of Physics, Jadavpur University, Kolkata- 700032, INDIA.

ABSTRACT

Background: Free radicals are known to cause severe damage to most of the biomolecules in the human system and are responsible for various illnesses including neurodegenerative, cardiovascular and autoimmune disorders. Antioxidants can reduce effects of free radicals and are given to patients suffering from such diseases. There are certain natural antioxidants like flavonoids which possess free radical scavenging activities. The flavonoid quercetin is one such compound among naturally occurring antioxidants. The present study has been designed to determine the antioxidant activity in the synthetic antidepressant drug imipramine which is structurally similar to quercetin. **Method:** Specific standard procedures like ferric ion reducing capacity by FRAP assay, phosphomolybdenum assay and cupric ion reducing (CUPRAC) assay were carried out keeping ascorbic acid as the known standard. **Results:** Ferric ion reducing property of imipramine by FRAP assay revealed that reducing power of imipramine augmented with increasing amounts of the drug. In the phosphomolybdenum assay antioxidant capacity of imipramine increased in a dose dependent manner. In both these studies imipramine showed greater antioxidant action than ascorbic acid. In CUPRAC assay as the amount of imipramine was increased there was a definite elevation in antioxidant activity; however, it was comparatively less active than ascorbic acid. **Conclusion:** The highly potent antioxidant property in the antidepressant synthetic compound imipramine may be recognized by physicians involved in treatment of psychosis since patients receiving this drug regularly will certainly be in an advantageous position. The parent structure of imipramine can be modified further to potentiate antioxidant property of the drug.

Key words: Antioxidant, Antidepressant drug, Flavonoids, Imipramine, Quercetin, Reactive Oxygen Species.

Correspondence :

Sujata Dastidar,
Department of Microbiology, Herbicure Healthcare Bio-Herbal Research Foundation,
Saraldighi (E), Boral, Kolkata-700154, INDIA.
Landline No.: +913322903135, Mobile No.: +919836029744

E-mail: jumicrobiol@yahoo.co.in
DOI: 10.5530/fra.2016.2.4

INTRODUCTION

Transfer of an electron from electron rich to electron deficient entity is termed as oxidation. The common natural oxidizing agents include metals and metallic compounds that are present naturally in all ecosystems.[1] A large number of studies have repeatedly proved the toxigenic and carcinogenic potentialities of heavy metals.[2] Such toxic metals have been found to interact with deoxyribonucleic acid (DNA) as well as proteins resulting in oxidative denaturation of biological macromolecules. Several heavy metals like lead, arsenic, mercury, iron, cadmium, chromium and cobalt are capable of producing reactive free radical species that may finally terminate in lipid peroxidation and oxidation of DNA and ribonucleic acid (RNA).[3] Prevention and slow reduction of such oxidative processes can be carried out by a variety of agents termed as antioxidants. An antioxidant is able to trap free radicals resulting in termination of a chain reaction by chelating the respective metal ion or by inhibiting the process of free radical generation and also direct scavenging of free radicals by preventing the reaction of biomolecules with the Reactive Oxygen Species (ROS). Along with ROS Reactive Nitrogen Species (RNS) is also capable of damaging biomolecules both *in vitro* and *in vivo*. Various harmful effects of ROS can be neutralized by non-enzymatic antioxidants as well as antioxidant enzymes.[4] Generation of free radicals is balanced by the antioxidative defense system in healthy individuals, but oxidative stress is revealed in individuals suffering from various ailments that favour free radical generation due to depletion of antioxidant levels.[5] Antioxidants are primarily of two types, enzymatic and non-enzymatic. Among the non-enzymatic antioxidants apart from vitamins C, E and carotenoids there is a large variety of flavonoids that are important antioxidants.

One of the most important properties of flavonoids is their protection against oxidative stress.[6] Flavonoids are polyphenolic compounds possessing 15 carbon atoms, two benzene rings which are joined by a linear three carbon atom chain. The flavonoid quercetein is known to be present in many fruits, vegetables, olive oil, red wine and tea.[7] During the past few years presence of quercetin has been reported in different parts of several higher plants.[8-13] Mishra and Flora observed further that administration of quercetin could successfully protect arsenic induced oxidation in experimental animals.[14] Based on these studies, the tricyclic antidepressant drug imipramine which is structurally similar to quercetin and a member of the dibenzazepine group of compounds was selected to determine its antioxidant potentiality.

MATERIALS AND METHODS

Drug: The drug imipramine (Sigma Aldrich, USA) was received as a gift from Dr. J. Christensen, University of Copenhagen, Copenhagen, Denmark.

Chemicals

All the chemicals and reagents used in this study were of analytical grade. Ascorbic acid was purchased from Sisco Research Laboratory (SRL, India). For ferric ion reducing assay ethanol, hydrochloric acid, potassium ferrocyanide and ferric chloride were obtained from Merck, India; and sodium dodecyl sulphate was from SRL, India. For phosphomolybdenum assay the chemicals ammonium molybdate and phosphoric acid were received from Merck, India. For cupric ion reducing assay cupric chloride, trisodium citrate and neocuproine were procured from Loba Chemie, India.

THE ANTIDEPRESSANT DRUG DOXEPIN: A PROMISING ANTIOXIDANT

SHAUROSENI PALCHOUDHURI[1], DEBANJAN MUKHOPADHYAY[2], DEBALINA SINHA ROY[1], BIDISHA GHOSH[3], SUKHEN DAS[3], SUJATA G DASTIDAR[1]*

[1]Department of Micrbiology, Herbicure Healthcare Bio-Herbal Research Foundation, Saraldighi (E), Kolkata, West Bengal, India.
[2]Department of Pathology, Microbiology and Immunology, School of Veterinary Medicine, University of California, Davis, CA, USA.
[3]Department of Physics, Jadavpur University, Kolkata, West Bengal, India. Email: jumicrobiol@yahoo.co.in

ABSTRACT

Objective: Oxidative stress contributes to the pathophysiology of exposure to environmental pollutants and to different free radical generating biochemical reactions in a human system leading to various types of age-related ailments. An antioxidant is a substance capable of preventing or slowing down oxidation of other molecules. Administration of different natural or synthetic antioxidants can ably lead to prevention and attenuation of such stress-induced biochemical alterations. Best examples of natural antioxidants are plant-derived flavonoids. The present study has been designated to determine antioxidant properties in antidepressant compound doxepin which is structurally similar to flavonoid quercetin.

Methods: Antioxidant capacity in doxepin was determined with help of several standard conventional procedures such as phosphomolybdenum assay, Ferric ion and cupric ion reducing power assays, ferrous ion chelating activity assay, hydrogen peroxide, and nitric oxide scavenging activity assays.

Results: Doxepin showed a stable rise in its antioxidant activity in a dose-dependent manner as determined by ferric as well as cupric ion reducing capacity and by phosphomolybdenum assay. An almost identical observation was noted while determining ferrous ion chelating activity. Furthermore, doxepin showed a strong nitric oxide scavenging activity in all the concentrations used in the study while its hydrogen peroxide scavenging activity was only observed at 500 µg/ml of doxepin.

Conclusion: Thus, our study opens up a new vista in search for antioxidants not only from plant sources but also from clinically established pharmaceutical compounds that are already in practical use among patients.

Keywords: Antioxidant, Antidepressant, Doxepin, Quercetin, Flavanol, Flavonoids.

INTRODUCTION

The driving forces to sustain life are some of the processes of biochemical reactions which continue till death of human beings. Such incessant processes in our bodies generate several bio-molecules, of which some are reactive oxygen species (ROSs) and free radicals [1]. Occupational exposure to environmental pollutants such as pesticides, toxic chemical wastes, direct as well as indirect cigarette smoke, gasoline exhaust, urban air pollutants ozone and radiation, and physical stress have been demonstrated to produce similar reactive molecular species in our bodies [2]. These molecules cause oxidative degradation of lipids, proteins, and DNA, activation of procarcinogens, inhibition of cellular and antioxidant defense system, depletion of sulfhydryls, altered calcium homeostasis, changes in gene expression, and induction of abnormal proteins and contribute significantly to human disease pathophysiology [3-5]. Certain substances known as antioxidants act as preventive oxidants caused by such free radicals and ROS. Halliwell [6] defined antioxidants as "any substance that delays, prevents or removes oxidative damage to a target molecule." The antioxidant vitamins such as vitamins C and E, ß-carotene and proanthocyanidins, antioxidant minerals such as zinc and selenium, and antioxidant enzymes such as glutathione, superoxide dismutase, and catalase, have been vividly studied for their potential role in the prevention of degenerative diseases including tumor growth and carcinogenesis [5-8]. Research evidence has suggested a link between increased levels of ROS and disturbed activities of enzymatic and nonenzymatic antioxidants in diseases associated with aging [9].

Through several studies, the different modes of action of various antioxidants have been observed: As preventers of oxidation reactions caused by free radicals, free lipid radical formation inhibitors, by breaking the chain of auto-oxidation reactions, as quenchers of singlet oxygen, by converting the hydroperoxides through reduction and the metal pro-oxidants by chelating metals into stable compounds, and finally as inhibitors of pro-oxidative enzymes [10-14].

Flavonoids are a class of naturally occurring polyphenolic compounds, isolated from a wide range of vascular plants. They generally occur in plants as glycosylated derivatives, and they contribute to the brilliant shades of blue, scarlet, and orange, in leaves, flowers, and fruits. Apart from various vegetables and fruits, flavonoids are found in seeds, nuts, grains, spices, and different medicinal plants as well in beverages, such as wine particularly red wine, tea, and at lower levels in beer [15]. The basic flavonoid structure is the flavan nucleus, which consists of 15 carbon atoms arranged in three rings. Different biological activities of flavonoids had been the subject of several studies in the past years, and it has been revealed that they exhibit antimicrobial, antiallergenic, antiviral, anti-inflammatory, and vasodilating actions. However, most interests have been devoted to the antioxidant activity of flavonoids, which is due to their ability to reduce free radical formation and to scavenge free radicals [16].

Among the flavonol subclass of flavonoids, quercetin is a major representative. Quercetin is the flavonoid widely distributed in nature and is one of the most abundant dietary flavonoids with an average

1st Virtual International Conference on Biotechnology and Bioinformatics (ICBB-2022)

On 26th-27th February 2022

Organized by

Insight BioSolutions, France

In technical collaboration with

Indian Science and Technology Foundation, India

CONFERENCE CERTIFICATE

This is to certify that Miss Bidisha Ghosh has participated in the ICBB 2022 conference and presented a poster title *"Fluorometric Sensing of hexavalent chromium in waste water and living cells by C dot decorated biocompatible FeOOH nanoparticles"* in the conference. Her poster got best poster Award.

Organizer, IBS

President
National Head Quarter
Indian Science and Technology Foundation
C-1/31, Yamuna Vihar, New Delhi- 110053

President, ISTF

ONE DAY NATIONAL LEVEL SEMINAR

on

Modern Trends in Chemistry for Sustainable Development

This is to certify that Prof./ Dr./Mr./Ms. ....Bidisha....Ghosh...........................

of ....Dept...of...Physics...Jadavpur...University... delivered (Poster/Oral) Presentation

entitled ...Synthesis..of..Bimetallic...........Biological..Application.. and was selected as

best presentation in the National Seminar on *"Modern Trends in Chemistry for Sustainable Development"* organized by the Department of Chemistry, Vijaygarh Jyotish Ray College, Kolkata and the Indian Chemical Society, Kolkata on March 03, 2020.

Prof. Chittaranjan Sinha
Honorary Secretary
Indian Chemical Society

Dr. Rajyasri Neogi
Principal
Vijaygarh Jyotish Ray College

Dr. Dasarath Mal
Convener
Vijaygarh Jyotish Ray College

National Conference on Recent Developments in Nanoscience & Nanotechnology,
29th -31st January 2019

NCRDNN

This is to certify that _Bidisha Ghosh_ of _Jadavpur University_ has ~~participated~~/presented a paper as ~~oral~~/poster presentation in the National Conference on Recent Developments in Nanoscience & Nanotechnology, 29th -31st January 2019, organized by the School of Materials Science and Nanotechnology, Jadavpur University.

31.1.2019

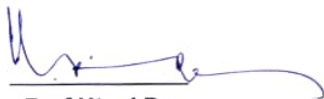Prof. Kalyan Kumar Chattopadhyay

Convener

CENTRE FOR INTERDISCIPLINARY RESEARCH AND EDUCATION

404-B Jodhpur Park, Kolkata 700068 :: Email: ciresdu@yahoo.in
(Registered under W.B.Registration of Societies Act XXVI of 1961, Reg.No. 75637 of 2010-11)

Best Poster Award 2016

This is to certify that the team of Bidisha Ghosh, Prgiya Nandy, Sukhen Das, Rajkumar Manchanda, et al has been selected for the Best Poster Award 2016 for their poster entitled PP.10 : The wonder drug Zincum oxydatum. presented at the National Symposium on Science Behind Homeopathy held on 20th February 2016 at the Birla Industrial and Technological Museum, Kolkata, organized jointly by the Centre for Interdisciplinary Research and Education, the National Council of Science Museums, the Birla Industrial and Technological Museum, the West Bengal Academy of Science and Technology (Section XI) and the Central Council for Research in Homeopathy, Dept of AYUSH, Govt. of India, New Delhi.

Prof Utpal De
President, CIRE

Dr R K Manchanda
Director General, CCRH

Shri G S Rautela
Director General, NCSM

20th February 2016

9TH ANNUAL CONFERENCE
INDIAN ASSOCIATION OF MEDICAL MICROBIOLOGISTS
WEST BENGAL CHAPTER

Certificate

The organising committee of 9ᵗʰ annual conference of Indian Association

Of Medical Microbiologists, West Bengal Chapter, 2014 appreciates the

participation of ...... Bidisha Ghosh ...... as

delegate and ..... Poster presentation .....

in the state conference held at Nil Ratan Sircar Medical College and Hospital,

Kolkata on the 7ᵗʰ December, 2014.

Prof. Manju Banerjee
Principal, NRSMCH

Prof. Satadal Das
President, IAMM, WB chapter

Prof. N.K Pal
Organising President

Prof. Susmita Bhattacharya
Organising Secretary

Insight
BioSolutions

CERTIFICATE OF COMPLETION

This is to certify that <u>**Miss Bidisha Ghosh**</u> has participated in our one-day workshop on "*DRUGS VIRTUAL SCREENING BY AUTODOCK VINA AND TOXICITY PREDICTION BY QSAR*" on 26th March 2022.

Organizer, IBS   Instructor   President, ISTF

President
National Head Quarter
Indian Science and Technology Foundation
C-1/31, Yamuna Vihar, New Delhi- 110053

CERTIFIED

CENTRE OF EXCELLENCE, TEQIP–II

IN

PHASE TRANSFORMATION AND PRODUCT CHARACTERISATION

JADAVPUR UNIVERSITY

Two-Day Workshop

On

Materials Characterisation Techniques

This is to certify that

Prof./Dr./Mr./Ms. *Bidisha Ghosh*

of *Jadavpur University*

has participated in the Workshop during 4-5 October, 2016.

Dr. Amrita Kundu
Organizing Secretary

Prof. Pravash Chandra Chakraborti
Coordinator, CoE, TEQIP-II